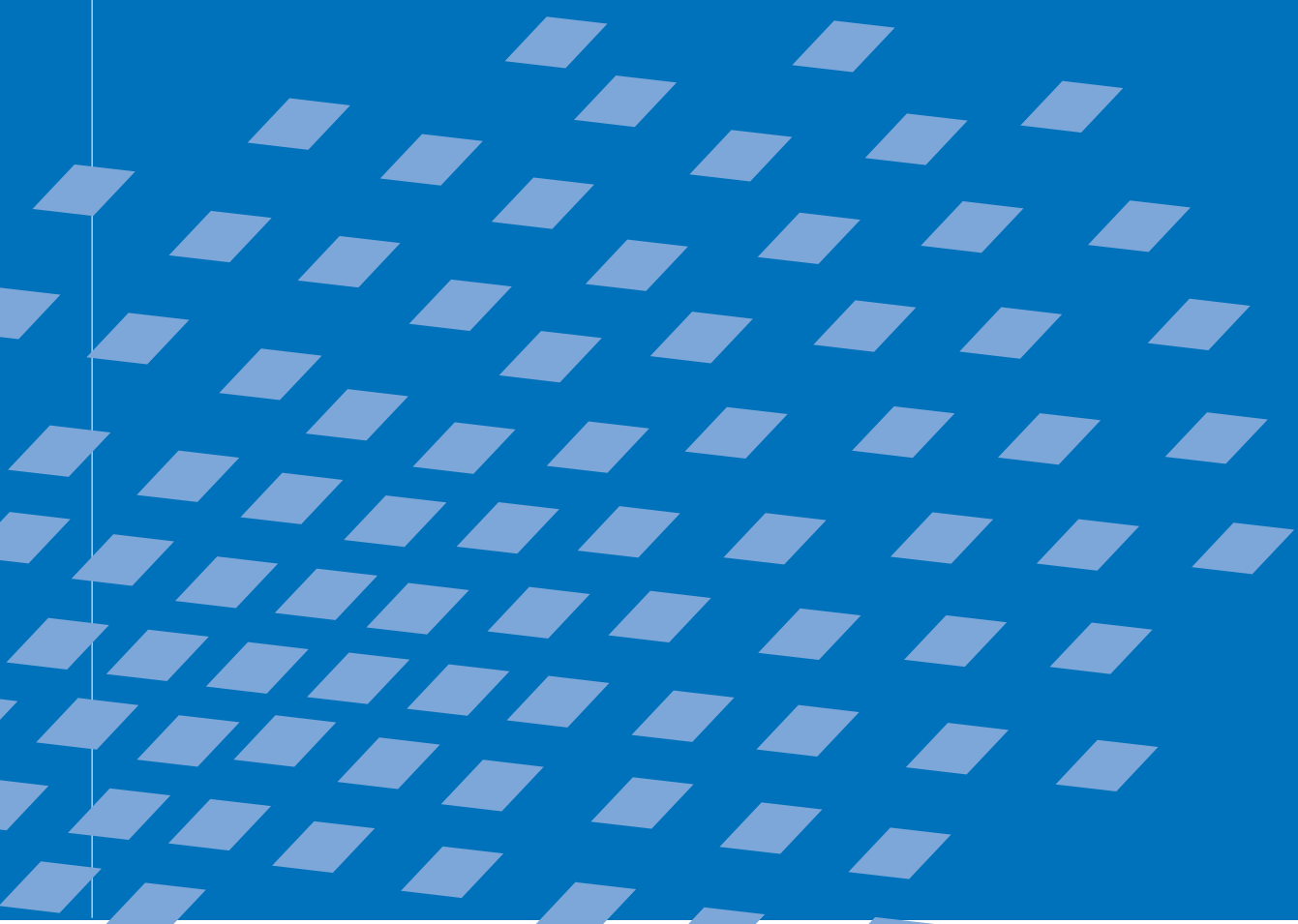




**Robust methods
for fluid–structure interaction
with stabilised finite elements**

Christiane Förster



Robust methods for fluid-structure interaction with stabilised finite elements

von

Christiane Förster

Bericht Nr. 51 (2007)
Institut für Baustatik und Baudynamik der Universität Stuttgart
Professor Dr.-Ing. M. Bischoff
Stuttgart 2007

© Christiane Förster

Berichte können bezogen werden über: / Reports are distributed by:

Institut für Baustatik und Baudynamik

Universität Stuttgart

Pfaffenwaldring 7

D-70550 Stuttgart

Tel.: ++49(0)711/685 66123

Fax: ++49(0)711/685 66130

<http://www.ibb.uni-stuttgart.de/>

Alle Rechte, insbesondere das der Übersetzung in andere Sprachen, vorbehalten. Ohne Genehmigung des Autors ist es nicht gestattet, diesen Bericht ganz oder teilweise auf photomechanischem, elektronischem oder sonstigem Wege zu kommerziellen Zwecken zu vervielfältigen.

All rights reserved. In particular, the right to translate the text of this thesis into another language is reserved. No part of the material protected by this copyright notice may be reproduced or utilized in any form or by any means, electronic or mechanical, including photocopying, recording or by any other information storage and retrieval system, without written permission of the author.

D93 - Dissertation an der Universität Stuttgart
ISBN 978-3-00-022267-2

Robust methods for fluid-structure interaction with stabilised finite elements

Von der Fakultät Bau- und Umweltingenieurwissenschaften
der Universität Stuttgart zur Erlangung der Würde eines Doktors der
Ingenieurwissenschaften (Dr.-Ing.) genehmigte Abhandlung

vorgelegt von

Christiane Förster

aus Zwickau

Hauptberichter: Prof. Dr.-Ing. Dr.-Ing. E.h. Dr. h.c. Ekkehard Ramm
1. Mitberichter: Prof. Dr. Ramon Codina
2. Mitberichter: Prof. Dr.-Ing. Wolfgang A. Wall
Tag der mündlichen Prüfung: 13. Juli 2007

Institut für Baustatik und Baudynamik der Universität Stuttgart
Stuttgart 2007

Zusammenfassung

In nahezu allen Bereichen des Ingenieurwesens treten Mehrfeldprobleme auf, zu denen auch Fluid-Struktur-Interaktionen (FSI) zu zählen sind. Diese Arbeit trägt zur Entwicklung eines stabilen und robusten numerischen Verfahrens zur Lösung solcher FSI-Probleme bei. Hier werden speziell zwei- und dreidimensionale Strukturen betrachtet, die in Wechselwirkung mit inkompressiblen Flüssigkeiten treten. Dabei ist das Strukturverhalten durch die nichtlinearen Gleichungen der Elastodynamik bestimmt. Die Dynamik des Fluids wird durch die inkompressiblen NAVIER-STOKES-Gleichungen beschrieben. Beide Felder werden mit Hilfe finiter Elemente im Raum und mittels Differenzenverfahren in der Zeit diskretisiert. Um das gekoppelte Problem zu lösen, kommt ein iterativ gestaffeltes partitioniertes Kopplungsverfahren mit Relaxation zum Einsatz.

Der Schwerpunkt dieser Arbeit liegt auf methodischen Aspekten. Insbesondere sollen die theoretischen Grundlagen des numerischen Verfahrens verbessert werden. Dabei ist das Ziel sicherzustellen, daß das Verfahren stabil läuft und für einen weiten Parameterbereich Ergebnisse von verlässlicher Genauigkeit liefert. Besondere Aufmerksamkeit gilt dem Fluidlöser, der in „Arbitrary LAGRANGEan EULERian“ (ALE) Betrachtungsweise formuliert ist. Das Verhalten des Fluids wird also in Bezug auf ein bewegtes Koordinatensystem beschrieben. Daher gilt es hier, neben den klassischen Erhaltungssätzen für Masse, Impuls und Energie auch die geometrische Erhaltung zu beachten. Der Zusammenhang zwischen den verschiedenen Erhaltungssätzen und der Stabilität des numerischen Verfahrens wird untersucht und es können Stabilitätsgrenzen in Form von maximalen Zeitschrittweiten für verschiedene Verfahren angegeben werden. Weiterhin kann gezeigt werden, wie ein unbedingt stabiles ALE Verfahren formuliert werden muß. Ein nächstes Schwerpunktthema ist das stabilisierte Finite-Element-Verfahren auf dem bewegten Gebiet. Es wird eine Version des Stabilisierungsverfahrens hergeleitet, deren Stabilität von der Netzbewegung nahezu unberührt bleibt. Weitere Untersuchungen betreffen die Empfindlichkeit des Verfahrens in Bezug auf kritische Parameter wie sehr kleine Zeitschritte, steile Gradienten oder auch stark verzerrte Netze. Für Elemente höherer Ordnung ist das stabilisierte Verfahren vollständig konsistent. Es wird gezeigt, daß mit solchen Elementen auch auf deutlich verzerrten Netzen sehr genaue Ergebnisse erzielt werden können.

Besonderes Augenmerk wird auch auf die Fluid-Struktur-Kopplung im Rahmen partitionierter Verfahren gelegt. In diesem Zusammenhang betrifft eine erste Frage den Austausch genauer und methodisch konsistenter Kopplungsinformation an der Grenzfläche zwischen Fluid und Struktur. Weiterhin wird der sogenannte „artificial added mass effect“ analysiert. Dieser Effekt bezeichnet die inherente Instabilität, die bei sequentiell gestaffelten Verfahren auftritt, wenn leichte Strukturen mit inkompressiblen Fluiden gekoppelt werden. Dabei ist letztendlich die Inkompressibilität dafür verantwortlich, daß einfache sequentiell gestaffelte Verfahren nicht erfolgreich verwendet werden können. Die mathematische Analyse, die im Rahmen dieser Arbeit vorgenommen wird, zeigt, warum die Instabilität nicht nur vom Massenverhältnis der beteiligten Kontinua, sondern auch von der Zeitdiskretisierung der Felder abhängt. Es wird deutlich, warum genauere zeitliche Diskretisierungsansätze ein früheres Eintreten der Instabilität zur Folge haben.

Die theoretischen Ergebnisse werden durch begleitende kleine Beispielrechnungen veranschaulicht. Einige größere Anwendungen des Verfahrens werden am Schluß der Arbeit präsentiert.

Abstract

Various multifield problems and among them fluid-structure interaction applications arise in nearly all fields of engineering. The present work contributes to the development of a stable and robust approach for the numerical simulation of fluid-structure interaction problems. In particular two-dimensional and three-dimensional elastic structures interacting with incompressible flow are considered. The structural field is governed by the nonlinear elastodynamic equations while the dynamics of the fluid field are described by the incompressible NAVIER-STOKES equations. Both fields are discretised by finite elements in space and finite difference methods in time. An iteratively staggered partitioned coupling procedure with relaxation is applied to obtain the overall coupled solution.

This work focuses on methodological aspects and contributes to a deeper understanding of the theoretical foundations of the approach. This is necessary to ensure that the formulation is stable and offers reliable results for a wide range of parameters. In particular the flow solver formulated in an arbitrary LAGRANGEan EULERian approach is considered. In addition to the classical conservation laws of mass, linear momentum and energy geometric conservation has to be considered. This is a consequence of the formulation of the flow equations with respect to a moving frame of reference. The relationship of these conservation laws and the stability of the numerical scheme is investigated and stability limits in terms of maximal time step sizes for different formulations are established. It is further shown how an unconditionally stable ALE formulation has to be constructed. Another key issue is the stabilised finite element method employed on the fluid domain. The derivation of the method from a virtual bubble approach is revisited while special attention is turned to the fact that the domain is moving. A version of the stabilisation is derived which is nearly unaffected by the motion of the frame of reference. Further the sensitivity of the stabilised formulation with respect to critical parameters such as very small time steps, steep gradients and distorted meshes is assessed. At least for higher order elements where full consistency of the formulation is assured very accurate results can be obtained on highly distorted meshes.

As another main issue the coupling of fluid and structure within a partitioned scheme is considered. A first concern in this context is the exchange of proper coupling data at the interface which is crucial for the consistency of the overall scheme. Subsequently the so-called artificial added mass effect is analysed. This effect is responsible for an inherent instability of sequentially staggered coupling schemes applied to the coupling of lightweight structures and incompressible flow. It is essentially the influence of the incompressibility which excludes the successful use of simple staggered schemes. The analysis derived in the course of this work reveals why the artificial added mass instability depends upon the mass ratio but further on the specific time discretisation used on the fluid and structural field. In particular it is shown why more accurate temporal discretisation results in an earlier onset of the instability.

While the theoretical considerations are accompanied by small numerical examples highlighting particular aspects some larger applications of the method are finally presented.

Vorwort

Die vorliegende Arbeit entstand in der Zeit von Ende 2002 bis Anfang 2007 während meiner Tätigkeit zunächst am Institut für Baustatik und nach der Umbenennung im Sommer 2006 am Institut für Baustatik und Baudynamik der Universität Stuttgart. In dieser Zeit genoß ich das Privileg als wissenschaftlicher Mitarbeiter an diesem renomierten Institut und gleichzeitig als Mitglied des Sonderforschungsbereiches 404 „Mehrfeldprobleme in der Kontinuumsmechanik“ arbeiten zu dürfen.

Meinem Doktorvater Herrn Prof. Dr.-Ing. Dr.-Ing. E.h. Dr. h.c. Ekkehard Ramm möchte ich an dieser Stelle außerordentlich herzlich für die Möglichkeiten danken, die er mir an seinem Institut eröffnet hat. Er hat eine Atmosphäre geschaffen, in der ich mich wohl gefühlt und sehr gern gearbeitet habe. Von dem Vertrauen und dem Rückhalt, den er meiner Arbeit gegeben hat, habe ich nicht nur wissenschaftlich profitieren können. Auch für private Probleme hatte er stets ein offenes Ohr. Vielen Dank dafür!

Auch Herrn Prof. Dr.-Ing. habil. Manfred Bischoff, der das Institut kurz vor dem Ende dieser Arbeit übernommen hat, danke ich für die großzügige fachliche und persönliche Unterstützung, die mir als gleichsam adoptiertem Doktoranden zuteil wurde. Er hat das beispiellos gute Arbeitsumfeld am Institut erhalten und mit neuem Elan gefüllt. Jeder Tag der Zusammenarbeit mit ihm war eine echte Bereicherung.

Herrn Prof. Dr. Codina vom „Departament de Resistencia de Materials i Estructures a l'Enginyeria“ der „Universitat Politecnica de Catalunya“ in Barcelona danke ich für die Übernahme des Mitberichtes, die gründliche Durchsicht des Manuskriptes sowie Kommentare und Verbesserungsvorschläge. Sein Interesse an meiner Arbeit ist mir eine unverdient große Ehre und hat mich sehr gefreut.

Ohne das Wirken von Prof. Dr.-Ing. Wolfgang A. Wall vom Lehrstuhl für numerische Mechanik der TU München wäre diese Arbeit so nicht zustande gekommen. Seine hervorragende Dissertation hatte das Thema Fluid-Struktur-Interaktion am Institut für Baustatik in Stuttgart einst etabliert und ist damit Wegbereiter und Basis der vorliegenden Arbeit. Ich danke Prof. Wall für seine fachliche Unterstützung in den letzten Jahren, die mir trotz seines stets übervollen Terminkalenders zuteil wurde. Auch für so manchen privaten Zuspruch danke ich ihm sehr herzlich.

Bedanken möchte ich mich auch bei den Kollegen am Institut für Baustatik und Baudynamik für die gute Zusammenarbeit, gegenseitiges Vertrauen und freundschaftlichen Umgang miteinander. Besonderer Dank gilt Herrn Malte von Scheven, der mit seinem selbstlosen Bemühen um die Pflege und Betreuung des institutseigenen Quellcodes zum Gelingen dieser Arbeit beigetragen hat.

Wertvolle Unterstützung und Hilfe habe ich auch von meinem Bruder Ulrich Küttler erfahren. Herzlich danke ich ihm für die Durchsicht meiner schriftlichen Arbeit, das stete Interesse an meinem Vorankommen und meinen Ergebnissen und seinen vielfachen guten Rat in Computerfragen.

Ein wesentlicher Teil der vorliegenden Arbeit wurde am mathematischen Department der „Kungliga Tekniska Högskolan“ (KTH) in Stockholm zusammengeschrieben. Ich bedanke mich beim gesamten Department und ganz besonders bei Prof. Dr. Ari Laptev für die herzliche Aufnahme, die ich dort erfahren habe.

Ganz herzlicher Dank gilt an dieser Stelle meinem Mann Clemens. Er hat meine Ar-

beit fachlich bereichert und mit bewundernswerter Geduld und Ausdauer bedingungslos unterstützt. Ich danke ihm für sein unerschütterliches liebevolles Verständnis. Herzlichen Dank möchte ich auch meinen Eltern, Geschwistern und Großeltern sagen. Unterstützung und Rückhalt aus der Familie waren nicht nur für diese Arbeit von unschätzbarem Wert.

Schließlich danke ich der deutschen Forschungsgemeinschaft für die Finanzierung meiner Arbeit im Rahmen eines herausfordernden Sonderforschungsbereiches.

Es ist berechtigt, wenn hier der Eindruck entsteht, daß ich nahezu ausschließlich mit fachlich herausragenden und menschlich großartigen Kollegen und Chefs zusammenarbeiten durfte. Die Zeit in Stuttgart und Umgebung war herausfordernd, spannend, interessant und bereichernd. Allen, die dazu beigetragen haben, sei ganz herzlich gedankt.

Christiane Förster

Drakonisches Gesetz gegen Schriftsteller. – Man sollte einen Schriftsteller als einen Missethäter ansehen, der nur in den seltensten Fällen Freisprechung oder Begnadigung verdient: das wäre ein Mittel gegen das Überhandnehmen der Bücher.

Friedrich Nietzsche, Menschliches Allzumenschliches

Contents

Contents	i
List of Figures	v
List of Tables	vii
Nomenclature	ix
1 Introduction	1
1.1 Motivation	1
1.2 Scope and objective	3
1.3 Overview	5
2 Governing equations and model problems	7
2.1 Systems of reference	7
2.2 Structure	7
2.2.1 Modelling	8
2.2.2 Kinematics	8
2.2.3 Constitutive equation	9
2.2.4 Balance of linear momentum	10
2.2.5 Initial conditions and boundary conditions	10
2.2.6 Weak formulation	11
2.2.7 Discretisation in space and time	12
2.3 Fluid	14
2.3.1 Modelling	14
2.3.2 Kinematics	14
2.3.3 Constitutive equation	14
2.3.4 Conservation of mass	15
2.3.5 Conservation of linear momentum	16
2.3.6 Conservation of energy	17
2.3.7 Properties of the incompressible Navier-Stokes equations	18
2.3.8 Initial conditions and boundary conditions	18
2.4 Coupling conditions	20
2.5 Model problems	20
2.5.1 STOKES problem	21
2.5.2 Transient advection-diffusion equation	21
2.5.3 Singular diffusion	22

3	Flow solver on moving meshes	23
3.1	Introduction	23
3.2	ALE forms of the Navier-Stokes equations	24
3.2.1	The ALE system of reference	24
3.2.2	Convective formulation	26
3.2.3	Divergence formulation	26
3.3	Discretisation	27
3.3.1	Discretisation in time	27
3.3.2	Discretisation in space	30
3.4	Conservation laws on deforming domains	33
3.4.1	Conservation of linear momentum	34
3.4.2	Geometric conservation	34
3.4.3	Conservation of energy	38
3.5	Stability of ALE formulations	40
3.5.1	Stability of the convective ALE formulation of the advection-diffusion equation	41
3.5.2	Stability of the divergence ALE formulation of the advection-diffusion equation	44
3.5.3	An unconditionally stable formulation on deforming domains	46
3.6	Summary	47
4	Stabilised finite element methods for incompressible flow	49
4.1	Wiggles and the need for stabilisation	49
4.1.1	Convection dominated problems	50
4.1.2	Spurious pressure oscillations and the LBB condition	51
4.2	Stabilisation – omnipresent in flow solvers	52
4.2.1	Convection stabilisation	52
4.2.2	Circumventing the LBB condition - pressure stabilisation	54
4.3	Residual based stabilisation methods	58
4.3.1	Virtual bubbles	59
4.3.2	A look beyond – the variational multiscale method	62
4.3.3	Generalisation and relatives	63
4.3.4	A comment on conservation in stabilised problems	66
4.3.5	Stabilised equal order elements and discretely divergence free functions	66
4.3.6	Stabilised formulation in matrix notation	68
4.3.7	Stabilisation parameter	70
4.3.8	Element length definitions	72
4.3.9	Residual based stabilisation and linear elements	73
4.4	Stability of a stabilised method on a moving mesh	74
4.4.1	Coercivity of GLS stabilised ALE formulation	75
4.4.2	Coercivity of USFEM stabilised ALE formulation	76
4.5	Summary	80
5	Stabilised finite element methods at critical parameters	81
5.1	Introduction	81
5.2	Residual based stabilisation at small time steps	82

5.2.1	Dominating zeroth order terms	84
5.2.2	A closer look at stabilisation for dominating zeroth order terms	87
5.2.3	Coercivity analysis of advection-diffusion-reaction model problem	88
5.2.4	Example at small time steps	94
5.3	Residual based stabilisation on distorted meshes	99
5.3.1	Sensitivity of USFEM stabilisation variant	99
5.3.2	Kim-Moin flow	100
5.3.3	Flow past cylinder	107
5.4	Summary	112
6	FSI coupling	113
6.1	Introduction	113
6.2	Partitioned FSI algorithm and its details	114
6.2.1	A general partitioned algorithm	114
6.2.2	Structural predictor	115
6.2.3	Fluid velocity boundary condition	116
6.2.4	Structural force boundary condition	117
6.3	Artificial added mass effect	118
6.3.1	Introduction	118
6.3.2	Added mass operator for LBB stable fluid elements	118
6.3.3	Added mass operator for stabilised finite elements	121
6.3.4	Influence of the discretisation in time	124
6.3.5	Consequences of the artificial added mass effect	129
6.3.6	General instability	130
6.3.7	Further influences on the artificial added mass effect	131
6.3.8	Numerical investigation	131
6.4	Stable partitioned schemes	136
6.4.1	Iteratively staggered schemes and the need for relaxation	136
6.4.2	Projection based semi-implicit scheme	137
6.5	Summary	138
7	Numerical Examples	139
7.1	Introduction	139
7.1.1	General algorithmic information and modelling	139
7.1.2	A few comments on computational tools	139
7.2	Bridge cross section in laminar flow	140
7.2.1	Geometry and material data	140
7.2.2	Modelling and discretisation	141
7.2.3	Results	142
7.3	Channel with backward facing step and membrane	145
7.3.1	Geometry and material data	145
7.3.2	Discretisation and initial membrane relaxation	145
7.3.3	Results on two meshes	146
7.4	Vibrating U-pipe	151
7.4.1	Geometry and material data	151
7.4.2	Modelling and discretisation	152

7.4.3	Results	153
8	Summary and Conclusions	155
8.1	Summary	155
8.2	Prospectus	156
A	Appendix	159
A.1	The kinematic formulae in a deforming frame of reference	159
A.1.1	Geometric conservation law	159
A.1.2	REYNOLDS transport theorem	160
A.2	Some mathematical background	161
A.2.1	The scalar product	161
A.2.2	LAX-MILGRAM lemma	161
A.2.3	Some inequalities	161
A.3	Errors in Kim-Moin flow	162
A.4	Flow around rigid cylinder	165
	References	169
	Index	182

List of Figures

1.1	Sample fluid-structure interaction problems	1
3.1	Sketch of ALE measuring of the fluid domain	25
3.2	Driven cavity flow example - problem description	37
3.3	Error in horizontal reaction force	37
3.4	Sketch of mesh velocity	43
5.1	Velocity oscillations on driven cavity problem	82
5.2	Model problem, solutions at different levels of discretisation	85
5.3	Problem setting of driven cavity example	95
5.4	Temporal evolution of top force at driven cavity problem	96
5.5	Driven cavity solved with linear elements and full USFEM operator	97
5.6	Driven cavity solved with linear elements and reduced USFEM operator	97
5.7	Driven cavity solved with quadratic elements and full USFEM operator	98
5.8	Driven cavity solved with quadratic elements and reduced USFEM operator	98
5.9	Driven cavity problem solved on reference mesh	98
5.10	Kim-Moin flow - velocity vectors on pressure field	101
5.11	Distorted meshes used for error evaluation	102
5.12	Velocity errors in KIM-MOIN flow	103
5.13	Velocity error depending on mesh distortion	103
5.14	Pressure error depending on mesh distortion	104
5.15	Meshes with offset edge nodes	106
5.16	Evolution of normalised errors for SUPG and GLS	106
5.17	Evolution of normalised error for USFEM	107
5.18	Flow past cylinder, geometry and mesh data	108
5.19	Lift coefficient on mesh A4	109
5.20	Drag coefficient on mesh A4	109
5.21	Pressure profile on mesh A4	110
5.22	Slightly oscillating pressure profile with close-up view obtained on Mesh C9 with minimal element length ν_i	110
5.23	Lift and drag coefficients on mesh C9	111

6.1	Polynomial $p(\lambda_i)$ according to (6.44) for different values of μ_i	126
6.2	Geometry and material data of driven cavity example with flexible bottom	132
6.3	Evolution of coupling force with different structural densities and BE . . .	132
6.4	Evolution of coupling force with different structural densities and BDF2 . .	133
6.5	Evolution of coupling force with different predictors	134
6.6	Evolution of coupling force with different time step sizes	135
6.7	Evolution of coupling force for consistent and inconsistent stabilisation . .	136
7.1	Geometry of bridge cross section in flow field	141
7.2	Evolution of vertical force on bridge deck	142
7.3	Evolution of angular momentum on bridge deck	143
7.4	Stream lines on pressure field	143
7.5	Bridge deck at different time instants	144
7.6	Initial geometry of backward facing step problem	145
7.7	Membrane problem: velocity on mesh of linear elements	148
7.8	Membrane problem: velocity on mesh of quadratic elements	149
7.9	Temporal evolution of vertical displacement of membrane mid point	150
7.10	Close-up view of membrane problem	150
7.11	Geometry and material of flowmeter tube	151
7.12	Boundary conditions of flowmeter	152
7.13	Vertical displacements at A and B	153
7.14	Results of U-pipe simulation	154
A.1	Lift, drag and pressure on mesh B4	165
A.2	Lift, drag and pressure on mesh C4	166
A.3	Lift, drag and pressure on mesh A9	167
A.4	Lift, drag and pressure on mesh B9	168

List of Tables

3.1	Conservation properties of ALE forms	47
4.1	Notation used to distinguish different versions of the stabilisation operator	65
5.1	Velocity and pressure error in normalised H^1 seminorm for linear elements	104
5.2	Velocity and pressure error in normalised H^1 seminorm for quadratic elements	105
5.3	STROUHAL number for flow past cylinder	108
6.1	Instability constants	127
A.1	L^2 error on undistorted mesh of linear elements	163
A.2	L^2 error on undistorted mesh of quadratic elements	163
A.3	L^2 error on mode 1 distorted mesh of linear elements	163
A.4	L^2 error on mode 1 distorted mesh of quadratic elements	164
A.5	L^2 error on mode 2 distorted mesh of linear elements	164
A.6	L^2 error on mode 2 distorted mesh of quadratic elements	164

Nomenclature

Abbreviations

ALE	Arbitrary LAGRANGEan EULERian
BDF2	Second order Backward Differentiation Formula
BE	Backward EULER time integration
CBS	Characteristic-Based Split
CFD	Computational Fluid Dynamics
DGCL	Discrete Geometric Conservation Law
FEM	Finite Element Method
FSI	Fluid-Structure Interaction
GCL	Geometric Conservation Law
GLS	GALERKIN/Least-Squares
ODE	Ordinary Differential Equation
PSPG	Pressure Stabilised PETROV-GALERKIN
SUPG	Streamline upwind PETROV-GALERKIN
TR	Trapezoidal rule
USFEM	Unusual Stabilised Finite Element Method

Spaces

$H^1(\Omega)$	SOBOLEV space of square-integrable functions with square-integrable derivatives
$L^2(\Omega)$	SOBOLEV space of square-integrable functions
\mathbb{C}	complex numbers
\mathbb{R}	real numbers
$B(\Omega_e)$	bubble space on element e
V_B^h	discrete finite element space enriched by bubble functions

$\mathbf{V}_{S,0}$	weighting function space for structural displacement
$\mathbf{V}_{S,D}$	solution function space for structural displacement
$\mathbf{V}_{S,0}^h$	discrete weighting function space for structural displacement
$\mathbf{V}_{S,D}^h$	discrete solution function space for structural displacement
\mathbf{V}_F^h	discrete solution function space for fluid velocity
$\mathbf{V}_{F,0}^h$	discrete weighting function space for fluid velocity
P^h	discrete function space for fluid pressure
P_m	continuous polynomial space of order m
$[P_m]$	discontinuous polynomial space of order m

Domains

Γ	fluid-structure interface
Ω_0	initial and reference domain of model problem
Ω_F	fluid domain
Ω_F^0	fluid reference domain
Ω_G	mesh domain
Ω_S	structural domain
Ω_S^0	structural reference domain
Ω_t	time dependent spatial domain of advection-diffusion problem
Ω_e	elemental domain
Ω_{n+1}	spatial domain of advection-diffusion problem at time level $n + 1$

Norms and derivatives

$(\dot{\cdot})$	material time derivative of (\cdot)
$\frac{D}{Dt}$	material time derivative
Grad	gradient with respect to the material system \mathbf{X}
Δ	LAPLACE operator with respect to the spatial system \mathbf{x}
∇	gradient with respect to spatial system \mathbf{x}
Div	divergence with respect to material system \mathbf{X}
$\ \cdot\ _{L^\infty(\Omega)}$	L^∞ -norm on Ω
$\ \cdot\ _\Omega$	L^2 -norm in Ω

$|\mathbf{x}|$ EUCLIDIAN norm of the vector \mathbf{x} , i.e. its length

Operators

$\mathcal{L}_M^{\text{stab}}$	stabilisation operator for momentum equation
\mathcal{R}_M	residual of temporally discretised balance of linear momentum in the fluid
\mathcal{L}_C	stabilisation operator for continuity equation
\mathcal{R}_C	residual of fluid continuity equation
Π	projection operator onto the space $[P_m]$
\mathcal{P}_B	projection operator on bubble space
\mathcal{R}	Residual of the advection-diffusion-problem
\mathcal{S}_B	solution operator in bubble space
tr	trace operator

Discrete matrices and vectors

\mathcal{M}_A	added mass operator
$\mathcal{M}_{Al}, \mathcal{M}_{A\text{stab}}$	added mass operator based on lumped mass matrices and on stabilised formulations
$\ddot{\mathbf{d}}$	vector of nodal structural accelerations
$\dot{\mathbf{d}}$	vector of nodal structural velocities
\mathbf{d}	vector of nodal structural displacements
\mathbf{D}^S	structural damping matrix
\mathbf{f}_b^F	right hand side vector of discrete fluid momentum balance obtained from history values and body forces
\mathbf{f}_h^F	right hand side vector of discrete fluid momentum balance obtained from traction forces
$\mathbf{F}_{\text{ext}}^S$	external structural forces
$\mathbf{F}_{\text{int}}^S$	internal structural forces
\mathbf{f}_Γ	nodal force vector at interface containing physical coupling force values
\mathbf{G}	discrete gradient operator
\mathbf{K}^F	fluid stiffness matrix obtained from viscous term
\mathbf{M}^F	fluid mass matrix

\mathbf{M}^S	structural mass matrix
\mathbf{N}	matrix of shape functions
$\mathbf{N}(\mathbf{u})$	fluid coefficient matrix stemming from convective term
\mathbf{p}	vector of nodal values of fluid pressure
\mathbf{u}	vector of nodal values of fluid velocity

Subscripts and superscripts

$(\cdot)^n$	value at time level n
$(\cdot)_0, (\cdot)_+$	stabilisation operator or weak form including zeroth order weighting function
$(\cdot)_B$	referring to bubble space
$(\cdot)_C$	referring to continuity equation
$(\cdot)_d$	referring to divergence formulation
$(\cdot)_e$	referring to element e
$(\cdot)_F$	referring to fluid field
$(\cdot)^{GLS}, (\cdot)^{USFEM}$	GLS or USFEM version of stabilisation operator or stabilised weak form
$(\cdot)_{gal}$	referring to GALERKIN weak form
$(\cdot)_G$	referring to mesh field
$(\cdot)_{mod}$	referring to model problem
$(\cdot)_M$	referring to momentum balance equation
$(\cdot)_S$	referring to structural field
$(\cdot) _{\mathbf{X}}$	evaluate at fixed material coordinate \mathbf{X}
$(\cdot) _{\mathbf{x}}$	evaluate at fixed spatial coordinate \mathbf{x}
$(\cdot)_\Gamma$	interface degrees of freedom of matrix (\cdot)
$(\cdot) _{\boldsymbol{\chi}}$	evaluate at fixed ALE coordinate $\boldsymbol{\chi}$

Symbols

A_e	elemental area
\mathbf{b}^F	specific fluid body forces
\mathbf{b}^S	specific structural body force vector
B_{mod}	bilinear form of model problem

⁽⁴⁾ \mathbf{C}	elasticity tensor
\mathbf{C}	right CAUCHY-GREEN tensor
C_e	constant of an elemental inverse inequality
d	number of spatial dimensions
\mathbf{E}	GREEN-LAGRANGEan strain tensor
E	YOUNG's modulus of the structural material
e	element counter
E_{kin}	kinetic energy
\mathbf{F}	deformation gradient tensor
\mathbf{h}_d	total momentum flux
\mathbf{h}	fluid traction vector
h_e	characteristic element length
J_t	time dependent JACOBIan determinant of the ALE mapping
k	polynomial order order of finite element space
L	characteristic length of a flow problem
m_e	elemental polynomial interpolation parameter
\mathbf{n}	outward normal vector
\bar{p}	physical fluid pressure
Pe	PECLET number
Pe^e	elemental PECLET number
p	kinematic fluid pressure
$\mathbf{r}, \mathbf{r}_\theta, \mathbf{r}_{\text{BDF2}}$	right hand side (data) of time discretised flow equations in convective formulation
$\mathbf{r}_d, \mathbf{r}_{d,\theta}, \mathbf{r}_{d,\text{BDF2}}$	right hand side (data) of time discretised flow equations in divergence formulation
Re	REYNOLDS number
Re^e	elemental REYNOLDS number
r_G	effective reaction coefficient in stabilisation operator
St	STROUHAL number
\mathbf{S}	second PIOLA-KIRCHHOFF stress tensor
T	time interval of interest

t	time
\mathbf{u}	fluid velocity field
\mathbf{u}^G	mesh velocity of ALE mesh
v	control volume in EULERian coordinates
W_S	specific strain energy of the structure
\mathbf{X}	material system of reference
\mathbf{x}	spatial system of reference
α, β, η	parameter determining the version of the stabilisation
$\delta, \delta_\theta, \delta_{\text{BDF2}}$	parameter stemming from time discretisation of the flow equations
$\boldsymbol{\varepsilon}$	strain rate tensor of the fluid
κ	diffusivity in advection-diffusion problem
λ_i	amplification coefficient for i th mode
μ	dynamic fluid viscosity
μ_i	i th eigenvalue of added mass operator
ν	kinematic fluid viscosity
ν^S	POISSON's ratio of the structural material
ϕ	scalar transport quantity
ρ^F	fluid density
ρ^S	structural mass density
σ_{0e}	lower bound on effective elemental reaction coefficient in convective ALE formulation
$\boldsymbol{\sigma}_F$	CAUCHY stresses of the fluid
$\boldsymbol{\sigma}_S$	structural CAUCHY stress tensor
τ_e	general stabilisation parameter
τ_{Ce}	elemental stabilisation parameter for continuity stabilisation
τ_{Me}	elemental stabilisation parameter for momentum stabilisation
$\boldsymbol{\tau}$	shear stresses of the fluid
$\boldsymbol{\chi}$	ALE system of reference

Chapter 1

Introduction

1.1 Motivation

Problem and applications

Fluid-structure interaction (FSI) describes a very general class of physical problems. A wide variety of FSI problems arises in engineering and technology but also in understanding and treatment of biological phenomena FSI plays a key role. Sample FSI applications from very different backgrounds are depicted in figure 1.1. The first sub figure shows a CORIOLIS mass flowmeter which serves as a measuring tool for the flow rate in a pipe. The amount of liquid passing the omega-shaped tube can be deduced from tube oscillations which are influenced by the passing flow. Mass flowmeters at very different scales are used in a multitude of technical applications. An undesired FSI takes place when wide-span bridges oscillate due to wind forces. Reliable predictions of the mutual influence of structural motion and surrounding air flow might well reduce the need for expensive wind channel tests and eventually help to increase the safety of buildings.



Figure 1.1: Coriolis mass flowmeter, Cable stayed bridge and human lung; source and copyright of images from left to right “RHEONIK Messgeräte GmbH” [203] MAGEBA [170] and HEINEMANN [124]

On top of all the engineering applications FSI is omnipresent in biological phenomena. The dynamical behaviour within a human lung as depicted figure 1.1c is governed by the interaction of air and soft tissue.

These and many more applications of FSI vary widely with respect to their characteristic scales in time and space but share the challenge of being coupled problems. Consequently the understanding and eventually the simulation of such problems tends to be tricky and time-consuming. However there is an immense interest in reliable predictions of the behaviour of FSI systems.

In a first classification FSI phenomena are distinguished in surface coupled problems and volume coupled problems. While in the first class the fluid and structural domain coincide along the common interface, i.e. the wet boundary of the structure the latter class contains problems like flow in porous media where the fluid and the structure commonly occupy a domain of interest.

Within this work surface-coupled problems are considered. Examples of such FSI problems in technical applications include besides the already mentioned ones tank sloshing, airbag deployment, parachute development, wind-force analysis on tall buildings or also earthquake response analysis of liquid storage tanks to name but a view.

But tools which are used to simulate those engineering applications are also applicable to enhance the understanding of biological processes which usually happen on very different scales. FSI occurs in the interaction of blood flow and vessels, air and lung or blood and heart valve. An increased understanding in particular of these latter processes gives rise to the hope that medical treatment can be improved, eventually increasing the quality of life for patients or even helping to reduce the number of premature death cases.

It is thus not surprising that the increase in computer power in terms of CPU and memory boosts the efforts made to simulate and predict the physics of multifield phenomena such as FSI. The present work has been undertaken within the collaborative research centre “Sonderforschungsbereich 404” on multifield problems at the University of Stuttgart. An overview over the numerical approach developed within this research project is given in [85].

Besides the research institutes an impressive number of scientific conferences indicates the high interest in the field of FSI. In the meantime FSI and other multifield modules have also been incorporated into commercial software packages reflecting the practical importance of the matter.

Modelling and approaches

Models of various levels of complexity have been derived to predict the behaviour of mechanical systems of fluids and structures influencing each other. A classical civil engineering problem including FSI is sloshing in liquid filled tanks under earthquake loading. A simple approach to such applications dates back to HOUSNER in 1963 who proposed to model the effect of the sloshing fluid by a system of horizontal springs, masses and damping. Similar applications are considered by RAMMERSTORFER et al. [198] who also couple a complex structural model with a simple added mass approach for the fluid.

However many applications deserve more accurate modelling. If the interaction of fluid and structure shall be simulated realistically including local effects at the interface both fields have to be modelled at a high level of complexity. This is particularly the case for problems where structural stresses as well as properties of the flow are of interest as in many biomechanical applications. Further problems where the structural response is particularly requested may require a complex flow description offering a prediction of the fluid forces which is sufficiently accurate.

Approaches combining advanced models for the structural and fluid description can be found among many others in DETTMER and PERIĆ [64], DONEA et al. [68], ENGEL and GRIEBEL [72], FARHAT et al. [77], FERNANDEZ et al. [80], FÖRSTER et al. [85], HEIL [123], HÜBNER et al. [130], LE TALLEC and MOURO [166], LÖHNER et al. [169],

MASSJUNG [174], PIPERNO and FARHAT [193, 194], TEZDUYAR et al. [222] and WALL and RAMM [229].

While doubtless an immense amount of research effort has already been put into accurate simulation of coupled FSI problems the challenge has by far not been solved to full satisfaction. Many recent publications indicate the persistent interest in the theory of coupled formulations. Sound mathematical formulations are required in order to guarantee that simulations offer reliable results.

A common characteristic of a large class of surface coupled FSI problems is the slenderness of the participating structure. Thin-walled structures are particularly sensitive to fluid forces and tend to exhibit large deformation which highly influence the dynamics of the flow. Thus numerical models need to include at least geometrical nonlinearities of the structure. The effect of non-linear elastic material behaviour may also be introduced into the structural solver if required. Numerical methods for this kind of structures are largely available. An overview of models and finite elements for thin-walled structures has recently been presented by BISCHOFF et al. in [16]. Within the present work the family of nonlinear three-dimensional finite shell elements as described by BISCHOFF [14] is employed which goes back to works of BÜCHTER et al. [36, 37] in the early 1990s. For two-dimensional examples geometrically nonlinear wall elements are applied.

In the present context the term *fluid* denotes materials that cannot resist shear stresses while being at rest. Thus fluids include liquids such as water, blood, oil or glycerol but also gases such as air as indicated in figure 1.1. In the regime of low MACH number, i.e. whenever the characteristic flow speed is considerably lower than the speed of sound in the fluid the flow behaves almost incompressible (see FERZIGER and PERIĆ [81]). Consequently compressibility or incompressibility is a problem dependent property rather than a material feature.

A restriction to incompressible flows of NEWTONian fluids puts the scope of the fluid field to the incompressible NAVIER-STOKES equations. For most technical applications the assumption of a linear relation between fluid shear strain rate and the corresponding stress is reasonably accurate. In a number of other cases as for example in blood flow the assumption of NEWTONian fluid behaviour allows to obtain a good first impression of the flow field and to assess the need for more appropriate material models.

On top of a structural and flow solver the *interaction* has to be managed, i.e. the ideal coupling algorithm is sought-after. Such an ideal algorithm would be efficient while not affecting accuracy and stability. It has to be admitted that despite all improvements the perfect algorithm has not yet been established.

1.2 Scope and objective

This work can in some sense be regarded a follow-up of the comprehensive dissertation of WALL [227] who introduced the topic of FSI at the Institute of Structural Mechanics at the University of Stuttgart. Within a subsequent work of MOK [182] the coupling issue was focused.

Within this work the flow problem is discretised by finite elements in space and finite difference methods in time similar to the structural equations. A stabilised Finite Element Method (FEM) the origin of which dates back to the works of HUGHES in the late 1970s

(see e.g. [135]) is used to treat convection dominated cases as well as to overcome the inf-sup condition. The flow equations are formulated in an Arbitrary LAGRANGEan EULERian (ALE) scheme which combines the possibility of considerable deformation of the fluid field with acceptable accuracy in particular at the interface.

Building upon an existing algorithm and code the present work is dedicated to a revisit of the methodological fundamentals and aims at improvements in accuracy, efficiency and stability. The focus is set on the flow simulation on a moving flow field and the coupling of the physical fields. In particular the ALE flow solver for a deforming domain deserves special attention to establish a scheme which is accurate and reliable. Therefore the effect of discrete versions of different ALE formulations on various conservation laws shall be considered. In addition to the conservation of linear momentum, mass and energy the matter of geometric conservation has to be settled in this context. Closely related to these conservation laws is the question of the numerical stability of the respective ALE schemes. Considering the model problem of advection-diffusion this stability issue shall be clarified. Limiting time steps sizes with respect to the mesh velocity will be derived and interpreted for different ALE formulations of the problem. A discrete ALE scheme which is stable irrespective of the mesh velocity shall be formulated.

Besides the clarification of the precise effect of mesh velocity the common occurrence of a time dependent domain and stabilisation of the fluid elements shall be considered by revisiting the derivation of a stabilised fluid formulation from a virtual bubble context. The ambition is to establish a numerical scheme for flow on deforming domains which inherits the defined stability with respect to mesh motion that is obtained for the unstabilised model problem. A modification of the stabilisation terms is searched for which guarantees that the stabilised flow element works independently of the mesh motion.

An ALE scheme does not only introduce a mesh velocity but goes along with potentially significantly distorted elements. The influence of mesh distortion on the accuracy of stabilised fluid elements shall be assessed and element formulations shall be found which are highly insensitive to mesh distortion. A robust and reliable FSI algorithm further requires that all related modules are not just stable but offer accurate results even at critical parameters such as very small time steps or steep gradients in space and time. In particular very small time steps result in a dominating zeroth order term within the semidiscrete equation which might give rise to local oscillations in the velocity and eventually also the pressure field. The effect of the stabilisation of such oscillations in the context of the unusual stabilised FEM including a zeroth order weighting function within the stabilisation terms shall be investigated. Altogether the reliability of different versions of the flow solver at such critical parameters will be assessed and improved.

Another important issue regarding the stability of the entire FSI algorithm rather than just the flow solver is the so-called *artificial added mass effect*. This effect is an inherent instability of weakly coupled partitioned FSI schemes coupling incompressible flow and light-weight structures. This topic taken up from the dissertation of MOK [182] where the effect was observed and studied numerically. A detailed stability analysis which was missed since shall be given here. This analysis will show why more accurate time discretisation on the participating fields strengthen the effect of the instability. Further the nature of the strong influence of the mass density ratio between fluid and structure will be clarified.

The present work focuses primarily on methodological aspects and intends to provide a

profound understanding of the schemes under consideration. Numerical examples shall be reported throughout the work verifying theoretical considerations and providing further insight into particular matters. Some larger applications will be presented in a final chapter. In this context modelling aspects and simulation issues of FSI problems will particularly be addressed.

1.3 Overview

Finishing this introduction an outline of the single chapters shall be provided offering a first impression of the subsequent matters.

In **chapter 2** the governing equations of the single fields are summarised. Further the discretisation of the structural equations in space and time is briefly presented. The flow equations are introduced in an EULERian framework where particular emphasise is put on the conservation structure of the respective equations. Within the chapter also a number of model problems is introduced which are used subsequently to analyse particular effects of interest.

Chapter 3 is devoted to the ALE scheme for flow on deforming domains. A convective and a divergence ALE formulation of the flow equations are introduced. A comparison with respect to the conservation properties of discrete versions of the two alternative formulations is given and the stability with respect to the mesh motion is considered. It turns out that an ALE formulation can be found which is stable irrespective of the mesh velocity.

Within **chapter 4** stabilised finite element methods are considered. An initial discussion concerns the reasons of numerical oscillations and thus the need for some kind of stabilisation. Residual based stabilisation methods for flow problems are reviewed and a family of the stabilisation methods which are applicable for ALE formulations is introduced along with all required details. Subsequently the performance of the stabilised finite element method on moving meshes is considered.

An investigation of stabilised methods at critical parameters is presented in **chapter 5** where the common occurrence of stabilisation and very small time steps or distorted meshes is considered. By means of a coercivity analysis the effect of very small time steps on different versions of the stabilisation is investigated. A numerical example confirms the theoretical observations. In a subsequent part of this chapter numerical tests are reported to evaluate the sensitivity of the method with respect to different kinds of mesh distortion.

The matter of **chapter 6** is the coupling of fluid and structural field. The correct exchange of interface data is discussed in the first place while subsequently a popular class of partitioned FSI algorithms is described. An analysis of the sequentially staggered version of the partitioned algorithm is presented. This analysis provides an explanation of the inherent instability of sequentially staggered schemes, the artificial added mass effect.

Within **chapter 7** some larger numerical examples are given highlighting the capabilities of the approach. Particular emphasise is put on the complete presentation of all modelling and discretisation details which have been crucial to obtain results.

It is the scope of **chapter 8** to offer an overall summary of the work along with conclusions and indications of future work. Within the **appendix A** some further information

is provided. In the first place a derivation of the basic kinematic formulae is presented and some extra mathematical background is provided. Subsequently additional result data of numerical test cases is appended completing the examples presented in chapter 5.

Chapter 2

Governing equations and model problems

This chapter reviews the continuum mechanical basis of solids and structures to the extent required within the present work. As the focus of this work is on the fluid and interaction rather than the structural part of FSI problems the discretisation of the structural equations is also briefly covered within this chapter.

Subsequent to the governing equations of the flow problem a number of model problems is presented which are used throughout this work to highlight particular effects of the flow problem.

2.1 Systems of reference

Three different systems of reference shall be used within this work. Structural deformations are most conveniently described in the so-called LAGRANGEan or material formulation. The corresponding LAGRANGEan coordinate system denoted by \mathbf{X} is associated with the particular material points.

The EULERian or spatial system of reference denoted by \mathbf{x} is most appropriate for pure fluid dynamics problems. The observer in an EULERian system is fixed in space and watches the fluid passing. Within a fluid-structure interaction problem a time dependent fluid domain has to be considered. Thus a third system of reference $\boldsymbol{\chi}$ is introduced. This Arbitrary LAGRANGEan-EULERian reference system follows the motion of the flow at the respective boundaries while deforming arbitrary in between. An introduction to the ALE formulation can be found in [69, 227]. Within the present work the ALE formulation of the flow equations is covered in chapter 3.

2.2 Structure

This section is devoted to a brief introduction to the basic structural continuum equations. Verbose explanations can be found in a broad variety of textbooks. In particular the field of structural continuum mechanics is covered by an overwhelming amount of literature of which the book by MARS DEN and HUGHES [173], the classical textbook by MALVERN [171] and the German texts by STEIN [207] and also the one by ALTENBACH and ALTENBACH [2] shall be given here to name but a view.

The basics of continuum mechanics are also covered by many books concerned with numerical approximations of continuum mechanics equations as for example in the second

volume of the finite element series of ZIENKIEWICZ and TAYLOR [236] or the monograph by BONET and WOOD [26].

2.2.1 Modelling

The fluid-structure interaction applications considered here include large structural deformations and thus geometric nonlinearities have to be considered. There is a broad range of problems dealing with thin-walled structures where the structural strains remain small and thus the assumption of linear elastic material behaviour is justified. However the iterative algorithm also allows to include nonlinear elastic materials.

2.2.2 Kinematics

The structural material initially occupies the domain $\Omega_S^0 \subset \mathbb{R}^d$ with $d \in \{2, 3\}$ and undergoes a displacement defined by the field $\mathbf{d}(\mathbf{X}, t)$. The structural reference configuration is conveniently identified with the initial configuration Ω_S^0 even if other choices are equally well possible. Ω_S denotes the time dependent domain currently occupied by the structure. The deformation gradient tensor \mathbf{F} relates a line element in the reference configuration $d\mathbf{X}$ to its image in the current configuration via

$$d\mathbf{x} = \mathbf{F} d\mathbf{X}. \quad (2.1)$$

The deformation gradient tensor \mathbf{F} is given by

$$\mathbf{F} = \text{Grad } \mathbf{x}, \quad (2.2)$$

where Grad denotes the spatial gradient operator with respect to the reference configuration, i.e. \mathbf{X} . The deformation gradient tensor is a two-field tensor connecting material and current configuration.

In contrast to \mathbf{F} the right CAUCHY-GREEN tensor

$$\mathbf{C} = \mathbf{F}^T \cdot \mathbf{F} \quad (2.3)$$

is symmetric and does not contain the rotational part of the deformation any more. It might thus be used as a strain measure if the material law accounts for the fact that $\mathbf{C} = \mathbf{I}$ for rigid body motions.

The GREEN-LAGRANGEan strain tensor \mathbf{E} is defined as a proper strain measure by normalising the right CAUCHY-GREEN tensor with respect to rigid body translations.

$$\mathbf{E} = \frac{1}{2} (\mathbf{F}^T \cdot \mathbf{F} - \mathbf{I}). \quad (2.4)$$

A graphical interpretation of the GREEN-LAGRANGEan strains \mathbf{E} shows that in an one-dimensional setting it relates the difference in the squares of a deformed and undeformed line element to the reference configuration, i.e.

$$E = \frac{1}{2} \frac{(dx)^2 - (dX)^2}{(dX)^2}.$$

2.2.3 Constitutive equation

The second PIOLA-KIRCHHOFF stress tensor \mathbf{S} is obtained from the physical CAUCHY stresses $\boldsymbol{\sigma}_S$ of the structural point by

$$\mathbf{S} = (\det \mathbf{F}) \mathbf{F}^{-1} \cdot \boldsymbol{\sigma}_S \cdot \mathbf{F}^{-T}. \quad (2.5)$$

This work is restricted to hyper elastic materials possessing an energy density function with potential character, i.e. satisfying

$$\dot{W}_S = \frac{\partial W_S}{\partial \mathbf{E}} : \dot{\mathbf{E}}. \quad (2.6)$$

As the second PIOLA-KIRCHHOFF stresses and the GREEN-LAGRANGEan strains are a work conjugate pair of stresses and strains the specific strain energy density rate is also given by $\dot{W}_S = \mathbf{S} : \dot{\mathbf{E}}$. Thus the second PIOLA-KIRCHHOFF stresses can be derived from

$$\mathbf{S} = \frac{\partial W_S(\mathbf{d})}{\partial \mathbf{E}}. \quad (2.7)$$

From the balance of angular momentum the symmetry of the CAUCHY stresses is obtained which is inherited by the second PIOLA-KIRCHHOFF stress tensor.

St.Venant-Kirchhoff material

In the case of linear ST.VENANT-KIRCHHOFF material the specific strain energy density depends linearly upon the strains according to

$$\mathbf{S} = \overset{(4)}{\mathbf{C}} : \mathbf{E} \quad (2.8)$$

where $\overset{(4)}{\mathbf{C}}$ denotes the fourth order material tensor. The over set number is used to distinguish the material tensor from the right CAUCHY-GREEN tensor.

Due to the symmetry of \mathbf{S} and \mathbf{E} and the potential character of W_S the number of independent material parameters in $\overset{(4)}{\mathbf{C}}$ reduces to 21. Assuming further isotropic behaviour the fourth order tensor of linear elasticity is given by

$$C^{ijkl} = \lambda^S g^{ij} g^{kl} + \mu^S (g^{ik} g^{jl} + g^{il} g^{jk}) \quad (2.9)$$

depending on two constants only. If the material law is expressed with respect to a Cartesian system of reference the contravariant coordinates of the metric tensor g^{ij} can be identified with the KRONECKER delta δ^{ij} . The LAMÉ constants λ^S and μ^S are related to the engineering material parameters YOUNG's modulus E and POISSON's ratio ν^S via

$$\lambda^S = \frac{E\nu^S}{(1 + \nu^S)(1 - 2\nu^S)}, \quad \mu^S = \frac{E}{2(1 + \nu^S)}. \quad (2.10)$$

Due to the linearisation of the stress-strain relationship inherent in the ST.VENANT-KIRCHHOFF material this model applies to small strain elasticity only. If large strains in particular large compressive strains are expected more appropriate material models have to be chosen.

Compressible Neo-Hookean material

In contrast to the linear elastic material law (2.8) a Neo-HOOKEAN material is capable of representing an infinite internal energy at both limits of infinite deformation, i.e. if a portion of material is either stretched infinitely long or compressed to just one point. Compressible Neo-HOOKEAN material behaviour yields the second PIOLA-KIRCHHOFF stresses

$$\mathbf{S} = \frac{\lambda^S}{2} ((\det \mathbf{F})^2 - 1) \mathbf{C}^{-1} + \mu^S (\mathbf{I} - \mathbf{C}^{-1}) \quad (2.11)$$

depending on the left CAUCHY-GREEN tensor \mathbf{C} (see e.g. WRIGGERS [234]). In (2.11) λ^S and μ^S denote the LAME constants (2.10).

2.2.4 Balance of linear momentum

NEWTON'S second law of motion states the dynamic equilibrium at a structural point and reads

$$\frac{D}{Dt} \left(\rho^S \frac{D\mathbf{d}}{Dt} \right) - \nabla \cdot \boldsymbol{\sigma}_S = \rho^S \mathbf{b}^S, \quad \text{in } \Omega_S \times T, \quad (2.12)$$

where D/Dt denotes the material time derivative and ρ^S represents the structural mass density in the deformed configuration. The balance equation applies the points within the structural domain Ω_S for all times of the time interval T . A reformulation of (2.12) with respect to the reference configuration yields

$$\rho^0 \ddot{\mathbf{d}} - \text{Div}(\mathbf{F} \cdot \mathbf{S}) = \rho^0 \mathbf{b}^S \quad \text{in } \Omega_S^0 \times T \quad (2.13)$$

where Div denotes the divergence in the LAGRANGEAN reference system and $\ddot{\mathbf{d}}$ represents the second material time derivative of the displacement field, i.e. the material acceleration. In contrast to (2.12) which refers to Ω_S a weak form of equation (2.13) has to be integrated over the time independent reference structural domain Ω_S^0 which is much more convenient as a starting point of a FEM formulation. Correspondingly ρ^0 denotes the structural mass density referring to Ω_S .

Along with a constitutive equation (2.8) or (2.11) and the kinematic equation (2.3) or (2.4) the balance of linear momentum (2.13) defines a system of coupled hyperbolic partial differential equations governing the temporal evolution of the displacement field \mathbf{d} , the stresses and strains.

2.2.5 Initial conditions and boundary conditions

At $t = 0$ the initial structural displacement field as well as its first material time derivative, the velocity, is employed to serve as initial conditions

$$\mathbf{d}(t = 0) = \mathbf{d}^0, \quad \dot{\mathbf{d}}(t = 0) = \dot{\mathbf{d}}^0 \quad \text{in } \Omega_S^0. \quad (2.14)$$

The boundary of the structural domain $\partial\Omega_S$ is decomposed into the disjoint portions $\Gamma_{S,D}$ and $\Gamma_{S,N}$ where displacement and traction boundary conditions are prescribed, respectively. The boundary portions satisfy

$$\partial\Omega_S = \Gamma_{S,D} \cup \Gamma_{S,N} \quad \text{and} \quad \Gamma_{S,D} \cap \Gamma_{S,N} = \emptyset. \quad (2.15)$$

The system of differential equations (2.13) (along with the kinematic and constitutive equation) is formulated with the displacement field as primary unknown thus $\Gamma_{S,D}$ is the DIRICHLET portion and $\Gamma_{S,N}$ the NEUMANN part of the structural boundary. The applied displacement boundary conditions are given by

$$\mathbf{d} = \bar{\mathbf{d}} \quad \text{on } \Gamma_{S,D} \quad (2.16)$$

while force boundary conditions read

$$\mathbf{N} \cdot \mathbf{S} = \mathbf{T} \quad \text{on } \Gamma_{S,N}^0, \quad (2.17)$$

where the vector \mathbf{T} is the pseudo traction vector referring to the initial configuration and \mathbf{N} denotes the normal vector on $\Gamma_{S,N}^0$. The boundary portion $\Gamma_{S,N}^0$ represents the image of the NEUMANN boundary $\Gamma_{S,N}$ in the reference configuration.

2.2.6 Weak formulation

In order to derive a finite element approximation to the structural system of equations an integral formulation is required. If all occurring energies exhibit potential character which implies that also the material law possesses a potential, the weak form can be derived from minimising the total potential energy.

Another approach to the principle of virtual work is obtained from the formal application of the method of weighted residuals which paves the way to a much wider class of test functions differing from the variation of the displacement.

The weak form of the structural balance equation (2.13) is to find $\mathbf{d} \in \mathbf{V}_{S,D} \times T$ such that

$$\left(\rho^0 \ddot{\mathbf{d}}, \delta \mathbf{d} \right)_{\Omega_S^0} + (\mathbf{S}, \delta \mathbf{E})_{\Omega_S^0} = (\rho^0 \mathbf{b}^S, \delta \mathbf{d})_{\Omega_S^0} + (\mathbf{T}, \delta \mathbf{d})_{\Gamma_{S,N}^0} \quad \text{for all } \delta \mathbf{d} \in \mathbf{V}_{S,0} \quad (2.18)$$

where the space $\mathbf{V}_{S,D} = \{ \mathbf{d} \in \mathbf{H}^1(\Omega_S^0) | \mathbf{d} = \bar{\mathbf{d}} \text{ on } \Gamma_{S,D}^0 \}$ contains all functions that satisfy the DIRICHLET boundary conditions while all functions comprised in the space $\mathbf{V}_{S,0} = \{ \mathbf{d} \in \mathbf{H}^1(\Omega_S^0) | \mathbf{d} = \mathbf{0} \text{ on } \Gamma_{S,D}^0 \}$ are zero on $\Gamma_{S,D}^0$. By $(\cdot, \cdot)_{\Omega_S^0}$ and $(\cdot, \cdot)_{\Gamma_{S,N}^0}$ the standard inner product evaluated over the reference domain or its NEUMANN boundary portion is denoted. Further $\delta \mathbf{E}$ denotes the variation of the GREEN-LAGRANGEAN strains due to a variation $\delta \mathbf{d}$ of the displacement field.

Remark 2.2.1 The symbol δ used here represents a variation and should not be mixed up with the δ introduced in a subsequent chapter along the time discretisation of the fluid equations. However the meaning of δ is obvious from the respective context.

Remark 2.2.2 The use of the notation $\delta \mathbf{d}$ for the weighting function of the structural balance of linear momentum shall indicate that a variation of the unknown displacement field \mathbf{d} is utilised to serve as test function. This yields a BUBNOV-GALERKIN type of weak formulation. In contrast different symbols will be used to represent the unknown field and its corresponding weighting function on the fluid domain. In this latter case the test function is understood as a general (somewhat arbitrary) function in the sense of a general weighted residual method and pointing towards PETROV-GALERKIN type of methods.

2.2.7 Discretisation in space and time

The structural formulation employed within this work is based on a large number of previous works in the fields of nonlinear structural dynamics at the Institute of Structural Mechanics. Thus detailed information can be found among others in the dissertations of BISCHOFF [14], KUHL [162] and GEE [99] as well as in KUHL and RAMM [163].

The integral equation (2.18) which represents the underlying structural field equations along with the corresponding boundary conditions is discretised in space by means of finite elements. Subsequently a finite-difference method is applied to discretise the resulting differential algebraic system of equations in time. Linearisation and an iterative solution method is required to eventually obtain a numerical approximation of the nonlinear partial differential equations governing the motion of the structure.

Discretisation in space

The finite element method applied here is a powerful tool in engineering and particularly applicable to structural mechanics applications. An almost infinite amount of work has been put into the method since it was first cast into a book by ZIENKIEWICZ in 1967. A broad overview covering the basics as well as numerous recent developments can be found in the sixth edition of the famous book by ZIENKIEWICZ and TAYLOR [236, 238]. One should further mention the monographs by BATHE [9] and HUGHES [134].

An early book covering the theory of finite elements is the one by ODEN [185]. The mathematics of the FEM are dealt with by BRAESS [28], BRENNER and SCOTT [30] or also by the series edited by CIARLET and LIONS [44, 45]. Another mathematically oriented classic is the monograph by CIARLET [43]. A recently given overview on finite element methods from a mathematical point of view can be found in the encyclopedia article by BRENNER and CARSTENSEN [29]. Clearly this collection is by far not complete. A list of literature entitled ‘some books on finite elements’ and occupying more than two pages is given in the introduction of the monograph by GRESHO and SANI [107].

The GALERKIN weak form (2.18) is discretised in space by replacing the function spaces $\mathbf{V}_{S,D}$ and $\mathbf{V}_{S,0}$ by discrete spaces $\mathbf{V}_{S,D}^h$ and $\mathbf{V}_{S,0}^h$, respectively. $\mathbf{V}_{S,D}^h$ and $\mathbf{V}_{S,0}^h$ contain C^0 -continuous piecewise polynomial functions defined on the single elements. Within this work the class of LAGRANGEan polynomials as well as SERENDIPity elements are considered.

Thus the unknown displacement field \mathbf{d} is replaced by the approximation

$$\mathbf{d}^h = \mathbf{N} \mathbf{d}, \quad \delta \mathbf{d}^h = \mathbf{N} \delta \mathbf{d}, \quad \ddot{\mathbf{d}}^h = \mathbf{N} \ddot{\mathbf{d}} \quad (2.19)$$

where \mathbf{N} is the matrix of the shape functions while \mathbf{d} and $\ddot{\mathbf{d}}$ denote the vector of all time dependent nodal displacement and acceleration values, respectively.

Introducing the discrete approximation (2.19) into the weak form (2.18) and noting that an arbitrary variation of the nodal displacements $\delta \mathbf{d}$ is possible yields a system of nonlinear differential algebraic equations which in matrix notation read

$$\mathbf{M}^S \ddot{\mathbf{d}} + \mathbf{D}^S \dot{\mathbf{d}} + \mathbf{F}_{\text{int}}^S(\mathbf{d}) = \mathbf{F}_{\text{ext}}^S, \quad (2.20)$$

where the viscous damping term $\mathbf{D}^S \dot{\mathbf{d}}$ has been added. In (2.20) \mathbf{M}^S denotes the symmetric positive definite structural system mass matrix while $\mathbf{F}_{\text{int}}^S$ represents the internal force

vector the linearisation of which eventually yields the tangential stiffness matrix. $\mathbf{F}_{\text{ext}}^{\text{S}}$ is the external force vector and collects the discrete representation of the right hand side in (2.18).

Discretisation in time

Subsequent to the spatial discretisation finite difference schemes shall be applied to discretise the semi-discrete system (2.20) in time. A general overview over time discretisation schemes for the structural system of equations can be found in the sound textbook by HUGHES [134]. Further references are the volumes by HAIRER et al. [111, 112]. The time discretisation of the nonlinear structural equations shall yield a stable and accurate approximation of the temporal derivatives. A nonlinear version of the generalised- α time integration scheme of CHUNG and HULBERT [42] has shown to offer the desired properties [162] and is used here.

The generalised- α method is based on the NEWMARK scheme replacing the newest displacement and velocity by expressions in terms of accelerations. Denoting the time step size by Δt the nodal displacements and velocities at the new time level are approximated by

$$\mathbf{d}^{n+1} = \mathbf{d}^n + \Delta t \dot{\mathbf{d}}^n + \Delta t^2 \left(\left(\frac{1}{2} - \beta \right) \ddot{\mathbf{d}}^n + \beta \ddot{\mathbf{d}}^{n+1} \right) \quad (2.21)$$

$$\dot{\mathbf{d}}^{n+1} = \dot{\mathbf{d}}^n + \Delta t \left((1 - \gamma) \ddot{\mathbf{d}}^n + \gamma \ddot{\mathbf{d}}^{n+1} \right). \quad (2.22)$$

Further the balance of linear momentum is satisfied at an intermediate time level t^α between t^n and t^{n+1}

$$\mathbf{M}^{\text{S}} \ddot{\mathbf{d}}^\alpha + \mathbf{D}^{\text{S}} \dot{\mathbf{d}}^\alpha + \mathbf{F}_{\text{int}}^{\text{S}}(\mathbf{d}^\alpha) = \mathbf{F}_{\text{ext}}^{\text{S},\alpha}, \quad (2.23)$$

where special care has to be taken in the treatment of the nonlinear internal force vector $\mathbf{F}_{\text{int}}^{\text{S}}(\mathbf{d}^\alpha)$ as shown in [60, 163].

Displacements, velocities and accelerations of the structure are interpolated between the discrete time levels by

$$\mathbf{d}^\alpha = (1 - \alpha_f) \mathbf{d}^{n+1} + \alpha_f \mathbf{d}^n, \quad (2.24)$$

$$\dot{\mathbf{d}}^\alpha = (1 - \alpha_f) \dot{\mathbf{d}}^{n+1} + \alpha_f \dot{\mathbf{d}}^n, \quad (2.25)$$

$$\ddot{\mathbf{d}}^\alpha = (1 - \alpha_m) \ddot{\mathbf{d}}^{n+1} + \alpha_m \ddot{\mathbf{d}}^n. \quad (2.26)$$

The integration constants are chosen such that the overall scheme has the desired spectral radius ρ_∞ while also minimal damping on low frequency modes is ensured. Evaluating the parameters α_m , α_f , β and γ according to

$$\begin{aligned} \alpha_m &= \frac{2\rho_\infty - 1}{\rho_\infty + 1}, & \alpha_f &= \frac{\rho_\infty}{\rho_\infty + 1} \\ \beta &= \frac{1}{4} (1 - \alpha_m + \alpha_f)^2, & \gamma &= \frac{1}{2} - \alpha_m + \alpha_f \end{aligned}$$

and satisfying

$$\alpha_m \leq \alpha_f \leq \frac{1}{2}$$

yields a second order accurate system.

2.3 Fluid

Within this section the basic fluid equations are introduced in EULERian notation while the required ALE formulations of the balance of linear momentum in a fluid are derived and discussed in chapter 3. The intention of this section is to provide a brief presentation of the basic equations and notations required within this work rather than giving a profound introduction into the broad topic of continuum fluid mechanics. Some more detailed presentations of the fundamental equations used here can be found in WALL [227] and GRAVEMEIER [103].

A presentation of the continuum mechanics of fluid flow along with historical remarks is given by MALVERN [171] who offers a sound introduction to both, fluid and solid continuum mechanics. Among others one may also consult FLECHTER [82], PIRONNEAU [196], WARSI [230] and the book by FERZIGER and PERIĆ [81] covering also computational techniques besides the mechanical basis.

2.3.1 Modelling

The flow problems here are considered incompressible. Further it is focused at low and moderate REYNOLDS numbers where the viscosity cannot be neglected. In particular in the vicinity of a structure the flow may exhibit a viscous boundary layer the dynamics of which significantly influence the physics of the overall coupled problem. A discussion of the model restrictions which also applies to the present work has been given by WALL [227].

2.3.2 Kinematics

The primary kinematic unknown of a flow problem is the velocity field $\mathbf{u}(\mathbf{x})$. The symmetric gradient of $\mathbf{u}(\mathbf{x})$ is called strain rate tensor

$$\boldsymbol{\varepsilon}(\mathbf{u}) = \frac{1}{2} \left(\boldsymbol{\nabla} \mathbf{u} + (\boldsymbol{\nabla} \mathbf{u})^T \right), \quad (2.27)$$

where the gradient operator $\boldsymbol{\nabla}$ denotes spatial derivatives with respect to the fixed EULERian system \mathbf{x} .

The acceleration of a fluid particle is given by the material time derivative of the respective velocity. In an EULERian formulation however this velocity is given as a function of spatial rather than material coordinates. Thus the material time derivative of the velocity field reads

$$\frac{D \mathbf{u}}{D t} = \frac{\partial \mathbf{u}}{\partial t} \Big|_{\mathbf{x}} = \frac{\partial \mathbf{u}}{\partial t} \Big|_{\mathbf{x}} + \mathbf{u} \cdot \boldsymbol{\nabla} \mathbf{u} \quad (2.28)$$

containing a nonlinear convective term.

2.3.3 Constitutive equation

As a portion of fluid at rest cannot carry any shear forces it is reasonable to decompose the CAUCHY stresses $\boldsymbol{\sigma}_F$ at a fluid point into a hydrostatic pressure \bar{p} and a tensor of

shear stresses $\boldsymbol{\tau}$. Denoting the identity tensor by \mathbf{I} this decomposition reads

$$\boldsymbol{\sigma}_F = -\mathbf{I}\bar{p} + \boldsymbol{\tau}. \quad (2.29)$$

Dating from STOKES is the assumption that the shear stress tensor $\boldsymbol{\tau} = f(\boldsymbol{\varepsilon})$ is a function of the strain rate tensor where STOKES considered a linear relationship. However, flows with a linear relation between shear stresses and strains are nowadays called NEWTONian [171]. Symmetry considerations reduce the number of independent material parameters to two, λ and μ , determining the viscosity of the fluid. Thus the constitutive equation for a NEWTONian flow reads

$$\boldsymbol{\sigma}_F = -\mathbf{I}\bar{p} + \lambda \operatorname{tr}(\boldsymbol{\varepsilon})\mathbf{I} + 2\mu \boldsymbol{\varepsilon}. \quad (2.30)$$

The assumption that mean pressure of the fluid equals the thermodynamic pressure \bar{p} holds if and only if either the flow is incompressible, i.e. $\operatorname{tr}(\boldsymbol{\varepsilon}) = 0$ or the bulk viscosity $\kappa = \lambda + 2/3 \mu$ vanishes [171].

Within this work incompressibility is assumed yielding the constitutive equation

$$\boldsymbol{\sigma}_F = -\mathbf{I}\bar{p} + 2\mu \boldsymbol{\varepsilon}. \quad (2.31)$$

Thus the only remaining material constant of the fluid is the viscosity μ of the dimension stress \times time. The parameter μ is also termed *dynamic viscosity* to distinguish it from the *kinematic viscosity*

$$\nu = \frac{\mu}{\rho^F} \quad (2.32)$$

which is normalised by the fluid mass density ρ^F . Similarly the kinematic pressure $p = \bar{p}/\rho^F$ will be used.

2.3.4 Conservation of mass

In an EULERian control volume v the rate of mass change of the mass m^F enclosed in v is directly related to the inflow and outflow to the respective boundaries if no mass sources or sinks are present

$$\left. \frac{\partial m^F}{\partial t} \right|_{\mathbf{x}} = \int_v \left. \frac{\partial \rho^F}{\partial t} \right|_{\mathbf{x}} dv = - \int_{\partial v} \rho^F \mathbf{u} \cdot \mathbf{n} d\gamma = - \int_v \nabla \cdot (\rho^F \mathbf{u}) dv, \quad (2.33)$$

where \mathbf{n} denotes the outward normal of the control volume. As (2.33) is valid for every possible control volume one obtains the local form of the mass balance reading

$$\left. \frac{\partial \rho^F}{\partial t} \right|_{\mathbf{x}} + \nabla \cdot (\rho^F \mathbf{u}) = 0. \quad (2.34)$$

For flows which exhibit a maximal velocity significantly smaller than the speed of sound in the respective medium, i.e. a small MACH number the effect of compressibility can be neglected. Thus the mass balance also termed continuity equation reduces to

$$\nabla \cdot \mathbf{u} = 0 \quad \text{in } \Omega_F \times T. \quad (2.35)$$

a scalar but powerful condition omnipresent in the fluid domain Ω_F .

2.3.5 Conservation of linear momentum

Convective form

Analogously to the dynamic equilibrium at a structural point (2.12) the balance of linear momentum at a fluid particle inside the domain Ω_F is given by

$$\rho^F \frac{\partial \mathbf{u}}{\partial t} \Big|_{\mathbf{x}} + \rho^F \mathbf{u} \cdot \nabla \mathbf{u} - \nabla \cdot \boldsymbol{\sigma}_F = \rho^F \mathbf{b}^F \quad \text{in } \Omega_F \times T, \quad (2.36)$$

where \mathbf{b}^F denotes specific fluid body forces. In (2.36) use has been made of the material acceleration in EULERian formulation (2.28). Inserting further the constitutive equation (2.31) and dividing by the density yields the EULERian formulation of the momentum balance of the incompressible NAVIER-STOKES equations in the *convective* form

$$\frac{\partial \mathbf{u}}{\partial t} \Big|_{\mathbf{x}} + \mathbf{u} \cdot \nabla \mathbf{u} - 2\nu \nabla \cdot \boldsymbol{\varepsilon}(\mathbf{u}) + \nabla p = \mathbf{b}^F \quad \text{in } \Omega_F \times T \quad (2.37)$$

which is accompanied by the continuity equation (2.35). As a result of the incompressibility the strain rate tensor $\boldsymbol{\varepsilon}$ is a traceless tensor containing shear strains only.

An interpretation of (2.37) naturally refers to a single fluid particle at which forces due to inertia, viscosity and the pressure gradient are in (dynamic) equilibrium with the external body forces. The formulation of the momentum balance given in (2.37) is frequently called *non-conservative* formulation.

Divergence form

The respective *conservative* or *divergence* form is given by

$$\frac{\partial \mathbf{u}}{\partial t} \Big|_{\mathbf{x}} + \nabla \cdot (\mathbf{u} \otimes \mathbf{u} - 2\nu \boldsymbol{\varepsilon}(\mathbf{u}) + \mathbf{I}p) = \mathbf{b}^F \quad \text{in } \Omega_F \times T, \quad (2.38)$$

where the continuity equation (2.35) has been employed. This version of the balance equation suggests an interpretation referring to a control volume rather than a single fluid particle. Integrating (2.38) over an arbitrary control volume v which is fixed in EULERian coordinates yields

$$\int_v \frac{\partial \mathbf{u}}{\partial t} \Big|_{\mathbf{x}} dv + \int_{\partial v} (\mathbf{u} \otimes \mathbf{u} - 2\nu \boldsymbol{\varepsilon}(\mathbf{u}) + \mathbf{I}p) \cdot \mathbf{n} d\gamma = \int_v \mathbf{b}^F dv, \quad (2.39)$$

where GAUSS' theorem has been applied. The integral equation (2.39) reveals why (2.38) is called conservative: A temporal change of the velocity in a control volume v is balanced by sources or sinks in v and fluxes over the boundary of the control volume.

Clearly both formulations are equal in the continuous setting. However their discrete solutions differ as in a discrete setting the continuity equation (2.35) is approximated rather than satisfied exactly. This opens the question of the better formulation or rather the one which is more appropriate in a particular case. The problem of conservation properties of various discrete versions of the flow equation will be discussed in chapter 3.

2.3.6 Conservation of energy

The energy is another conservative quantity of the flow. For the incompressible flows considered here energy conservation is not an independent equation. It is rather closely related to the balance of linear momentum (2.36). The kinetic energy E_{kin} inside a control volume v_c is given by

$$E_{\text{kin}} = \frac{1}{2} \int_v \rho^{\text{F}} |\mathbf{u}|^2 dv = \frac{1}{2} \|\sqrt{\rho^{\text{F}}} \mathbf{u}\|_v^2, \quad (2.40)$$

where $|\mathbf{u}| = \sqrt{\mathbf{u} \cdot \mathbf{u}}$ denotes the EUCLIDIAN norm of the velocity and $\|\cdot\|_v$ represents the L^2 -norm in the control volume v . Following the lines of [107] to derive the energy balance equation the equilibrium equation (2.36) is multiplied by the velocity \mathbf{u} and integrated over v yielding

$$\left(\rho^{\text{F}} \frac{\partial \mathbf{u}}{\partial t} \Big|_{\mathbf{x}}, \mathbf{u} \right)_v + (\rho^{\text{F}} \mathbf{u} \cdot \nabla \mathbf{u}, \mathbf{u})_v - (\nabla \cdot \boldsymbol{\sigma}_{\text{F}}, \mathbf{u})_v = (\rho^{\text{F}} \mathbf{b}^{\text{F}}, \mathbf{u})_v. \quad (2.41)$$

The first term in (2.41) can be recognised as temporal change of the kinetic energy inside the volume v while the convective term is reformulated using the continuity equation (2.35). Further the viscous contribution to the energy rate is integrated by parts yielding a boundary term and the internal energy dissipation rate $\boldsymbol{\sigma}_{\text{F}} : \nabla \mathbf{u}$ which reduces to $\boldsymbol{\tau} : \nabla \mathbf{u}$ since the pressure does not contribute to the internal viscous work. Using the symmetry of the shear stress tensor $\boldsymbol{\tau}$ this term can further be reformulated to

$$\boldsymbol{\tau} : \nabla \mathbf{u} = \boldsymbol{\tau} : \frac{1}{2\mu} \boldsymbol{\tau} = \frac{1}{2\mu} |\boldsymbol{\tau}|^2 \geq 0.$$

Thus inserting all these terms back into (2.41) and employing GAUSS' divergence theorem conservation of the kinetic energy is obtained according to

$$\frac{\partial E_{\text{kin}}}{\partial t} \Big|_{\mathbf{x}} + \frac{1}{2} \rho^{\text{F}} (|\mathbf{u}|^2 \mathbf{n}, \mathbf{u})_{\partial v} - (\mathbf{n} \cdot \boldsymbol{\sigma}_{\text{F}}, \mathbf{u})_{\partial v} + \frac{1}{2\mu} \|\boldsymbol{\tau}\|_v^2 = \int_v \rho^{\text{F}} \mathbf{b}^{\text{F}} \cdot \mathbf{u} dv. \quad (2.42)$$

Equation (2.42) states that a change of the kinetic energy inside the control volume is balanced by the inflow of kinetic energy, the work done by the traction along the boundary of the control volume, the work of body forces and the energy dissipated by internal friction. From (2.42) it can be observed that in every volume with homogeneous DIRICHLET boundary conditions and zero body forces the kinetic energy has to decay monotonously.

Analytical solutions of either the convective or the divergence formulation of the fluid momentum balance satisfy energy conservation. However this does not necessarily apply to the respective spatially discrete equations as the discrete velocity field will not be exactly divergence free. To carry conservation of energy over to the discrete version the balance of linear momentum has to be written in the form (consult also [107, 197] in this issue)

$$\frac{\partial \mathbf{u}}{\partial t} \Big|_{\mathbf{x}} + \mathbf{u} \cdot \nabla \mathbf{u} + \frac{1}{2} \nabla \cdot \mathbf{u} \mathbf{u} - 2\nu \nabla \cdot \boldsymbol{\varepsilon}(\mathbf{u}) + \nabla p = \mathbf{b}^{\text{F}} \quad \text{in } \Omega_{\text{F}} \times T. \quad (2.43)$$

The energy conservation equation (2.42) can be derived from (2.43) without requiring an exactly divergence free velocity field. It is noteworthy that (2.43) is the average of the convective formulation and the divergence form of the incompressible NAVIER-STOKES equations in a fixed EULERian system of reference.

2.3.7 Properties of the incompressible Navier-Stokes equations

The transient incompressible NAVIER-STOKES equations are a nonlinear system of mixed hyperbolic-parabolic partial differential equations for the primary unknown fields of the velocity \mathbf{u} and the kinematic pressure p .

As a result of the incompressibility a local change in the pressure is instantly carried to the entire domain, i.e. the fluid exhibits an infinite speed of sound.

The incompressible NAVIER-STOKES equations contain two main challenges. The first one is the saddle point structure of the problem caused by the mixed formulation in velocity and pressure. A second problem is the hyperbolic convective term which also introduces a nonlinearity.

The properties of a particular flow can be measured by dimensionless numbers representing a ratio of forces which govern the problem. The most famous of these measures is the REYNOLDS number given by

$$\text{Re} = \frac{L |\mathbf{u}|}{\nu}, \quad (2.44)$$

where L is a characteristic length of the respective flow problem while \mathbf{u} and ν denote a representative scalar velocity and the kinematic viscosity, respectively. The REYNOLDS number gives the ratio of stationary inertial forces and viscous forces. The higher the REYNOLDS number gets the lower is the influence of the elliptic viscous term. Consequently very thin internal and boundary layer may develop at high REYNOLDS number.

A further dimensionless measure required within the present work is the STROUHAL number defined by

$$\text{St} = \frac{L}{t_c u} \quad (2.45)$$

where the characteristic period length t_c enters. The STROUHAL number is a dimensionless frequency representing the ratio of transient and stationary inertial forces.

An exhaustive discussion of alternative formulations of the single terms as well as expressions in alternative variables is given by GRESHO and SANI in [107]. Mathematical properties of incompressible viscous flow are also discussed by RANNACHER in [202].

2.3.8 Initial conditions and boundary conditions

The initial condition of the momentum balance is an initial velocity field in the initial fluid domain Ω_{F}^0

$$\mathbf{u}(t = 0) = \mathbf{u}^0 \quad \text{in } \Omega_{\text{F}}^0 \quad (2.46)$$

which has to be solenoidal, i.e. to satisfy $\nabla \cdot \mathbf{u}^0 = 0$ to guarantee a well posed problem. It is important to note that the fact that the initial velocity field has to be divergence free excludes impulsive starts of the velocity perpendicular to the boundary.

There is no initial condition for the pressure in an incompressible flow. It rather acts as a LAGRANGE multiplier for the incompressibility condition and instantly adjusts to the velocity field. For a broad discussion of the initial condition one should consult [107].

In accordance to the structural boundary conditions the boundary of the fluid domain $\partial\Omega_F$ is decomposed into

$$\partial\Omega_F = \Gamma_{F,D} \cup \Gamma_{F,N} \quad \text{with} \quad \Gamma_{F,D} \cap \Gamma_{F,N} = \emptyset \quad (2.47)$$

where the respective DIRICHLET and NEUMANN boundary conditions are prescribed as

$$\mathbf{u} = \bar{\mathbf{u}} \quad \text{on } \Gamma_{F,D} \quad \text{and} \quad \frac{1}{\rho^F} \mathbf{n} \cdot \boldsymbol{\sigma}_F = \mathbf{h} \quad \text{on } \Gamma_{F,N}. \quad (2.48)$$

Here \mathbf{h} denotes the specific traction vector.

The incompressibility condition (2.35) demands that on a fixed control volume the inflow and outflow balance, i.e.

$$\int_{\Gamma_F} \mathbf{u} \cdot \mathbf{n} \, d\gamma = 0. \quad (2.49)$$

Clearly (2.49) puts a restriction if the fluid is fully constraint by DIRICHLET type of boundary conditions.

It is of interest to interpret particular boundary conditions with respect to their physical meaning.

- *No-slip boundary conditions* can be chosen as the NAVIER-STOKES equations include viscous effects. Assuming that the fluid particles at the boundary stick to the fixed or moving surface DIRICHLET boundary conditions for the velocity are prescribed in the normal and tangential component. A prescribed tangential velocity typically causes a boundary layer where the physics are dominated by internal friction.
- *Slip boundary conditions* consequently have to be used if the EULER equations are considered, i.e. if no viscosity occurs. In the case of slip boundary conditions the first equation of (2.48) is replaced by

$$\mathbf{u} \cdot \mathbf{n} = \bar{\mathbf{u}} \cdot \mathbf{n} \quad \text{on } \Gamma_{F,D}. \quad (2.50)$$

For viscous flow problems these boundary conditions may be used to model an artificial boundary of the domain.

- *Slip with friction boundary conditions* are a choice between the above two. Thus the fluid particles are allowed to slip tangentially to the boundary line but the slip results in shear forces due to a linear friction law. These boundary conditions require an additional material type of parameter. This friction coefficient heavily depends upon the property of the respective surface and the viscosity of the flow. Suggested by GALDI and LAYTON [97] in the context of large eddy simulations such boundary conditions have been used by JOHN, e.g. [148, 151].
- *Outflow boundary conditions* are a particular challenge. Caused rather by the need to limit the computational domain than by any physically reasonable boundary neither essential nor natural boundary data is available. Within this work the popular ‘do nothing’ boundary condition is used which implies the assumption of a zero NEUMANN boundary condition. The question of outflow boundary conditions is discussed by HEYWOOD et al. [125].

- A *pressure boundary condition* is required as the pressure is determined by the incompressible NAVIER-STOKES equations up to a constant. For pure flow problems the pressure constant is usually fixed implicitly by a NEUMANN boundary condition or directly at a particular point. Alternatively the mean value of the pressure can be fixed. The influence of the pressure boundary condition in a coupled FSI problem will be touched upon again in section 2.4.

Further possible boundary conditions such as symmetry boundary conditions, periodic boundary conditions or free surfaces will not be used within this work. For an exhaustive discussion of appropriate boundary conditions and their effects one may consult GRESHO, SANI and coauthors, i.e. in [107, 206].

2.4 Coupling conditions

In order to reach at the coupled FSI problem the structural and fluid field have to be connected along the interface Γ .

The solution of the overall problem requires kinematic and dynamic continuity across Γ for all times in T

$$\mathbf{x}_0^S + \mathbf{d} = \mathbf{x}, \quad \dot{\mathbf{d}} = \mathbf{u}, \quad \ddot{\mathbf{d}} = \dot{\mathbf{u}} \quad \text{on } \Gamma \times T \quad (2.51)$$

and

$$\mathbf{n} \cdot \boldsymbol{\sigma}_S = \mathbf{n} \cdot \boldsymbol{\sigma}_F \quad \text{on } \Gamma \times T \quad (2.52)$$

where \mathbf{x} denotes the position of the fluid boundary and \mathbf{x}_0^S represents the initial position of the structural point. In most cases \mathbf{x}_0^S will be identified with the LAGRANGEAN coordinate \mathbf{X} . In (2.51) no-slip boundary conditions at the interface Γ have been assumed. If slip shall be possible the normal components of the kinematic variables are coupled exclusively.

It is worth noting that the dynamic coupling condition (2.52) connects the fluid pressure level with the structural stresses. Thus for problems where the structure is not fully immersed in the fluid the free pressure constant implicitly depends upon the external structural loads. Correspondingly the interface displacement has to satisfy the global mass conservation of the fluid field. Particularly partitioned solution approaches may fail for some problems due to these implicit coupling conditions. Approaches to solve this incompressibility dilemma are discussed by KÜTTLER et al. in [164].

2.5 Model problems

Within this section a number of model problems is introduced which will be used subsequently to study particular numerical effects of the flow field. These differential equations can be regarded as special simplifications of the incompressible NAVIER-STOKES equations while they also possess a physical interpretation on their own.

The STOKES equations modelling creeping flow state an important simplification of the incompressible NAVIER-STOKES equations. The STOKES problem is a classical model problem to study the effect of the incompressibility condition.

Mixed convective-diffusive transport of a quantity is modelled by the advection-diffusion equation. A scalar advection-diffusion problem suffices to investigate the ability of a numerical method to properly reproduce transport including significant convection.

2.5.1 Stokes problem

In the limit of very small flow velocities \mathbf{u} the effect of the convective term might be neglected. Such creeping flows are governed by the incompressible STOKES equations reading

$$\begin{aligned} \left. \frac{\partial \mathbf{u}}{\partial t} \right|_{\mathbf{x}} - 2\nu \nabla \cdot \boldsymbol{\varepsilon}(\mathbf{u}) + \nabla p = \mathbf{b}^F & \quad \text{in } \Omega_F \times T \\ \nabla \cdot \mathbf{u} = 0 & \quad \text{in } \Omega_F \times T \end{aligned} \quad (2.53)$$

along with appropriate initial- and boundary conditions.

While still exhibiting the problem of the incompressibility the STOKES problem is linear and does not contain a hyperbolic term any more. It is thus used to model the saddle point structure of the incompressible NAVIER-STOKES equations.

2.5.2 Transient advection-diffusion equation

The advection-diffusion equation governs the transport of a scalar quantity ϕ as for example the concentration of milk in a cup of coffee which is stirred up. The milk diffuses depending on the gradient in milk concentration while it is moved by the underlying velocity field at the same time. The function ϕ may also represent the temperature distribution in a medium which is moving with the velocity field \mathbf{a} .

In the convective formulation on a potentially time dependent domain Ω_t the advection-diffusion problem reads

$$\left. \frac{\partial \phi}{\partial t} \right|_{\mathbf{x}} + \mathbf{a} \cdot \nabla \phi - \kappa \Delta \phi = f \quad \text{in } \Omega_t \times T, \quad (2.54)$$

$$\phi(t=0) = \phi^0 \quad \text{in } \Omega_0, \quad (2.55)$$

where f denotes a source or sink, κ the diffusivity and the advective velocity field \mathbf{a} is divergence free.

The advection-diffusion equation is accompanied by appropriate DIRICHLET and NEUMANN boundary conditions given by

$$\phi = \bar{\phi} \quad \text{on } \Gamma_D \quad \mathbf{n} \cdot \kappa \nabla \phi = h \quad \text{on } \Gamma_N. \quad (2.56)$$

Equation (2.54) is a linear model problem of (2.37) combining diffusive and convective transport. It allows to study the properties of a mixed hyperbolic-elliptic differential equation in a linear context. As a measure of the ratio of the convective and diffusive transport the PECLET number

$$\text{Pe} = \frac{|\mathbf{a}|L}{\kappa} \quad (2.57)$$

is used. This number is the analogue to the REYNOLDS number for the NAVIER-STOKES equation as given in (2.44).

A temporally discretised version of (2.54) in convective formulation takes the form

$$\phi + \delta \mathbf{a} \cdot \nabla \phi - \delta \kappa \Delta \phi = r, \quad \text{in } \Omega_t \quad (2.58)$$

where the symbol r denotes the right hand side term consisting of body forces and contributions from temporal discretisation and δ represents a coefficient stemming from time discretisation. Equation (2.58) is also termed advection-diffusion-reaction equation. The zeroth order term is called reactive as in certain reactive processes sources depend upon the unknown quantity ϕ itself. In the context of this work the term is used to model the effect of the zeroth order term introduced by time discretisation of the flow equations.

Remark 2.5.1 The parameter δ depends upon the time step size and the choice of the time discretisation scheme as defined in (3.17).

2.5.3 Singular diffusion

A further reduction of the advection-diffusion-reaction equation (2.58) yields the singular diffusion problem

$$\phi - \delta \kappa \Delta \phi = r, \quad (2.59)$$

along with appropriate boundary conditions. Differential equations of this kind are obtained from temporally discretised diffusion problems or transient heat conduction. The singular diffusion problem is employed to model the effect of the zeroth order term stemming from time discretisation and its relationship to elliptic diffusion.

Chapter 3

Flow solver on moving meshes

Within this chapter the ALE formulations of the flow equations are derived and discussed. Similar to the convective and divergence formulation in an EULERIAN setting a convective and divergence formulation on a moving domain can be derived. Discretising these formulations in time and space yields schemes with different discrete properties and potentially different discrete solutions. In particular the conservation features of these discrete forms are considered.

3.1 Introduction

Fluid-structure interaction problems have to deal with temporally changing domains. While the structural equations are written in a LAGRANGEAN formulation and thus track the moving interface Γ the balance of linear momentum in the flow field (2.37) poses a difficulty. The use of an ALE formulation removes the problem. It allows to define a reference system following the moving boundaries while not being attached to the motion of the fluid particles inside the deforming domain.

ALE schemes have gained significant popularity for simulations which have to treat temporally changing domains and in particular for flow simulations with free surfaces or FSI problems [131]. The original development of the method was done in the context of finite difference methods in the 1960s. The formulation was later adopted for finite element schemes. Early applications with moving finite element meshes have among others been presented by DONEA et al. [67] in 1977 and BELYTSCHKO and KENNEDY [13] in 1978. In [13] the flow formulation is termed ‘quasi-Eulerian’. Apparently the term ALE was established by HIRT et al. in 1974 in an article that was reprinted in 1997 [127, 128]. Applications of the method in the finite element context from the early 1980s and are reported by DONEA in [66, 68]. ALE methods in the finite element context are covered in the book by DONEA and HUERTA [69] where also some more references to the history of ALE methods can be found. An overview including information on mesh update procedures is also given in the encyclopedia article by DONEA et al. [70].

It is obviously desirable to transfer the temporal order of accuracy obtained on a fixed reference system to the deforming domain problem. Additionally stability of the ALE formulation is required. Stability of different ALE formulations is a persistent problem of interest [5, 83, 84, 175]. The matter of accurate and stable computations on deforming domains is further closely linked to the question of geometric conservation, an additional conservation property on moving frames of reference. However, geometric conservation of a numerical scheme should not be discussed independently of conservation of linear momentum and energy as no numerical approximation will be able to satisfy simultaneously

all conservation laws exactly.

Within this work the focus is set on the flow solver on deforming domains rather than the treatment of mesh motion itself. Some comments on the mesh update shall thus be added here. Various mesh motion schemes have been proposed over the last few decades. For simple shaped domains heuristic or interpolation methods as the one described in [156] are used. Such approaches may be formulated rather efficient, i.e. without the need to solve a large system of equations. For complicated geometries and arbitrary motion of the boundary pseudo-structural approaches are frequently preferred for their generality. Pseudo-structural methods can be found for example in CHIANDUSSI et al. [39] and LÖHNER and YANG [168]. Within such schemes locally varying stiffnesses are used to maintain an optimal mesh quality close to the moving boundary. The same motivation is behind the idea of discontinuous pseudo-structural schemes based on a spring analogy. In such formulations the mesh motion is determined from the displacement of a system of translational and possibly torsional springs attached to the edges, diagonals and vertices of the elements. Two-dimensional applications of the spring analogy can be found in BLOM [18] and FARHAT et al. [74]. The three-dimensional case is considered by DEGAND and FARHAT in [61] and very recently by MARKOU et al. in [172].

Within the present work pseudo-structural approaches as well as spring-type mesh motion schemes are employed.

3.2 ALE forms of the Navier-Stokes equations

Analogously to the convective and divergence form of the momentum balance in an EULERian setting the respective formulations can be recovered on a deforming domain. The derivation of the ALE formulation of the flow equations can be found in the book by DONEA and HUERTA [69]. A graphical interpretation has also been given by WALL [227].

3.2.1 The ALE system of reference

A sketch of the ALE system of reference is given in figure 3.1. The spatial coordinates of a particular point $\mathbf{x} \in \Omega_F$ are given by the unique mapping

$$\mathbf{x} = \varphi(\boldsymbol{\chi}, t) \quad \text{for all } t \in T. \quad (3.1)$$

The reference system $\boldsymbol{\chi}$ tracks the moving boundaries of Ω_F and is allowed to move arbitrarily and independent of the fluid flow inside the domain. It can be identified with a particular temporal configuration for example the initial configuration. Within this work the elemental parameter space is considered as reference configuration in the discrete case.

Jacobian determinant of the ALE frame of reference

The ALE mapping (3.1) allows to introduce the strictly positive JACOBIAN determinant

$$J_t = \det \left(\frac{\partial \mathbf{x}}{\partial \boldsymbol{\chi}} \right) \quad (3.2)$$

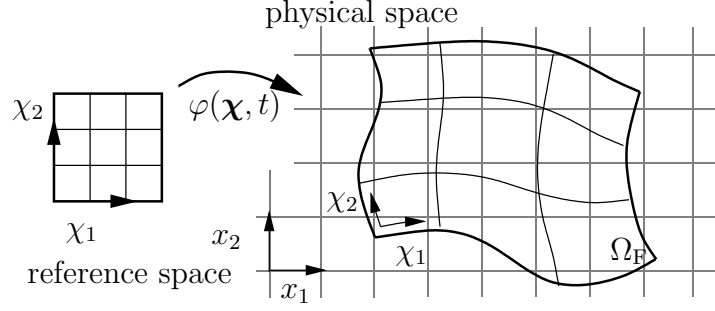


Figure 3.1: Sketch of ALE measuring of the fluid domain

relating the differential portions of volume in the spatial and reference domain according to

$$d\Omega_F = J_t d\Omega_F^0. \quad (3.3)$$

The reference fluid domain Ω_F^0 is time independent. The temporal change of the fluid domain Ω_F is caused by the normal velocity of its boundary according to

$$\frac{\partial}{\partial t} \Big|_{\mathbf{x}} \int_{\Omega_F} d\Omega_F = \int_{\Omega_F^0} \frac{\partial J_t}{\partial t} \Big|_{\boldsymbol{\chi}} d\Omega_F^0 = \int_{\partial\Omega_F} \mathbf{u}^G \cdot \mathbf{n} d\partial\Omega_F. \quad (3.4)$$

The local form of (3.4) yields the well known EULER expansion formula [3] also termed EULER's formula by WARSI in [230]

$$\frac{\partial J_t}{\partial t} \Big|_{\mathbf{x}} = J_t \nabla \cdot \mathbf{u}^G. \quad (3.5)$$

In the context of ALE formulations (3.5) is called *geometric conservation law* (GCL). A less illustrative and more mathematical derivation of this equation is given in appendix A.1.

Material time derivative in the ALE frame of reference

In order to formulate the flow equations in the moving frame of reference $\boldsymbol{\chi}$ the material time derivative of a quantity $f(\mathbf{x}(\boldsymbol{\chi}, t), t)$ shall be expressed in the deforming reference system. Application of the chain rule yields

$$\frac{Df}{Dt} = \frac{\partial f(\boldsymbol{\chi}, t)}{\partial t} \Big|_{\mathbf{x}} + \frac{\partial f(\boldsymbol{\chi}, t)}{\partial \boldsymbol{\chi}} \frac{\partial \boldsymbol{\chi}}{\partial t} \Big|_{\mathbf{x}} = \frac{\partial f(\boldsymbol{\chi}, t)}{\partial t} \Big|_{\mathbf{x}} + \frac{\partial f(\mathbf{x}, t)}{\partial \mathbf{x}} \frac{\partial \mathbf{x}}{\partial \boldsymbol{\chi}} \frac{\partial \boldsymbol{\chi}}{\partial t} \Big|_{\mathbf{x}}. \quad (3.6)$$

The material time derivative of the spatial coordinate \mathbf{x} , i.e. the temporal change of the spatial position of a material point is the velocity \mathbf{u} . Expressing this derivative according to (3.6) in the moving frame of reference reads

$$\mathbf{u} = \frac{D\mathbf{x}}{Dt} = \frac{\partial \mathbf{x}(\boldsymbol{\chi}, t)}{\partial t} \Big|_{\mathbf{x}} + \frac{\partial \mathbf{x}(\boldsymbol{\chi}, t)}{\partial \boldsymbol{\chi}} \frac{\partial \boldsymbol{\chi}}{\partial t} \Big|_{\mathbf{x}}, \quad (3.7)$$

where the temporal change of the spatial position of a reference point $\partial \mathbf{x}(\boldsymbol{\chi}, t)/\partial t|_{\boldsymbol{\chi}}$ can be identified with the velocity of the reference system \mathbf{u}^G . Inserting (3.7) into (3.6) yields the ALE expression of the material time derivative of a function f

$$\frac{Df}{Dt} = \left. \frac{\partial f(\boldsymbol{\chi}, t)}{\partial t} \right|_{\boldsymbol{\chi}} + (\mathbf{u} - \mathbf{u}^G) \cdot \nabla f. \quad (3.8)$$

Equation (3.8) also termed *fundamental ALE equation* allows to express the material time derivative of a quantity f as a temporal change of f in the reference system and a convective term accounting for the relative motion of this system. As a special case of (3.8) the material time derivative in EULERian coordinates (2.28) is recovered by setting $\boldsymbol{\chi} = \mathbf{x}$ which implies $\mathbf{u}^G = \mathbf{0}$.

3.2.2 Convective formulation

By means of the fundamental ALE equation (3.8) an ALE formulation of the momentum balance equation (2.37) is easily obtained reading

$$\left. \frac{\partial \mathbf{u}}{\partial t} \right|_{\boldsymbol{\chi}} + (\mathbf{u} - \mathbf{u}^G) \cdot \nabla \mathbf{u} - 2\nu \nabla \cdot \boldsymbol{\varepsilon}(\mathbf{u}) + \nabla p = \mathbf{b}^F \quad \text{in } \Omega_F \times T. \quad (3.9)$$

In (3.9) the EULERian material time derivative has been replaced by the fundamental ALE equation employed on the velocity field \mathbf{u} .

The convective formulation in the EULERian or ALE form is commonly used as a base for spatial discretisation by means of finite elements (as for example in [103, 107, 109, 227]). It is also the preferred version within the present work. Equation (3.9) is frequently termed non-conservative ALE formulation.

Remark 3.2.1 All spatial derivatives occurring in (3.9) refer to the EULERian system \mathbf{x} while only the time derivative has been transferred to the moving frame of reference $\boldsymbol{\chi}$. Consequently the continuity equation (2.35) remains unchanged and applies to the moving domain formulation as well.

3.2.3 Divergence formulation

Analogous to the EULERian formulation (2.38) a divergence or conservative form of (3.9) can be obtained. To serve this purpose the convective term in (3.9) is reformulated

$$(\mathbf{u} - \mathbf{u}^G) \cdot \nabla \mathbf{u} = \nabla \cdot ((\mathbf{u} - \mathbf{u}^G) \otimes \mathbf{u}) + \mathbf{u} \nabla \cdot \mathbf{u}^G, \quad (3.10)$$

where the continuity equation $\nabla \cdot \mathbf{u} = 0$ has been used. Employing (3.10) and (3.5) a divergence form of the ALE formulation is recovered.

$$\left. \frac{\partial (J_t \mathbf{u})}{\partial t} \right|_{\boldsymbol{\chi}} + J_t \nabla \cdot ((\mathbf{u} - \mathbf{u}^G) \otimes \mathbf{u} - 2\nu \boldsymbol{\varepsilon}(\mathbf{u}) + \mathbf{I}p) = J_t \mathbf{b}^F \quad \text{in } \Omega_F^0 \times T \quad (3.11)$$

On a deforming domain the convective and the divergence form of the momentum balance equation (or indeed of every conservation law) differ not only in the appearance of the convective term but also the time derivative. This has a significant impact on the discrete versions of the respective equations.

Remark 3.2.2 Alternatively to using the fundamental ALE equation (3.8) the convective and divergence ALE formulation of a conservation law can also be derived from integral forms as it has been done for example in [86].

3.3 Discretisation

The flow equations are discretised in a sequential manner, i.e. discretisation in space and time are performed (at least to some extent) independently and by different methods. This allows to employ the finite element method for the spatial discretisation and to use a finite difference method in time. An alternative to this approach provide space-time elements allowing to simultaneously discretise all dimensions by a finite element concept. This approach pursued among others by the group of TEZDUYAR (see e.g. [213, 218] or [221, 224] for more recent applications). A space-time formulation for moving domain problems has also been proposed by MASUD and HUGHES in [176] where a discontinuous GALERKIN method based on the physical entropy variables is used. The main disadvantage of space-time formulations is the significantly increased size of the resulting equation systems. In particular when higher order accuracy in time is desired sequential discretisation is preferred.

With respect to the stabilised finite element flow formulation introduced in chapter 4 the time discretisation is performed prior to the discretisation in space. In contrast to the usual sequential discretisation in space and subsequently in time, i.e. the method of lines, this approach is also termed *horizontal method of lines* or ROTHE method inspired by an article of ROTHE in 1930 [204].

3.3.1 Discretisation in time

Introduction

With respect to time the incompressible NAVIER-STOKES equations (3.9) and (2.35) pose a coupled problem composed of a partial differential equation and the constraint of the incompressibility. Anticipating discretisation in space one notes that the discrete NAVIER-STOKES equations yield a differential-algebraic problem. Thus the incompressible NAVIER-STOKES equations might be regarded as infinitely stiff partial differential equation. A rough definition of stiffness of ordinary differential equations (ODE) in time is the presence of a very large range of characteristic time scales. And indeed without specifically determining the largest time scale one can easily observe that the incompressibility condition introducing an infinite speed of sound also introduces an infinitely small time scale.

Relaxation of the incompressibility condition will be introduced by using a stabilised finite element method for spatial discretisation. Thus eventually the resulting discrete equations will be of large but finite stiffness.

Time integration of stiff problems requires implicit methods. For the present problem where the stiffness is related to the incompressibility implicit methods have to be used at least to integrate the pressure field. Explicit methods would demand a step size able to resolve the dynamics of the smallest occurring time scale. Therefore such methods show

tremendously inefficient on stiff problems. However not only efficiency but also stability requirements limit the possible time discretisation methods for stiff problems [112].

The method of choice to discretise the incompressible NAVIER-STOKES equations in time therefore has to be stiffly stable at least. (See GEAR [98] for a definition of stiff stability.) A subset of stiffly stable methods are A-stable. Applying an A-stable method to the linear ODE

$$\dot{y}(t) = -\lambda y(t) \quad \lambda \in \mathbb{C}, \quad \text{Re}(\lambda) < 0 \quad (3.12)$$

yields $\lim_{n \rightarrow \infty} y^n = 0$ independent of the fixed time step size Δt . DAHLQUIST's test equation (3.12) can be regarded a model of an advective-diffusive equation where the real part of λ represents the diffusive effect and the imaginary contribution models advective transport. Consult GRESHO and SANI [107] for an explanation of this analogy.

The time discretisation schemes employed within this work are further limited by a theorem known by the name *second DAHLQUIST barrier* which states that an A-stable multistep method does not exceed order two. It further says that the most accurate second order A-stable scheme is the well known trapezoidal rule. For a detailed discussion of stiffness and stable numerical step methods the reader is referred to the book by HAIRER and WANNER [112].

The present work thus aims at a second order accurate time discretisation of the incompressible NAVIER-STOKES equations on a deforming domain which is (at least conditionally) stable. An analysis comparing temporal discretisation schemes for the particular use to integrate the stabilised FEM of the NAVIER-STOKES equations can be found in DETTMER and PERIĆ [62].

One-step- θ

The one-step- θ method is one of the integration schemes considered within this work. Applied on the general first order ODE $\dot{y} = f(y, t)$ one-step θ time integration yields

$$\frac{y^{n+1} - y^n}{\Delta t} = \theta f(y^{n+1}, t^{n+1}) + (1 - \theta) f(y^n, t^n), \quad (3.13)$$

where Δt denotes the time step size. The method is A-stable if $1/2 \leq \theta \leq 1$ and contains the special cases of backward EULER (BE) time discretisation at $\theta = 1$ and the trapezoidal rule (TR) for $\theta = 1/2$. The TR is a second order accurate scheme while a deviation from $\theta = 1/2$ yields a method which is just first order accurate. Another advantage of the TR is that it is free of spurious damping. It is thus the method of choice for long time simulations. However the lack of numerical damping frequently results in a tendency to spurious oscillations caused by unresolved transients or initial inaccuracy. As the numerical stability of (3.13) increases with increasing parameter θ a slight shift of θ towards a higher value frequently cures the oscillations but sacrifices second order accuracy.

Second order backward differencing

The second order representative of the backward differentiation formulae (BDF2) applied to the general first order ODE $\dot{y} = f(y, t)$ reads

$$\frac{y^{n+1} - y^n}{\Delta t} = \frac{1}{3} \frac{y^n - y^{n-1}}{\Delta t} + \frac{2}{3} f(y^{n+1}, t^{n+1}). \quad (3.14)$$

The method combines second order accuracy and some numerical dissipation. It thus guarantees that errors are always damped. BDF2 is A-stable (or more precisely even L-stable see [112]). A disadvantage of BDF2 is its need for a starting algorithm.

The method has been preferred within this work for its robustness and accuracy.

Time discretisation of the convective form

The temporally discretised equation is cast into a unified concept. Applying (3.13) and (3.14) to the convective form of the ALE momentum balance (3.9) and the continuity equation yields

$$\mathbf{u}^{n+1} + \delta [(\mathbf{u}^{n+1} - \mathbf{u}^{G,n+1}) \cdot \nabla \mathbf{u}^{n+1} - 2\nu \nabla \cdot \boldsymbol{\varepsilon}(\mathbf{u}^{n+1}) + \nabla p^{n+1}] = \mathbf{r}^{n+1} \quad \text{in } \Omega_{\text{F}}^{n+1}, \quad (3.15)$$

$$\delta \nabla \cdot \mathbf{u}^{n+1} = 0 \quad \text{in } \Omega_{\text{F}}^{n+1}, \quad (3.16)$$

where δ represents a scalar depending on the discretisation scheme:

$$\delta_{\theta} = \theta \Delta t, \quad \delta_{\text{BDF2}} = \frac{2}{3} \Delta t. \quad (3.17)$$

The vector valued function \mathbf{r} contains history terms of the velocity and depends on the time integration scheme. Possible body forces \mathbf{f} are also included in \mathbf{r} according to

$$\mathbf{r}_{\theta}^{n+1} = \delta_{\theta} \mathbf{b}^{\text{F},n+1} + (1 - \theta) \Delta t \dot{\mathbf{u}}^n + \mathbf{u}^n \quad \mathbf{r}_{\text{BDF2}}^{n+1} = \delta_{\text{BDF2}} \mathbf{b}^{\text{F},n+1} + \frac{4}{3} \mathbf{u}^n - \frac{1}{3} \mathbf{u}^{n-1}.$$

Equation (3.15) can be interpreted as a differential equation in space which refers to a different domain in every time step.

Remark 3.3.1 The time parameter δ introduced in (3.16) does not emerge from temporal discretisation. It is rather introduced to scale the continuity equation for better conditioning of the resulting effective fluid coefficient matrix and to preserve the last bit of symmetry of the mixed formulation.

Time discretisation of the divergence form

Time integration of the divergence ALE form (3.11) requires to discretise the temporal change of the product $J_t \mathbf{u}$ yielding

$$J^{n+1} \mathbf{u}^{n+1} + \delta J^{n+1} \nabla \cdot ((\mathbf{u}^{n+1} - \mathbf{u}^{\text{G},n+1}) \otimes \mathbf{u}^{n+1} - 2\nu \boldsymbol{\varepsilon}(\mathbf{u}^{n+1}) + \mathbf{I} p^{n+1}) = \mathbf{r}_{\text{d}}^{n+1} \quad \text{in } \Omega_{\text{F}}^0, \quad (3.18)$$

$$\delta J^{n+1} \nabla \cdot \mathbf{u}^{n+1} = 0 \quad \text{in } \Omega_{\text{F}}^0,$$

where the above definition of the parameter δ applies. However the right hand side contribution significantly differs from the one obtained for the convective formulation. It now reads

$$\mathbf{r}_{\text{d},\theta}^{n+1} = \delta_{\theta} J^{n+1} \mathbf{b}^{\text{F},n+1} + J^n \mathbf{u}^n + \Delta t (1 - \theta) \overline{(\dot{J}\mathbf{u})}^n \quad (3.19)$$

and

$$\mathbf{r}_{\text{d},\text{BDF2}}^{n+1} = \delta_{\text{BDF2}} J^{n+1} \mathbf{b}^{\text{F},n+1} + \frac{4}{3} J^n \mathbf{u}^n - \frac{1}{3} J^{n-1} \mathbf{u}^{n-1} \quad (3.20)$$

for one-step- θ and BDF2, respectively, including terms that refer to previous positions of the reference system. Compared to the convective ALE equation this results in a slightly increased effort as previous node positions have to be tracked.

Remark 3.3.2 The subscript ‘d’ is used here and subsequently to denote symbols that refer to the divergence formulation and differ from the respective term of the convective form.

3.3.2 Discretisation in space

Spatial discretisation by means of finite elements is introduced here in order to discuss the conservation properties of the convective and divergence ALE formulation on the fully discretised equations. With this in mind the GALERKIN weak form is considered in this section. Additional stabilisation terms which complete the spatial discretisation will be regarded in chapter 4. Suffice it here to assure that the instabilities requiring stabilisation terms are (at least to some extent) independent of the fundamental conservation properties of the equations and the potential loss of stability due to mesh motion.

Finite element discretisation is covered subsequently to the extent required for the present work. A presentation of the details and problems encountered on the way of using finite elements for flow problems can be found in the exhaustive monograph by GRESHO and SANI [107] which has already been mentioned several times. The book by DONEA and HUERTA [69] also covers the subject including ALE formulations. Further the third volume of the classic books on FEM by ZIENKIEWICZ and TAYLOR [237] should be mentioned along the engineering books on the subject. A more mathematical view on the FEM for incompressible flows can be found in the book by GUNZBURGER [109] or also the volume by GIRAULT and RAVIART [102].

Spatial discretisation of convective form

In order to discretise the semi-discrete convective ALE equation (3.15) in space the domain Ω_{F} is divided into non-overlapping patches, the elements. The spatial discretisation maintains its topology while following the deformation of the domain. The reference domain Ω_{F}^0 is then associated with the elemental parameter spaces, such that J_t is identified with the elemental JACOBIAN determinant.

To define the discrete GALERKIN form the finite element spaces $\mathbf{V}_{\text{F},0}^h \subset \mathbf{H}_0^1(\Omega_{\text{F}})$ and $\mathbf{V}_{\text{F}}^h \subset \mathbf{H}^1(\Omega_{\text{F}})$ are selected, where \mathbf{V}_{F}^h satisfies the time dependent DIRICHLET boundary

conditions of the problem while all functions in $\mathbf{V}_{F,0}^h$ are zero on $\Gamma_{F,D}$. The pressure is taken from the space $P^h \subset L^2(\Omega_F)$ of square integrable functions.

The discrete variational statement then reads: seek the solution at $\mathbf{u} \in \mathbf{V}_{F,n+1}^h$, $p \in P_{n+1}^h$ at the new time level $n + 1$ such that

$$B_{\text{gal}}(\{\mathbf{u}, p\}, \{\mathbf{v}, q\}) = (\mathbf{r}^{n+1}, \mathbf{v})_{\Omega_F^{n+1}} + \delta (\mathbf{h}^{n+1}, \mathbf{v})_{\Gamma_{F,N}^{n+1}} \quad \text{for all } (\mathbf{v}, q) \in (\mathbf{V}_{F,0,n+1}^h, P_{n+1}^h), \quad (3.21)$$

where the discrete operator in convective form $B_{\text{gal}}(\{\mathbf{u}, p\}, \{\mathbf{v}, q\})$ is given by

$$\begin{aligned} B_{\text{gal}}(\{\mathbf{u}, p\}, \{\mathbf{v}, q\}) &= (\mathbf{u}, \mathbf{v})_{\Omega_F^{n+1}} + (\delta (\mathbf{u} - \mathbf{u}^{G,n+1}) \cdot \nabla \mathbf{u}, \mathbf{v})_{\Omega_F^{n+1}} + (\delta 2\nu \boldsymbol{\varepsilon}(\mathbf{u}), \boldsymbol{\varepsilon}(\mathbf{v}))_{\Omega_F^{n+1}} \\ &\quad - (\delta p, \nabla \cdot \mathbf{v})_{\Omega_F^{n+1}} - (\delta \nabla \cdot \mathbf{u}, \beta q)_{\Omega_F^{n+1}}. \end{aligned} \quad (3.22)$$

It is pointed out that the superscript $n+1$ is dropped at the unknown velocity and pressure field at the new time level for clarity of the presentation. The parameter $\beta \in \{-1, 1\}$ carries the sign of the pressure test function q . This parameter is introduced here with respect to the general stabilised formulation that shall be considered in chapter 4.

From (3.21) and (3.22) it can be observed that all inner products refer to the actual time instant, i.e. the time discretisation of the convective ALE formulation does not interfere with the temporal mesh evolution.

Discrete flow equations in matrix notation

Denoting the vectors of unknown nodal velocity values by \mathbf{u} and the corresponding nodal pressure values by \mathbf{p} , i.e. bold face non-serif upright letters which are generally used here for discrete matrices and vectors, the fluid system of equations can conveniently be cast into matrix form reading

$$\mathbf{M}^F \mathbf{u} + \delta \mathbf{N}(\mathbf{u}) + \delta \mathbf{K}^F \mathbf{u} + \delta \mathbf{G} \mathbf{p} = \mathbf{f}_b^F + \mathbf{f}_h^F \quad (3.23)$$

$$\delta \mathbf{G}^T \mathbf{u} = \mathbf{0}, \quad (3.24)$$

where fluid mass matrix is obtained from the bilinear form

$$\mathbf{v}^T \mathbf{M}^F \mathbf{u} = (\mathbf{u}, \mathbf{v})_{\Omega_F^{n+1}}.$$

The fluid ‘stiffness’ is derived from the discrete nonlinear convective term reading

$$\mathbf{v}^T \mathbf{N}(\mathbf{u}) = ((\mathbf{u} - \mathbf{u}^{G,n+1}) \cdot \nabla \mathbf{u}, \mathbf{v})_{\Omega_F^{n+1}}$$

and a symmetric positive definite matrix stemming from the viscous term

$$\mathbf{v}^T \mathbf{K}^F \mathbf{u} = (2\nu \boldsymbol{\varepsilon}(\mathbf{u}), \boldsymbol{\varepsilon}(\mathbf{v}))_{\Omega_F^{n+1}}.$$

The discrete gradient operator is obtained from

$$\mathbf{v}^T \mathbf{G} \mathbf{p} = -(p, \nabla \cdot \mathbf{v})_{\Omega_F^{n+1}}$$

while the discrete divergence operator is given by

$$\mathbf{q}^T \mathbf{G}^T \mathbf{u} = -\beta (\nabla \cdot \mathbf{u}, q)_{\Omega_{\mathbb{F}}^{n+1}}.$$

The vector $\mathbf{f}_b^{\mathbb{F}}$ collects the right hand side terms from history values and body forces

$$\mathbf{v}^T \mathbf{f}_b^{\mathbb{F}} = (\mathbf{r}^{n+1}, \mathbf{v})_{\Omega_{\mathbb{F}}^{n+1}}$$

while $\mathbf{f}_h^{\mathbb{F}}$ represents tractions

$$\mathbf{v}^T \mathbf{f}_h^{\mathbb{F}} = (\mathbf{h}^{n+1}, \mathbf{v})_{\Gamma_{\mathbb{F},N}^{n+1}}.$$

On deforming domains all coefficient matrices are time dependent.

Spatial discretisation of divergence form

A spatial discretisation of the divergence formulation (3.18) depends upon the particular time discretisation scheme. In the case of one-step- θ it reads: find the velocity and pressure $\mathbf{u} \in \mathbf{V}_{\mathbb{F},n+1}^h$, $p \in P_{n+1}^h$ at the new time instant $n+1$ such that

$$\begin{aligned} B_{\text{gal,d}}(\{\mathbf{u}, p\}, \{\mathbf{v}, q\}) &= (\delta \mathbf{b}^{\mathbb{F},n+1}, \mathbf{v})_{\Omega_{\mathbb{F}}^{n+1}} + (\mathbf{u}^n, \mathbf{v})_{\Omega_{\mathbb{F}}^n} + \left(\Delta t (1-\theta) \overline{(\mathbf{J}\mathbf{u})}^n, \mathbf{v} \right)_{\Omega_{\mathbb{F}}^0} \\ &+ (\delta \mathbf{h}_d^{n+1}, \mathbf{v})_{\Gamma_{\mathbb{F},N}^{n+1}} \quad \text{for all } (\mathbf{v}, q) \in (\mathbf{V}_{\mathbb{F},0}^h \subset \mathbf{H}_0^1(\Omega_{\mathbb{F}}^0), P^h \subset L^2(\Omega_{\mathbb{F}}^0)). \end{aligned} \quad (3.25)$$

After time discretisation by BDF2 the GALERKIN weak formulation reads: seek $\mathbf{u} \in \mathbf{V}_{\mathbb{F},n+1}^h$, $p \in P_{n+1}^h$ such that

$$\begin{aligned} B_{\text{gal,d}}(\{\mathbf{u}, p\}, \{\mathbf{v}, q\}) &= (\delta \mathbf{b}^{\mathbb{F},n+1}, \mathbf{v})_{\Omega_{\mathbb{F}}^{n+1}} + \frac{4}{3} (\mathbf{u}^n, \mathbf{v})_{\Omega_{\mathbb{F}}^n} - \frac{1}{3} (\mathbf{u}^{n-1}, \mathbf{v})_{\Omega_{\mathbb{F}}^{n-1}} \\ &+ (\delta \mathbf{h}_d^{n+1}, \mathbf{v})_{\Gamma_{\mathbb{F},N}^{n+1}} \quad \text{for all } (\mathbf{v}, q) \in (\mathbf{V}_{\mathbb{F},0}^h \subset \mathbf{H}_0^1(\Omega_{\mathbb{F}}^0), P^h \subset L^2(\Omega_{\mathbb{F}}^0)). \end{aligned} \quad (3.26)$$

In both cases the weighting functions for velocity and pressure are defined with respect to the reference system, i.e. on the elemental parameter spaces and integrated over domains referring to different time levels. The discrete operator in the divergence form is given by

$$\begin{aligned} B_{\text{gal,d}}(\{\mathbf{u}, p\}, \{\mathbf{v}, q\}) &= (\mathbf{u}, \mathbf{v})_{\Omega_{\mathbb{F}}^{n+1}} - (\nabla \cdot \mathbf{u}, q)_{\Omega_{\mathbb{F}}^{n+1}} \\ &+ \delta \left(-(\mathbf{u} - \mathbf{u}^{\text{G},n+1}) \otimes \mathbf{u} + 2\nu \boldsymbol{\varepsilon}(\mathbf{u}) - \mathbf{I}p^{n+1}, \nabla \mathbf{v} \right)_{\Omega_{\mathbb{F}}^{n+1}} \end{aligned} \quad (3.27)$$

applying to either of the above cases.

Remark 3.3.3 In the divergence or conservative form (3.27) the integration by parts refers to the total momentum flux including the convective one. Thus the corresponding NEUMANN boundary condition is

$$\mathbf{h}_d^{n+1} = \mathbf{n} \cdot (\boldsymbol{\sigma} - (\mathbf{u}^{n+1} - \mathbf{u}^{\text{G},n+1}) \otimes \mathbf{u}^{n+1}) = \mathbf{h}^{n+1} - \mathbf{n} \cdot (\mathbf{u}^{n+1} - \mathbf{u}^{\text{G},n+1}) \otimes \mathbf{u}^{n+1}. \quad (3.28)$$

On boundaries with a local LAGRANGEan formulation, i.e. $\mathbf{u} = \mathbf{u}^G$ or where the velocity vector is tangential to the boundary the total momentum flux equals the traction force vector \mathbf{h} . Alternatively to (3.27) it is possible to use a weak formulation of the divergence form where the integration by parts exclusively refers to the viscous and pressure term as it is not strictly necessary to integrate the convective term by parts. If such an approach is followed the NEUMANN boundary condition is not altered.

Remark 3.3.4 The weighted residual of the divergence ALE formulation (3.25) or (3.26) can also be used to derive a finite volume method by choosing \mathbf{v} to be element wise constant. In such a case the second line in (3.27) vanishes and it remains to balance the total fluxes \mathbf{h}_d^{n+1} over the boundaries of the control volumes.

3.4 Conservation laws on deforming domains

It is worthwhile to open the discussion of conservation with the words of HUGHES and coauthors [137]: “*Let us take the point of view here that local conservation is at least desirable, possibly helpful, and certainly not harmful.*” indicating that discrete conservation is not unconditionally mandatory. While the stated sentence refers to the conserved quantity which is actually discretised, i.e. in the present case to the conservation of linear momentum, it is of interest to simultaneously have a look at the various other conservation laws which are met on the way of discretising the flow equations on a deforming domain.

The matter of conservation properties of discrete equations arises when discrete representations of conservation laws are considered. In general such a law governing the temporal evolution of a quantity f can be written as

$$\frac{\partial f}{\partial t} + \nabla \cdot \mathbf{F} = s \quad (3.29)$$

or more obviously

$$\frac{\partial}{\partial t} \int_{v_c} f \, dv_c + \int_{\partial v_c} \mathbf{n} \cdot \mathbf{F} \, d\partial v_c = \int_{v_c} s \, dv_c \quad (3.30)$$

stating that *the temporal change of f inside the fixed control volume v_c is balanced by a source term s and the fluxes \mathbf{F} passing the control volume boundary.*

It is easy to observe that the divergence formulation of the momentum balance in EULERian formulation (2.38) as well as its ALE version (3.11) pose special cases of conservation laws of the type (3.29). Further conservation laws which have been touched so far are the energy conservation within the fluid (2.42), the geometric conservation law (3.5) and the conservation of mass (2.35) equation. The latter posing a special case neither containing a temporal change of the conserved quality nor source terms.

Clearly the structural momentum balance equation (2.12) is another conservation law even if rarely called so. Structural engineers are used to prefer the idea of force equilibrium rather than conservation of linear momentum in the above sense.

3.4.1 Conservation of linear momentum

As the divergence formulation of the flow balance appears in the form (3.29) it is frequently termed *conservative* formulation while the convective form is called *non-conservative* (see e.g. FORMAGGIA and NOBILE [83, 84]). The rigorous equality of the two is lost as soon as the continuity equation is approximated rather than strictly satisfied.

Using a conservative instead of a non-conservative formulation of the respective equations for discretisation ensures that the conservation property of the quantity of interest is carried over to the discrete version. For equation (3.11) this means that the temporal change of linear momentum within one element is balanced by the elemental body forces and the total momentum fluxes \mathbf{h}_d across the element boundaries. This conservation property cannot directly be observed any more when the convective formulation (3.9) is discretised which suggests the idea of force balance at a time instant rather than conservation of a quantity over time. However, it is worth noting that *conservation* does not necessarily imply *accuracy* (even if it evidently does not contradict it either). Quoting HUGHES again one may even state that “*advective forms are often preferred on grounds of accuracy despite violation of conservation*” [144].

There are two main reasons to prefer the conservative form of the equations. The first one is the intention to use a finite volume method which relies on a divergence expression. The second reason is the desire to simulate problems with shock discontinuities which may be present for high speed compressible flow (see ZIENKIEWICZ et al. [237]).

As neither of the reasons is apparent for the present work the convective formulation is used preferably here. Nevertheless some properties of divergence formulations of ALE schemes shall also be considered in the sequel.

Remark 3.4.1 Using the divergence formulation (3.11) implies discrete conservation of linear momentum in an integral sense. It yields, however, neither energy nor geometric conservation on the same control volume. Both conservation laws are spoiled by discretisation errors. Thus the more neutral terms *divergence formulation* and *convective formulation* rather than *conservative scheme* and *non-conservative scheme* are preferred within this work.

Remark 3.4.2 Returning to the initially cited paper by HUGHES et al. another aspect has to be mentioned when conservation is considered. Continuous GALERKIN methods are frequently accused of not being locally conservative irrespective of the form of the discretised equations. HUGHES and coauthors [137] clarify this issue demonstrating that local conservation is well achieved by continuous GALERKIN approximations if the conservative fluxes are deduced from the consistent nodal forces.

3.4.2 Geometric conservation

Geometric conservation poses a difficulty particularly when the divergence ALE formulation (3.11) is applied. The matter of geometric conservation is not restricted to incompressible flow but arises also when compressible flow problems on moving domains are investigated. Consequently the need for geometric conservation was pointed out first by THOMAS and LOMBARD [223] in 1979 who solved the GCL numerically along with the

flow equations using difference operators. In the sequel the GCL was discussed in relation with the accuracy of finite volume or finite difference methods by FARHAT et al. [108, 161].

A desirable property of a numerical scheme is that it is able to predict exactly a constant flow. LESOINNE and FARHAT showed that this condition is satisfied if the scheme under consideration satisfies a discrete version of the GCL [167]. Discrete geometric conservations laws (DGCL) for finite volume schemes were suspected to be necessary for the stability of the overall scheme [75, 76, 73] while it was also shown that it is neither necessary nor sufficient to guarantee that the discrete scheme on a moving domain preserves the order of accuracy in time of the respective fixed grid version [101]. BOFFI and GASTALDI proved that the GCL is neither necessary nor sufficient for stability [25].

Nevertheless it remains desirable to satisfy geometric conservation at least for incompressible flow where it is closely related to mass conservation.

The GCL can be satisfied in different ways. Using a convective ALE formulation of the flow equations intrinsically satisfies (3.5) exactly as shown for example in [86]. When a divergence formulation is employed the GCL can either be stated as a separate equation to be solved e.g. as in [72, 223] or a discrete GCL can be used to determine some free time integration parameters subsequent to temporal discretisation as done in [75, 101].

Subsequently the geometric conservation properties of the discrete schemes (3.22) and (3.27) are considered by testing the requirement that a constant solution has to be reproduced exactly.

Convective formulation

To show that geometric conservation is assured in the discrete convective form a spatial and temporal constant solution $\bar{\mathbf{u}}$ is inserted into the discrete equation (3.21). A uniform velocity field is accompanied by a pressure field that carries the body forces and surface tractions. Thus depending on the time discretisation scheme this yields

$$(\bar{\mathbf{u}}, \mathbf{v})_{\Omega_{\mathbb{F}}^{n+1}} = (\bar{\mathbf{u}}, \mathbf{v})_{\Omega_{\mathbb{F}}^{n+1}} \quad \text{and} \quad (\bar{\mathbf{u}}, \mathbf{v})_{\Omega_{\mathbb{F}}^{n+1}} = \left(\frac{4}{3}\bar{\mathbf{u}}, \mathbf{v}\right)_{\Omega_{\mathbb{F}}^{n+1}} - \left(\frac{1}{3}\bar{\mathbf{u}}, \mathbf{v}\right)_{\Omega_{\mathbb{F}}^{n+1}} \quad (3.31)$$

for one-step θ and BDF2, respectively. Consequently geometric conservation reduces to the demand that at least all mass like terms in (3.22) have to be integrated over the same domain $\Omega_{\mathbb{F}}$, i.e. at the same instant in time. This condition is met by the discrete formulation (3.21).

The convective ALE formulation is inherently geometrically conservative irrespective of the employed time discretisation scheme. Interestingly geometric conservation is satisfied independent of the mesh velocity which does not occur in (3.31). Nevertheless the determination of \mathbf{u}^G has a significant impact on the order of accuracy of the overall scheme.

Determination of the mesh velocity

The mesh motion is governed by the first order ODE

$$\left. \frac{\partial \mathbf{x}}{\partial t} \right|_{\mathbf{x}} = \mathbf{u}^G \quad (3.32)$$

which is a vector equation including the information of the scalar geometric conservation law (3.5). It has to be remarked here that in the derivation of the GCL 3.5 the definition of the mesh velocity (3.32) has already been utilised. Within numerical FSI schemes the new position of the mesh \mathbf{x}^{n+1} is determined by a mesh motion algorithm and thus treated as known here. Hence (3.32) can be discretised in time yielding

$$\mathbf{u}^{\text{G},n+1} = \frac{\mathbf{x}^{n+1} - \mathbf{x}^n}{\theta \Delta t} - \frac{1 - \theta}{\theta} \mathbf{u}^{\text{G},n} \quad \text{and} \quad \mathbf{u}^{\text{G},n+1} = \frac{3\mathbf{x}^{n+1} - 4\mathbf{x}^n + \mathbf{x}^{n-1}}{2\Delta t} \quad (3.33)$$

for one-step θ and BDF2, respectively. Setting $\theta = 1$ in the first equation of (3.33) recovers the popular step wise constant mesh velocity

$$\mathbf{u}^{\text{G},n+1} = \frac{\mathbf{x}^{n+1} - \mathbf{x}^n}{\Delta t}$$

as backward EULER time discretisation of the mesh motion ODE (3.32). Both ways of discretising (3.32) in time satisfy the geometric conservation condition (3.5).

However care has to be taken if a temporally second order discretisation of the fluid velocity is desired. In this case the mesh motion equation has to be integrated at least second order accurately. An analysis of the local truncation error indicates that it should be possible to use the trapezoidal rule ($\theta = 1/2$) for the mesh movement while using BDF2 for the solution of the Navier-Stokes equations and still obtain second order convergence. This is indeed the case, however, the trapezoidal rule tends to introduce oscillations into the scheme. Therefore the second equation of (3.33) is used here for second order accurate schemes to obtain the new mesh velocity $\mathbf{u}^{\text{G},n+1}$.

Subsequently a numerical investigation confirming the accuracy observations is reported.

Remark 3.4.3 It is not necessary to use the same time integration scheme for the mesh velocity that is used for the momentum balance. Any other implicit multistep method can also be chosen provided it offers the desired accuracy.

Numerical accuracy check for convective ALE formulation

In order to show that second order accuracy in time can be obtained from the discrete convective formulation (3.22) a numerical example is investigated. The problem is the well known driven cavity flow where the parameters used here are given in figure 3.2. The cavity occupies the unit square and the horizontal flow in x -direction prescribed on the top is parabolic in space and follows sinusoidal function in time according to $u_x(x, t) = 4(x - x^2) \sin(\pi/4 t)$. Nine-noded quadratic elements in space are used. To investigate a moving mesh, the horizontal mesh middle line as indicated in figure 3.2 is moved vertically following $y_m(t) = 0.35 \sin(\pi/2 t)$. The convergence of the horizontal reaction force F_x at the top of the cavity at time $t = 1.0$ is investigated for different temporal discretisations of the mesh velocity \mathbf{u}^{G} .

For both lines in figure 3.3 the overall time stepping scheme has been BDF2. The figure confirms that using constant mesh velocities within the single time steps effectively sacrifices one order of temporal accuracy. Using a second order accurate scheme to obtain the new grid velocity restores the overall temporal convergence to second order on moving meshes without introducing extra effort.

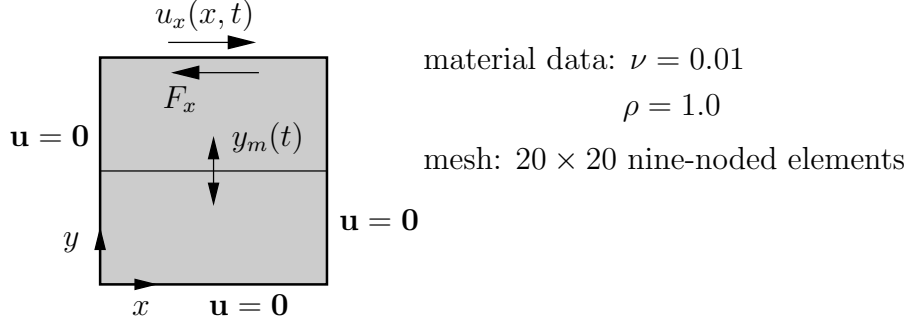


Figure 3.2: Driven cavity flow example - problem description

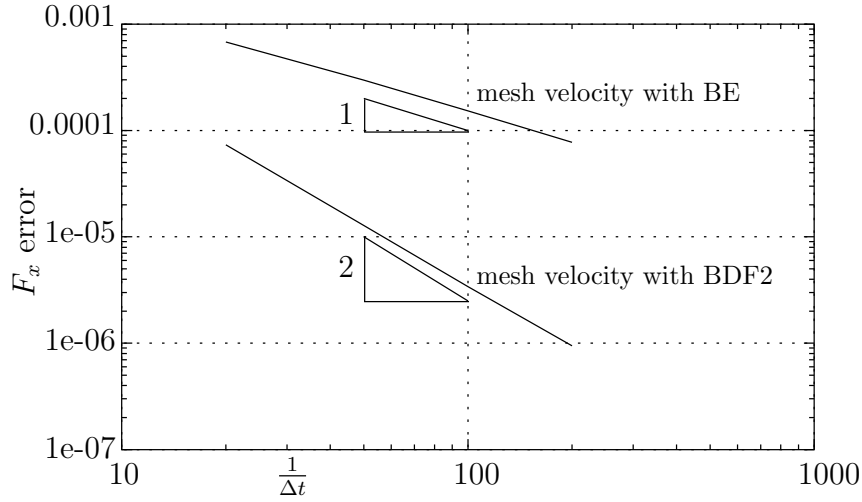


Figure 3.3: Error in horizontal reaction force

Divergence formulation

To find the inherent geometric conservation properties of the divergence formulation of the ALE equations a spatially and temporally constant solution $\bar{\mathbf{u}}$ is inserted into the discrete equation (3.25), i.e. the one-step- θ case is considered. As all spatial velocity gradients vanish one obtains

$$\begin{aligned}
 (\bar{\mathbf{u}}, \mathbf{v})_{\Omega_{\mathbb{F}}^{n+1}} - \theta \Delta t \left((\bar{\mathbf{u}} - \mathbf{u}^{\text{G},n+1}) \otimes \bar{\mathbf{u}}, \nabla \mathbf{v} \right)_{\Omega_{\mathbb{F}}^{n+1}} &= (\bar{\mathbf{u}}, \mathbf{v})_{\Omega_{\mathbb{F}}^n} + \left(\Delta t (1 - \theta) j^n \bar{\mathbf{u}}, \mathbf{v} \right)_{\Omega_{\mathbb{F}}^0} \\
 &\quad + \left(\Delta t (\mathbf{h}_d^{n+1} - \mathbf{h}^{n+1}), \mathbf{v} \right)_{\Gamma_{\mathbb{F},\mathbb{N}}^{n+1}}, \quad (3.34)
 \end{aligned}$$

where the pressure field balances the body forces and tractions. To simplify (3.34) further the convective flux term is integrated by parts which gives

$$\left((\bar{\mathbf{u}} - \mathbf{u}^{\text{G},n+1}) \otimes \bar{\mathbf{u}}, \nabla \mathbf{v} \right)_{\Omega_{\mathbb{F}}^{n+1}} = \left(\mathbf{n} \cdot (\bar{\mathbf{u}} - \mathbf{u}^{\text{G},n+1}) \otimes \bar{\mathbf{u}}, \mathbf{v} \right)_{\Gamma_{\mathbb{F},\mathbb{N}}^{n+1}} + \left(\nabla \cdot \mathbf{u}^{\text{G},n+1} \bar{\mathbf{u}}, \mathbf{v} \right)_{\Omega_{\mathbb{F}}^{n+1}}, \quad (3.35)$$

where the fact that $\bar{\mathbf{u}}$ is constant in space has been used. Inserting (3.35) back into the weak formulation (3.34) the boundary terms cancel due to (3.28) and the weak form

$$(\bar{\mathbf{u}}, \mathbf{v})_{\Omega_{\mathbb{F}}^{n+1}} - \theta \Delta t (\nabla \cdot \mathbf{u}^{\mathbb{G}, n+1} \bar{\mathbf{u}}, \mathbf{v})_{\Omega_{\mathbb{F}}^{n+1}} = (\bar{\mathbf{u}}, \mathbf{v})_{\Omega_{\mathbb{F}}^n} + \left(\Delta t (1 - \theta) j^n \bar{\mathbf{u}}, \mathbf{v} \right)_{\Omega_{\mathbb{F}}^0} \quad (3.36)$$

is obtained. For arbitrary $\bar{\mathbf{u}}$ the EULER equation of (3.36) is a discrete representation of the geometric conservation law (3.5)

$$\frac{J^{n+1} - J^n}{\Delta t} = \theta J^{n+1} \nabla \cdot \mathbf{u}^{\mathbb{G}, n+1} + (1 - \theta) j^n. \quad (3.37)$$

Equation (3.37) has to be satisfied in order to enable the discrete scheme (3.25) to reproduce an uniform velocity field exactly, i.e. to make the scheme geometrically conservative.

A similar expression can be obtained for the discrete scheme employing BDF2 time discretisation (3.26). Inserting a constant solution in (3.26) yields after some algebra

$$\frac{J^{n+1} - J^n}{\Delta t} = \frac{1}{3} \frac{J^n - J^{n-1}}{\Delta t} + \frac{2}{3} J^{n+1} \nabla \cdot \mathbf{u}^{\mathbb{G}, n+1}. \quad (3.38)$$

The discrete geometric conservation laws (3.37) and (3.38) are temporally discretised versions of the GCL (3.5) by the same scheme that has been used for the governing equations themselves. However, discretising the mesh velocity by the same scheme that has been used for the ALE formulation of the NAVIER-STOKES equations does generally not also satisfy (3.37) or (3.38) as the JACOBIAN determinant $J_t = \det(\partial \mathbf{x} / \partial \boldsymbol{\chi})$ is a nonlinear function of the current spatial position \mathbf{x} .

Discrete geometric conservation laws for temporally second order schemes and finite volume discretisations on deforming domains have been developed by FARHAT et al. e.g. in [75, 101].

3.4.3 Conservation of energy

In contrast to the EULERian setting considered in section 2.3.6 the effect of domain motion upon the energy balance equation shall be investigated here. Conservation of energy in a discrete scheme is closely linked to stability [107, 197]. Thus the energy conservation property of the discrete schemes for the incompressible NAVIER-STOKES equations is of particular interest.

To investigate the energy conservation properties of the ALE versions of the momentum balance (3.9) and (3.11) the continuous formulations are considered. The effect of the spatial discretisation is accounted for by keeping in mind that the continuity condition $\nabla \cdot \mathbf{u}$ will not be strictly valid in a discrete scheme.

The kinetic energy E_{kin} enclosed in a volume of fluid which is fixed in the reference system $\boldsymbol{\chi}$ reads

$$E_{\text{kin}} = \frac{1}{2} \rho^{\mathbb{F}} \int_{\Omega_{\mathbb{F}}} |\mathbf{u}|^2 \, d\Omega_{\mathbb{F}} = \frac{1}{2} \rho^{\mathbb{F}} \int_{\Omega_{\mathbb{F}}^0} |\mathbf{u}|^2 J_t \, d\Omega_{\mathbb{F}}^0. \quad (3.39)$$

Hence the temporal change of kinetic energy inside $\Omega_{\mathbb{F}}$ is given by

$$\left. \frac{\partial E_{\text{kin}}}{\partial t} \right|_{\boldsymbol{\chi}} = \rho^{\mathbb{F}} \int_{\Omega_{\mathbb{F}}^0} \left. \frac{\partial \mathbf{u}}{\partial t} \right|_{\boldsymbol{\chi}} \cdot \mathbf{u} J_t \, d\Omega_{\mathbb{F}}^0 + \frac{\rho^{\mathbb{F}}}{2} \int_{\Omega_{\mathbb{F}}^0} |\mathbf{u}|^2 \nabla \cdot \mathbf{u}^{\mathbb{G}} J_t \, d\Omega_{\mathbb{F}}^0, \quad (3.40)$$

where the geometric conservation law (3.5) has been used.

Convective formulation

To derive the energy conservation equation on a deforming domain the convective momentum balance is multiplied by the velocity \mathbf{u} and integrated over a domain fixed in the reference system yielding

$$\begin{aligned} \rho^F \int_{\Omega_F} \left. \frac{\partial \mathbf{u}}{\partial t} \right|_{\mathbf{x}} \cdot \mathbf{u} \, d\Omega_F + \rho^F \int_{\Omega_F} (\mathbf{u} - \mathbf{u}^G) \cdot \nabla \mathbf{u} \cdot \mathbf{u} \, d\Omega_F - \int_{\Omega_F} \nabla \cdot \boldsymbol{\sigma} \cdot \mathbf{u} \, d\Omega_F \\ = \rho^F \int_{\Omega_F} \mathbf{b}^F \cdot \mathbf{u} \, d\Omega_F. \end{aligned} \quad (3.41)$$

The convective term in (3.41) can be integrated by parts and reformulated using GAUSS'S divergence theorem

$$\begin{aligned} \int_{\Omega_F} (\mathbf{u} - \mathbf{u}^G) \cdot \nabla \mathbf{u} \cdot \mathbf{u} \, d\Omega_F = -\frac{1}{2} \int_{\Omega_F} |\mathbf{u}|^2 \nabla \cdot \mathbf{u} \, d\Omega_F + \frac{1}{2} \int_{\Omega_F} |\mathbf{u}|^2 \nabla \cdot \mathbf{u}^G \, d\Omega_F \\ + \frac{1}{2} \int_{\partial\Omega_F} |\mathbf{u}|^2 (\mathbf{u} - \mathbf{u}^G) \cdot \mathbf{n} \, d\partial\Omega_F \end{aligned}$$

Inserting this into (3.41) and reformulating the viscous term in the same way as in (2.42) yields

$$\begin{aligned} \left. \frac{\partial E_{\text{kin}}}{\partial t} \right|_{\mathbf{x}} - \frac{\rho^F}{2} \int_{\Omega_F} |\mathbf{u}|^2 \nabla \cdot \mathbf{u} \, d\Omega_F + \frac{\rho^F}{2} \int_{\partial\Omega_F} |\mathbf{u}|^2 (\mathbf{u} - \mathbf{u}^G) \cdot \mathbf{n} \, d\partial\Omega_F \\ - \int_{\partial\Omega_F} \mathbf{n} \cdot \boldsymbol{\sigma} \cdot \mathbf{u} \, d\partial\Omega_F + \frac{1}{2\mu} \|\boldsymbol{\tau}\|_{\Omega_F}^2 = \rho^F \int_{\Omega_F} \mathbf{b}^F \cdot \mathbf{u} \, d\Omega_F \end{aligned} \quad (3.42)$$

where the temporal change of the kinetic energy according to (3.40) has been identified. Equally to the energy balance on a fixed reference system (2.42) equation (3.42) states that the temporal change of energy inside Ω_F is balanced by an inflow of energy, the work done by tractions and body forces and the energy which is dissipated by the internal friction. However the second term in the first line of (3.42) which vanishes for strictly divergence free velocity fields might spoil the correct balance in a spatially discretised version. Thus conservation of energy cannot be recovered exactly in a discrete scheme basing on the convective ALE formulation (3.9).

Divergence formulation

A similar energy balance expression to (3.42) is obtained by starting from the divergence ALE form (3.11), multiplying it with the velocity field \mathbf{u} and integrating over a domain which is constant in the reference system. In this case the resulting energy balance reads

$$\begin{aligned} \left. \frac{\partial E_{\text{kin}}}{\partial t} \right|_{\mathbf{x}} + \frac{\rho^F}{2} \int_{\Omega_F} |\mathbf{u}|^2 \nabla \cdot \mathbf{u} \, d\Omega_F + \frac{\rho^F}{2} \int_{\partial\Omega_F} |\mathbf{u}|^2 (\mathbf{u} - \mathbf{u}^G) \cdot \mathbf{n} \, d\partial\Omega_F \\ - \int_{\partial\Omega_F} \mathbf{n} \cdot \boldsymbol{\sigma} \cdot \mathbf{u} \, d\partial\Omega_F + \frac{1}{2\mu} \|\boldsymbol{\tau}\|_{\Omega_F}^2 = \rho^F \int_{\Omega_F} \mathbf{b}^F \cdot \mathbf{u} \, d\Omega_F, \end{aligned} \quad (3.43)$$

i.e. the sign of the energy error term $\rho^F/2 \int_{\Omega_F} |\mathbf{u}|^2 \nabla \cdot \mathbf{u} \, d\Omega_F$ has changed.

Equation (3.43) highlights that discrete schemes derived from the divergence ALE form (3.11) will also be unable of exactly conserving the energy. It further shows that the potential energy error is of the same order of magnitude for the divergence form and the convective formulation provided that the deviation from exact fulfilment of the continuity equation is comparable.

A combined ALE formulation

A comparison of (3.42) and (3.43) suggests that an energy conserving discrete formulation could be derived from an average of the convective and divergence formulation. This is well known for EULERIAN flow formulations where it yields the form (2.43). Consult GRESHO and SANI [107] or also QUATERONI and VALLI [197] for a detailed discussion in the EULERIAN case. Also on deforming domains the average of the convective ALE form and the respective divergence formulation yields a discretely energy conserving scheme. However in this case it is not only the convective term which is affected by ‘averaging’ the two equations but also the time derivative, i.e. the mass term. The energy conserving formulation reads

$$\begin{aligned} \frac{\rho^F}{2} \left(\frac{\partial (J_t \mathbf{u})}{\partial t} \Big|_{\mathbf{x}} + J_t \frac{\partial \mathbf{u}}{\partial t} \Big|_{\mathbf{x}} \right) + J_t \rho^F (\mathbf{u} - \mathbf{u}^G) \cdot \nabla \mathbf{u} + \frac{J_t \rho^F}{2} \nabla \cdot (\mathbf{u} - \mathbf{u}^G) \mathbf{u} \\ + J_t \nabla \cdot \boldsymbol{\sigma} = J_t \rho^F \mathbf{b}^F \quad \text{on } \Omega_{\mathbb{F}}^0 \times T. \end{aligned} \quad (3.44)$$

Unfortunately (3.44) contains time derivatives of different fields and is thus not accessible to straightforward temporal discretisation. Nevertheless it is of theoretical interest as it indicates how to design an unconditionally stable scheme on a deforming domain.

3.5 Stability of ALE formulations

Numerical schemes for the approximation of initial value problems require to be consistent and stable in order to be convergent. Also for boundary value problems consistency and stability are highly desired. Consistency is obvious for weighted residual methods which will always be satisfied by the analytical solution.

The stability of temporally discretised ALE formulations, however, is a persistent matter of concern. In [83, 84] FORMAGGIA and NOBILE conclude that the convective ALE formulation was potentially unstable. According to the latter paper the divergence formulation discretised in time by BE is the only scheme for which unconditional temporal stability can be shown. However it is also stated there that the authors “*were actually unable to find a test case where the simulation would blow-up*”. Recent contributions to the question of stability of ALE based schemes have been made by BADIA and CODINA [5] and MASUD [175].

Stability of a discrete problem requires that for a finite right hand side the solution does not exhibit unbounded growth. Thus it demands that the discrete operator can be inverted which is the case if the operator is coercive. However, coercivity is a sufficient but not a necessary condition for stability. In the present context of the incompressible NAVIER-STOKES equations a coercivity estimate can also be interpreted as a lower bound

on the energy which is generated if inertial forces, convective forces, viscous forces and pressure forces which are due to a velocity field \mathbf{u} act along the direction of \mathbf{u} .

The subsequent analysis is considered with stability within one time step which is a kind of local stability (with respect to time) in contrast to long-term stability considered in [5, 83, 84]. Conditions are obtained here that guarantee that the operator can be inverted within a particular step. Thus these conditions could also be termed solvability condition to distinguish it clearly from a stability condition obtained from a long-term stability analysis.

Stability within one time step is necessary but not sufficient for long-term stability which is hard to show. The present considerations shed light on why and how the mesh motion affects stability of a numerical scheme.

A stability analysis is performed here on the model problem of the transient advection-diffusion equation (2.55). This allows to assess the effect of the domain motion on the stability independent of the other difficulties contained in the incompressible NAVIER-STOKES equations, i.e. the velocity-pressure coupling and the nonlinearity.

3.5.1 Stability of the convective ALE formulation of the advection-diffusion equation

The discrete model problem in convective formulation

The convective ALE form of the model problem reads

$$\left. \frac{\partial \phi}{\partial t} \right|_{\boldsymbol{\chi}} + (\mathbf{a} - \mathbf{u}^G) \cdot \nabla \phi - \kappa \Delta \phi = f \quad \text{in } \Omega_t \times T \quad (3.45)$$

with an initial field $\phi(t, \boldsymbol{\chi}) = \phi^0(\boldsymbol{\chi})$ and homogeneous DIRICHLET boundary conditions $\phi = 0$ on $\partial\Omega_t$ assumed for brevity of the presentation. After discretisation in time by one-step- θ or BDF2 this yields in every time step

$$\phi^{n+1} + \delta \{ (\mathbf{a}^{n+1} - \mathbf{u}^{G,n+1}) \cdot \nabla \phi^{n+1} - \kappa \Delta \phi^{n+1} \} = r^{n+1} \quad \text{in } \Omega_{n+1} \quad (3.46)$$

where the parameter δ is given by (3.17) and the right hand side term r^{n+1} depends on the particular choice of the time discretisation scheme according to

$$r_{\theta}^{n+1} = \delta_{\theta} f^{n+1} + (1 - \theta) \Delta t \dot{\phi}^n + \phi^n, \quad r_{\text{BDF2}}^{n+1} = \delta_{\text{BDF2}} f^{n+1} + \frac{4}{3} \phi^n - \frac{1}{3} \phi^{n-1}.$$

Thus the GALERKIN weak form is given by: find $\phi \in V_{0,n+1}^h \subset H^1$ such that

$$(\phi, \omega)_{\Omega_{n+1}} + \delta \left((\mathbf{a}^{n+1} - \mathbf{u}^{G,n+1}) \cdot \nabla \phi, \omega \right)_{\Omega_{n+1}} + \delta \kappa (\nabla \phi, \nabla \omega)_{\Omega_{n+1}} = (r^{n+1}, \omega)_{\Omega_{n+1}} \quad (3.47)$$

is satisfied for all ω in $V_{0,n+1}^h \subset H^1$ which is the discrete space that satisfies the homogeneous DIRICHLET boundary conditions.

Coercivity analysis

It is worth noting that the convective ALE formulation of the present model problem (3.46) is not affected by the motion of the mesh within one time step. The problem rather

takes the form of an advection-diffusion-reaction equation with an underlying velocity field $\mathbf{a} - \mathbf{u}^G$ which is not divergence free. The stability limits of convective problems with non-solenoidal velocity fields are well known, consult for example KNABNER and ANGERMANN [157], and transfer to the present case as shall be shown subsequently.

A weak formulation of the right hand side of (3.47) defines the bilinear form

$$B_{\text{mod}}(\phi, \omega) = (\phi, \omega)_{\Omega_{n+1}} + \delta \left((\mathbf{a}^{n+1} - \mathbf{u}^{G,n+1}) \cdot \nabla \phi, \omega \right)_{\Omega_{n+1}} + \delta \kappa (\nabla \phi, \nabla \omega)_{\Omega_{n+1}} \quad (3.48)$$

coercivity of which is required for the stability of the discrete problem (3.47). Inserting $\omega = \phi$ yields

$$B_{\text{mod}}(\phi, \phi) = \|\phi\|_{\Omega_{n+1}}^2 + \delta \int_{\Omega_{n+1}} (\mathbf{a}^{n+1} - \mathbf{u}^{G,n+1}) \cdot \nabla \phi \phi \, d\Omega_t + \delta \kappa \|\nabla \phi\|_{\Omega_{n+1}}^2. \quad (3.49)$$

The second term in (3.49) can be reformulated by integration by parts and employing $\nabla \cdot \mathbf{a} = 0$. Using further that the boundary integral term vanishes due to the boundary conditions one obtains

$$\int_{\Omega_{n+1}} (\mathbf{a}^{n+1} - \mathbf{u}^{G,n+1}) \cdot \nabla \phi \phi \, d\Omega_{n+1} = \frac{1}{2} \int_{\Omega_{n+1}} \nabla \cdot \mathbf{u}^{G,n+1} |\phi|^2 \, d\Omega_{n+1}. \quad (3.50)$$

Inserting (3.50) into (3.49) allows to obtain the coercivity estimate

$$B_{\text{mod}}(\phi, \phi) \geq \left(1 + \delta \frac{1}{2} \min(\nabla \cdot \mathbf{u}^{G,n+1}) \right) \|\phi\|_{\Omega_{n+1}}^2 + \delta \kappa \|\nabla \phi\|_{\Omega_{n+1}}^2. \quad (3.51)$$

which is sharp if $\nabla \cdot \mathbf{u}^G$ is constant in space, i.e. if the domain expands or contracts uniformly.

Thus the formulation is stable within one time step if

$$1 + \delta \frac{1}{2} \min(\nabla \cdot \mathbf{u}^{G,n+1}) > 0 \quad (3.52)$$

is satisfied, i.e. if the coefficient of the L^2 -norm in (3.51) is strictly bounded away from zero. This condition on the solvability of convection dominated problems can also be found in [157].

Consequently a discrete scheme based on the convective ALE formulation is only conditionally stable. A similar result has also been obtained by BADIA and CODINA who consider the long-term stability of the convective ALE formulation in [5].

Interpretation of stability result

However the situation is not as bad as it might seem. A first soothing observation is the fact that a positive divergence of the mesh velocity will never yield instability but rather stabilise the bilinear form. Thus element contraction has to be considered dangerous. Recalling the value of δ for one-step- θ and BDF2 time discretisation upper limits on the time step size are obtained. The time step size has to obey

$$\Delta t < \frac{2}{\theta \max |\nabla \cdot \mathbf{u}^{G,n+1}|} \quad \text{and} \quad \Delta t < \frac{3}{\max |\nabla \cdot \mathbf{u}^{G,n+1}|} \quad (3.53)$$

for one-step- θ and BDF2, respectively, to yield a stable method. The strictest time step limit according to (3.53) is observed for BE time integration. Assuming linear approximation in space and time the divergence of the mesh velocity of an element in d dimensions that shrinks uniformly can be expressed by

$$\nabla \cdot \mathbf{u}^{\text{G},n+1} = d \frac{h^{n+1} - h^n}{\Delta t h^{n+1}}, \quad (3.54)$$

which is negative for a contracting element with a size of $h^{n+1} = \gamma h^n$ and $\gamma < 1$. The derivation of (3.54) is illustrated in figure 3.4 where a rectangular element is considered which is aligned in global coordinate directions. However, as the divergence of the mesh

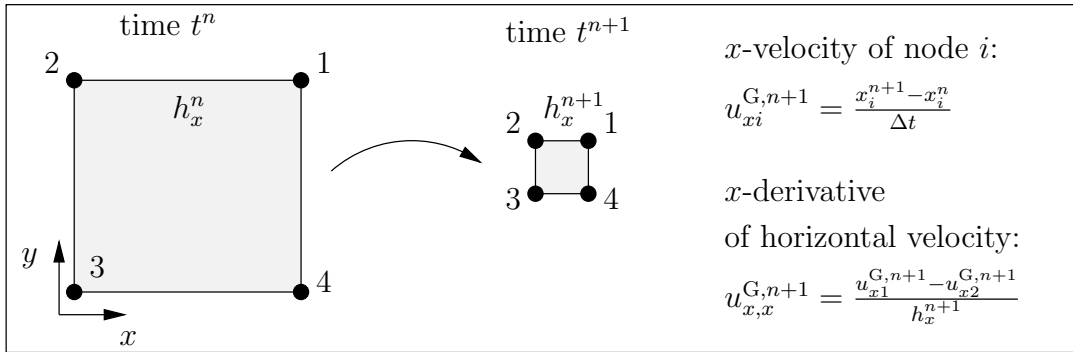


Figure 3.4: Sketch of linear finite element within the time step from t^n to t^{n+1} and the resulting mesh velocity derivative assuming linear interpolation in time and space

velocity actually is a measure of a volume ratio it is clear that (3.54) applies for all elements which expand and shrink uniformly.

Inserting this divergence expression into the time step limit obtained for BE time discretisation (3.53a) with $\theta = 1$ yields the maximal allowable contraction within one time step. Depending on the dimension of the problem d the bilinear form remains coercive for a uniform contraction satisfying

$$d/(2 + d) < \gamma. \quad (3.55)$$

Thus in the three-dimensional case the element can contract to nearly 60% of the previous length h^n in every direction and the scheme is still stable on the deforming domain. Schemes with $\theta < 1$ or BDF2 are even more permissive. Similarly more rapid contraction is possible in lower dimensional cases. Presumably this is the reason why the suspected instability of a convective ALE formulation could not be confirmed numerically [84].

It is more complicated to evaluate (3.53) for higher order schemes, when more than two time levels are involved. A much more unfavourable divergence of the mesh velocity can be constructed for higher order schemes by assuming that an element expands in one time step and contracts rapidly in the subsequent one. If the approximation of the mesh velocity within one element is linear in space which means that either linear elements are used for the mesh motion or quadratic elements are involved with perfectly placed edge and centre nodes, a divergence of the mesh velocity within an element can be deduced from (3.33b).

To sample the following case shall be considered: a three-dimensional element has a characteristic length of h^{n+1} at time level $n + 1$ and was larger in the previous step

$h^n = \gamma h^{n+1}$ with $\gamma > 1$ and of the same small size at the time level $n-1$, i.e. $h^{n-1} = h^{n+1}$. The expansion and subsequent contraction shall happen uniformly in space which is the worst case. Thus one coordinate of the mesh velocity according to (3.33b) evaluates to

$$u^G = \frac{2(1-\gamma)h^{n+1}}{\Delta t}.$$

In a three-dimensional case this yields a negative divergence of the mesh velocity of

$$\nabla \cdot \mathbf{u}^G = \frac{6(1-\gamma)}{\Delta t}.$$

It shall further be assumed that BDF2 has been used to discretise the overall equations and thus (3.53b) has to hold. The maximal expansion factor γ of such a scenario is $\gamma = 1.5$ which means that the scheme is at its limit if an element uniformly expands to $h^n = 1.5 h^{n-1}$ and shrinks back to $h^{n+1} = h^{n-1}$ within the next step. However such a scenario for the mesh motion should irrespective of stability issues not be considered trustworthy.

These results transfer to the respective ALE formulation of the incompressible NAVIER-STOKES equations if the divergence of the mesh velocity is replaced by $-\nabla \cdot (\mathbf{u} - \mathbf{u}^{G,n+1})$ to account for the divergence error of the discrete velocity field. Hence it is advisable to check the stability limits (3.53) during a computation and issuing a warning that causes the user to restart the problem with a smaller time step if necessary.

3.5.2 Stability of the divergence ALE formulation of the advection-diffusion equation

The discrete model problem in divergence form

Analogously to the NAVIER-STOKES equations a divergence ALE form of the model problem can be found reading

$$\left. \frac{\partial (J_t \phi)}{\partial t} \right|_{\mathbf{x}} + J_t \nabla \cdot \{(\mathbf{a} - \mathbf{u}^G) \phi - \kappa \nabla \phi\} = f \quad \text{in } \Omega_0 \times T \quad (3.56)$$

accompanied by initial conditions and homogeneous DIRICHLET boundary conditions. A temporal discretisation of this divergence expression yields

$$J^{n+1} \phi^{n+1} + \delta J^{n+1} \nabla \cdot \{(\mathbf{a}^{n+1} - \mathbf{u}^{G,n+1}) \phi^{n+1} - \mu \nabla \phi^{n+1}\} = r_d^{n+1} \quad \text{in } \Omega_0, \quad (3.57)$$

where r_d contains right hand side terms analogously to the respective terms for the flow momentum balance in divergence form (3.20).

$$r_{d,\theta}^{n+1} = \delta_\theta J^{n+1} f^{n+1} + J^n \phi^n + (1-\theta) \Delta t \dot{J} \phi^n, \quad (3.58)$$

$$r_{d,BDF2}^{n+1} = \delta_{BDF2} J^{n+1} f^{n+1} + \frac{4}{3} J^n \phi^n - \frac{1}{3} J^{n-1} \phi^{n-1}. \quad (3.59)$$

The GALERKIN weak formulation of the discretised problem reads: find $\phi \in V_0^h(\Omega_0)$ such that

$$\begin{aligned} (J^{n+1} \phi^{n+1}, \omega)_{\Omega_0} + \delta (J^{n+1} \nabla \cdot \{(\mathbf{a}^{n+1} - \mathbf{u}^{G,n+1}) \phi^{n+1}\}, \omega)_{\Omega_0} + \delta \kappa (J^{n+1} \nabla \phi^{n+1}, \nabla \omega)_{\Omega_0} \\ = (r_d^{n+1}, \omega)_{\Omega_0} \quad \text{for all } \omega \text{ in } V_0^h \end{aligned} \quad (3.60)$$

is satisfied where V_0^h denotes the discrete space that satisfies the homogeneous DIRICHLET boundary conditions.

Coercivity analysis

Equation (3.60) defines the bilinear form

$$B_{\text{mod,d}}(\phi, \omega) = (\phi, \omega)_{\Omega_{n+1}} + \delta (\nabla \cdot \{(\mathbf{a}^{n+1} - \mathbf{u}^{\text{G},n+1}) \phi\}, \omega)_{\Omega_{n+1}} + \delta \kappa (\nabla \phi, \nabla \omega)_{\Omega_{n+1}} \quad (3.61)$$

coercivity of which is required for stability. Inserting $\omega = \phi$ yields

$$B_{\text{mod,d}}(\phi, \phi) = \|\phi\|_{\Omega_{n+1}}^2 + \delta \int_{\Omega_{n+1}} \nabla \cdot \{(\mathbf{a}^{n+1} - \mathbf{u}^{\text{G},n+1}) \phi\} \phi \, d\Omega_{n+1} + \delta \kappa \|\nabla \phi\|_{\Omega_{n+1}}^2. \quad (3.62)$$

Evaluating the second term in (3.62) gives

$$\int_{\Omega_{n+1}} \nabla \cdot \{(\mathbf{a}^{n+1} - \mathbf{u}^{\text{G},n+1}) \phi\} \phi \, d\Omega_{n+1} = -\frac{1}{2} \int_{\Omega_{n+1}} \nabla \cdot \mathbf{u}^{\text{G},n+1} |\phi|^2 \, d\Omega_{n+1},$$

where $\nabla \cdot \mathbf{a} = 0$ and (3.50) have been used. This reformulation yields the stability result of the divergence ALE formulation

$$B_{\text{mod,d}}(\phi, \phi) \geq \left(1 - \delta \frac{1}{2} \max(\nabla \cdot \mathbf{u}^{\text{G},n+1})\right) \|\phi\|_{\Omega_{n+1}}^2 + \delta \kappa \|\nabla \phi\|_{\Omega_{n+1}}^2. \quad (3.63)$$

The estimate (3.63) is sharp if the domain contracts or expands uniformly. Thus the stability limit obtained for the conservative ALE scheme is given by

$$1 - \delta \frac{1}{2} \max(\nabla \cdot \mathbf{u}^{\text{G}}) > 0 \quad (3.64)$$

showing that a discrete scheme obtained from the divergence ALE form is also conditionally stable. This result is remarkably similar to the stability condition obtained for the convective ALE formulation. However the divergence ALE formulation might get unstable at sudden element expansion rather than contraction. Transferring (3.64) into a specific time step limit yields

$$\Delta t < \frac{2}{\theta \max(\nabla \cdot \mathbf{u}^{\text{G},n+1})} \quad \text{and} \quad \Delta t < \frac{3}{\max(\nabla \cdot \mathbf{u}^{\text{G},n+1})} \quad (3.65)$$

for one-step- θ and BDF2, respectively, which apply for positive divergence of the mesh velocity only.

In order to estimate the practical meaning of the time step limits (3.65) a d -dimensional element is considered again subject to uniform expansion. The initial length h^n is stretched to $h^{n+1} = \gamma h^n$ with $\gamma > 1$. Assuming linear interpolation in space and time the divergence of the mesh velocity is evaluates to

$$\nabla \cdot \mathbf{u}^{\text{G},n+1} = d \frac{h^{n+1} - h^n}{h^{n+1} \Delta t} = d \frac{\gamma - 1}{\gamma \Delta t}. \quad (3.66)$$

The lowest time step limit in (3.65) obtained for BE states that the divergence of the mesh velocity (3.66) has to be smaller than $2/\Delta t$. If the dimension is lower than three this is satisfied for all finite γ . In the three dimensional case stability is conditional upon $\gamma < 3$. Thus a three-dimensional element may stably undergo an expansion to up to three times the original length in each direction within one time step. Clearly this limit has not been met in practical computations.

Similar to what is observed for the convective ALE formulation further unstable cases can be constructed for higher dimensional interpolations of the mesh velocity. However such scenarios are likewise not of high interest in practical computations.

Remark 3.5.1 (on comparison) The obvious unsymmetry between element contraction and expansion is caused by the fact that the divergence of the actual mesh velocity $\nabla \cdot \mathbf{u}^{\text{G},n+1}$ refers to the most recent configuration. Thus an element contracting to zero will always yield an infinitely negative divergence of the mesh velocity and thus certainly violate the condition (3.53) with every time step. However both of the limiting time step sizes hardly determine the maximal time step for a given physical problem as rapid changes of the element lengths are caused by rapid motion of the fluid-structure interface Γ which indicates highly transient dynamics. Such situations anyway deserve small time steps to resolve the physical problem adequately.

3.5.3 An unconditionally stable formulation on deforming domains

A comparison of the stability estimates obtained for the convective formulation (3.51) and the divergence form (3.63) indicates how to construct an unconditionally stable ALE formulation of conservation laws on deforming domains. An energy conserving ALE form results from averaging the convective and divergence ALE formulation, however, this partial differential equation cannot straightforwardly be discretised in time.

An unconditionally stable discrete formulation is obtained by averaging the *discrete convective and divergence* ALE form (3.21) and (3.25) or (3.26) for one-step- θ and BDF2, respectively. In the case of the present model problem this means averaging of the weak forms (3.47) and (3.60) yielding the discrete problem of finding $\phi \in V_0^h(\Omega_{n+1})$ such that

$$\begin{aligned} (\phi, \omega)_{\Omega_{n+1}} + \delta \left((\mathbf{a}^{n+1} - \mathbf{u}^{\text{G},n+1}) \cdot \nabla \phi, \omega \right)_{\Omega_{n+1}} + \frac{1}{2} \delta \left(\nabla \cdot (\mathbf{a}^{n+1} - \mathbf{u}^{\text{G},n+1}) \phi, \omega \right)_{\Omega_{n+1}} \\ + \delta \kappa (\nabla \phi, \nabla \omega)_{\Omega_{n+1}} = \frac{1}{2} (r^{n+1}, \omega)_{\Omega_{n+1}} + \frac{1}{2} (r_d^{n+1}, \omega)_{\Omega_0} \end{aligned} \quad (3.67)$$

is satisfied for all $\omega \in V_0^h$. Indeed repeating the stability analysis one obtains coercivity of the bilinear form $B_{\text{mod,av}}$ defined by the left hand side of (3.67). The respective analysis yields after some algebra

$$B_{\text{mod,av}}(\phi, \phi) = \|\phi\|_{\Omega_{n+1}}^2 + \delta \kappa \|\nabla \phi\|_{\Omega_{n+1}}^2 \quad (3.68)$$

confirming that the problem (3.67) can stably be integrated irrespective of the time step size or the mesh motion.

However there is nothing for free. While guaranteeing stability with respect to the mesh motion the weak form (3.67) has lost the exact geometric conservation property of the convective ALE form as well as the conservation property of the divergence formulation.

3.6 Summary

There are different ways to formulate conservation laws on moving domains. While in a continuous setting all these formulations are equal, discrete versions thereof exhibit differences with respect to the exact fulfillment of conservation laws. A summary of the conservation laws inherently satisfied by different ALE formulations is given in table 3.1.

Table 3.1: Short summary of inherent conservation properties of different ALE formulations

ALE formulation	conservation of energy	conservation of momentum	conservation of mass	conservation of geometry
divergence form	no	yes	yes	no
convective form	no	no	yes	yes
average form	yes	no	yes	no

It has been shown that the convective ALE formulation inherently satisfies geometric conservation while a discretisation error enters the conservation of linear momentum and energy. Schemes basing on the convective ALE formulation share the temporal order of accuracy of their fixed grid counterpart as soon as the mesh velocity is interpolated sufficiently high.

A temporally discretised scheme of the divergence formulation guarantees exact conservation of momentum. However, extra effort has to be made here in order to approach geometric conservation. Similarly to the convective formulation the discrete versions of the divergence form do not satisfy energy conservation exactly. Both schemes are conditionally stable where an upper bound on the time step size can be obtained which depends upon the divergence of the mesh velocity as well as on the particular time discretisation scheme.

Similar to what is well known for EULERian methods an energy-conserving ALE formulation can be obtained by averaging the convective and divergence formulation. Averaging time discretised versions of the convective and divergence formulation a temporally discrete scheme is obtained which is unconditionally stable on moving domains.

Chapter 4

Stabilised finite element methods for incompressible flow

Within this chapter the temporally discretised flow equations are discretised in space. Along with the spatial discretisation stabilisation has to be introduced. This need for stabilisation of the discrete flow equations is explained and a number of stabilisation methods are discussed. After briefly reviewing the reason for the observed numerical oscillations some more or less popular methods to circumvent these oscillations are considered. The main part of the chapter is devoted to the family of residual based stabilisation methods which are discussed and analysed in some detail.

The focus is set on introducing and formulating a stabilised finite element method on a deforming domain such that no additional stability restrictions arise.

4.1 Wiggles and the need for stabilisation

It is well known that finite element methods based on weak GALERKIN forms such as (3.21), (3.25) or (3.26) frequently fail as soon as significant convection occurs. Another important challenge in incompressible flow is the incompressibility condition and thus the role of the pressure. In particular a close look at the weak forms (3.22) and (3.27) reveals that the pressure variable acts as a LAGRANGE multiplier to enforce the incompressibility condition (2.35). Thus the restrictions imposed by the inf-sup condition or LBB (LADYSHENSKAYA-BABUŠKA-BREZZI) condition have to be considered.

Increasing the flow velocity on a given mesh, i.e. increasing the convective transport, as well as violating the inf-sup condition introduces spurious oscillations also termed *wiggles*. GRESHO and SANI [107] give an exhaustive discussion on such wiggles and wiggle-generating situations while they insist that wiggles are a self-diagnosis property, indicating inappropriate resolution and the difficulty of the numerical method to come up with a suitable approximation of the physical problem. The risk of over-stabilisation by damping out numerical problems while at the same time changing the physics of the problem solved has to be kept in mind when stabilisation methods shall be developed.

This section is devoted to briefly highlighting the cause of the occurring unphysical oscillations. For more exhaustive explanations and examples one might consult the dissertations of GRAVEMEIER and WALL [103, 227] as well as the book by DONEA and HUERTA [69]. With respect to the LBB condition mathematical literature on mixed variational problems and fluid dynamics as for example the monograph by GIRAULT and RAVIART [102] or the one by GUNZBURGER [109] should be consulted. A standard reference for mixed methods problems is further the book by BREZZI and FORTIN [32].

4.1.1 Convection dominated problems

Mathematical analysis

Numerical oscillations induced by dominating convection are conveniently analysed by means of the advection-diffusion equation (2.54). Thus the result of a coercivity analysis of the discrete transient advection-diffusion problem with homogeneous DIRICHLET boundary conditions obtained in section 3.5 is recalled. From (3.51), (3.63) and (3.68) it can be observed that irrespective of the underlying ALE formulation (and indeed also on fixed grids) the transient advection-diffusion problem yields a coercivity estimate of the form

$$B_{\text{mod}}(\phi, \phi) \geq C \|\phi\|_{\Omega_{n+1}}^2 + \delta\kappa \|\nabla\phi\|_{\Omega_{n+1}}^2 \quad (4.1)$$

where C is a positive constant. Thus the corresponding numerical method is stable in the sense that the corresponding discrete coefficient matrix is non-singular. However the convective term $\mathbf{a} \cdot \nabla\phi$ does not contribute to the coercivity. So if the influence of the convection is much larger than the effect of the diffusion governed by κ the coercivity estimate (4.1) might be arbitrarily small indicating that the control over the H^1 norm of the solution is gradually lost leaving the discrete solution with the freedom to oscillate.

In the special case of a stationary advection-diffusion problem a coercivity consideration yields

$$B_{\text{mod,stationary}}(\phi, \phi) = \kappa \|\nabla\phi\|_{\Omega_{n+1}}^2$$

further highlighting the potential loss of stability at small κ compared to the convection, i.e. at high elemental PécLET number $\text{Pe}^e = ah/2\kappa$. An error estimate for stationary advective-diffusive transport obtained by HUGHES [132] reads

$$\|\nabla e\| = O((1 + \text{Pe}^e) h^k)$$

where k denotes the polynomial order of the element. Thus the gradient of the error $e = \phi^h - \phi$ depends on Pe^e indicating that oscillations are well possible at convection dominated flows while the bound behaves optimal for diffusion dominated problems.

Properties and interpretation of convective wiggles

Spurious convection oscillations emanated at unresolved gradients tend to spread over the entire domain. In particular in time dependent calculations the solution is polluted by such wiggles globally after just a few steps.

In order to increase the understanding of the deficiency of GALERKIN schemes in convection dominated problems and indicate ways to overcome it, different interpretations of the problem have been given some of which shall be summarised here.

- Analysing the discrete equations in one dimension DONEA and HUERTA [69] show that centred schemes are under-diffusive compared to schemes which would yield nodally exact solutions. This suggests stabilisation by a proper amount of additional numerical diffusion.

- It can also be argued that the solution at a particular node at time level $n + 1$ is much more influenced by the behaviour of the function ϕ upstream than by the situation downstream at time level n . A numerical scheme to simulate advective transport should thus include an upwinding of the weighting function rather than being centred.
- Another view on the problem reveals that the wiggly numerical approximation is caused by non-resolved physics, i.e. badly represented higher modes. Thus introducing additional subscale degrees of freedom might cure the deficiencies.
- A further approach is inspired by the coercivity estimate (4.1) in which an advective term of the form $\|\mathbf{a} \cdot \nabla \phi\|^2$ is missing; enriching the weighting function space such that it includes a convective term would yield the desired control in the bilinear form.

4.1.2 Spurious pressure oscillations and the LBB condition

In order to study the role of the inf-sup condition the STOKES equations (2.53) are recalled. A discrete weak form of the STOKES problem reads on a fixed domain: find the velocity $\mathbf{u} \in \mathbf{V}_F^h$ and pressure field $p \in P^h$ at the new time level such that

$$\begin{aligned} (\mathbf{u}, \mathbf{v})_{\Omega_F} + \delta (2\nu \boldsymbol{\varepsilon}(\mathbf{u}), \boldsymbol{\varepsilon}(\mathbf{v}))_{\Omega_F} - \delta (p, \nabla \cdot \mathbf{v})_{\Omega_F} - \delta (q, \nabla \cdot \mathbf{u})_{\Omega_F} \\ = (\mathbf{r}^{n+1}, \mathbf{v})_{\Omega_F} + \delta (\mathbf{h}^{n+1}, \mathbf{v})_{\Gamma_{F,N}} \quad \text{for all } (\mathbf{v}, q) \in (\mathbf{V}_{F,0}^h, P^h) \end{aligned} \quad (4.2)$$

is satisfied. In matrix notation the system might be written as

$$\begin{bmatrix} \mathbf{M}^F + \delta \mathbf{K}^F & \delta \mathbf{G} \\ \delta \mathbf{G}^T & \mathbf{0} \end{bmatrix} \begin{bmatrix} \mathbf{u} \\ \mathbf{p} \end{bmatrix} = \begin{bmatrix} \mathbf{f}^F \\ \mathbf{0} \end{bmatrix}. \quad (4.3)$$

The discrete system (4.2) is stable if the finite element spaces \mathbf{V}_F^h and P^h and thus the elements are chosen such that the discrete version of the well-known LBB or inf-sup condition is satisfied. This condition reads (see for example GUNZBURGER [109]): Given any $p \in P^h$,

$$\sup_{\mathbf{0} \neq \mathbf{v} \in \mathbf{V}_{F,0}^h} \left(\frac{-(p, \nabla \cdot \mathbf{v})}{|\mathbf{v}|_1} \right) \geq \gamma \|p\|, \quad (4.4)$$

where the positive constant γ is independent of the mesh size h and the particular choice of $p \in P^h$. The condition states that for every admissible non-zero pressure field a velocity test function \mathbf{v} is contained in $\mathbf{V}_{F,0}^h$ which yields a contribution of the pressure to the total internal energy.

Employing the matrix \mathbf{G} , the discrete LBB condition can be written

$$\sup_{\mathbf{0} \neq \mathbf{v} \in \mathbf{V}_0^h} \left(\frac{\mathbf{v}^T \mathbf{G} \mathbf{p}}{|\mathbf{v}|_1} \right) \geq \gamma \|p\|. \quad (4.5)$$

Equation (4.5) shows that in the case of LBB stable discretisation the matrix \mathbf{G} is of full rank which is clearly a necessary condition for the solvability of the discrete system (4.3) as well as discrete versions of the incompressible NAVIER-STOKES equations.

Unfortunately the inf-sup condition is frequently violated for desirable combinations of velocity and pressure spaces. However there are two different grades of violation. A number of elements can be found which might be used – at least with some care concerning the boundary conditions – even if they do not satisfy (4.4). Examples of such elements can be found in the list of possible elements for the incompressible NAVIER-STOKES equations given by GRESHO and SANI in [107]. Such elements violate the inf-sup condition in the sense that they do not exhibit a stability constant γ independent of the mesh size h . Thus they might get unstable in the limit $h \rightarrow 0$, a case rarely met in practical computations.

A much more severe problem occurs if (4.5) is violated such that the discrete operator \mathbf{G} exhibits a rank deficiency. In this case the coefficient matrix in (4.3) will be singular and no unique solution can be obtained. Consequently the discrete solution of the pressure – while possibly accompanied by a reasonable velocity approximation – exhibits devastating spurious oscillations. Examples of such spurious pressure modes have been computed e.g. by WALL [227].

4.2 Stabilisation – omnipresent in flow solvers

Wherever flow problems with considerable convective transport have to be dealt with stabilisation is considered. Occasionally it might not be called ‘stabilisation’ but rather come along termed ‘upwinding’ or ‘balancing diffusion’. However in all those cases some extra effort has been made in order to overcome the unstable wiggly solution of a pure BUBNOV-GALERKIN scheme.

Analogously the restriction imposed by the LBB condition occurs as soon as an incompressible process is considered. And it is generally taken as an advantage of a numerical scheme if it allows to circumvent this condition opening the full range of velocity and pressure space combinations.

Before introducing the residual based stabilisation methods which have been used primarily within this work a short overview over some alternative stabilisation methods shall be given. It is far beyond the scope of the present work to introduce a wide range of flow solvers in detail. The intention is rather to highlight that there is no stable flow solver without extra effort. The focus is put on stabilisation methods applied in conjunction with finite elements. However, very similar methods are used when finite volumes or difference methods are considered where analogous instabilities arise.

4.2.1 Convection stabilisation

Inspired by the fact that information is propagated by an underlying velocity field, upwind schemes have been proposed for convection dominated flow. In the context of weighted residual methods upwinding is introduced by choosing a weighting function which puts more weight to the upstream than to the downstream part of the flow, i.e. a PETROV-GALERKIN scheme is employed. Adjusting the amount of upwinding to the Péclet number allows to obtain nodally exact values for the one-dimensional advection-diffusion problem [69, 237].

The situation is more difficult in the higher dimensional case. A certain amount of upwinding corresponds to a particular portion of artificial diffusivity introduced in the

scheme [69, 237]. But introducing numerical viscosity goes along with the so-called ‘cross-wind diffusion’, i.e. artificial diffusivity perpendicular to the convective velocity severely harming the accuracy of the approximation.

In order to overcome these difficulties the streamline upwind PETROV-GALERKIN (SUPG) method has been developed by HUGHES and colleagues in [135, 136, 153]. The method shall be touched upon again in Section 4.3 as this is one of the early members of the family of residual based stabilisation methods. A next one is the GALERKIN/Least-Squares (GLS) method which has also been proposed by HUGHES and coworkers [140].

Finite increment calculus

Stabilisation terms can be derived by employing the so-called finite increment calculus suggested by OÑATE [188]. Recent formulations of stabilisation based on finite calculus can be found in [190, 191] where the method has also been used to treat incompressible flows on moving domains. Application of the method to ship hydrodynamics is presented in [189].

The basic idea of the formulation shall be explained briefly here on the scalar advection-diffusion equation

$$\mathbf{a} \cdot \nabla \phi - \kappa \Delta \phi - f = 0 \quad \text{in } \Omega. \quad (4.6)$$

In view of the desired numerical solution of (4.6) by means of a discrete method which considers finite portions of the domain the residual (4.6) is expanded in space in a TAYLOR series yielding

$$\mathbf{a} \cdot \nabla \phi - \kappa \Delta \phi - f + \frac{\boldsymbol{\delta}}{2} \cdot \nabla (\mathbf{a} \cdot \nabla \phi - \kappa \Delta \phi - f) = 0 \quad \text{in } \Omega, \quad (4.7)$$

where $\boldsymbol{\delta}$ is a spatial distance vector pointing in the direction of the expansion. It is smaller or as long as an elemental length and scales the stabilisation terms. In order to ensure streamline oriented stabilisation the expansion is performed in the direction of the underlying velocity field, i.e. $\boldsymbol{\delta} = c \mathbf{a}/|\mathbf{a}|$ where c is a constant to be chosen appropriately.

Characteristic Galerkin procedure

Another way of obtaining stabilisation terms is the so-called characteristic-GALERKIN procedure extensively used in [237], where the path of a fluid particle is called its characteristic. This approach departs from the LAGRANGEAN formulation of the transient flow problem which for the advection-diffusion equation (2.54) reads

$$\left. \frac{\partial \phi(\mathbf{x}(t), t)}{\partial t} \right|_{\mathbf{x}} - \kappa \Delta \phi = f(\mathbf{x}), \quad (4.8)$$

where the convective term disappears and the material time derivative of the transport variable is involved. A temporal discretisation of (4.8) by the one-step- θ method then yields terms to be evaluated at different spatial positions

$$\phi_{\mathbf{x}^{n+1}}^{n+1} - \phi_{\mathbf{x}^n}^n = \theta \Delta t [\kappa \Delta \phi + f]_{\mathbf{x}^{n+1}}^{n+1} + (1 - \theta) \Delta t [\kappa \Delta \phi + f]_{\mathbf{x}^n}^n \quad (4.9)$$

where the subscripts \mathbf{x}^{n+1} and \mathbf{x}^n denote the actual and the previous position of the fluid particle. Discretising (4.9) directly in space requires a LAGRANGEan mesh motion which is highly undesirable. Thus the old value $\phi_{\mathbf{x}^n}^n$ is approximated by a TAYLOR series expansion backward in space truncated after the second term.

$$\phi_{\mathbf{x}^n}^n \approx \phi_{\mathbf{x}^{n+1}}^n - \boldsymbol{\delta} \cdot \nabla \phi_{\mathbf{x}^{n+1}}^n + \frac{1}{2} \boldsymbol{\delta} \cdot \mathbf{H} \phi_{\mathbf{x}^{n+1}}^n \cdot \boldsymbol{\delta} + O(\Delta t^3)$$

where the distance vector $\boldsymbol{\delta} = \mathbf{x}^{n+1} - \mathbf{x}^n = \bar{\mathbf{a}} \Delta t$ is the way of the respective particle within the time step and can be obtained if an average convective velocity $\bar{\mathbf{a}}$ within the time step is available. The symbol \mathbf{H} denotes the HESSEan matrix, i.e. second spatial derivatives.

Similarly the diffusive and load term at the old time level and spatial position \mathbf{x}^n are expanded in a TAYLOR series yielding

$$\begin{aligned} \Delta \phi_{\mathbf{x}^n}^n &\approx \Delta \phi_{\mathbf{x}^{n+1}}^n - \boldsymbol{\delta} \cdot \nabla \Delta \phi_{\mathbf{x}^{n+1}}^n + O(\Delta t^2), \\ f_{\mathbf{x}^n}^n &\approx f_{\mathbf{x}^{n+1}}^n - \boldsymbol{\delta} \cdot \nabla f_{\mathbf{x}^{n+1}}^n + O(\Delta t^2). \end{aligned}$$

Introducing these expansions back into (4.9) yields a scheme with possible second order temporal accuracy reading

$$\begin{aligned} \phi^{n+1} - \phi^n &= \theta \Delta t [\kappa \Delta \phi + f]^{n+1} + (1 - \theta) \Delta t [\kappa \Delta \phi + f]^n - \Delta t \bar{\mathbf{a}} \cdot \nabla \phi^n \\ &+ \frac{1}{2} \Delta t^2 \bar{\mathbf{a}} \cdot \mathbf{H} \phi^n \cdot \bar{\mathbf{a}} - (1 - \theta) \Delta t^2 \bar{\mathbf{a}} \cdot \nabla (\kappa \Delta \phi^n + f^n) \end{aligned} \quad (4.10)$$

where all terms refer to the present positions of the particles \mathbf{x}^{n+1} . In the first line of (4.10) it can be observed that the transformation of the LAGRANGEan equation (4.8) to an EULERian mesh via TAYLOR series expansions effectively reintroduces the convective term. Additionally the second line of (4.8) emerges containing terms that enhance the stability of the formulation. In particular the first term on the second line of (4.8) offers the desired stabilisation diffusion in the streamline direction.

It is noteworthy that the characteristic procedure in the formulation sketched above is restricted to a temporal accuracy up to second order due to the truncations in the TAYLOR series. The method of characteristics further applies to transient problems exclusively.

Flow conditioned based interpolation

An alternative way to cope with convection domination has been suggested by BATHE. Within the scheme proposed in [10] an exponential weighting function for the velocity is used which depends upon the underlying flow field and thus introduces an appropriate amount of upwinding within each element. In a subsequent publication [11] the method was modified such that the convective velocity itself is interpolated by exponential trial functions depending upon the velocity field.

Recent developments of the method can be found in [158, 159, 160].

4.2.2 Circumventing the LBB condition - pressure stabilisation

Several methods have been proposed to circumvent the restrictions imposed by the inf-sup condition. This is desirable in particular for low order approximations of pressure

and velocity most of which do not satisfy the LBB condition. However low order pairs of velocity and pressure are of special interest as they yield small bandwidths and a low number of non zero values per line of the coefficient matrix also in three-dimensional problems.

It is further regarded a general advantage if the choice of the discrete velocity and pressure space can be made freely. This significantly enlarges the set of possible elements for incompressible flow simulations. Typically the relaxation of the incompressibility condition yields contributions on the pressure main diagonal block of the overall coefficient matrix making this matrix significantly easier to solve by iterative solvers. In other words a slight relaxation of the incompressibility condition weakens the pressure shock which results from a deviation from a velocity field which is divergence free in the proper weak sense. The issue of stabilised versus a priori stable elements shall be touched upon later again in the context of residual based stabilisation methods.

Penalty formulations have been used to formulate the incompressibility constraint allowing to uncouple the pressure and velocity equation (see e.g. [135]). In contrast to these methods stabilisation aims at relaxing the incompressibility condition such that LBB incompatible spaces can safely be used.

Pressure stabilisation can be designed basing on a variety of projection schemes. One of the possibilities is to relax the continuity equation in the context of operator splitting projection methods such as the characteristic-based split (CBS) algorithm of ZIENKIEWICZ et al. [237] which is briefly described in the sequel. The possibility of pressure stabilisation in the context of projection schemes for transient problems has already been shown by KAWAHARA and OHMIYA in [152].

As an extension of the operator splitting methods CODINA and BLASCO proposed a pressure stabilisation method for the STOKES equations which does not rely on the time discretisation of the transient problem [54]. This pressure gradient projection method analysed by CODINA and coworkers in [17, 55, 56] is designed for elements with discontinuous pressure spaces. The incompressibility constraint is then relaxed by using the difference between the discontinuous pressure gradient and its projection onto the continuous velocity space. However, this stabilisation method comes along with the need for an inversion of a global matrix in order to perform the projection.

Residual based stabilisation methods for the STOKES problem have been proposed by HUGHES and coworkers [139]. Comparisons of stabilised finite elements and a priori stable schemes have shown that stabilised formulations compete well with their inherently stable counterparts as shown by NORBURN and SILVESTER in [184].

Recent work on the Pressure POISSON stabilisation has been reported by BOCHEV et al. [8, 20].

Pressure stabilisation within projection based algorithms

A popular family of flow solvers is based on projection and operator splitting. One well-known representation thereof is the so-called characteristic-based split (CBS) algorithm described in the third volume of the finite element trilogy of ZIENKIEWICZ et al. [237]. A comparison of CBS and GLS stabilisation used to stabilise the incompressible NAVIER-STOKES equations can be found in [59] where CODINA and ZIENKIEWICZ show that both methods introduce similar stabilising terms.

The basic idea of the CBS algorithm and similar schemes is to employ the HELMHOLTZ decomposition also known as the fundamental theorem of vector calculus stating that every vector field can uniquely be decomposed into a curl-free vector field and the gradient of a scalar field. In the present context this allows to decompose the unknown solenoidal velocity field \mathbf{u} according to

$$\mathbf{u} = \mathbf{u}^* - \nabla\varphi \quad (4.11)$$

where the scalar field φ is closely related to the kinematic pressure p . Employing (4.11) the solution of the incompressible NAVIER-STOKES equations might be split into two steps; first solving for the intermediate velocity field \mathbf{u}^* while ignoring the incompressibility condition. This step can be done in an explicit or semi-implicit manner. Subsequently the final solution \mathbf{u} is obtained by projecting \mathbf{u}^* into the space of (discretely) divergence free functions. This projection method goes back to the works of CHORIN in the context of finite difference methods [40, 41]. It is also described by TEMAM in [212]. The projection method or closely related schemes is also termed fractional step method, (operator) splitting method or pressure correction method.

The version of the projection method which is used within the CBS algorithm described in the book by ZIENKIEWICZ et al. [237] can be formulated such that the LBB condition is circumvented. The basic idea of the formulation shall be sketched here by means of the STOKES problem a temporally discretised version of which reads on a fixed grid

$$\mathbf{u}^{n+1} - \delta 2\nu \nabla \cdot \boldsymbol{\varepsilon}(\mathbf{u}^n) + \delta \nabla p^{n+1} = \mathbf{r}^{n+1} \quad \text{in } \Omega_F \quad (4.12)$$

$$\nabla \cdot \mathbf{u}^{n+1} = 0 \quad \text{in } \Omega_F, \quad (4.13)$$

where the viscous term is treated explicitly. In view of (4.11) equation (4.12) is rewritten in the form

$$\mathbf{u}^{n+1} + \delta \nabla p^{n+1} = \delta 2\nu \nabla \cdot \boldsymbol{\varepsilon}(\mathbf{u}^n) + \mathbf{r}^{n+1} = \mathbf{u}^* \quad (4.14)$$

which can be solved explicitly for the intermediate velocity field \mathbf{u}^* entirely ignoring the pressure. Taking the divergence of (4.14) allows to obtain an elliptic equation for the pressure reading

$$\delta \Delta p^{n+1} = \nabla \cdot \mathbf{u}^* \quad (4.15)$$

that can be solved as soon as \mathbf{u}^* is known. Thus the desired divergence free velocity field \mathbf{u} is eventually obtained in a third step from the initial split, i.e.

$$\mathbf{u}^{n+1} = \mathbf{u}^* - \delta \nabla p^{n+1}.$$

From a spatially discretised version of the above algorithm it can be observed that the restrictions of the inf-sup condition have been circumvented. A matrix representation of (4.12) reads

$$\mathbf{M}^F \mathbf{u}^{n+1} + \delta \mathbf{K}^F \mathbf{u}^n + \delta \mathbf{G} \mathbf{p}^{n+1} = \mathbf{f}^F. \quad (4.16)$$

From the matrix expressions of (4.14) and (4.15), i.e. from

$$\mathbf{M}^F \mathbf{u}^{n+1} + \delta \mathbf{G} \mathbf{p}^{n+1} = \mathbf{M}^F \mathbf{u}^* \quad \text{and} \quad \delta \mathbf{H} \mathbf{p}^{n+1} = \mathbf{G}^T \mathbf{u}^*,$$

where \mathbf{H} denotes the negative discrete LAPLACE operator on the pressure, the intermediate nodal velocities \mathbf{u}^* can be eliminated yielding the equation

$$\mathbf{G}^T \mathbf{u}^{n+1} + \left(\delta \mathbf{G}^T (\mathbf{M}^F)^{-1} \mathbf{G} - \delta \mathbf{H} \right) \mathbf{p}^{n+1} = \mathbf{0}. \quad (4.17)$$

Combining (4.16) and (4.17) shows that the above split algorithm corresponds to solving the discrete system

$$\begin{bmatrix} \mathbf{M}^F & \delta \mathbf{G} \\ \mathbf{G}^T & \delta \left(\mathbf{G}^T (\mathbf{M}^F)^{-1} \mathbf{G} - \mathbf{H} \right) \end{bmatrix} \begin{bmatrix} \mathbf{u}^{n+1} \\ \mathbf{p}^{n+1} \end{bmatrix} = \begin{bmatrix} \mathbf{f}^F - \delta \mathbf{K}^F \mathbf{u}^n \\ \mathbf{0}, \end{bmatrix} \quad (4.18)$$

which is nonsingular irrespective of the choice of the discrete velocity and pressure space due to the strictly positive definite matrix \mathbf{H} [237]. This additional freedom is gained from a relaxation of the incompressibility condition by the difference of two discrete representations of the LAPLACEan operator on the pressure. It has to be noted, however, that this relaxation depends on the time step size and thus the formulation does not work to circumvent the LBB condition when a stationary solution is sought.

The algorithm is doubtless an interesting one in particular as it allows to solve an implicit equation for the pressure while the diffusive (and convective) operator are integrated explicitly. However the problems of the projection method are hidden within the details. In particular the proper choice of the boundary conditions for the intermediate velocity field \mathbf{u}^* is challenging. The interested reader may consult also [107, 227] in this context.

Within the CBS algorithm the projection idea presented here has been combined with the convection stabilisation resulting from the characteristic procedure which is sketched in section 4.2.1. A detailed description of this algorithm can be found in the third volume of the finite element trilogy of ZIENKIEWICZ et al. [237].

Pressure stabilisation based on polynomial pressure projection

Pressure projection methods have been designed by DOHRMANN and BOCHEV [19, 65] with particular respect to the lowest order velocity-pressure pairs such as linear velocity and pressure approximation as well as linear velocities along with piecewise constant pressures. It works, however, to stabilise all equal order pairs of velocity and pressure.

The basic idea of the method can be explained by considering the deficiency of such elements with respect to the inf-sup condition (4.4). While not satisfying this conditions the linear equal order interpolation spaces obey a weaker inequality reading

$$\sup_{\mathbf{0} \neq \mathbf{v} \in \mathbf{V}_{F,0}^h} \left(\frac{-(p, \nabla \cdot \mathbf{v})}{|\mathbf{v}|_1} \right) \geq \gamma_1 \|p\| - \gamma_2 h \|\nabla p\|, \quad (4.19)$$

for any $p \in P^h$, where γ_1 and γ_2 are two positive constants independent of h [19, 209]. The last term on the right hand side of (4.19) quantifies the LBB deficiency of the equal order interpolation spaces. It can be shown that this term can be bounded from above by

$$\gamma_3 h \|\nabla p\| \leq \|p - \Pi p\| \quad \text{for all } p \in P^h \quad (4.20)$$

where γ_3 is a positive constant independent of the element length h [19]. In order to stabilise equal order interpolations, Π denotes the projection operator for a projection onto the discontinuous polynomial space which is one order lower than the interpolation space for velocity and pressure and which is defined on the single elemental domains Ω_e , i.e.

$$\Pi p \in [P_m] = \{q \in L^2(\Omega) \mid q|_{\Omega_e} \in P_m(\Omega_e); \text{ for all } \Omega_e\}$$

where P_m denotes the polynomial space of order m .

The L^2 -projection is then given by

$$(r, \Pi p - p)_{\Omega_F} = 0 \quad \text{for all } r \in [P_m].$$

In order to remove the inf-sup deficiency (4.19) and hence stabilise the discrete weak problem the bilinear form

$$\mathbf{q}^T \mathbf{C} \mathbf{p} := \frac{1}{2\nu} (p - \Pi p, q - \Pi q) \quad (4.21)$$

is added to the weak form of the incompressible STOKES equations (4.2). Due to the discontinuity of the projection the stabilised method fits into a finite element code with just minor modifications on element level. Analogously to (4.3) the discrete stabilised problem reads

$$\begin{bmatrix} \mathbf{M}^F + \delta \mathbf{K}^F & \delta \mathbf{G} \\ \delta \mathbf{G}^T & -\delta \mathbf{C} \end{bmatrix} \begin{bmatrix} \mathbf{u} \\ \mathbf{p} \end{bmatrix} = \begin{bmatrix} \mathbf{f}^F \\ \mathbf{0} \end{bmatrix},$$

which shows that the polynomial pressure projection allows to retain the symmetry of the STOKES problem. Further the method does not require to calculate higher order derivatives and comes along without the need for a stabilisation parameter. It might, however, be useful to scale the amount of stabilisation introduced. Such a scaling allows to use the amount of stabilisation required to avoid zero pressure modes while ensuring that the continuity equation is not relaxed more than necessary. However the proper amount of stabilisation is hard to determine and it might be regarded a disadvantage of the method that the additional terms do not vanish when the analytical solution is inserted into the weak form. Unlike residual based stabilisation methods it is thus not consistent.

4.3 Residual based stabilisation methods

Residual based stabilisation methods have been developed in order to combine consistency and accuracy for transport problems with considerable advection. Suggested by HUGHES and coworkers first in the context of advective-diffusion equation [135] the SUPG method was developed. Similar methods have been proposed by the same group in order to circumvent the LBB condition in the STOKES problem [139]. A combination of these two ideas in order to stabilise the incompressible NAVIER-STOKES equations goes back to TEZDUYAR et al. [219], where the approach was termed SUPG/PSPG (Streamline Upwind PETROV-GALERKIN/Pressure Stabilised PETROV-GALERKIN). A review of the

history of residual based stabilisation methods can be found in BREZZI et al. [33], the book by DONEA and HUERTA [69] or also in the comprehensive dissertation of WALL [227]. Also the encyclopedia article by HUGHES et al. on multiscale and stabilised methods [143] should be mentioned in this context. An overview of stabilised finite element methods for the advection-diffusion problem and the history thereof has recently been given by FRANCA et al. [94].

A close relationship between residual based stabilisation and a standard GALERKIN approach enriched with bubble functions has been established by BREZZI et al. [31] and further elaborated for example in [6, 34]. Basing on this insight the so-called unusual stabilised finite element method (USFEM) has been proposed by FRANCA and coauthors [91, 92, 96]. A comparison of stabilisation methods for the advection-diffusion equation has been given by CODINA in [47] where the close relationship of different stabilisation methods is highlighted. It is shown in [47] that most classical stabilisation methods can be written as residual based approaches and differ mainly in the stabilisation operator and the stabilisation parameter. CODINA also contributed significantly to the analysis of these methods, so in [17, 48, 51, 53, 55, 57].

Residual based stabilisation methods are closely related to error estimation as the stabilisation is designed such that optimal convergence rates can be achieved. This connection of error analysis and design of finite element methods yields numerical schemes that require mesh dependent terms [116]. A basic introduction to finite element error analysis can be found in [210] where STEWART and HUGHES also give special attention to the advection-diffusion equation. A recent note of ZIENKIEWICZ sheds light on the background of error estimation in prose rather than by formulas [235]. A posteriori error estimation in least-squares stabilised finite element schemes has been covered by RANACHER in [201] and more recently HAUKE et al. considered a posteriori error estimation in a variational multiscale approach in [122].

Recent developments of residual based stabilisation methods include the work by CODINA and coworkers who proposed to use orthogonal subscales for stabilisation [50, 52, 53, 58]. WHITING et al. used a hierarchical basis to formulate stabilised methods [232, 233]. A comparison of the classical residual based SUPG/PSPG method and recent developments of symmetric stabilisation techniques has been published by BRAACK et al. [27]. In this paper the generalised OSEEN problem is analysed in a fixed grid setting.

Very few analysis can be found of numerical schemes considering stabilised finite element methods on deforming ALE domains one of which is a very recent paper of BADIA and CODINA [5]. Applications of a stabilised ALE formulations for fluid-structure interaction or problems with moving boundaries have been reported by KHURRAM and MASUD [154] and TEZDUYAR [217].

Within the present work residual based stabilisation is employed and analysed in the context of ALE methods. Additional parameters are introduced in order to ensure that no destabilising effect results from the coexistence of stabilisation terms and domain motion.

4.3.1 Virtual bubbles

A derivation of the stabilising terms from bubble elimination of a classical BUBNOV-GALERKIN scheme appears to be the least miraculous one. This derivation reveals that the stabilising terms can be interpreted as statically condensed bubbles, i.e. the effect

of smaller scales. The term *virtual bubbles* was first used by BAIOCCHI et al. [6] and indicates that an enrichment by bubble functions which are not specifically defined is used to achieve the desired stabilisation properties. BAIOCCHI et al. show that under certain conditions there exists a bubble the static condensation of which yields the stabilisation term of interest.

The derivation of a stabilisation method from bubble enrichment makes use of the linearity of the underlying operator and is thus performed on the advection-diffusion equation (2.54). In accordance with the scope of this work this derivation is performed on the convective ALE formulation of the model problem. Thus domain motion is considered which yields an additional term compared to fixed grid stabilisation methods.

The weak form of the temporally discretised advection-diffusion on a deforming domain is given by equation (3.47) reading

$$a(\phi, \omega) = (r^{n+1}, \omega)_{\Omega_{n+1}}$$

where the bilinear form $a(\phi, \omega)$ contains an inertia term, a convective term and the viscous contribution according to

$$a(\phi, \omega) := (\phi, \omega)_{\Omega_{n+1}} + \delta \left((\mathbf{a}^{n+1} - \mathbf{u}^{\text{G},n+1}) \cdot \nabla \phi, \omega \right)_{\Omega_{n+1}} + \delta \kappa (\nabla \phi, \nabla \omega)_{\Omega_{n+1}}. \quad (4.22)$$

The superscript $n + 1$ has been dropped on the unknown transport variable at the new time level for brevity.

Rather than approximating the unknown function ϕ and the weighting function ω by the usual piecewise polynomial functions (or mappings thereof into the physical space) the respective functions are now taken from the space

$$V_{\text{B}}^h = \{ \omega \in H^1(\Omega_0) \mid \omega|_{\Omega_{e,0}} \in P_k(\Omega_{e,0}) \oplus B(\Omega_{e,0}) \}, \quad (4.23)$$

defined over the reference domain, i.e. the elemental parameter spaces. V_{B}^h is enriched by element wise bubble functions $\omega_{\text{B}} \in B(\Omega_{e,0})$ satisfying homogeneous DIRICHLET boundary conditions on the elemental boundaries $\omega_{\text{B}} = 0$ on $\partial\Omega_{e,0}$. The linear independence of the polynomial and the bubble space allows an additional decomposition of the discrete trial and weighting functions according to

$$\phi^h = \phi_k + \phi_{\text{B}} \quad \text{and} \quad \omega = \omega_k + \omega_{\text{B}}. \quad (4.24)$$

Using the decomposition (4.24) in the weak form (3.47) allows to solve (at least formally) for the bubble degrees of freedom. Due to the bubble property of ω_{B} the bubble equations decouple and can be solved independently on the single elements where

$$a(\phi_k, \omega_{\text{B}}) + a(\phi_{\text{B}}, \omega_{\text{B}}) = (r^{n+1}, \omega_{\text{B}})_{\Omega_e} \quad (4.25)$$

has to be satisfied for all $\omega_{\text{B}} \in B$. Noting that after integrating the viscous term by parts

$$\delta \kappa (\nabla \phi_k, \nabla \omega_{\text{B}})_{\Omega_e} = \delta \kappa (\nabla \phi_k \cdot \mathbf{n}, \omega_{\text{B}})_{\partial\Omega_e} - \delta \kappa (\Delta \phi_k, \omega_{\text{B}})_{\Omega_e}$$

the elemental boundary term vanishes due to the zero boundary condition of ω_{B} on the element boundaries, (4.25) can be reformulated to

$$a(\phi_{\text{B}}, \omega_{\text{B}}) = (r^{n+1} - \phi_k - \delta (\mathbf{a}^{n+1} - \mathbf{u}^{\text{G},n+1}) \cdot \nabla \phi_k + \delta \kappa \Delta \phi_k, \omega_{\text{B}})_{\Omega_e}. \quad (4.26)$$

Equation (4.26) is a variational problem in the bubble space which has a unique solution. The right hand side driving the bubble on a single element can easily be recognised as the negative residual of the original advection-diffusion-reaction problem

$$\mathcal{R}(\phi_k) = \phi_k + \delta (\mathbf{a}^{n+1} + \mathbf{u}^{G,n+1}) \cdot \nabla \phi_k - \delta \kappa \Delta \phi_k - r^{n+1}$$

in the polynomial space (3.46). Hence whenever the polynomial space suffices to describe the correct solution within one element the contribution of the respective bubble vanishes. This property eventually transfers to the consistency of the stabilised finite element method derived.

The bubble in one particular element is then found by solving (4.26), i.e.

$$\phi_B = -\mathcal{S}_B \mathcal{P}_B (\mathcal{R}(\phi_k)), \quad (4.27)$$

where \mathcal{P}_B denotes the L^2 -projection onto the bubble space B and \mathcal{S}_B is the solution operator in the bubble space. In other words the magnitude of the bubble within one element is found by performing two steps. First the bubble which is closest to $\mathcal{R}(\phi_k)$ on the element e in a least-squares sense is searched. In a second step the negative of this bubble is taken as the right hand side of an advection-diffusion problem in the bubble space on the element and this problem is solved as indicated by the solution operator \mathcal{S}_B .

The so found bubble ϕ_B can now be used in the second part of the weak form which is weighted by the polynomial test function ω_k .

$$a(\phi_k, \omega_k) = (r^{n+1}, \omega_k)_{\Omega_{n+1}} - a(\phi_B, \omega_k)$$

After integrating some terms by parts and inserting (4.27), the discrete weak problem reads: find ϕ_k in P_k such that

$$a(\phi_k, \omega_k) = (r^{n+1}, \omega_k)_{\Omega_{n+1}} + (\mathcal{S}_B \mathcal{P}_B (\mathcal{R}(\phi_k)), \mathcal{L}^{\text{stab}}(\omega_k)) \quad \text{for all } \omega_k \in P_k \quad (4.28)$$

is satisfied, where the operator $\mathcal{L}^{\text{stab}}$ is given by

$$\mathcal{L}^{\text{stab}} \omega_k = (1 + \delta \nabla \cdot \mathbf{u}^{G,n+1}) \omega_k - \delta (\mathbf{a} - \mathbf{u}^{G,n+1}) \cdot \nabla \omega_k - \delta \kappa \Delta \omega_k. \quad (4.29)$$

In equation (4.28) the weak formulation of the original advection-diffusion equation is augmented by the perturbation term $(\mathcal{S}_B \mathcal{P}_B (\mathcal{R}(\phi_k)), \mathcal{L}^{\text{stab}}(\omega_k))$ providing additional stability. On a fixed grid, where the mesh velocity vanishes the operator $\mathcal{L}^{\text{stab}}$ is the adjoint of the original advection-diffusion operator.

It has been shown by BAIOCCHI et al. [6] that under certain conditions there exists a bubble space B such that

$$(\mathcal{S}_B \mathcal{P}_B (\mathcal{R}(\phi_k)), \mathcal{L}^{\text{stab}}(\omega_k))_{\Omega_e} = (\tau_e \mathcal{R}(\phi_k), \mathcal{L}^{\text{stab}}(\omega_k))_{\Omega_e}, \quad (4.30)$$

i.e. the projection of $\mathcal{R}(\phi_k)$ onto the bubble space, the subsequent solution of the bubble problem on the element and a projection back into the space of the operator $\mathcal{L}^{\text{stab}}$ reproduces a linear operator for a particular bubble function.

Assuming that such a bubble has been chosen and inserting (4.30) back into (4.28) yields the stabilised weak problem to find $\phi_k \in P_k$ such that

$$a(\phi_k, \omega_k) - \sum_e (\tau_e \mathcal{R}(\phi_k), \mathcal{L}^{\text{stab}}(\omega_k))_{\Omega_e} = (r^{n+1}, \omega_k)_{\Omega_{n+1}} \quad (4.31)$$

is satisfied. The effect of the bubble is now condensed in the elemental stabilisation parameter τ_e which will be discussed in section 4.3.7.

Remark 4.3.1 A similar approach also works to derive stabilisation terms for the incompressible STOKES problem [7].

Remark 4.3.2 The stabilisation operator (4.29) derived for the model problem on a deforming domain contains the divergence of the mesh velocity within the coefficient of the zeroth order term. This additional term is required to preserve the stability of the method if $\nabla \cdot \mathbf{u}^{G,n+1} < 0$ while it destabilises as soon as an element expands, i.e if $\nabla \cdot \mathbf{u}^{G,n+1} > 0$. It will thus be modified within the stabilisation of the NAVIER-STOKES equations.

Remark 4.3.3 The virtual bubble approach is frequently also termed concept of residual-free bubbles as for example in [138, 205]. However the latter term is somewhat misleading as it suggests that an analytical fine scale solution - at least on the elemental level - is available which hardly happens to be the case in real-world problems.

4.3.2 A look beyond – the variational multiscale method

The virtual bubble derivation of a stabilised finite element method reveals that residual based stabilisation can be regarded a special application of a much wider approach, the variational multiscale method. The method was proposed by HUGHES in 1995 [133] and is a very general tool to treat physical problems the solution of which exhibits a multiscale behaviour.

The basic idea of the variational multiscale method is a split of the trial and weighting spaces into subspaces referring to different scales [133, 138]. Initially the method was proposed in order to design formulations which treat large resolved scales in the usual way while additional terms are considered accounting for the effect of the small, unresolved scale upon the larger ones of interest. However, the method is by far not limited there. It allows a split of the solution into more than two scales. For instance a three level method for the incompressible NAVIER-STOKES equations has been developed by GRAVEMEIER [103, 105, 106]. There a distinction is made between large resolved scales, small resolved scales and unresolved scales.

A key application of the variational multiscale method is turbulent flow where a wide range of scales is involved. A large eddy simulation developed from the variational multiscale method was proposed by HUGHES and coworkers [141, 142] and also the work of GRAVEMEIER [103, 106] treats turbulent flows. A state of the art review on the variational multiscale method for laminar and turbulent flow can be found in [104]. However, the variational multiscale method is not at all limited to fluid mechanics. Applications to structural problems include the development of methods for incompressible materials [178, 177] or also the modelling of structural nonlinearities caused by phenomena on different scales as done in [145]. An overview of state of the art contributions to the theory of multiscale and stabilised methods can be found in the special issue edited by FRANCA [90].

In the light of the variational multiscale method the stabilisation term in (4.31) can be interpreted as the influence of unresolved fine scales upon the resolved scale represented by the polynomial finite element space V^h . However it has to be kept in mind that two important simplifications have been made in order to arrive at (4.31). Firstly the static elimination of the bubble terms relies on the assumption that the fine scale contribution is

local, i.e. restricted to each element. A second simplification is less obvious. Introducing one stabilisation parameter per element effectively reduces the fine-scale space within each element to a one-dimensional space. Consequently the stabilisation term is far from representing the effect of the unresolved scales *exactly*.

Nevertheless the derivation of stabilisation terms from a variational multiscale approach reveals that these additional terms are an appropriate model of fine scale effects rather than a purely numerical or arbitrary stabilisation tool.

4.3.3 Generalisation and relatives

The stabilisation method resulting from the virtual bubble approach can be extended and generalised to a wider class of methods which are used within the present work. Applying the stabilisation obtained in the previous section to the incompressible flow problem of interest yields the variational problem of finding $\mathbf{u} \in \mathbf{V}_{F,n+1}^h$, $p \in P_{n+1}^h$ such that

$$\begin{aligned} B_{\text{gal}}(\{\mathbf{u}, p\}, \{\mathbf{v}, q\}) &= \sum_e (\tau_{Me} \mathcal{R}_M(\mathbf{u}, p), \mathcal{L}_M^{\text{stab}}(\mathbf{u}, \{\mathbf{v}, q\}))_{\Omega_e} \\ &+ \sum_e (\tau_{Ce} \mathcal{R}_C(\mathbf{u}), \mathcal{L}_C(\mathbf{v}))_{\Omega_e} \\ &= (\mathbf{r}^{n+1}, \mathbf{v})_{\Omega_F^{n+1}} + (\mathbf{h}^{n+1}, \mathbf{v})_{\Gamma_{F,N}^{n+1}} \quad \text{for all } (\mathbf{v}, q) \in (\mathbf{V}_{F,0,n+1}^h, P_{n+1}^h), \end{aligned} \quad (4.32)$$

where e counts all elements of the triangulation. The GALERKIN weak form B_{gal} in (4.32) is the one defined in (3.22). The first stabilisation term in the above weak formulation corresponds to the one obtained in (4.31) while the latter one introduced by FRANCA and HUGHES [95] provides additional stability at high REYNOLDS numbers [12].

The residual of the momentum equation in convective form and the residual of the continuity equation at the new time level read

$$\mathcal{R}_M(\mathbf{u}, p) = \mathbf{u} + \delta [(\mathbf{u} - \mathbf{u}^{G,n+1}) \cdot \nabla \mathbf{u} - 2\nu \nabla \cdot \boldsymbol{\varepsilon}(\mathbf{u}) + \nabla p] - \mathbf{r}^{n+1}, \quad (4.33)$$

$$\mathcal{R}_C(\mathbf{u}) = \nabla \cdot \mathbf{u}, \quad (4.34)$$

which can be regarded purely spatial differential equations. It has to be remarked there that the unknown velocity and pressure field at the new time level is denoted by \mathbf{u} and p for clarity. Data and right hand side terms remain labelled by a time level superscript.

As well as the residuals the stabilisation operators are based upon the temporally discretised equation. The general form of the momentum stabilisation operator which is considered here is given by

$$\mathcal{L}_M^{\text{stab}}(\mathbf{u}, \{\mathbf{v}, q\}) = r_G \eta \mathbf{v} + \delta [-(\mathbf{u} - \mathbf{u}^{G,n+1}) \cdot \nabla \mathbf{v} - \alpha 2\nu \nabla \cdot \boldsymbol{\varepsilon}(\mathbf{v}) + \beta \nabla q] \quad (4.35)$$

while

$$\mathcal{L}_C^{\text{stab}}(\mathbf{v}) = \mathcal{L}_C(\mathbf{v}) = \nabla \cdot \mathbf{v} \quad (4.36)$$

is used on the continuity equation. In contrast to the convective term in (4.36) a bubble condensation yields a term of the form

$$-\nabla \cdot ((\mathbf{u} - \mathbf{u}^{G,n+1}) \otimes \mathbf{v})$$

as it can be observed from (4.29). This term is reformulated to

$$-\nabla \cdot ((\mathbf{u} - \mathbf{u}^{G,n+1}) \otimes \mathbf{v}) = -\nabla \cdot (\mathbf{u} - \mathbf{u}^{G,n+1}) \mathbf{v} - (\mathbf{u} - \mathbf{u}^{G,n+1}) \cdot \nabla \mathbf{v} \quad (4.37)$$

and the first contribution on the right hand side of (4.37) is added to the zeroth order term of $\mathcal{L}_M^{\text{stab}}$, i.e. it is included in the effective reaction coefficient r_G . However, while the divergence of the convective velocity $\mathbf{u} - \mathbf{u}^{G,n+1}$ helps to ensure stability for $\nabla \cdot (\mathbf{u} - \mathbf{u}^{G,n+1}) > 0$ it may spoil stability if $\nabla \cdot (\mathbf{u} - \mathbf{u}^{G,n+1}) < 0$. Thus the effective reaction coefficient r_G in (4.35) is defined by

$$r_G = \min(1 - \delta \nabla \cdot (\mathbf{u} - \mathbf{u}^{G,n+1}), 1). \quad (4.38)$$

The influence of r_G on the stability of the stabilised problem will be discussed again in section 4.4.

The parameters $\alpha \in \{-1, 0, 1\}$ and $\eta \in \{1, 0\}$ within the general operator (4.35) along with the previously introduced β from equation (3.22) allow to distinguish a variety of closely related but different stabilisation methods. An overview over the properties of the different schemes in the case of the stationary STOKES problem has been given by BOCHEV in [8]. All of the possible methods are consistent in the sense that sufficiently smooth solutions of the strong equations (3.15) and (3.16) satisfy the stabilised discrete form (4.32).

Due to the nonlinearity of the NAVIER-STOKES equations the stabilisation operator (4.35) depends on the unknown velocity field \mathbf{u} and hence adds to the nonlinearity of the stabilised equation. As a result all coefficient matrices of the stabilised discrete fluid equations depend on the velocity.

Two terms of the momentum stabilisation operator (4.35) are of particular importance. The first one is the gradient of the weighting function for the pressure which provides pressure stabilisation. A residual based stabilisation of the STOKES problem where the stabilisation operator is given by ∇q has been termed PSPG, Pressure Stabilised PETROV-GALERKIN method. The second necessarily required contribution of the stabilisation operator is the convective term serving to stabilise convection induced wiggles. Using this term exclusively to stabilise advective problems yields the SUPG method [136]. The zeroth order term given in the first line of the stabilisation operator (4.35) is of particular importance in the context of very small time steps and will be considered in section 5.2. All the remaining terms in (4.35) do not directly contribute to stabilise the problem and can thus be played around with which yields an entire family of stabilisation methods. The notation employed within this work to distinguish the single family members is summarised in Table 4.1.

- Using $\alpha = 1$, $\beta = -1$ and $\eta = 1$ on a fixed grid recovers the adjoint $\mathcal{L}_M^*(\mathbf{u}, \{\mathbf{v}, q\}) = \mathcal{L}_+^{\text{USFEM}}(\mathbf{u}, \{\mathbf{v}, q\})$ of the original temporally discretised NAVIER-STOKES momentum operator (3.15). This version of the method which is also termed *Unusual Stabilised Finite Element Method* (USFEM) was introduced by FRANCA and FARHAT in [91] and is closely related to bubble functions [6, 92]. Extending this notation within the present work all methods with $\alpha = 1$ within the operator (4.35) shall be denoted by the superscript ‘USFEM’.
- On a fixed mesh the negative of the original operator can be recovered by setting $\eta = -1$, $\alpha = -1$ and $\beta = -1$ which would thus yield the correct GLS version of the

stabilisation. However, as will be shown in section 5.2 $\eta = -1$ further increases instabilities due to dominating zeroth order terms and thus yields an unstable method. Nevertheless modified GLS versions are of interest with $\eta \in \{1, 0\}$ where the superscript ‘GLS’ subsequently denotes all stabilisation methods of the type (4.32) with $\alpha = -1$.

- As the required stabilisation of convection and pressure instabilities is independent of the zeroth order weighting term within the stabilisation operator it appears interesting to consider also stabilisation by operators which are derived from the corresponding stationary problem i.e. $\eta = 0$. The subscript ‘+’ or ‘0’ at the stabilisation operator or the stabilised form refers to the sign of η and denotes the full or stationary operator, respectively.

Table 4.1: Notation used to distinguish different versions of the stabilisation operator

notation	α	η	stabilisation operator
$\mathcal{L}_+^{\text{USFEM}}$	1	1	$r_G \mathbf{v} + \delta \left(- \left(\mathbf{u} - \mathbf{u}^{\text{G},n+1} \right) \cdot \nabla \mathbf{v} - 2\nu \nabla \cdot \boldsymbol{\varepsilon}(\mathbf{v}) - \nabla q \right)$
$\mathcal{L}_+^{\text{GLS}}$	-1	1	$r_G \mathbf{v} + \delta \left(- \left(\mathbf{u} - \mathbf{u}^{\text{G},n+1} \right) \cdot \nabla \mathbf{v} + 2\nu \nabla \cdot \boldsymbol{\varepsilon}(\mathbf{v}) - \nabla q \right)$
$\mathcal{L}_0^{\text{USFEM}}$	1	0	$\delta \left(- \left(\mathbf{u} - \mathbf{u}^{\text{G},n+1} \right) \cdot \nabla \mathbf{v} - 2\nu \nabla \cdot \boldsymbol{\varepsilon}(\mathbf{v}) - \nabla q \right)$
$\mathcal{L}_0^{\text{GLS}}$	-1	0	$\delta \left(- \left(\mathbf{u} - \mathbf{u}^{\text{G},n+1} \right) \cdot \nabla \mathbf{v} + 2\nu \nabla \cdot \boldsymbol{\varepsilon}(\mathbf{v}) - \nabla q \right)$

Remark 4.3.4 It has been shown by CODINA that subscale based methods, which in the present context corresponds to the USFEM version of the stabilisation are superior in the sense that the stabilisation is invariant with respect to a change of variables when used for linear systems of convection-diffusion-reaction equations [49].

Remark 4.3.5 An interesting method extending the concept of virtual bubble stabilisation has recently been proposed by CODINA and coworkers [52, 57]. Deriving a stabilised method for the incompressible NAVIER-STOKES equations they not only pay special attention to the nonlinear term which opens a door to turbulence but also suggest to track the fine scale solution, i.e. the bubble part, in time. The approach can be regarded to be turned over half way from a stabilised method to a full multiscale formulation. On the price of additional internal variables representing the subscales at previous time levels this approach offers an elegant way to abolish the dependency of a stationary solution on the time step size otherwise inherent in stabilised methods and offers the hope for more temporal accuracy.

Remark 4.3.6 An alternative to deriving a stabilised formulation from elimination of virtual bubble degrees of freedom is to regard it as a PETROV-GALERKIN type of discretisation method where the weighting function for the velocity is $\tilde{\mathbf{v}} = \mathbf{v} - \tau_{\text{Me}} \mathcal{L}_M^{\text{stab}}(\mathbf{u}, \{\mathbf{v}, q\})$ rather than \mathbf{v} and the modified pressure test function reads $\tilde{q} = q + \tau_{\text{Ce}} \mathcal{L}_C^{\text{stab}}(\mathbf{v})$.

Remark 4.3.7 A comment on equal order interpolation for velocity and pressure in the context of residual based stabilisation appears appropriate here. It has already been mentioned that relaxation of the incompressibility condition yields advantages with respect to an iterative solution of the resulting system of equations. From the initial discussion of the present chapter it is further obvious that LBB stable elements might well still require

stabilisation whenever it comes to highly convective flows. It is thus regarded a particular advantage of residual based stabilisation methods that both potential instabilities are treated within a unified framework which is further consistent at least for higher order elements.

Reconsidering the derivation of residual based stabilisation from virtual bubble functions further shows that the principal difference of the present stabilised finite element and LBB stable elements is not as fundamental as it might seem at the first sight. A popular way to stable elements is to enhance an unstable one with internal velocity degrees of freedom such as the first order MINI element which is enriched by a cubic bubble. Static condensation of such internal degrees of freedom yields terms that might be termed *stabilisation*.

4.3.4 A comment on conservation in stabilised problems

It appears interesting to reconsider the issue of conservation of linear momentum for the stabilised discrete problem. Here strict equivalence of convective and divergence formulation is lost as the continuity equation is relaxed by stabilisation terms rather than weakly satisfied. Thus conservation of linear momentum in the sense that the acceleration of a portion of fluid is exactly balanced by the integral forces over the boundaries is approximated rather than strictly satisfied.

An approach to reestablish conservation in the context of a stabilised method appears first in a paper by TAYLOR et al. [211], can be found in the dissertation of WHITING [231] and is eventually explained in a paper by HUGHES and WELLS [144]. There it is shown how global conservation can approximately be preserved through a small residual-based modification of conventional stabilised formulations. This correction is based on multiscale considerations and the fact that an elemental fine-scale velocity is approximated by the negative coarse-scale residual within this element weighted by the stabilisation parameter. However the additional term which is introduced to reestablish conservation is of advective type and needs to be stabilised itself. Consequently further higher order stabilisation terms enter the formulation.

Within the present work the modification of HUGHES and WELLS has not been used. Conservation while being desirable is not a crucial matter for viscous flows at low or moderate REYNOLDS numbers. Thus the price of further stabilisation terms including an additional stabilisation parameter appears to high for the gain of a closer approximation of conservation.

It has also to be mentioned that these additional terms include second derivatives of the velocity and its weighting function. Consistency of the method including the effect of largely restored conservation can thus be expected only for higher order elements.

4.3.5 Stabilised equal order elements and discretely divergence free functions

Prior to proceeding with a matrix notation of the stabilised discrete flow problem a somewhat un-pleasing issue shall be discussed. It has been mentioned in chapter 2 that an initial velocity field needs to be divergence free to define a well posed problem. In the

discrete setting this demands that the initial velocity field has to be discretely divergence free in the sense imposed by the corresponding LAGRANGE multiplier space, i.e. the space of the pressure.

Stabilisation opens the way for a broad variety of velocity and pressure space combinations. However at the same time this complicates the important issue of correct initial conditions. This question also arises whenever a velocity field has to be mapped from one mesh to another, i.e. when remeshing takes place. A closely related matter is the determination of the unavoidable interpolation error on a given mesh or - which is essentially the same problem - the norm in which a certain discrete solution is optimal.

Whenever LBB stable elements are employed an appropriate discrete initial velocity field $\mathbf{u}^{0,h}$ is obtained from a L^2 -projection of a known velocity field \mathbf{u}^0 under the constraint of incompressibility. This condition is imposed by a LAGRANGE multiplier field spanned by the same functions as the discrete pressure. Thus $\mathbf{u}^{0,h} \in \mathbf{V}_E^h$ and $\lambda \in P^h$ are determined from a stationary point of the augmented functional

$$\Pi(\mathbf{u}^{0,h}, \lambda) = \frac{1}{2} \|\mathbf{u}^{0,h} - \mathbf{u}^0\|^2 - (\nabla \cdot \mathbf{u}^{0,h}, \lambda), \quad (4.39)$$

where the discrete space \mathbf{V}_E^h contains all those functions that satisfy the normal component of the velocity boundary condition $\mathbf{n} \cdot \mathbf{u}^{0,h} = \mathbf{n} \cdot \mathbf{u}^0$ on $\Gamma_{F,D}$ in an appropriate weak sense. A variation of the functional (4.39) yields the saddle point problem

$$\begin{aligned} (\mathbf{u}^{0,h} + \nabla \lambda, \mathbf{v}) - (\mathbf{n} \cdot \mathbf{v}, \lambda)_{\Gamma_{F,N}} &= (\mathbf{u}^0, \mathbf{v}) \\ - (\nabla \cdot \mathbf{u}^{0,h}, q) &= 0, \end{aligned} \quad (4.40)$$

where $\mathbf{v} \in \mathbf{V}_0^h$ and $q \in P^h$ denote the variation of the velocity field and LAGRANGE multiplier, respectively.

Equivalently to the incompressible NAVIER-STOKES equations the mixed problem defined by (4.40) is unstable for combinations of the spaces \mathbf{V}_E^h and P^h that do not satisfy the LBB condition. Consequently (4.40) cannot be inverted for equal-order interpolation of velocity and pressure. A correct way to project a known initial velocity field to a particular mesh that works for stabilised finite elements with equal order interpolation could not be found in the literature. Apparently the problem is frequently circumvented rather than solved. Simulations are started from an incorrect (not discretely divergence free) initial condition and the corresponding peak in the pressure required to adjust the incompressibility within the next time step is simply ignored.

However the interpretation of stabilised methods in the virtual bubble context gives some hints how the problem should be tackled. If the virtual bubble space was known an admissible projection could be found by projecting onto a velocity in the discrete polynomial space enriched by bubble functions \mathbf{V}_B^h . Such an approach could be formulated as a ‘stabilised projection’ and would allow to circumvent the LBB condition and to compute initial conditions which are discretely divergence free in the sense that suits the discrete spaces of velocity and pressure which are used.

Unfortunately the shape of the virtual bubble remains untold. Consequently the certainly unsatisfactory start from an ill posed problem has to be chosen whenever an initial velocity field is required. Most simulations however start from a zero velocity field and demand a starting phase.

Nevertheless the issue of correct projection onto a velocity field which is divergence free in a proper weak sense is of higher interest as it might seem at the first glance. An L^2 -projection like (4.40) does not require that the original velocity field \mathbf{u}^0 is solenoidal. In order to abbreviate the start phase of a fluid or FSI simulation a function \mathbf{u}^0 might thus be constructed that satisfies the DIRICHLET boundary conditions and is as close as possible to an estimated velocity function within the domain. A projection of such a function onto a discretely divergence free vector field could possibly serve as a good initial condition and is potentially much faster than accelerating the flow from zero.

4.3.6 Stabilised formulation in matrix notation

Evaluating the weak form (4.32) with discrete finite element spaces $\mathbf{V}_{F,n+1}^h$ and P_{n+1}^h spanned by nodal based polynomial functions allows to obtain a discrete matrix representation corresponding to (3.23) and (3.24) in the unstabilised case. The stabilised discrete matrix equations read

$$\overline{\mathbf{M}}^F(\mathbf{u})\mathbf{u} + \delta \overline{\mathbf{K}}^F(\mathbf{u})\mathbf{u} + \delta \overline{\mathbf{N}}(\mathbf{u}) + \delta \overline{\mathbf{G}}(\mathbf{u})\mathbf{p} = \overline{\mathbf{f}}_b^F + \mathbf{f}_h^F \quad (4.41)$$

$$\overline{\mathbf{G}}_M^T \mathbf{u} + \delta \overline{\mathbf{G}}_K^T(\mathbf{u})\mathbf{u} - \delta \overline{\mathbf{C}}\mathbf{p} = \overline{\mathbf{f}}_C, \quad (4.42)$$

where an top bar indicates that the respective matrix contains contributions emerging from stabilisation terms. Thus all matrices depend upon the stabilisation parameters τ_{Me} and such on the fluid viscosity, the flow regime and the time step size. Additionally the stabilisation adds different terms on the two \mathbf{G} -matrices and introduces an acceleration dependent term into the second line altogether destroying the formal symmetry of the system.

The stabilised mass matrix reads

$$\begin{aligned} \mathbf{v}^T \overline{\mathbf{M}}^F(\mathbf{u}) \mathbf{u} &= (\mathbf{u}, \mathbf{v})_{\Omega_F^{n+1}} - \eta \sum_e \tau_{Me} (\mathbf{u}, r_G \mathbf{v})_{\Omega_e} + \sum_e \tau_{Me} (\mathbf{u}, \delta (\mathbf{u} - \mathbf{u}^{G,n+1}) \cdot \nabla \mathbf{v})_{\Omega_e} \\ &+ \alpha \sum_e \tau_{Me} (\mathbf{u}, \delta 2\nu \nabla \cdot \boldsymbol{\varepsilon}(\mathbf{v}))_{\Omega_e}. \end{aligned}$$

The mass matrix contribution to the continuity equation is given by

$$\mathbf{q}^T \overline{\mathbf{G}}_M^T \mathbf{u} = -\beta \sum_e \tau_{Me} (\mathbf{u}, \delta \nabla q)_{\Omega_e},$$

while the stabilised viscous term is composed by the sum

$$\begin{aligned} \mathbf{v}^T \overline{\mathbf{K}}^F(\mathbf{u}) \mathbf{u} &= (2\nu \boldsymbol{\varepsilon}(\mathbf{u}), \boldsymbol{\varepsilon}(\mathbf{v}))_{\Omega_F^{n+1}} + \sum_e \tau_{Ce} (\nabla \cdot \mathbf{u}, \nabla \cdot \mathbf{v})_{\Omega_e} \\ &+ \eta \sum_e \tau_{Me} (2\nu \nabla \cdot \boldsymbol{\varepsilon}(\mathbf{u}), r_G \mathbf{v})_{\Omega_e} \\ &- \sum_e \tau_{Me} (2\nu \nabla \cdot \boldsymbol{\varepsilon}(\mathbf{u}), \delta (\mathbf{u} - \mathbf{u}^{G,n+1}) \cdot \nabla \mathbf{v})_{\Omega_e} \\ &- \alpha \sum_e \tau_{Me} (2\nu \nabla \cdot \boldsymbol{\varepsilon}(\mathbf{u}), \delta 2\nu \nabla \cdot \boldsymbol{\varepsilon}(\mathbf{v}))_{\Omega_e}, \end{aligned}$$

where the continuity stabilisation has been added. Further the convective part is determined from

$$\begin{aligned} \mathbf{v}^T \bar{\mathbf{N}}(\mathbf{u}) &= ((\mathbf{u} - \mathbf{u}^G) \cdot \nabla \mathbf{u}, \mathbf{v})_{\Omega_{\mathbb{F}}^{n+1}} - \eta \sum_e \tau_{Me} ((\mathbf{u} - \mathbf{u}^{G,n+1}) \cdot \nabla \mathbf{u}, r_G \mathbf{v})_{\Omega_e} \\ &\quad + \sum_e \tau_{Me} ((\mathbf{u} - \mathbf{u}^{G,n+1}) \cdot \nabla \mathbf{u}, \delta (\mathbf{u} - \mathbf{u}^{G,n+1}) \cdot \nabla \mathbf{v})_{\Omega_e} \\ &\quad + \alpha \sum_e \tau_{Me} ((\mathbf{u} - \mathbf{u}^{G,n+1}) \cdot \nabla \mathbf{u}, \delta 2\nu \nabla \cdot \boldsymbol{\varepsilon}(\mathbf{v}))_{\Omega_e}, \end{aligned}$$

while the discrete gradient operator in the stabilised case reads

$$\begin{aligned} \mathbf{q}^T \bar{\mathbf{G}}_K^T(\mathbf{u}) \mathbf{u} &= -\beta (\nabla \cdot \mathbf{u}, q)_{\Omega_{\mathbb{F}}^{n+1}} - \beta \sum_e \tau_{Me} ((\mathbf{u} - \mathbf{u}^{G,n+1}) \cdot \nabla \mathbf{u}, \delta \nabla q)_{\Omega_e} \\ &\quad + \beta \sum_e \tau_{Me} (2\nu \nabla \cdot \boldsymbol{\varepsilon}(\mathbf{u}), \delta \nabla q)_{\Omega_e}. \end{aligned}$$

The stabilised discrete divergence operator is given by

$$\begin{aligned} \mathbf{v}^T \bar{\mathbf{G}}(\mathbf{u}) \mathbf{p} &= -(p, \nabla \cdot \mathbf{v})_{\Omega_{\mathbb{F}}^{n+1}} - \eta \sum_e \tau_{Me} (\nabla p, r_G \mathbf{v})_{\Omega_e} \\ &\quad + \sum_e \tau_{Me} (\nabla p, \delta (\mathbf{u} - \mathbf{u}^{G,n+1}) \cdot \nabla \mathbf{v})_{\Omega_e} + \alpha \sum_e \tau_{Me} (\nabla p, \delta 2\nu \nabla \cdot \boldsymbol{\varepsilon}(\mathbf{v}))_{\Omega_e}, \end{aligned}$$

and the stabilising pressure matrix is obtained from

$$\mathbf{q}^T \bar{\mathbf{C}} \mathbf{p} = \beta \sum_e \tau_{Me} (\nabla p, \delta \nabla q)_{\Omega_e}.$$

Similar to the matrices also the right hand sides in (4.41) and (4.42) contain additional terms emerging from stabilisation. The right hand side vector of the momentum equation is a sum of two contributions the first of which stems from body forces and history terms along with the respective stabilisation and reads

$$\begin{aligned} \mathbf{v}^T \bar{\mathbf{f}}_b^F &= (\mathbf{r}^{n+1}, \mathbf{v})_{\Omega_{\mathbb{F}}^{n+1}} - \eta \sum_e \tau_{Me} (\mathbf{r}^{n+1}, r_G \mathbf{v})_{\Omega_e} + \sum_e \tau_{Me} (\mathbf{r}^{n+1}, \delta (\mathbf{u} - \mathbf{u}^{G,n+1}) \cdot \nabla \mathbf{v})_{\Omega_e} \\ &\quad + \alpha \sum_e \tau_{Me} (\mathbf{r}^{n+1}, \delta 2\nu \nabla \cdot \boldsymbol{\varepsilon}(\mathbf{v}))_{\Omega_e}, \end{aligned}$$

while the second accounts for external tractions

$$\mathbf{v}^T \bar{\mathbf{f}}_h^F = \delta (\mathbf{h}^{n+1}, \mathbf{v})_{\Gamma_{\mathbb{F},N}^{n+1}}.$$

Also the continuity equation gets a right hand side contribution from stabilisation terms reading

$$\mathbf{q}^T \bar{\mathbf{f}}_C = -\beta \sum_e \tau_{Me} (\mathbf{r}^{n+1}, \delta \nabla q)_{\Omega_e}.$$

It remains to remark that all the stabilisation terms have to be integrated over the actual element domain at time level $n + 1$.

Within the present work the above terms have been re-implemented into the research code at the Institute of Structural Mechanics `ccarat` including a linearisation of the stabilisation terms except the stabilisation parameters τ_{Me} and τ_{Ce} which have not been linearised. Consequently quadratic convergence within the flow solver is observed for problems with almost constant stabilisation parameters.

4.3.7 Stabilisation parameter

The stabilisation parameter is a crucial ingredient of the entire stabilised method. Consequently the method is frequently criticised for requiring a problem dependent parameter. However stable definitions of τ_{Me} and τ_{Ce} can be found which work well independently of the problem.

From convergence studies the required order of the stabilisation parameter $\tau_{M,e}$ has been obtained. According to the respective limit case $\tau_{M,e}$ has to satisfy

$$\tau_{Me} = O\left(\frac{h_e}{|\mathbf{u} - \mathbf{u}^G|}\right) \quad \text{for } \text{Re}^e \gg 1 \quad \text{and} \quad \tau_{Me} = O\left(\frac{h_e^2}{\nu}\right) \quad \text{for } \text{Re}^e \ll 1, \quad (4.43)$$

where Re^e denotes the elemental REYNOLDS number. In the limit of a dominating zeroth order term, i.e. if very small time steps are considered the stabilisation terms have to be proportional to δ . Thus for the present formulation which is based on time discretised operators τ_{Me} has to be of order one in δ .

Various definitions in particular for τ_{Me} have been proposed in the literature which in many cases exhibit just slight differences. Recent contributions to the proper evaluation of stabilisation parameters in the context of USFEM have been made by FRANCA and VALENTIN [96], BARRENECHEA and VALENTIN [7], CODINA [47, 51, 52, 58] as well as the group of TEZDUYAR [1, 214, 215, 216]. In [220] TEZDUYAR and OSAWA propose to determine stabilisation parameters directly from elemental matrices and vectors, i.e. circumventing the determination of element lengths.

Further comments on the history of the stabilisation parameter today widely known as τ can be found in the dissertation of WALL [227]. In every case a useful stabilisation parameter has to obey the limit behaviour according to (4.43). Numerical simulations indicate that on meshes up to moderate mesh distortion the influence of the particular choice of the stabilisation parameter is a minor issue provided that the parameter exhibits the correct overall asymptotics and excessive over-stabilisation is avoided.

The parameter used preferably within this work is a combination of the stabilisation parameter derived from bubble condensation by BARRENECHEA and VALENTIN for the linear STOKES problem in [7] and by FRANCA and VALENTIN for the reaction-advection-diffusion equation in [96]. The parameter which has been generalised within the present work to yield stable formulations in the ALE cases reads

$$\tau_{Me} = \min\left(\frac{h_e^2}{h_e^2 \xi_1 + \frac{4\delta\nu}{m_e} \xi_2}, \sigma_{0e}\right) \quad (4.44)$$

where the new elemental parameter σ_{0e} is the lower bound on the generalised reaction coefficient of the convective ALE formulation

$$\sigma_{0e} = \begin{cases} 1 - \delta/2 \max(\nabla \cdot (\mathbf{u} - \mathbf{u}^{\text{G},n+1})) & \text{for } \nabla \cdot (\mathbf{u} - \mathbf{u}^{\text{G},n+1}) > 0 \\ 1 & \text{for } \nabla \cdot (\mathbf{u} - \mathbf{u}^{\text{G},n+1}) \leq 0 \end{cases} . \quad (4.45)$$

For the fixed grid variant of the method just $\nabla \cdot \mathbf{u}$ has to be considered which is close to zero and so $\sigma_{0e} \approx 1$ and is thus hardly significant in (4.44). For deforming meshes the divergence is dominated by $\nabla \cdot \mathbf{u}^{\text{G},n+1}$ and thus the first line in (4.45) corresponds to contracting elements while the second line covers the case of expanding elements. In this case σ_{0e} will never be relevant in (4.44). On contracting elements, where $\nabla \cdot (\mathbf{u} - \mathbf{u}^{\text{G},n+1}) > 0$ the stability of the method is affected by the mesh motion and the influence of σ_{0e} has to be considered. Stability of convective ALE formulations with solenoidal convective velocity is conditional upon (3.52) as shown in section 3.5.1. For the present case this condition transfers to

$$1 - \delta \frac{1}{2} \max(\nabla \cdot (\mathbf{u} - \mathbf{u}^{\text{G},n+1})) > 0, \quad (4.46)$$

i.e. the discretisation error in the divergence of the fluid velocity has to be considered. From (4.46) it can be observed that the coefficient σ_{0e} is strictly positive.

The stabilisation parameter (4.44) obeys the asymptotics (4.43) and is strictly smaller than one. This is caused by the fact that discretisation in time was performed prior to discretisation in space and thus stabilisation is based upon the time discretised residuals and stabilisation operator.

The parameters ξ_1 and ξ_2 depend on the effects dominating the flow in a particular element according to

$$\xi_1 = \max(r^e, 1) \quad \xi_2 = \max(\text{Re}^e, 1), \quad (4.47)$$

where r^e denotes the ratio of the viscous, second order term to the zeroth order term introduced by the time integration. The ratios are obtained from

$$r^e = \frac{4\delta\nu}{m_e h_e^2} \quad \text{and} \quad \text{Re}^e = \frac{m_e |\mathbf{u} - \mathbf{u}^{\text{G}}| h_e}{2\nu}.$$

The elemental REYNOLDS number Re^e is evaluated at the element centre. The EUCLIDIAN norm of the velocity $|\mathbf{u} - \mathbf{u}^{\text{G}}|$ is a measure of the convective term, where the parameter m_e carries the influence of the particular discretisation. It is defined by (see also FRANCA and VALENTIN [96])

$$m_e = \min\left(\frac{1}{3}, C_e\right) \quad (4.48)$$

where C_e is the largest constant satisfying the inverse estimate

$$C_e h_e^2 \|\Delta \mathbf{v}\|_{\Omega_e}^2 \leq \|\nabla \mathbf{v}\|_{\Omega_e}^2 \quad \text{for all } \mathbf{v} \in \mathbf{V}_{\text{F},e}^h, \quad (4.49)$$

and $\mathbf{V}_{\text{F},e}^h$ denotes the restriction of the discrete space \mathbf{V}_{F}^h to the element e . The exact determination of m_e and thus the sharp constant C_e is discussed in section 5.3.1.

According to the estimates presented by HARARI and HUGHES in [116], $m_e = 1/3$ and $m_e = 1/12$ is used for linear and quadratic elements, respectively. However USFEM simulations rely on the correct parameter m_e according to (4.48) in order to guarantee a stable method. The determination of the correct constant C_e in (4.49) will be discussed subsequently in the context of distorted elements in section 5.3.1.

For the stabilisation parameter of the continuity equation τ_{C_e} the definition presented by CODINA in [52] is adopted reading

$$\tau_{C_e} = \delta \sqrt{4\nu^2 + \left(\frac{c_2}{c_1} |\mathbf{u} - \mathbf{u}^G| h_e \right)^2} \quad (4.50)$$

which has been derived from a FOURIER analysis. The constants c_1 and c_2 satisfy $c_2^2 \leq c_1$ and are explained further in [52]. Within the simulations presented in this work $c_1 = 2.0$ and $c_2 = 1.0$ have been used. Analogously to τ_{M_e} the parameter τ_{C_e} is evaluated once at the element centre and therefore treated as an elemental constant.

As the stabilised method is defined on the temporally discretised equation (3.15) and residual (4.33) the time discretisation parameter δ enters the stabilisation parameter. In the case of a stationary operator (i.e. $\eta = 0$) the entire stabilisation operator is multiplied by the factor δ stemming from temporal discretisation. Absorbing this factor into the stabilisation operator τ_{M_e} yields a stabilisation parameter of the dimension of a time, the familiar ‘intrinsic time scale’. However as also the full stabilisation operator containing a zeroth order term shall be considered the dimensionless stabilisation parameter (4.44) is preferred here.

4.3.8 Element length definitions

The characteristic element length h_e has a potentially significant impact on the actual amount of stabilisation employed as at the viscous limit the stabilisation parameter is proportional to h_e^2 while it is linear in the element length at the convective limit. Especially in the context of mesh distortion or highly elongated elements the element length definition has to be chosen carefully [181].

Various definitions have been suggested and discussed in the literature. An overview can be found in [227] where it is suggested to use different element lengths within the different terms. A geometric ‘isotropic’ element length definition (for example the square root of the elemental area) is suggested when the viscous terms dominate, while a stream-length is used for convection dominated flows. In chapter 5 a variety of definitions for the characteristic element lengths are compared by numerical investigations. The single definitions are

- i. square root of element area, i.e. $h_e = \sqrt{A_e}$
- ii. element length in flow direction according to [227] evaluated once at element centre,
- iii. approximate element length in flow direction as defined by CODINA in [58] $h_k = h_0 |\mathbf{u}| / |\mathbf{u}_0|$, where the subscript 0 refers to the reference configuration, and
- iv. element length for anisotropic meshes as defined by CODINA in [58], where the smallest eigenvalue of the operator \mathbf{B} is taken as characteristic element length. \mathbf{B}

stems from the polar decomposition of the JACOBIAN \mathbf{J} of the isoparametric mapping to the element domain, i.e. $\mathbf{J} = \mathbf{B}\mathbf{Z}$, where \mathbf{B} is symmetric and positive-definite while \mathbf{Z} is orthogonal.

Further an implicit definition of the element length which has been suggested by TAYLOR et al. [211] shall also be considered.

- v. Employing the covariant coordinates of the metric tensor g_{ij} of the mapping from global Cartesian coordinates to the element parameters the stabilisation parameter is given by

$$\tau_{Me} = \left(4 + \delta^2 (u_i g_{ij} u_j + c \nu^2 g_{ij} g_{ij})\right)^{-\frac{1}{2}},$$

where the constant c is set to 36 and to 60 for linear and quadratic elements, respectively [231, 232]. The corresponding stabilisation parameter for the continuum equation is given by

$$\tau_{Ce} = (8 \tau_{Me} \text{tr}(g_{ij}))^{-1}.$$

Additionally the element length definitions investigated by MITTAL [181] are considered as parts of the computations reported in [181] are repeated in section 5.3. These definitions are

- vi. minimal element length given by

$$h_e = h_{e,\min} = \frac{\sqrt{2}A_e}{\max(h_{\text{diag}})} \quad (4.51)$$

- vii. maximal element length defined as the edge length of a square with a diagonal of $\max(h_{\text{diag}})$

$$h_e = h_{e,\max} = \frac{\max(h_{\text{diag}})}{\sqrt{2}} \quad (4.52)$$

While the element length definitions i., iv. and v. to vii. are purely geometrical the stream-length (ii. and iii.) depends upon the velocity and hence adds to the overall nonlinearity. Consequently the convergence rate of the fluid iterations decreases when these stabilisation parameters are employed. In complex situations convergence may even be lost. In order to fix this problem linearisation of the stabilisation parameter with respect to the velocity could be performed. Numerical observations indicate however that streamlength computation is not essential and geometrical definitions of the characteristic element length may work equally well.

4.3.9 Residual based stabilisation and linear elements

The discrete finite element spaces \mathbf{V}_F^h and P^h within the stabilised form (4.32) can be of arbitrary polynomial order. Nevertheless the cheapest and most popular version is to use linear elements. However such elements do not allow to properly represent second

derivatives contained in the residual. Thus the residual of the momentum equation which is effectively ‘felt’ within the stabilisation terms of linear elements reduces to

$$\mathcal{R}_M^{\text{lin}}(\mathbf{u}, p) = \mathbf{u} + \delta \left((\mathbf{u} - \mathbf{u}^{\text{G},n+1}) \cdot \nabla \mathbf{u} + \nabla p \right) - \mathbf{r}^{n+1}.$$

The incompletely resolved second derivatives are included not only in the residual but also within the stabilisation operator as soon as USFEM or GLS type of stabilisation is employed (i.e. $\alpha \neq 0$). Numerical observations indicate that these derivatives in the weighting term are an additional source of inaccuracy if bilinear or trilinear elements are employed.

As the so introduced consistency error scales with the stabilisation parameter τ_{Me} it diminishes at spatial or temporal refinement. While not affecting convergence rates it is present for particular discretisations with linear elements. Thus in such simulations a portion of the error is observed which scales directly with the stabilisation parameter. Consequently it is of particular importance to employ a stabilisation parameter as small as possible when linear elements are used in conjunction with residual based stabilisation methods. However a lower bound on the stabilisation parameter is required to prevent artificial pressure modes resulting from the violation of the inf-sup condition.

Improvements which reintroduce some influence of the viscous part of the residual have been suggested by JANSEN et al. in [147] while such modifications fall into the category of ‘variational crimes’. One way to cope with linear elements and residual based stabilisation responsibly could be to control the stabilisation parameter, i.e. to ensure that the maximal amount of stabilisation within an element is limited to a tolerable amount. However this would not only require to define the tolerable amount of stabilisation but also yield frequent mesh refinement as soon as steeper gradients evolve in the solution. It thus appears worth to pay the price and go for higher order elements instead. The superiority of biquadratic elements for residual based stabilised problems has already been mentioned in an early paper on stabilisation by FRANCA et al. [93] where the advection-diffusion model problem as well as the STOKES problem are considered.

Higher order finite element methods for flow problems have been used by JOHN [149, 150]. Stabilised finite elements with a hierarchical basis have been developed by WHITING [231] and appear as an interesting choice.

4.4 Stability of a stabilised method on a moving mesh

It remains to show that the stability of the convective ALE formulation obtained for an unstabilised model problem in section 3.5.1 also applies for consistently stabilised NAVIER-STOKES equations on a deforming domain. Stability of the convective ALE formulation of the model problem is guaranteed if (3.52) is satisfied and thus the reaction coefficient σ_{0e} is strictly positive.

An upper bound on the time step size to integrate the model problem on a deforming domain has been obtained. Repeating the analysis of section 3.5.1 for the convective ALE formulation of the incompressible NAVIER-STOKES equations shows that with slight restrictions condition (3.52) also transfers to the present case, where the corresponding condition (4.46) has to be satisfied. The analysis presented here is restricted to the convective formulation however the results obtained in section 3.5 can similarly be transferred in the other cases.

With respect to the form of the stabilisation operator (4.35) two different cases shall be considered. The first variant is a classical GLS where the parameter in (4.35) are set to $\eta = 0$ and $\alpha = \beta = -1$. Additionally a full USFEM version of the stabilisation shall be of interest the parameters of which are $\eta = \alpha = 1$, and $\beta = -1$. In particular the analysis of this latter case is based on the newly introduced parameters r_G and σ_{0e} which depend upon mesh motion. In this latter case the analysis further relies on the additional condition that r_G and σ_{0e} are constant within the single elements. This condition is clearly not satisfied in the general case. However as the respective analysis is not very sharp it can be suspected that stability is not lost even when this condition is relaxed. Nevertheless a prove for the general case could not be found within this work.

As the stabilisation parameter is evaluated once per element it can be treated as an elemental constant and can thus be taken out of the respective integrals. The analysis is based on some basic inequalities which are also given in appendix A.2.3.

4.4.1 Coercivity of GLS stabilised ALE formulation

Coercivity of the form $B_0^{\text{GLS}}(\{\mathbf{u}, p\}, \{\mathbf{v}, q\})$ defined by (4.32) with the parameters $\eta = 0$ and $\alpha = \beta = -1$ requires that a set of weighting functions \mathbf{v} and q can be found such that the form is bounded from below. Inserting $\mathbf{v} = \mathbf{u} \in \mathbf{V}_{\mathbb{F},0,n+1}^h$ and $q = p \in P_{n+1}^h$ yields

$$\begin{aligned} B_0^{\text{GLS}}(\{\mathbf{u}, p\}, \{\mathbf{u}, p\}) &= \|\mathbf{u}\|_{\Omega_{\mathbb{F}}^{n+1}}^2 + \delta \left((\mathbf{u} - \mathbf{u}^{\text{G},n+1}) \cdot \nabla \mathbf{u}, \mathbf{u} \right)_{\Omega_{\mathbb{F}}^{n+1}} + \delta 2\nu \|\nabla \mathbf{u}\|_{\Omega_{\mathbb{F}}^{n+1}}^2 \\ &\quad + \sum_e \tau_{\text{Me}} \left\| \delta (\mathbf{u} - \mathbf{u}^{\text{G},n+1}) \cdot \nabla \mathbf{u} - \delta 2\nu \nabla \cdot \boldsymbol{\varepsilon}(\mathbf{u}) + \delta \nabla p \right\|_{\Omega_e}^2 \\ &\quad - \sum_e \tau_{\text{Me}} \left(\mathbf{u}, -\delta (\mathbf{u} - \mathbf{u}^{\text{G},n+1}) \cdot \nabla \mathbf{u} + \delta 2\nu \nabla \cdot \boldsymbol{\varepsilon}(\mathbf{u}) - \delta \nabla p \right)_{\Omega_e} \\ &\quad + \sum_e \tau_{\text{Ce}} \|\nabla \cdot \mathbf{u}\|_{\Omega_e}^2. \end{aligned} \quad (4.53)$$

There are two terms in (4.53) which may have a destabilising effect the first of which is the convective term in the first line. Similarly to what was done in (3.50) this term can be integrated by parts yielding

$$\begin{aligned} \delta \left((\mathbf{u} - \mathbf{u}^{\text{G},n+1}) \cdot \nabla \mathbf{u}, \mathbf{u} \right)_{\Omega_{\mathbb{F}}^{n+1}} &= -\delta \frac{1}{2} \left(\nabla \cdot (\mathbf{u} - \mathbf{u}^{\text{G},n+1}) \mathbf{u}, \mathbf{u} \right)_{\Omega_{\mathbb{F}}^{n+1}} \\ &\quad + \delta \frac{1}{2} \left(\mathbf{n} \cdot (\mathbf{u} - \mathbf{u}^{\text{G},n+1}) \mathbf{u}, \mathbf{u} \right)_{\Gamma_{\mathbb{F}}^{n+1}}. \end{aligned} \quad (4.54)$$

The boundary term in (4.54) vanishes at DIRICHLET boundaries where the weighting function is zero. It disappears further at all FSI interfaces and local LAGRANGEan boundaries where $\mathbf{n} \cdot \mathbf{u} = \mathbf{n} \cdot \mathbf{u}^{\text{G},n+1}$ applies. At outflow boundaries where $\mathbf{n} \cdot \mathbf{u} > \mathbf{n} \cdot \mathbf{u}^{\text{G},n+1}$ the boundary term adds stability. Free inflow boundaries where the boundary term in (4.54) would subtract stability yield ill-posed overall problems and are thus not applicable. Consequently the boundary term can be bound from below by zero, i.e. it can be omitted.

The first term in (4.54) subtracts stability on a particular element e if the divergence of the mesh velocity is negative, i.e. if the respective element is contracting. Thus the elemental contribution of the convective term can be estimated by

$$\delta \left| \left((\mathbf{u} - \mathbf{u}^{\text{G},n+1}) \cdot \nabla \mathbf{u}, \mathbf{u} \right)_{\Omega_e} \right| \leq \delta \frac{1}{2} \left\| \nabla \cdot (\mathbf{u} - \mathbf{u}^{\text{G},n+1}) \right\|_{L^\infty(\Omega_e)} \|\mathbf{u}\|_{\Omega_e}^2. \quad (4.55)$$

The remaining term in (4.53) which is not necessarily positive can easily be bounded from above by employing the CAUCHY-SCHWARZ inequality (A.15) and the ε -inequality (A.16). On every element e

$$\begin{aligned} & \left| \mathbf{u}, -\delta (\mathbf{u} - \mathbf{u}^{\text{G},n+1}) \cdot \nabla \mathbf{u} + \delta 2\nu \nabla \cdot \boldsymbol{\varepsilon}(\mathbf{u}) - \delta \nabla p \right|_{\Omega_e} \\ & \leq \|\mathbf{u}\|_{\Omega_e} \left\| \delta (\mathbf{u} - \mathbf{u}^{\text{G},n+1}) \cdot \nabla \mathbf{u} - \delta 2\nu \nabla \cdot \boldsymbol{\varepsilon}(\mathbf{u}) + \delta \nabla p \right\|_{\Omega_e} \\ & \leq \varepsilon \|\mathbf{u}\|_{\Omega_e}^2 + \frac{1}{4\varepsilon} \left\| \delta (\mathbf{u} - \mathbf{u}^{\text{G},n+1}) \cdot \nabla \mathbf{u} - \delta 2\nu \nabla \cdot \boldsymbol{\varepsilon}(\mathbf{u}) + \delta \nabla p \right\|_{\Omega_e}^2 \end{aligned} \quad (4.56)$$

holds for every strictly positive ε . Setting $\varepsilon = 1/2$ and using (4.55) and (4.56) in (4.53) yields

$$\begin{aligned} B_0^{\text{GLS}}(\{\mathbf{u}, p\}, \{\mathbf{u}, p\}) & \geq \sum_e \left(\sigma_{0e} - \frac{1}{2} \tau_{\text{Me}} \right) \|\mathbf{u}\|_{\Omega_e}^2 + \delta 2\nu \|\nabla \mathbf{u}\|_{\Omega_e}^2 \\ & \quad + \sum_e \tau_{\text{Me}} \frac{1}{2} \left\| \delta (\mathbf{u} - \mathbf{u}^{\text{G},n+1}) \cdot \nabla \mathbf{u} - \delta 2\nu \nabla \cdot \boldsymbol{\varepsilon}(\mathbf{u}) + \delta \nabla p \right\|_{\Omega_e}^2 \\ & \quad + \sum_e \tau_{\text{Ce}} \|\nabla \cdot \mathbf{u}\|_{\Omega_e}^2 \end{aligned} \quad (4.57)$$

where (4.45) has been employed. Thus with $\tau_{\text{Me}} \leq \sigma_{0e}$ the desired lower bound on the GLS stabilised form is obtained. The estimate (4.57) explains the restriction of the momentum stabilisation parameter with respect to σ_{0e} that has been introduced in (4.44). However while being formally necessary to obtain the above stability estimate this restriction is hardly significant in practical computations.

As a consequence of (4.57) the time step restrictions with respect to the mesh velocity obtained in section 3.5.1 also apply for the GLS stabilised NAVIER-STOKES equations if $\nabla \cdot \mathbf{u}^{\text{G},n+1}$ is replaced by $-\nabla \cdot (\mathbf{u} - \mathbf{u}^{\text{G},n+1})$.

4.4.2 Coercivity of USFEM stabilised ALE formulation

USFEM operator and initial discussion

It turns out to be more difficult to obtain coercivity of the unusual stabilised form $B_+^{\text{USFEM}}(\{\mathbf{u}, p\}, \{\mathbf{v}, q\})$. In this case the influence of a negative divergence of the mesh velocity entering the stabilised problem via the parameter r_{G} has to be considered.

Using the parameters $\eta = \alpha = 1$ and $\beta = -1$ and inserting $\mathbf{v} = \mathbf{u} \in \mathbf{V}_{\text{F},0,n+1}^h$ and

$q = p \in P_{n+1}^h$ yields

$$\begin{aligned}
B_+^{\text{USFEM}}(\{\mathbf{u}, p\}, \{\mathbf{u}, p\}) &= \|\mathbf{u}\|_{\Omega_F^{n+1}}^2 + \delta \left((\mathbf{u} - \mathbf{u}^{\text{G},n+1}) \cdot \nabla \mathbf{u}, \mathbf{u} \right)_{\Omega_F^{n+1}} + \delta 2\nu \|\nabla \mathbf{u}\|_{\Omega_F^{n+1}}^2 \\
&+ \sum_e \tau_{\text{Me}} \left\| \delta (\mathbf{u} - \mathbf{u}^{\text{G},n+1}) \cdot \nabla \mathbf{u} + \delta \nabla p \right\|_{\Omega_e}^2 \\
&- \sum_e \tau_{\text{Me}} \left(\delta (\mathbf{u} - \mathbf{u}^{\text{G},n+1}) \cdot \nabla \mathbf{u} + \delta \nabla p, (r_{\text{G}} - 1)\mathbf{u} \right)_{\Omega_e} \quad (4.58) \\
&- \sum_e \tau_{\text{Me}} \left\{ r_{\text{G}} \|\mathbf{u}\|^2 - (1 + r_{\text{G}}) \delta 2\nu (\mathbf{u}, \nabla \cdot \boldsymbol{\varepsilon}(\mathbf{u})) \right. \\
&\quad \left. + \delta^2 4\nu^2 \|\nabla \cdot \boldsymbol{\varepsilon}(\mathbf{u})\|^2 \right\}_{\Omega_e} \\
&+ \sum_e \tau_{\text{Ce}} \|\nabla \cdot \mathbf{u}\|_{\Omega_e}^2,
\end{aligned}$$

where the effective reaction coefficient r_{G} according to (4.38) differs from one only when local contraction takes place. In the case of rapid loss of element volume r_{G} can be negative. However due to the general stability condition (3.52) the parameter r_{G} satisfies

$$|r_{\text{G}}| \leq 1. \quad (4.59)$$

In (4.58) it has been assumed that r_{G} is constant over an element which means that the element shrinks or contracts uniformly if one ignores the divergence error of \mathbf{u} for interpretation purpose. This assumption is necessary for the analysis while the result is not sharp and numerical experience indicates that the method may well be generally stable even if this could not be shown here.

Considering the obvious zero order contributions in (4.58) the switch in the effective reaction coefficient r_{G} can be explained. From the GALERKIN terms one obtains the elemental contribution

$$\|\mathbf{u}\|_{\Omega_e}^2 - \frac{\delta}{2} (\nabla \cdot (\mathbf{u} - \mathbf{u}^{\text{G},n+1}) \mathbf{u}, \mathbf{u}) \quad (4.60)$$

whereas the stabilisation terms yield an elemental contribution of

$$-\tau_{\text{Me}} \left\{ \|\mathbf{u}\|_{\Omega_e}^2 - \delta (\nabla \cdot (\mathbf{u} - \mathbf{u}^{\text{G},n+1}) \mathbf{u}, \mathbf{u}) \right\} \quad (4.61)$$

if r_{G} contains the derivative of the mesh velocity. Expression (4.61) follows from the first term in the fourth line of (4.58) and thus the potential destabilising effect of the mixed terms has not yet been considered. As the stabilisation parameter τ_{Me} may approach one for $\delta > 0$ instability would be obtained in the case of expanding elements, i.e. if $\nabla \cdot (\mathbf{u} - \mathbf{u}^{\text{G},n+1}) < 0$. Consequently $r_{\text{G}} = 1$ is used in this case.

Bounding single terms

In order to show that (4.58) is strictly positive and thus the problem is stable all the mixed products which potentially subtract stability have to be bounded from above and subtracted. Thus the single terms are considered in a kind of worst-case scenario.

The product on the third line of (4.58) vanishes for all elements that expand and it is potentially destabilising in contracting areas. On every element it can be bounded from

above by means of the CAUCHY-SCHWARZ inequality (A.15) and the ε -inequality (A.16) with $\varepsilon = 1/2$ according to

$$\begin{aligned} & \left| (\delta (\mathbf{u} - \mathbf{u}^{\text{G},n+1}) \cdot \nabla \mathbf{u} + \delta \nabla p, (r_{\text{G}} - 1)\mathbf{u})_{\Omega_e} \right| \\ & \leq \left\| \delta (\mathbf{u} - \mathbf{u}^{\text{G},n+1}) \cdot \nabla \mathbf{u} + \delta \nabla p \right\|_{\Omega_e} |r_{\text{G}} - 1| \|\mathbf{u}\|_{\Omega_e} \\ & \leq \frac{1}{2} |r_{\text{G}} - 1| \left\| \delta (\mathbf{u} - \mathbf{u}^{\text{G},n+1}) \cdot \nabla \mathbf{u} + \delta \nabla p \right\|_{\Omega_e}^2 + \frac{1}{2} |r_{\text{G}} - 1| \|\mathbf{u}\|_{\Omega_e}^2 \end{aligned} \quad (4.62)$$

The mixed product within the fourth line of (4.58) is treated in a similar way

$$\begin{aligned} (1 + r_{\text{G}}) \left| \delta 2\nu (\mathbf{u}, \nabla \cdot \boldsymbol{\varepsilon}(\mathbf{u}))_{\Omega_e} \right| & \leq (1 + r_{\text{G}}) \|\mathbf{u}\|_{\Omega_e} \delta 2\nu \|\nabla \cdot \boldsymbol{\varepsilon}(\mathbf{u})\|_{\Omega_e} \\ & \leq \varepsilon (1 + r_{\text{G}}) \|\mathbf{u}\|_{\Omega_e}^2 + (1 + r_{\text{G}}) \frac{\delta^2 \nu^2}{\varepsilon} \|\nabla \cdot \boldsymbol{\varepsilon}(\mathbf{u})\|_{\Omega_e}^2, \end{aligned}$$

for all $\varepsilon > 0$. From (4.59) it can be observed that the coefficient $1 + r_{\text{G}}$ is never negative. Employing further the inverse inequality (4.49) allows to reformulate

$$(1 + r_{\text{G}}) \left| \delta 2\nu (\mathbf{u}, \nabla \cdot \boldsymbol{\varepsilon}(\mathbf{u}))_{\Omega_e} \right| \leq \varepsilon (1 + r_{\text{G}}) \|\mathbf{u}\|_{\Omega_e}^2 + (1 + r_{\text{G}}) \frac{\delta^2 \nu^2}{\varepsilon C_e h_e^2} \|\nabla \mathbf{u}\|_{\Omega_e}^2. \quad (4.63)$$

To complete the treatment of the single terms the estimate of the GALERKIN convective term (4.55) is recalled and the inverse inequality is used again to obtain

$$\delta^2 4\nu^2 \|\nabla \cdot \boldsymbol{\varepsilon}(\mathbf{u})\|_{\Omega_e}^2 \leq \frac{\delta^2 4\nu^2}{C_e h_e^2} \|\nabla \mathbf{u}\|_{\Omega_e}^2. \quad (4.64)$$

Equipped with bounds for all the terms the coefficients of the single norms can be evaluated. Here two cases have to be distinguished the first of which considers elements which contract within the present step, i.e. which exhibit $r_{\text{G}} < 1$.

Coefficients for contracting elements

First the coefficient of $\left\| (\mathbf{u} - \mathbf{u}^{\text{G},n+1}) \cdot \nabla \mathbf{u} + \delta \nabla p \right\|_{\Omega_e}^2$ shall be looked at. Using (4.58) and (4.62) one obtains

$$\tau_{\text{Me}} \left(1 - \frac{1}{2} \|r_{\text{G}} - 1\|_{L^\infty(\Omega_e)} \right) = \tau_{\text{Me}} \sigma_{0e}. \quad (4.65)$$

Second the coefficient of the L^2 -norm of the velocity $\|\mathbf{u}\|_{\Omega_e}^2$ is considered. Summarising the respective terms from (4.58), (4.55), (4.62) and (4.63) the elemental coefficient

$$\begin{aligned} & 1 - \frac{1}{2} \delta \|\nabla \cdot (\mathbf{u} - \mathbf{u}^{\text{G},n+1})\|_{L^\infty(\Omega_e)} \\ & - \tau_{\text{Me}} (1 - \delta \nabla \cdot (\mathbf{u} - \mathbf{u}^{\text{G},n+1})) - \tau_{\text{Me}} \frac{1}{2} \delta \|\nabla \cdot (\mathbf{u} - \mathbf{u}^{\text{G},n+1})\|_{L^\infty(\Omega_e)} \\ & - \tau_{\text{Me}} \varepsilon (2 + \delta \nabla \cdot (\mathbf{u} - \mathbf{u}^{\text{G},n+1})) \end{aligned} \quad (4.66)$$

is determined where the first line contains GALERKIN terms while the coefficients stemming from stabilisation are given in the subsequent lines. Recalling that here a positive

divergence of $\mathbf{u} - \mathbf{u}^{G,n+1}$ is considered and using (4.45) the coefficient of $\|\mathbf{u}\|_{\Omega_e}^2$ can be reformulated yielding

$$\sigma_{0e} - \tau_{Me} \sigma_{0e} - 2\tau_{Me} \varepsilon \sigma_{0e}. \quad (4.67)$$

Expression (4.67) is minimised if the stabilisation parameter takes on its maximal value. With

$$\tau_{Me} \leq \frac{h_e^2}{h_e^2 + \frac{4\delta\nu}{m_e}} \quad (4.68)$$

and $\varepsilon = \delta\nu / (m_e h_e^2)$ the coefficient of $\|\mathbf{u}\|_{\Omega_e}^2$ can be bounded by

$$\tau_{Me} \sigma_{0e} \frac{2\delta\nu}{m_e h_e^2}. \quad (4.69)$$

Finally the coefficient of the viscous term has to be evaluated. From (4.58), (4.63) and (4.64) coefficient of $\|\nabla\mathbf{u}\|_{\Omega_e}^2$ can be determined to

$$\delta 2\nu - \tau_{Me} \left(2 - \delta \nabla \cdot (\mathbf{u} - \mathbf{u}^{G,n+1})\right) \frac{\delta^2 \nu^2}{\varepsilon C_e h_e^2} - \tau_{Me} \frac{\delta^2 4\nu}{C_e h_e^2} \quad (4.70)$$

using further (4.45) and $\varepsilon = \delta\nu / (m_e h_e^2)$ yields the elemental coefficient

$$\delta 2\nu \left(1 - \tau_{Me} \sigma_{0e} - \tau_{Me} \frac{\delta^2 2\nu}{C_e h_e^2}\right)$$

which is again minimal for the maximal possible stabilisation parameter (4.68). Thus a lower bound for the viscous coefficient reads

$$\tau_{Me} \frac{\delta^2 4\nu^2}{m_e h_e^2} \quad (4.71)$$

where $\sigma_{0e} \leq 1$ has been used.

Coercivity estimate

According to the definition of the stabilisation operator (4.35) and the coefficient r_G (4.38) the divergence of the mesh velocity within the zeroth order term of the stabilisation operator is omitted for expanding elements. With $r_G = \sigma_{0e} = 1$ it can be observed that the previously obtained estimates also hold for expanding or rigid elements.

Summarising these results for all elements yields the lower bound on the unusual stabilised operator on a moving mesh reading

$$\begin{aligned} B_+^{\text{USFEM}}(\{\mathbf{u}, p\}, \{\mathbf{u}, p\}) &\geq \sum_e \tau_{Me} \sigma_{0e} \frac{2\delta\nu}{m_e h_e^2} \|\mathbf{u}\|_{\Omega_e}^2 + \sum_e \tau_{Me} \frac{\delta^2 4\nu^2}{m_e h_e^2} \|\nabla\mathbf{u}\|_{\Omega_e}^2 \\ &+ \sum_e \tau_{Me} \sigma_{0e} \|\delta(\mathbf{u} - \mathbf{u}^{G,n+1}) \cdot \nabla\mathbf{u} + \delta\nabla p\|_{\Omega_e}^2 \\ &+ \sum_e \tau_{Ce} \|\nabla \cdot \mathbf{u}\|_{\Omega_e}^2. \end{aligned} \quad (4.72)$$

The estimate (4.72) shows that the unusual stabilised version of the stabilisation method can be generalised in an ALE framework when the additional assumption of uniform expansion or contraction is made. The present work introduces a distinction between expanding and contracting elements via the parameter r_G in (4.38) which also applies to the closely related elemental parameter σ_{0e} (4.45). This distinction eventually allows that a coercivity estimate of the form (4.72) can be found.

The present analysis reveals that the conditional stability as obtained in section 3.5.1 which is typical for convective ALE formulations also applies to the residual based stabilised flow formulation. Thus no further restrictions due to the mesh motion have to be dealt with if the divergence error of the velocity is considered along with the divergence of the mesh velocity. The discussion about maximal time step sizes given in section 3.5.1 applies to the stabilised incompressible NAVIER-STOKES problem.

4.5 Summary

Stabilisation is an omnipresent matter in flow simulations which are based on the incompressible NAVIER-STOKES equations. There are two classical needs for stabilisation the first of which is dominating convective transport while the latter occurs if the LBB condition shall be circumvented. Various methods can be found to stabilise convection based wiggles. All those schemes have in common that they can be interpreted as a kind of upwinding or artificial viscosity introduced basing on a mesh dependent parameter. Pressure stabilisation can be achieved by some kind of relaxation of the incompressibility condition. The need for pressure stabilisation can be avoided when LBB stable elements are employed.

Residual based stabilisation methods are a means to deal simultaneously with both effects. The stabilisation is consistent and does not affect convergence rates even for higher order elements. Further it is robust if the correct stabilisation parameter is employed. For versions of the stabilisation which do not include a zeroth order term within the stabilisation operator stability also on deforming domains is straightforward. If such a term is used provable stability on moving domains requires a distinction between expanding and contracting elements as well as the assumption of uniform expansion or contraction of the elements. However, as the estimate is not sharp the latter assumption may not be required in practical applications. In particular stabilised formulations without zeroth order terms within the stabilisation operator can be used safely on deforming domains as they do not degenerate accuracy or stability properties of the original unstabilised formulations independently of the mesh motion.

Chapter 5

Stabilised finite element methods at critical parameters

Within this chapter the behaviour of the stabilised flow solver at very small time steps is considered and different versions of the stabilising scheme are compared. The efficiency of an ALE flow solver significantly relies on the performance of the mesh motion scheme. However, successful mesh motion necessarily introduces a significant amount of mesh distortion. A subsequent numerical investigation thus regards the accuracy of flow simulations obtained on distorted meshes.

5.1 Introduction

With respect to FSI applications the flow solver does not only need to be stable on a deforming ALE domain but also needs to offer reliable results at critical parameters. Unfortunately stability in the sense that the system can be solved does not guarantee that a smooth approximation is obtained. While a flow simulation may cope with a wiggly solution which is damped out after a few steps an error once introduced into an FSI computation has a potentially very significant impact on the coupled dynamics. In particular very thin structures are highly sensitive to slightly differing fluid forces.

Two very important critical situations shall be considered here. The first one regards very fine time steps and in particular a high temporal resolution on a mesh with unaltered spatial mesh size. Temporal refinement on a given mesh may well be of interest especially in three-dimensional FSI problems where the overall problem size is unfavourably limited by computational resources. Nevertheless a highly transient behaviour of the structure as it is observed in limit situations such as snap-through or buckling may well deserve very fine time steps.

Another crucial issue of ALE methods is the inherent need to solve the flow equations on a potentially heavily distorted mesh. A number of questions arise in this context that are hard to access analytically. A first matter is the general problem of how fast a solution deteriorates at successive mesh degeneration. In the present context of a stabilised flow formulation it might further be of interest if different versions of the stabilisation exhibit poorer or better behaviour on a distorted mesh. A special case of mesh distortion are highly stretched elements as used to resolve boundary layers. An investigation of the influence of the choice of the element length h_e within the stabilisation parameter has been reported by MITTAL in [181]. Some of the test cases reported there shall be repeated here along with a number of additional tests concerning the behaviour of quadratic elements in the same situation.

5.2 Residual based stabilisation at small time steps

Stabilised flow formulations have shown to work well for a wide variety of applications. However situations are encountered where unphysical oscillations are obtained within a fully stabilised formulation. In particular wiggles emerging when the time step is reduced on a given spatial mesh have been reported.

Such observations contradict the intuitive expectation that temporal refinement improves or at least does not harm a numerical approximation which is obtained with a consistent method. More importantly these oscillations have to be understood properly in the context of fluid-structure interaction problems where in critical situations the structure may experience a highly transient buckling or snap-through phase which dictates very small time steps and tends to be incredibly sensitive with respect to the flow behaviour.

Motivating example

A typical situation where oscillations occur when small time steps are used is the lid driven cavity problem at early time as depicted in Figure 5.1. The figure shows the cavity problem discretised by 20×20 linear elements in space and BDF2 in time after 20 time steps of $\Delta t = 0.003$ and a kinematic viscosity of $\nu = 0.001$. The horizontal top velocity has been increased linearly in time up to $u_x = 0.02$. The depicted oscillations get worse when the time step or the viscosity are reduced further. A regular mesh aligned with the flow direction and perpendicular to the flow eases the occurrence of such instabilities.

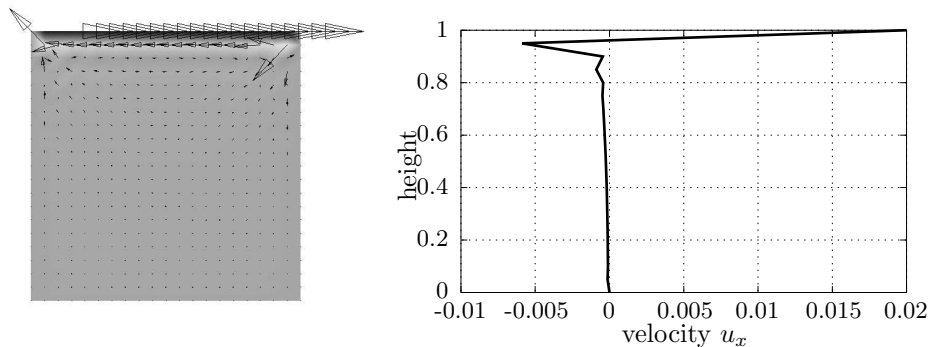


Figure 5.1: Velocity oscillations on driven cavity problem

Similar wiggles are frequently observed in the vicinity of no-slip boundaries if the mesh refinement towards the boundary does not suffice to resolve the wall gradient.

Potential instabilities at small time steps due to transient stabilisation terms

BOCHEV et al. investigate potentially destabilising effects at small time steps caused by the stabilisation terms themselves. Analysing the transient STOKES problem in [21, 22, 24] these authors argue that residual based stabilisation methods have been developed for stationary operators which do not contain an inertia term. Applying the same kind of stabilisation to transient problems requires to include the mass term into the residual within the stabilisation term in order to retain consistency. While these stabilisation terms on the mass matrix are necessary they may destabilise the discrete equations. In

particular it has been shown that the use of a purely spatial momentum stabilisation parameter which for the present formulation takes the form

$$\tau_{Me} = \frac{c_1 h_e^2}{\delta} \quad (5.1)$$

with a positive stability constant c_1 yields a stability condition linking the spatial and temporal discretisation. The stability condition induced by the transient terms then reads

$$h_e^2 < \frac{\delta}{c_1} \quad (5.2)$$

limiting the mesh size depending on the time step. Violating (5.2) while a stationary stabilisation parameter of the form (5.1) is used yields pressure instabilities. However employing a stabilisation parameter which at the limit of small time steps is of the order of one circumvents a condition like (5.2). The only problem remaining is the fact that at the limit of $\delta \rightarrow 0$ for fixed element size h_e the stabilisation terms diminish with δ eventually recovering the unstabilised GALERKIN formulation.

Remark 5.2.1 The spatial parameter in (5.1) has to be normalised by the time constant δ as in the present formulation of the residual based stabilisation method the stabilisation operator $\mathcal{L}_M^{\text{stab}}$ is defined one order higher in δ than in the cited references.

It has further been shown by BOCHEV et al. in [23] that SUPG methods used for the transient advection-diffusion problem do not introduce an instability caused by the mass terms emerging from stabilisation.

Within the present work a transient definition stabilisation parameter is employed while a re-entering of unstable pressure modes has not been observed in practical computations. The destabilising effect of the transient stabilisation terms is therefore regarded a minor issue.

However there is a further aspect that should be mentioned here. The choice of a transient stabilisation parameter has the consequence that stationary solutions depend upon δ and thus upon the time step size as soon as δ drops below a certain limit. Consequently care should be taken to employ time step sizes large enough when steady states are approached. This goes along with efficiency considerations which also strongly suggest larger time step sizes when steady state solutions shall be approximated.

A more elegant and more expensive way to avoid this dependency is to utilise time dependent subscales, i.e. take into account the temporal change of the bubble part of the solution. This approach which was suggested by CODINA in [52] and analysed by CODINA et al. in [57] requires that the actual fine scale solution of the velocity is computed from a nonlinear equation and stored at the elemental GAUSS points. This method which is half way turned over from a stabilised formulation to a proper multi-scale analysis allows to recover stability irrespective of the time step size and stationary solutions independent of the time step.

However in the context of fluid-structure interaction steady state solutions are hardly ever considered anyway.

Instabilities at small time steps due to dominating zeroth order terms

A more severe problem is due to the dominance of the zeroth order term of the unknown velocity within the temporally discretised momentum equation (3.15) or also in (3.18)

which occurs at small time steps. At very small time steps (3.15) can be regarded a singular perturbed problem where the spatial derivatives of \mathbf{u} have lost their influence compared to the undifferentiated zeroth order term. Solutions of singular perturbed problems frequently exhibit characteristic steep boundary layers the proper numerical approximation of which poses a challenge. Indeed the velocity oscillations observed in figure 5.1 are induced by a dominating zeroth order term.

In order to re-establish control over the derivatives in the context of dominating zeroth order terms HARARI and HUGHES [117] proposed to use a GLS approach in conjunction with a gradient least squares (GGLS) stabilisation. While achieving the desired stabilisation effects this method introduces not only a further stabilisation parameter but also a least square form of the gradient of the differential equation of concern and thus turns out rather cumbersome and expensive. It further requires at least third order finite element spaces if all the stabilisation shall be consistent.

A more appealing way to deal with dominating zeroth order terms arises in the context of consistently stabilised methods. A derivation of stabilisation terms from bubble condensation as performed in section 4.3.1 yields a zeroth order term within the stabilisation operator as soon as an undifferentiated term is contained within the original differential equation. The approach which suggests to subtract GALERKIN like terms has been proposed as a method applicable for dominating zeroth order term problems from its early days on (see e.g. FRANCA et al. in [91, 92]).

Similar methods containing a zeroth order term within the stabilisation operator, i.e. $\eta = 1$ have been used for problems with zeroth order terms as in BARRENECHEA and VALENTIN [7], CODINA [51] and FRANCA and VALENTIN [96]. In [113, 114] HARARI suggests to employ stabilisation of the unusual type to damp out oscillations in a discrete version of a modified HELMHOLTZ problem which emerges from time discretisation of a transient diffusion equation. In a very recent contribution to the issue by HARARI and HAUKE [115] the advection-diffusion-reaction problem is considered and stabilisation of the time-discretised problem is suggested.

The method has been extended by HAUKE [118] to deal with negative reaction terms. HAUKE and DOWEIDAR are concerned with the advection-diffusion-reaction equation also in [119, 120, 121] where an explicit treatment of the diffusion and advection is proposed along with an implicit treatment of the lumped mass and zeroth order terms.

However, care has to be taken if this kind of stabilisation is applied along with linear elements. In this case an immense stabilisation effect is observed which originates from the inability of linear elements to properly approximate second derivatives and potentially significantly changes the problem to be solved.

5.2.1 Dominating zeroth order terms

Model problem singular diffusion

The effect of a zeroth order term dominating the differential terms is modelled by the singular diffusion problem (2.59) which can be interpreted as the temporal discretisation of the transient diffusion problem

$$\frac{\partial \phi}{\partial t} - \kappa \Delta \phi = 0, \quad (5.3)$$

where the right hand side in (2.59) results from temporal discretisation and the parameter δ is proportional to the time step.

In order to highlight the nature of the instability the one-dimensional numerical example used by HARARI and reported in [113] is employed. On a domain of the length L the unknown field ϕ is interpreted as the temperature of a rod. Perfect insulation at $x = 0$ is assumed while zero temperature is prescribed at $x = L$. The initial temperature is constant at ϕ^0 . Following HARARI [113] the TR is used for time discretisation along with a time step size of $\Delta t = 1/100 \kappa$. The solution of the fully discretised problem after one time step obtained from a spatial discretisation with five linear elements is depicted in figure 5.2 along with the analytical solution of the partial differential equation (5.3) and the solution of the ODE (2.59) obtained after discretisation in time.

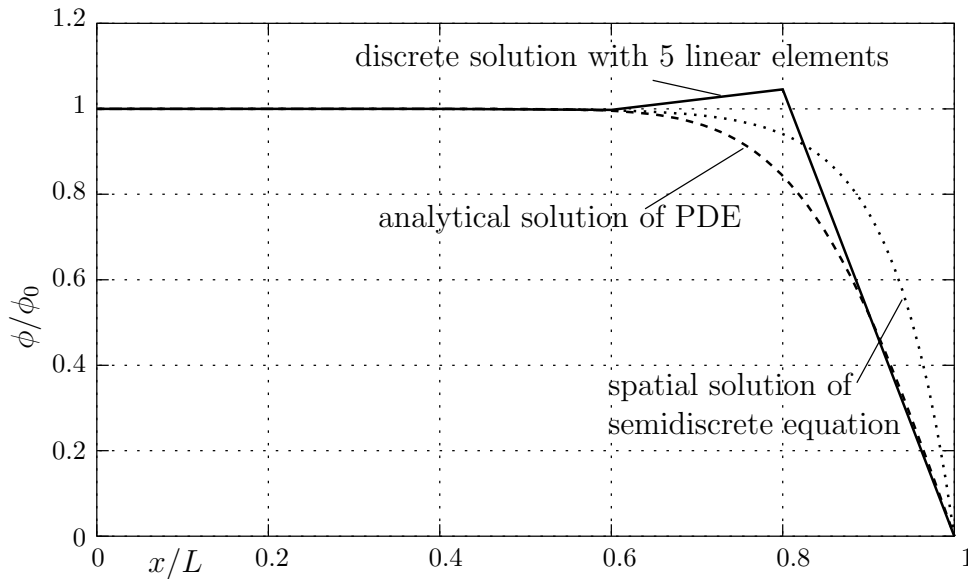


Figure 5.2: Model problem, solutions at different levels of discretisation

The difference between the two smooth curves in the diagram 5.2 can be identified as the temporal discretisation error within the first time step. As the trapezoidal rule is a convergent scheme, this error decreases if the temporal discretisation is refined. For the given time step size, however, the spatial discretisation of (2.59) has to converge to the solution analytic in space and discrete in time, given by the dotted line. In this context the overshoot apparent in the finite element solution can be interpreted as a necessary result of the method's attempt to reproduce both, the function values and its spatial derivatives on a coarse mesh.

Interestingly the slope of the analytical solution at $x = L$ is almost matched by the fully discrete approximation, i.e. in the present model problem the spatial and temporal discretisation error almost cancel with respect to this derivative. However this effect does not appear to be a reliable base for a numerical method.

If the overshoot in the discrete solution shall be removed by a stabilisation there remains the question for the ideal stabilised solution on the given mesh. An evident goal of stabilisation is to reproduce nodal exact values. This means, however, correcting the function values while increasing the errors in the derivatives. For the present example this has the consequence of an underestimated thermal flow at $x = L$. For the incompressible

NAVIER-STOKES problem the respective stabilisation yields a non-oscillatory solution that underestimates the viscous tractions.

Remark 5.2.2 The above discussion reveals that it is misleading to blame small time steps for the occurring oscillations which are initiated by unresolved spatial gradients. Problems which do not exhibit steep gradients (for example the KIM-MOIN problem) can be solved properly by almost arbitrarily small Δt .

Remark 5.2.3 A crude way to get rid of this kind of oscillations is mass matrix lumping. However this means increasing smoothness not accuracy and sacrifices the consistency of the scheme. Furthermore a mass matrix emerging from a stabilised formulation of the incompressible NAVIER-STOKES equations contains terms introduced by the stabilisation which are not symmetric. There is no straightforward lumping technique applicable in such cases.

Detection of oscillations induced by zeroth order terms by reaction forces

The wiggles induced by dominating zeroth order terms typically occur close to boundaries and are induced by unresolved gradients in particular gradients perpendicular to the flow direction. The flow gradient perpendicular to a no-slip boundary is intimately related to the respective reaction shear force. Thus shear boundary forces are used as a measure of the accuracy of a scheme in the small time step regime.

There are two possibilities to compute such shear reaction forces in a FEM setting. A first one is to determine and integrate the respective shear stresses along the boundary. However these stresses depend upon velocity derivatives and have to be expected one order lower in spatial accuracy than the velocity approximation.

A much more elegant way to compute reaction forces in a FEM context is to determine consistent nodal reaction forces by summarising the elemental node forces along the boundary. Consistent nodal forces share the order of accuracy of the primary variables and fit into a node based data structure. These forces are also used for FSI coupling purpose as described in chapter 6.

Obviously both possibilities of determining the shear forces have to converge to the same value at mesh refinement. Within the present work the reaction force has been computed on both ways for some problems. The results obtained indicate that oscillations within a boundary layer and which are due to dominating zeroth order terms go along with the two types of reaction forces converging from both sides. In smooth problems convergence from the same side was observed. Unfortunately this observation could not yet be confirmed by any theoretical analysis. Clarifying this issue could help to establish an indicator for local mesh refinement at unresolved gradients. While the difference between integrated stresses and consistent node forces can generally be regarded an error indicator it appears to be particularly appropriate to signal insufficient local resolution in space compared to the time step. In contrast to general relationships of spatial and temporal resolution such as (5.2) an indicator based on integrated stresses and consistent node forces would consider the physical configuration, i.e. indicate the need for finer meshes in the vicinity of steep gradients. This would be useful as small time steps can be employed safely on smooth problems.

5.2.2 A closer look at stabilisation for dominating zeroth order terms

Stabilisation parameters at small time steps

In the limit of $\delta \rightarrow 0$ and $h_e = \text{const}$, i.e. when the time step is refined but the spatial mesh size is retained, the ratio of the viscous forces to the inertia forces represented by the parameter r^e decreases with δ . Hence the first switch parameter in (4.47) is $\xi_1 = 1$. Thus depending on the elemental REYNOLDS number Re^e there are two cases to distinguish for the stabilisation parameter τ_{Me} given in equation (4.44) at the small time step limit. If significant convection is encountered the stabilisation parameter is given by

$$\lim_{\delta \rightarrow 0} \tau_{Me} = \frac{h_e}{h_e + 2\delta |\mathbf{u} - \mathbf{u}^G|} = 1 \quad (5.4)$$

while in the other case the limit

$$\lim_{\delta \rightarrow 0} \tau_{Me} = \frac{h_e^2}{h_e^2 + \frac{4\delta\nu}{m_e}} = 1 \quad (5.5)$$

is obtained. The continuity stabilisation parameter (4.50) vanishes at the small time step limit $\lim_{\delta \rightarrow 0} \tau_{Ce} = 0$.

Effect of zeroth order term in the stabilisation operator

The following consideration does not claim to be a rigorous mathematical analysis but rather a rough calculation giving an impression of the basic effect of the inclusion of a zeroth order term within the stabilisation operator.

In order to understand the effect of a zeroth order term within the stabilisation operator, i.e. $\eta = 1$ in (4.35), the stabilised formulation (4.32) is written in its possibly shortest way. The continuity stabilisation is ignored for brevity of the present discussion and the full adjoint stabilisation operator $\mathcal{L}_+^{\text{USFEM}}$ is applied such that the stabilised form of the momentum balance reads

$$(\mathcal{R}_M(\mathbf{u}, p), \mathbf{v})_{\Omega_F} - \sum_e (\mathcal{R}_M(\mathbf{u}, p), \tau_{Me} \mathcal{L}_+^{\text{USFEM}}(\mathbf{v}))_{\Omega_e} = 0 \quad (5.6)$$

where the first inner product (after integration by parts) yields the GALERKIN terms. The stabilisation might now be split up into the additional reaction stabilisation term and one term which uses the stationary stabilisation operator according to

$$\begin{aligned} (\mathcal{R}_M(\mathbf{u}, p), \mathbf{v})_{\Omega_F} - \sum_e (\mathcal{R}_M(\mathbf{u}, p), \tau_{Me} (1 - \delta \nabla \cdot (\mathbf{u} - \mathbf{u}^{G, n+1})) \mathbf{v})_{\Omega_e} \\ - \sum_e (\mathcal{R}_M(\mathbf{u}, p), \tau_{Me} \mathcal{L}_0^{\text{USFEM}}(\mathbf{v}))_{\Omega_e} = 0 \end{aligned} \quad (5.7)$$

The stabilisation terms due to the zeroth order weighting function within the stabilisation operator are GALERKIN like terms scaled by the stabilisation parameter τ_{Me} and a term depending on the mesh motion. It shall be assumed for the moment that these terms are constant and the equal for all elements. If further higher order elements ($k \geq 2$) are used

such that all terms of the residual $\mathcal{R}_M(\mathbf{u}, p)$ can be represented within the stabilised form, the GALERKIN like terms from the first line of (5.7) can be collected and after division by the term $1 - \tau_{Me} (1 + \delta \nabla \cdot \mathbf{u}^{G,n+1})$ the stabilised problem (5.7) is equivalent to

$$\sum_e (\mathcal{R}_M(\mathbf{u}, p), \mathbf{v})_{\Omega_e} - \sum_e (\mathcal{R}_M(\mathbf{u}, p), \tau_{Me}^{\text{mod}} \mathcal{L}_0^{\text{USFEM}}(\mathbf{v}))_{\Omega_e} = \mathbf{0} \quad (5.8)$$

with the modified elemental stabilisation parameter

$$\tau_{Me}^{\text{mod}} = \frac{\tau_{Me}}{1 - \tau_{Me} (1 - \delta \nabla \cdot (\mathbf{u} - \mathbf{u}^{G,n+1}))}. \quad (5.9)$$

Equation (5.8) shows that the additional reaction stabilisation which subtracts GALERKIN like terms can be reduced to a modified stabilisation parameter. Thus it does not introduce an new stabilising effect, it rather affects the ratio between GALERKIN and stabilising terms. In particular it can be observed from (5.9) and (5.4) or (5.5) that the modified stabilisation parameter increases for decreasing time steps. In the limiting case of $\delta \rightarrow 0$ the weak form (5.8) is dominated by the stabilisation terms while the influence of the GALERKIN terms becomes negligible. Consequently the solution is governed by numerical damping rather than the physics if small time steps along with reaction stabilisation are employed.

From (5.9) it can further be observed that the additional amount of stabilisation which is activated within an element is exclusively governed by the time step size rather than local solution properties. Thus an increase of stabilisation does not only occur in regions of unresolved gradients but also where the velocity field behaves smoothly. Thus the method exhibits a strong tendency to heavily change the physics of the problem at hand.

The situation is even worse when linear elements are used which are unable to represent the second derivatives included in the residual $\mathcal{R}_M(\mathbf{u}, p)$. While the first term of the stabilised equation (5.7), the GALERKIN term, has been integrated by parts the additional ‘reaction stabilisation’ term has not. Thus in the formulation (5.7) all GALERKIN terms are reduced except the viscous one which contains second derivatives within the original operator. So the stabilisation increases the viscosity within the GALERKIN terms on an elemental base and thus yields much more smooth solutions. However this effect is entirely due to the inconsistency of linear elements and does not give a reliable base for a stabilisation scheme!

5.2.3 Coercivity analysis of advection-diffusion-reaction model problem

To fully understand the stabilising effect of USFEM and the GLS method in the context of large zeroth order terms the advection-diffusion-reaction equation in a fixed grid formulation is employed. The results obtained on the scalar advection-diffusion-reaction equation also hold for the vector valued case which is covered in [88]. Numerical observations also show that the theoretical predictions are well transferable to the incompressible NAVIER-STOKES equations.

An accurate coercivity analysis of a numerical method allows to get an idea of the norm in which the approximation to the solution is controlled. Thus unphysical oscillations are indicated by improper balances of different terms within a coercivity estimate.

The convective ALE formulation of the scalar advection-diffusion-reaction problem (2.58) is considered reading

$$\mathcal{L}\phi = r \quad \text{in } \Omega \quad \text{with} \quad \phi = 0 \quad \text{on } \partial\Omega, \quad (5.10)$$

where homogeneous boundary conditions are assumed for clarity. The linear operator \mathcal{L} is defined by

$$\mathcal{L}\phi = \phi + \delta \mathbf{a} \cdot \nabla \phi - \delta \kappa \Delta \phi \quad (5.11)$$

while analogous to the NAVIER-STOKES case the stabilisation operator

$$\mathcal{L}^{\text{stab}}\omega = \eta\omega - \delta \mathbf{a} \cdot \nabla \omega - \alpha \delta \kappa \Delta \omega \quad (5.12)$$

is used.

From the coercivity analysis of a GALERKIN weak form of the problem (5.10) which was given in (4.1) not only a potential instability at dominating convection can be observed but also that the weak unstabilised form of the model problem B_{mod} is dominated by an L^2 -norm at small δ while the control in the H^1 sense is gradually lost (4.1). As a result oscillations induced by high gradients may spoil the solution.

The stabilisation parameter τ_e is the one proposed by FRANCA and VALENTIN [96].

$$\begin{aligned} \tau_e &= \frac{h_e^2}{h_e^2 \xi(r_{\text{mod}}^e) + \frac{2\delta\kappa}{m_e} \xi(\text{Pe}^e)} \quad \text{with} \quad \xi(x) = \max(x, 1) \quad \text{and} \quad (5.13) \\ r_{\text{mod}}^e &= \frac{2\delta\kappa}{m_e h_e^2}, \quad \text{Pe}^e = \frac{m_e |\mathbf{a}| h_e}{2\kappa}. \end{aligned}$$

If small time steps are considered in (5.13) the ratio of viscous and inertia forces r_{mod}^e is small and τ_e can take two different forms depending on the amount of advection. With only minor advection the stabilisation parameter accounts for the zeroth order term only and will be termed by τ_e^0 while $\tau_e^{\mathbf{a}}$ includes advection. The parameters read

$$\tau_e^0 = \left(1 + \frac{2\delta\kappa}{m_e h_e^2}\right)^{-1} \quad \text{and} \quad \tau_e^{\mathbf{a}} = \left(1 + \frac{\delta|\mathbf{a}|}{h_e}\right)^{-1}. \quad (5.14)$$

The elemental parameter m_e is the one defined in (4.48).

USFEM – the full operator

The unusually stabilised bilinear form of the advection-diffusion-reaction problem is given by

$$B_{\text{mod},+}^{\text{USFEM}}(\phi, \omega) = B_{\text{mod}}(\phi, \omega) - \sum_e (\mathcal{L}\phi, \tau_e \mathcal{L}_{\text{mod},+}^{\text{USFEM}}\omega)_{\Omega_e}, \quad (5.15)$$

with $\eta = 1$ and $\alpha = 1$

$$\mathcal{L}_{\text{mod},+}^{\text{USFEM}}\omega = \omega - \delta \mathbf{a} \cdot \nabla \omega - \delta \kappa \Delta \omega \quad (5.16)$$

according to (5.12) which is the adjoint operator of \mathcal{L} .

Inserting the weighting function $\omega = \phi$ into (5.15) yields

$$B_{\text{mod},+}^{\text{USFEM}}(\phi, \phi) = \|\phi\|^2 + \delta\kappa \|\nabla\phi\|^2 \quad (5.17)$$

$$- \sum_e \tau_e \left\{ \|\phi\|^2 - \delta^2 \|\mathbf{a} \cdot \nabla\phi\|^2 + \delta^2 \kappa^2 \|\Delta\phi\|^2 - 2(\delta\kappa\Delta\phi, \phi) \right\}_{\Omega_e}.$$

In order to show that (5.17) is strictly positive and to assess the ratio of the different terms the single contributions to the operator have to be evaluated.

From (5.17) it can be observed that a number of terms introduced within the stabilisation actually subtract stability. Employing the inverse inequality (4.49) the destabilising LAPLACEan term can be bounded by

$$\|\Delta\phi\|_{\Omega_e}^2 \leq \frac{1}{C_e h_e^2} \|\nabla\phi\|_{\Omega_e}^2. \quad (5.18)$$

For purely linear elements the destabilising second derivatives vanish. In all other cases the estimate is sharp in the sense that within every element a function $\phi \in V_e^h$ along with a constant C_e can be found such that the inverse inequality (4.49) is an equality.

A potentially destabilising effect is also due to the last term in (5.17). By means of the CAUCHY-SCHWARZ inequality (A.15) the absolute value of the mixed term can be bounded from above by

$$\begin{aligned} |(\delta\kappa\Delta\phi, \phi)_{\Omega_e}| &\leq C_{\text{cs}} \delta\kappa \|\Delta\phi\|_{\Omega_e} \|\phi\|_{\Omega_e} \\ &\leq \frac{C_{\text{cs}} \delta\kappa}{\sqrt{C_e} h_e} \|\nabla\phi\|_{\Omega_e} \|\phi\|_{\Omega_e}, \end{aligned} \quad (5.19)$$

where the inverse inequality (4.49) has been used again. The constant $C_{\text{cs}} < 1$ is introduced into (5.19) in order to include the sharp case. The CAUCHY-SCHWARZ inequality is sharp if the terms considered are linearly dependent. The discrete finite element space on one element V_e^h is spanned by polynomial functions and does not contain the eigenfunction of the LAPLACE operator. Thus the constant C_{cs} is strictly smaller than one. Applying further the ε -inequality (A.16) yields

$$|(\delta\kappa\Delta\phi, \phi)_{\Omega_e}| \leq \frac{\varepsilon C_{\text{cs}}^2 \delta^2 \kappa^2}{C_e h_e^2} \|\nabla\phi\|_{\Omega_e}^2 + \frac{1}{4\varepsilon} \|\phi\|_{\Omega_e}^2 \quad \text{for all } \varepsilon > 0, \quad (5.20)$$

where the parameter ε allows to shift weight between the L^2 norm and the gradient norm. With the aim of obtaining a correct estimate of the ratio of both terms ε cannot be chosen arbitrarily. The ε -inequality has a sharp case depending on ε which for the present case requires the constant to take on the value

$$\varepsilon_s = \frac{\sqrt{C_e} h_e \|\phi\|_{\Omega_e}}{2 C_{\text{cs}} \delta\kappa \|\nabla\phi\|_{\Omega_e}}. \quad (5.21)$$

Employing further a second inverse estimate reading

$$C_{0e} h_e^2 \|\nabla\phi\|_{\Omega_e}^2 \leq \|\phi\|_{\Omega_e}^2 \quad \text{for all } \phi \in V_e^h \quad (5.22)$$

allows to bound the sharp value for ε from below by

$$\varepsilon_s \geq \frac{\sqrt{C_e C_{0e}} h_e^2}{2 C_{\text{cs}} \delta\kappa}. \quad (5.23)$$

Instead of (5.23)

$$\varepsilon = \frac{C_e h_e^2}{2 C_{cs}^2 \delta \kappa} \quad (5.24)$$

shall be used within the present derivation. Inserting (5.18) and (5.20) back into the coercivity condition (5.17) yields

$$B_{\text{mod},+}^{\text{USFEM}}(\phi, \phi) \geq \sum_e \left\{ \left(1 - \tau_e - \frac{\tau_e}{2\varepsilon}\right) \|\phi\|^2 + \left(\delta\kappa - \frac{\tau_e \delta^2 \kappa^2}{C_e h_e^2} - \frac{\tau_e 2\varepsilon C_{cs}^2 \delta^2 \kappa^2}{C_e h_e^2}\right) \|\nabla\phi\|^2 + \tau_e \delta^2 \|\mathbf{a} \cdot \nabla\phi\|^2 \right\}_{\Omega_e}$$

Inserting also the parameter ε according to (5.24) and the stabilisation parameter according to (5.14) allows to obtain the single coefficients. In the case of minor advection this yields

$$1 - \tau_e^0 - \tau_e^0 \frac{1}{2\varepsilon} = \tau_e^0 \left((\tau_e^0)^{-1} - 1 - \frac{C_{cs}^2 \delta \kappa}{h_e^2 C_e} \right) = \tau_e^0 \delta \left(\frac{\kappa}{h_e^2} \left(\frac{2}{m_e} - \frac{C_{cs}^2}{C_e} \right) \right)$$

for the coefficient of $\|\phi\|^2$ and

$$\delta\kappa - \tau_e^0 \frac{\delta^2 \kappa^2}{C_e h_e^2} - \tau_e^0 \frac{2\varepsilon C_{cs}^2 \delta^2 \kappa^2}{C_e h_e^2} = \delta\kappa \tau_e^0 \left((\tau_e^0)^{-1} - \frac{\delta\kappa}{C_e h_e^2} - 1 \right) = \delta^2 \kappa \tau_e^0 \left(\frac{\kappa}{h_e^2} \left(\frac{2}{m_e} - \frac{1}{C_e} \right) \right)$$

for the coefficient of $\|\nabla\phi\|^2$.

In the other case when the advection dominates the diffusive term similar results are computed reading

$$1 - \tau_e^{\mathbf{a}} - \tau_e^{\mathbf{a}} \frac{1}{2\varepsilon} = \delta\tau_e^{\mathbf{a}} \left(\frac{|\mathbf{a}|}{h_e} - \frac{C_{cs}^2 \kappa}{h_e^2 C_e} \right)$$

$$\delta\kappa - \tau_e^{\mathbf{a}} \frac{\delta^2 \kappa^2}{C_e h_e^2} - \tau_e^{\mathbf{a}} \frac{2\varepsilon C_{cs}^2 \delta^2 \kappa^2}{C_e h_e^2} = \delta^2 \kappa \tau_e^{\mathbf{a}} \left(\frac{|\mathbf{a}|}{h_e} - \frac{\kappa}{h_e^2 C_e} \right).$$

Due to the definition of the elemental parameter m_e (4.49) both expressions are positive. Recalling $C_{cs} < 1$ theorem 1 can be concluded immediately.

Theorem 1 *If the stabilised bilinear form (5.15) employs the adjoint stabilisation operator $\mathcal{L}_{\text{mod},+}^{\text{USFEM}}$ along with the stabilisation parameter (5.13) and the method is formulated on a fixed grid than there exists a positive element based constant α_e such that*

$$B_{\text{mod},+}^{\text{USFEM}}(\phi, \phi) \geq \sum_e \tau_e \left\{ \alpha_e (\delta\|\phi\|^2 + \delta^2 \kappa \|\nabla\phi\|^2) + \delta^2 \|\mathbf{a} \cdot \nabla\phi\|^2 \right\}_e, \quad (5.25)$$

where the constant is given by

$$\alpha_e = \begin{cases} \frac{\kappa}{h_e^2} \left(\frac{2}{m_e} - \frac{1}{C_e} \right) & \text{if } \text{Pe}^e \leq 1 \\ \frac{|\mathbf{a}|}{h_e} - \frac{\kappa}{h_e^2 C_e} & \text{if } \text{Pe}^e > 1 \end{cases}. \quad (5.26)$$

A comparison of (5.25) with the coercivity of the GALERKIN weak form (4.1) shows the well known effect of advection stabilisation. It can also be observed that the order in δ of the zeroth order term has successfully been reduced. However the estimate (5.25) also indicates that the order of the derivative terms has been decreased as well. Thus the ratio of these terms remains unchanged. Nevertheless the order reduction has an important impact as it ensures that the advection stabilisation term remains comparable to the other terms which guarantees stable computations in the advection dominated regime even at small time step sizes.

However the warning should be repeated; the method's success is based on an amount of stabilisation increasing as the time step decreases. Thus the risk of over-stabilisation is rather present whenever $\eta = 1$ is used.

Remark 5.2.4 The effect of linear elements on the weak form and stability might be of interest. Equation (5.17) reveals that the stabilisation also introduces potential sources of instabilities. The only term within the curly brackets in (5.17) which definitely *adds* stability is the advective term. Approximating (5.15) with linear elements incapable of reproducing second derivatives effectively yields

$$B_{\text{mod},+, \text{lin}}^{\text{USFEM}}(\phi, \phi) = \|\phi\|^2 + \delta\kappa\|\nabla\phi\|^2 - \sum_e \tau_e \{ \|\phi\|^2 - \|\mathbf{a} \cdot \nabla\phi\|^2 \}_e$$

without the terms containing LAPLACE operators. Thus two potential sources of instabilities are excluded while full consistency has been sacrificed. Clearly the reduced form $B_{\text{mod},+, \text{lin}}^{\text{USFEM}}$ is coercive for all $\tau_e < 1$ which is always satisfied. Thus the inconsistency of linear elements significantly adds stability and yields the smoothing effect of 'reaction stabilisation'.

The price which is paid in terms of accuracy however is potentially immense. From (5.13) it can be observed that for small δ the stabilisation parameter can be expressed as $\tau_e = (1 + \epsilon)^{-1}$ with a small parameter ϵ . Assuming linear elements which are zero for all second derivatives the fully USFEM stabilised bilinear form yields

$$B_{\text{mod},+, \text{lin}}^{\text{USFEM}}(\phi, \omega) = \sum_e \tau_e \{ \epsilon(\phi, \omega) + \epsilon\delta(\mathbf{a} \cdot \nabla\phi, \omega) + (1 + \epsilon)\delta\kappa(\nabla\phi, \nabla\omega) \\ + \delta^2(\mathbf{a} \cdot \nabla\phi, \mathbf{a} \cdot \nabla\omega) + \delta(\phi, \mathbf{a} \cdot \nabla\omega) \}_e$$

where the first line contains the Galerkin like terms and the second line the remaining advection stabilisation. Thus the effective residual is a linear combination of the sums

$$\epsilon\phi + \epsilon\delta\mathbf{a} \cdot \nabla\phi - (1 + \epsilon)\delta\kappa\Delta\phi - \epsilon r \quad \text{and} \quad \phi + \delta\mathbf{a} \cdot \nabla\phi - r$$

where the contribution of either sum depends on the amount of advection involved. For small δ and thus small ϵ the potential loss of accuracy of this approach is obvious.

USFEM – the reduced operator

The stability result of the fully stabilised USFEM given in theorem 1 motivates the use of the simpler stabilisation operator

$$\mathcal{L}_{\text{mod},0}^{\text{USFEM}}\omega = -\delta\mathbf{a} \cdot \omega\phi - \delta\kappa\Delta\omega \tag{5.27}$$

which is the stabilisation operator for the respective stationary problem. By means of (5.27) the stabilised bilinear form

$$B_{\text{mod},0}^{\text{USFEM}}(\phi, \omega) = B_{\text{mod}}(\phi, \omega) - \sum_e \{(\mathcal{L}\phi, \tau_e \mathcal{L}_{\text{mod},0}^{\text{USFEM}} \omega)\}_e \quad (5.28)$$

is defined. Performing an analysis very similar to the previous case yields the following coercivity result.

Theorem 2 *If the reduced stabilisation operator (5.27) along with the previously defined stabilisation parameter (5.13) are employed the stabilised bilinear form $B_{\text{mod},0}^{\text{USFEM}}$ (5.28) is defined describing a fixed mesh problem which satisfies the coercivity condition*

$$B_{\text{mod},0}^{\text{USFEM}}(\phi, \phi) \geq \sum_e \tau_e \left\{ \alpha_e (\|\phi\|^2 + \delta\kappa \|\nabla\phi\|^2) + \frac{\delta^2}{2} \|\mathbf{a} \cdot \nabla\phi\|^2 \right\}_e, \quad (5.29)$$

where the positive elemental constant is given by

$$\alpha_e = \begin{cases} \frac{1}{2} + \frac{2\delta\kappa}{m_e h_e^2} - \frac{\delta\kappa}{C_e h_e^2} & \text{if } \text{Pe}^e \leq 1 \\ \frac{1}{2} + \frac{\delta|\mathbf{a}|}{h_e} - \frac{\delta\kappa}{C_e h_e^2} & \text{if } \text{Pe}^e > 1 \end{cases}. \quad (5.30)$$

A comparison of the estimate (5.29) and the coercivity result obtained for the operator that includes a zeroth order term (5.25) clearly shows that the effect of this term is a reduction of both, the L^2 term and the derivative. When the reduced stabilisation operator is employed, i.e. the estimate (5.29) holds, advection oscillations have to be expected in the small time step limit.

GLS method – the full operator

It is further of interest to investigate also the stability of the original GLS method applied to the advection-diffusion-reaction equation in the regime of dominating reaction caused by very small time step sizes. In contrast to USFEM, the stability of the GLS method does not depend upon the correctly determined parameter m_e and the latter method is thus better applicable to moving mesh schemes. The GLS stabilised form reads

$$B_{\text{mod},-}^{\text{GLS}}(\phi, \omega) = B_{\text{mod}}(\phi, \omega) + \sum_e (\mathcal{L}\phi, \tau_e \mathcal{L}\omega)_e. \quad (5.31)$$

i.e. the original operator is employed for stabilisation purpose. Formal coercivity of this least-square form is easily shown as

$$B_{\text{mod},-}^{\text{GLS}}(\phi, \phi) = \delta\kappa \|\nabla\phi\|^2 + \|\phi\|^2 + \sum_e \tau_e \|\mathcal{L}\phi\|_e^2. \quad (5.32)$$

However a close analysis reveals that this procedure yields a rather unfavourable stability norm which gives rise to even higher oscillation when the time step is very fine. Thus the method is not of practical interest.

GLS – the modified operator

To retain the advection stability in the GLS context

$$\mathcal{L}_{\text{mod},+}^{\text{GLS}}\omega = \omega - \delta\mathbf{a} \cdot \nabla\omega + \delta\kappa\Delta\omega \quad (5.33)$$

is used to serve as stabilisation operator. The operator is called modified as in comparison to the negative of the original operator which yields a complete GLS method the sign of the zeroth order term is reversed here. This operator cannot be derived from a multi scale analysis nor does it yield a proper least-squares form. It has rather been combined by using the stationary least-squares operator and subtracting a zeroth order term in order to balance the equations in the dominating reaction scheme. By means of (5.33) the stabilised form

$$B_{\text{mod},+}^{\text{GLS}}(\phi, \omega) = B_{\text{mod}}(\phi, \omega) - \sum_e (\mathcal{L}\phi, \tau_e \mathcal{L}_{\text{mod},+}^{\text{GLS}}\omega)_e \quad (5.34)$$

is defined. In this case a coercivity analysis yields the following estimate.

Theorem 3 *The stabilised bilinear form $B_{\text{mod},+}^{\text{GLS}}(\phi, \omega)$ defined in (5.34) satisfies the coercivity condition*

$$B_{\text{mod},+}^{\text{GLS}}(\phi, \phi) \geq \sum_e \tau_e \left\{ \alpha_e (\delta\|\phi\|^2 + \delta^2\kappa\|\nabla\phi\|^2) + \delta^2 \frac{C_e h_e^2}{\delta\kappa + C_e h_e^2} \|\mathbf{a} \cdot \nabla\phi\|^2 \right\}_e, \quad (5.35)$$

where the positive elemental constant is given by

$$\alpha_e = \begin{cases} \frac{2\kappa}{m_e h_e^2} & \text{if } \text{Pe}^e \leq 1 \\ \frac{|\mathbf{a}|}{h_e} & \text{if } \text{Pe}^e > 1 \end{cases}. \quad (5.36)$$

The stabilised method given by (5.34) shares the stability properties of the full USFEM formulation (5.15) while being insensitive with respect to the elemental parameter m_e . The role of m_e will be addressed again in the subsection 5.3.1.

Remark 5.2.5 A general comment concerning the above estimates has to be added. By means of the inverse estimate (5.22) it is in every case possible to transfer stability from the L^2 norm to the derivative. This reflects the fact that on a finite element, i.e. in a fixed discrete space the function and its derivatives are closely tied together. Consequently numerical oscillations will necessarily affect both the function itself as well as its derivatives.

Within the above estimates care has been taken to properly sort the influence of the particular terms in order to obtain an indication of the norm in which the solution actually is controlled. And indeed the results can be confirmed numerically as shown by the subsequent example.

5.2.4 Example at small time steps

The lid driven cavity is used to numerically verify the analytical results. A 2-D cavity is considered as depicted in figure 5.3. The x -direction of the top velocity is prescribed

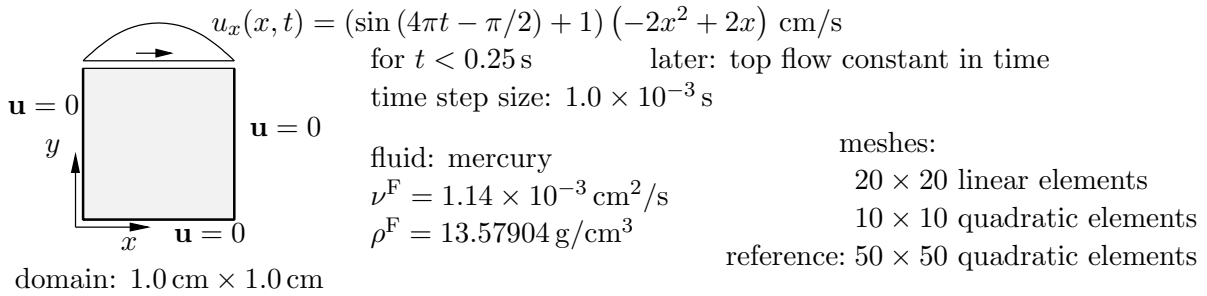


Figure 5.3: Problem setting of driven cavity example

parabolic in space and increases with a sin function in time. The parabolic profile in space serves to avoid corner singularities in the pressure result. Material and discretisation data is given in figure 5.3.

Different meshes and stabilisation methods are applied to compare the results. The behaviour of bilinear elements is investigated on a relatively coarse mesh of 20×20 elements. Nine-noded quadratic elements are applied on a discretisation of 10×10 elements which yields the same number of unknowns compared to the linear version. To obtain accurate results for reference purpose the domain is discretised by 50×50 nine-noded quadratic elements. The horizontal reaction force at the top of the cavity is used for comparison. This force is tangential to the boundary and thus unaffected by the pressure. It only depends upon the velocity derivatives and is thus an appropriate measure for the quality of the approximation of the velocity gradient $\partial u_x / \partial y$. The total horizontal force is obtained from the sum of the respective consistent nodal forces.

The problem is chosen such that an initially very steep gradient occurs at the top of the cavity which cannot be resolved by the coarse meshes used. After the circulating flow inside the cavity developed and the top velocity does not accelerate further the gradient significantly decreases and coarse meshes should be able to offer a reasonable solution.

The resulting reaction force obtained by the different meshes and stabilisation methods is depicted in figure 5.4. From the diagram in figure 5.4a) which has been computed with linear elements it can be observed that in this case full USFEM stabilisation including the zeroth order weighting term within the stabilisation operator yields devastatingly wrong results. The heavily overestimated viscosity yields a reaction force which is much too large in amplitude even for times later than 0.125 s when a smoother profile is developed in the original problem. An immense accuracy problem of linear elements used with full USFEM stabilisation can also be observed in figure 5.5, which show that irrespective of the low viscosity of mercury a Stokes flow type of behaviour is obtained.

In contrast linear elements stabilised by means of a stationary USFEM operator behave much better with respect to the horizontal top force as it can be observed from the diagram in figure 5.4. While they also fail to properly approximate the evolution of the boundary force during the initially very transient period they catch up as soon as the physics can be reasonably well resolved. Nevertheless advection type wiggles cannot be removed on the coarse mesh as figure 5.6 shows.

The diagram in figure 5.4b) displays the results obtained on a mesh of biquadratic elements. In this case both stabilised versions approximate the reaction force reasonably well on the coarse mesh confirming that the extra stabilisation effect of the zeroth order

term within the stabilisation operator is to a large extent due to the inability of linear elements to approximate second derivatives. Impressions of the velocity and pressure field obtained on the quadratic mesh are given in figures 5.7 and 5.8.

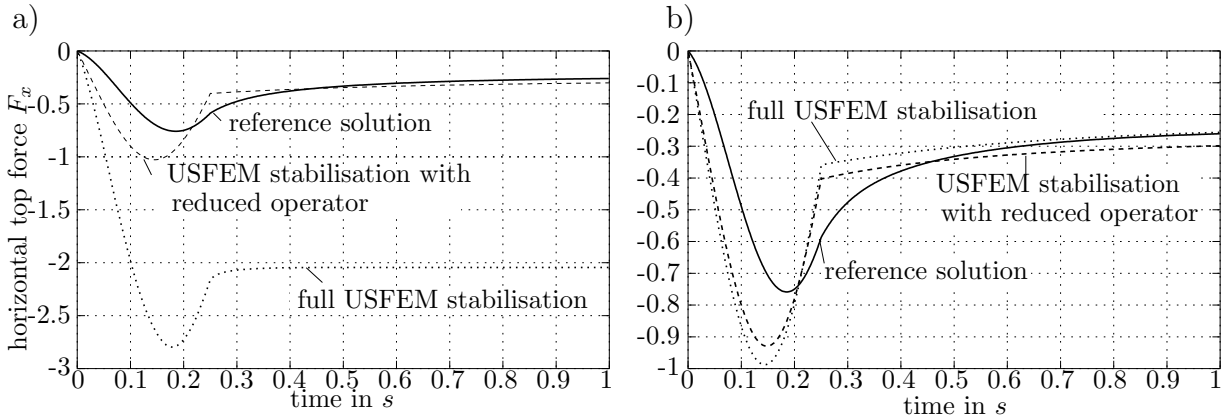


Figure 5.4: Temporal evolution of the horizontal top force in 10^{-5} N obtained a) from the linear and b) the quadratic elements compared to the reference solution

In the figures 5.5b) to 5.8b) the velocity arrows are plotted on the horizontal velocity component at time $t = 0.15$ s. The colour scale for the horizontal velocity is set to -0.05 to $+0.65$ cm/s in all images. The reference solution obtained on the fine quadratic mesh is given in figure 5.9b). The corresponding figures 5.5a) to 5.9a) depict the horizontal velocity profile at $t = 0.15$ s along a vertical cut in the centre of the corresponding velocity figure.

All results obtained on the coarse meshes display velocity and pressure oscillations except the fully USFEM stabilised linear elements in figure 5.5 which gives a perfectly smooth but inaccurate result as a comparison of figure 5.9 reveals. This confirms that the major part of reaction stabilisation is due to the inconsistency of linear elements. A comparison of figure 5.7b) and 5.8b) however reveals that while the fully stabilised version 5.7 exhibits oscillations only in the vicinity of the top layer, the stationary stabilisation operator yields additional convection type instabilities which spread all over the domain.

This interpretation of the results is also supported by the pressure fields depicted in figure 5.5c) to 5.8c) and 5.9c) where the solution in the almost stationary regime at $t = 1.0$ s is shown. The fully USFEM stabilised linear elements yield a smooth but wrong result which goes along with a pressure field exhibiting five to ten times higher values than the reference solution. All other pressure fields use the same colour scale between -0.1 and $+0.24$ Pa.

In all figures it can further be observed that velocity oscillations go along with oscillations in the pressure field which in the case of fully stabilised biquadratic elements are restricted to the vicinity of the steep top gradient. Mesh refinement in this area yields correct results at lowest possible cost when fully USFEM stabilised quadratic elements are employed.

The coarse grid results depicted in figure 5.5c) to 5.8c) highlight also a difficulty to accurately represent the continuity equation (2.35) which can be observed from non closing streamlines. This is a side effect of a large stabilisation parameter τ_{Mk} close to one which yields a significant relaxation of the continuity equation. Thus the user should be warned

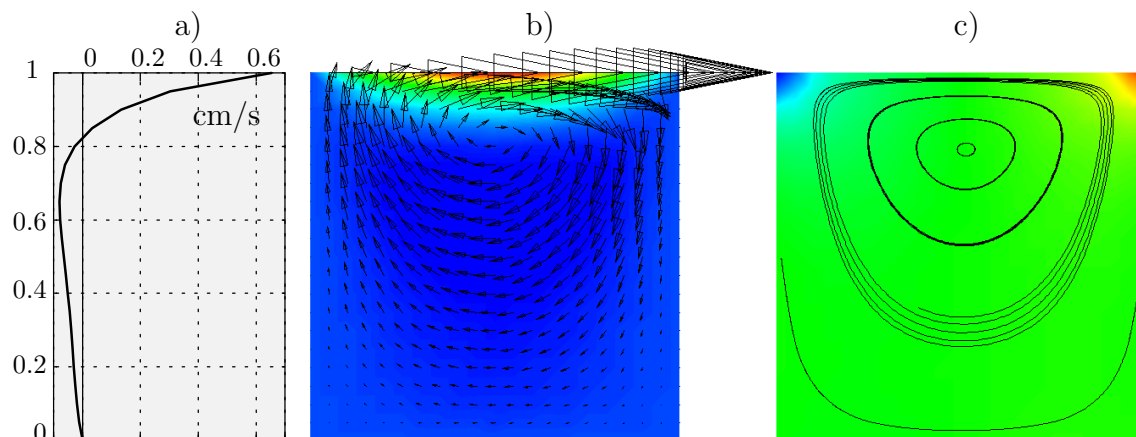


Figure 5.5: Solution obtained with linear elements and full USFEM operator: a) profile of horizontal velocity in a vertical cut through the centre at $t = 0.15$ s b) velocity arrows on horizontal velocity at $t = 0.15$ s c) streamlines on pressure at $t = 1.0$ s

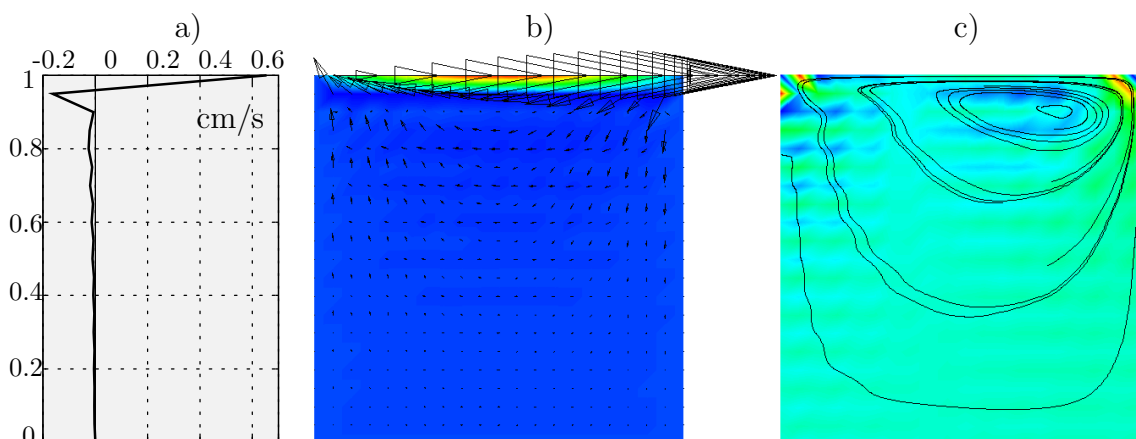


Figure 5.6: Solution obtained with linear elements and reduced USFEM operator: a) profile of horizontal velocity in a vertical cut through the centre at $t = 0.15$ s b) velocity arrows on horizontal velocity at $t = 0.15$ s c) streamlines on pressure at $t = 1.0$ s

and reminded to better balance temporal and spatial discretisation when the stabilisation parameter approaches one too closely.

From the streamlines in figure 5.7c) it can further be observed that the full USFEM stabilisation also in conjunction with quadratic elements does indeed introduce more numerical dissipation as the vortex centre is moved towards the centre of the cavity compared to the reference solution 5.9c).

When GLS type rather than USFEM stabilisation (i.e. $\alpha = -1$ in (4.35)) is employed the results are identical to the USFEM ones except that the computation is less sensitive to the parameter m_e . On the fine mesh used for reference all stabilisation methods yield almost identical results.

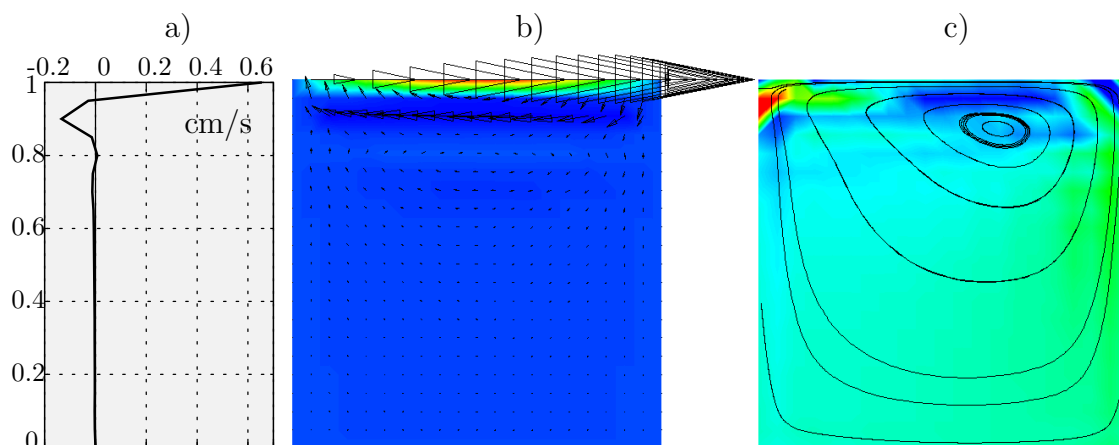


Figure 5.7: Solution obtained with quadratic elements and full USFEM operator: a) profile of horizontal velocity in a vertical cut through the centre at $t = 0.15$ s b) velocity arrows on horizontal velocity at $t = 0.15$ s c) streamlines on pressure at $t = 1.0$ s

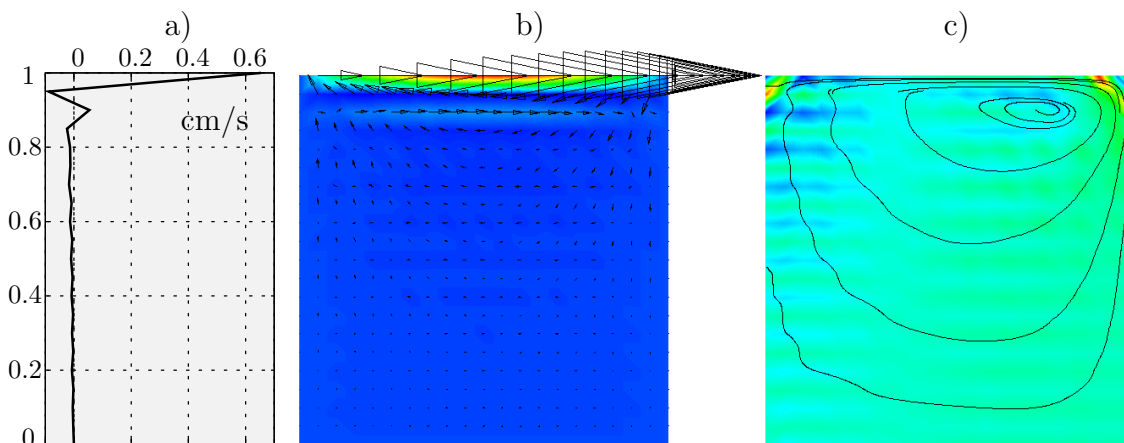


Figure 5.8: Solution obtained with quadratic elements and reduced USFEM operator: a) profile of horizontal velocity in a vertical cut through the centre at $t = 0.15$ s b) velocity arrows on horizontal velocity at $t = 0.15$ s c) streamlines on pressure at $t = 1.0$ s

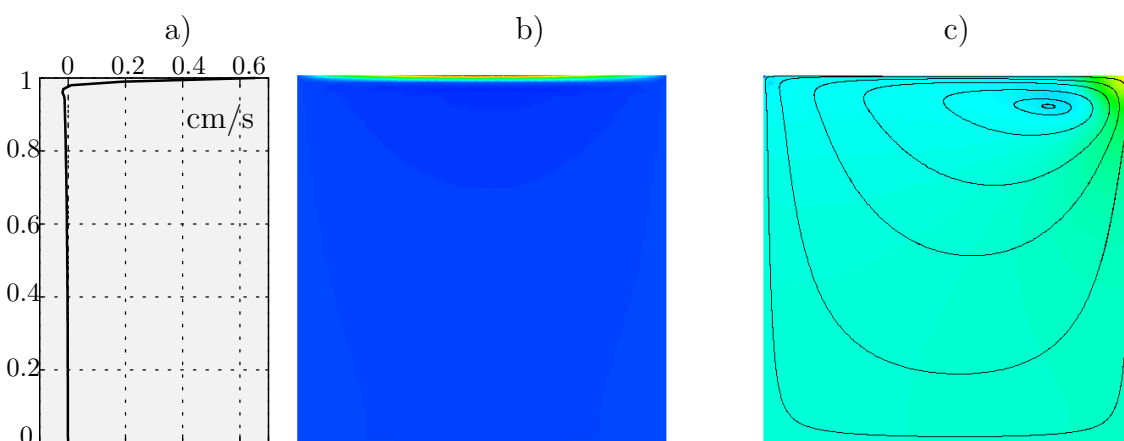


Figure 5.9: Solution obtained on fine reference mesh: a) profile of horizontal velocity in a vertical cut through the centre at $t = 0.15$ s b) horizontal velocity at $t = 0.15$ s c) streamlines on pressure at $t = 1.0$ s

5.3 Residual based stabilisation on distorted meshes

ALE methods inevitably come along with mesh motion and thus mesh distortion. Compared to fixed grid flow computations this introduces two additional challenges. The first one is related to the mesh motion itself and has been covered in chapter 3. A second problem is caused by the need to solve the flow equations on potentially heavily distorted meshes.

The sensitivity of stabilised methods with respect to distorted and unfavourably shaped elements is hard to access analytically. Thus numerical test cases are used here. These tests which are also reported in [89] are designed to compare the performance of different elements on typical distortion modes. The shape of the elements enters the residual based stabilised formulation via the elemental parameter m_e . In particular for the USFEM version of the stabilisation method the exact determination of this parameter is crucial for the stability of the method.

5.3.1 Sensitivity of USFEM stabilisation variant

Influence of the parameter m_e

Numerical investigations reveal that the USFEM implementation with $\alpha = 1$ and a fixed parameter m_e gets unstable at a certain level of mesh distortion. The observed instability is caused by a stabilisation term and can easily be shown at the model problem of an unusual stabilised diffusion problem given by: find $\phi \in V^h$ such that

$$(\kappa \nabla \phi, \nabla \omega) - \sum_e (\kappa \Delta \phi, \tau_e \kappa \Delta \omega)_{\Omega_e} = (f, \omega) - \sum_e (f, \tau_e \kappa \Delta \omega)_{\Omega_e} \quad \text{for all } \omega \in V_0^h. \quad (5.37)$$

The problem (5.37) represents an unusual stabilised formulation of the LAPLACE equation $-\kappa \Delta \phi = f$. It defines a symmetric bilinear form $B(\phi, \omega)$ coercivity of which depends upon the proper choice of the stabilisation parameter τ_e . The lowest eigenvalue of this bilinear form is bounded from below by

$$B(\phi, \phi) = \kappa \|\nabla \phi\|^2 - \sum_e \tau_e \kappa^2 \|\Delta \phi\|_{\Omega_e}^2.$$

Employing the inverse inequality (4.49) one obtains

$$B(\phi, \phi) \geq \sum_e \left(\kappa - \frac{\tau_e \kappa^2}{C_e h_e^2} \right) \|\nabla \phi\|_{\Omega_e}^2$$

yielding the condition

$$\tau_e \kappa < C_e h_e^2. \quad (5.38)$$

In the viscous limit of the stationary case the stabilisation parameter given by definition (5.13) reduces to

$$\tau_e = \frac{h_e^2 m_e}{4\kappa}.$$

Together with (5.38) this yields the stability condition

$$m_e < 4C_e. \quad (5.39)$$

The condition (5.39) is satisfied for m_e according to (4.48). Thus for a proper use of the USFEM on distorted meshes it proves essential to employ the correct definition of the parameter m_e rather than working with a fixed constant as it is commonly done for convenience and efficiency.

The parameter m_e enters the stabilisation parameter in order to account for the ratio of the first and second derivatives in the finite element space. Element distortion highly influences this ratio and thus accurate determination of m_e is required if USFEM shall be used on ALE meshes.

This potential instability disappears as soon as an SUPG ($\alpha = 0$) or GLS ($\alpha = -1$) method is used rather than the unusual stabilised version. In these cases the destabilising term is either not present (SUPG) or is added rather than subtracted and hence adds to the stability (GLS). The unconditional stability of the stabilised method obtained by setting $\alpha = 1$, denoted GLS within the present work, has already been noticed by DOUGLAS and WANG in 1989 [71] and is of particular interest in the context of deforming meshes.

Determination of the parameter m_e

The determination of the exact constant C_e satisfying the inverse estimate (4.49) for a particular element e yields an eigenvalue problem. Estimates of the constant for a variety of different elements have been provided by HARARI and HUGHES in [116]. The norms of the gradient and the LAPLACEAN define symmetric positive definite (or semi-definite) elemental operator matrices by

$$\|\nabla \mathbf{v}\|_{\Omega_e}^2 = \mathbf{v}_e^T \mathbf{K}_e \mathbf{v}_e \quad \text{and} \quad \|\Delta \mathbf{v}\|_{\Omega_e}^2 = \mathbf{v}_e^T \mathbf{L}_e \mathbf{v}_e,$$

where \mathbf{v}_e denotes the nodal degrees of freedom with respect to the nodal base of $\mathbf{V}_{F,e}^h$, the trial space of the element e which has to be free of rigid body modes. The maximal eigenvalue $\lambda_{e,1}$ of the generalised eigenvalue problem

$$\det(\mathbf{L}_e - \lambda_{e,i} \mathbf{K}_e) = 0 \quad (5.40)$$

yields the sharp constant $C_e = (\lambda_{e,1} h_e^2)^{-1}$.

As the correct value of the parameter C_e can be crucial in USFEM the solution of one eigenvalue problem per element is required. In the case of a moving ALE mesh a stable USFEM implementation is obtained only if C_e is determined for every element after each mesh motion step which makes the algorithm rather expensive and should be avoided. Alternatively GLS or SUPG versions of the stabilisation might be used which are stable irrespective of the parameter m_e .

5.3.2 Kim-Moin flow

A two-dimensional flow problem for which an analytical solution of the incompressible NAVIER-STOKES equations is known dates from KIM and MOIN in 1985 [155]. The

problem is stated by prescribing the exact velocity according to (5.41) and (5.42) along the boundary of the fluid domain.

The KIM-MOIN model problem is solved on the unit square $\Omega_F = [0, 1] \times [0, 1]$ and compared to its analytical solution which is given by

$$u_x(x, y, t) = -\cos(a\pi x) \sin(a\pi y) e^{-2a^2\pi^2 t\nu} \quad (5.41)$$

$$u_y(x, y, t) = \sin(a\pi x) \cos(a\pi y) e^{-2a^2\pi^2 t\nu} \quad (5.42)$$

$$p(x, y, t) = -\frac{1}{4} (\cos(2a\pi x) + \cos(2a\pi y)) e^{-4a^2\pi^2 t\nu}. \quad (5.43)$$

An impression of the flow field is given in figure 5.10 where velocity vectors on the corresponding pressure field are depicted. According to (5.41)-(5.43) velocity and pressure field remain in space and decrease monolithically in time.

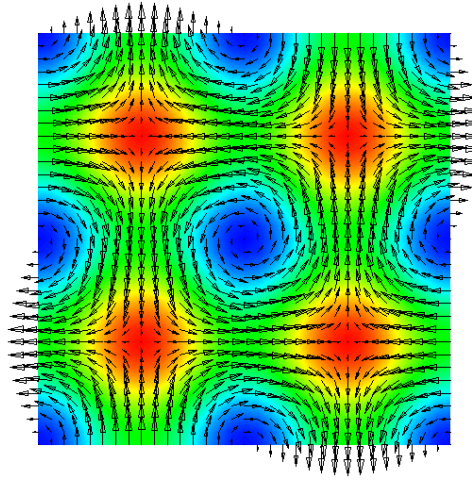


Figure 5.10: Kim-Moin flow - velocity vectors on pressure field

The solution (5.41)-(5.43) is a product of a spatial and a temporal function which allows easy scaling of the error in order to remove the temporal error decay which is due to the decay of the solution. The errors reported subsequently are absolute spatial errors defined by

$$\begin{aligned} err_{\mathbf{u}} &:= \|\mathbf{u}^h - \mathbf{u}\|_0 e^{2a^2\pi^2 t\nu} \\ err_p &:= \|p^h - p\|_0 e^{4a^2\pi^2 t\nu}. \end{aligned} \quad (5.44)$$

Characteristic maximal solution values of the spatial velocity and pressure fields are $\|\mathbf{u}\|_{L^\infty(\Omega_F)} = 1.0$ and $\|p\|_{L^\infty(\Omega_F)} = 0.5$ such that (5.44) might also be read as relative errors.

The calculations have been performed with the parameter $a = 2.0$ and a kinematic viscosity of $\nu = 0.01$. BDF2 has been used for temporal discretisation with a time step size of $\Delta t = 0.01$. The errors after 100 time steps are compared in different cases.

Remark 5.3.1 The determination of the spatial error of the KIM-MOIN problem opens the very interesting question of the unavoidable discretisation error on a given mesh. An approximation of this error could be obtained if an admissible L^2 -projection to the

discretely divergence free space would have been found. This issue turns out to be difficult in the context of stabilised methods as discussed in section 4.3.5. However the problem goes even further. The numerical solution on a given mesh will not be closest to the analytical solution in an L^2 -sense. So does a norm exist in which the error is minimised and what does it look like? The developer of numerical schemes might also turn around this question and ask for the norm in which the discrete solution should be optimal. Unfortunately no satisfying answer to these questions has been found. The problem remains open.

Sensitivity to mesh distortion – linear and quadratic elements

In a first test case different discretisations with 32×32 linear elements and 16×16 quadratic nine-noded elements are compared. Both meshes yield the same number of unknowns.

Within this example no steep gradients occur. Thus the stabilisation methods which are compared are the ones defined by $\eta = 0$, $\alpha = -1$, $\beta = -1$ (GLS) and $\eta = \alpha = 0$, $\beta = -1$ (SUPG) both with fixed m_e . Further an USFEM variant without zeroth order term, i.e. $\eta = 0$, $\alpha = 1$ and $\beta = -1$ is used where m_e is gradually reduced down to $1/200$ in order to obtain a convergent solution. In all cases the stabilisation parameter is calculated once per element at the element centre.

Two different distortion modes are investigated as depicted in figure 5.11 b) and c).

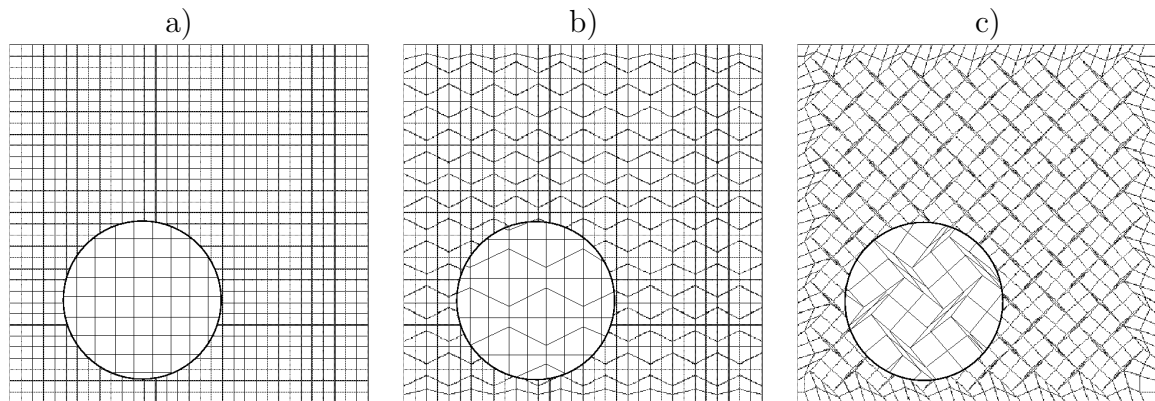


Figure 5.11: Meshes used for error evaluation with zoom area a) undistorted mesh for reference, b) distortion mode 1 and c) distortion mode 2

The first mode degenerates the quadratical elements to trapezoidals while the second introduces very slender rhombuses which turned out to appear easily when the mesh moves. The distorted quadratic elements work on the same nodal distributions, i.e. the quadratic mesh exhibits perfectly placed edge and centre nodes.

An impression of the error distribution in two examples is given in figure 5.12 where the absolute value of the difference of numerical and analytical solution, i.e. $|\mathbf{u}^h - \mathbf{u}| e^{2a^2\pi^2t\nu}$ is plotted. The figure shows results obtained with linear GLS stabilised elements with stabilisation parameter according to definition i. The error distribution on the undistorted mesh and the mesh in distortion mode 2 is presented. In the latter case the maximal deviation from the analytical solution is more than 250 times larger than on the regular mesh. However the error distribution itself appears remarkably similar and closely related

to the pattern of the solution. This indicates that in both cases the primary error source is numerical dissipation yielding a faster decay of the flow.

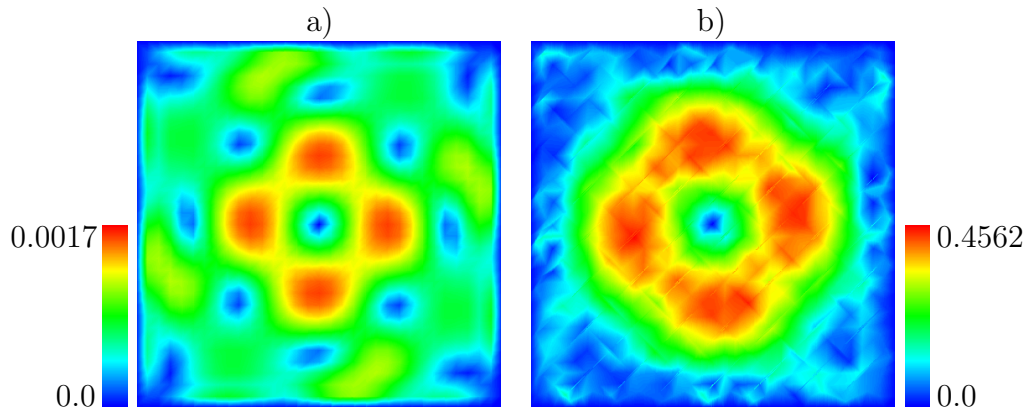


Figure 5.12: Distribution of absolute value of normalised velocity error obtained with linear elements after 100 time steps a) on distortion mode 0 and b) on distortion mode 2

Velocity and pressure errors according to (5.44) have been computed on the three meshes for the different stabilisation parameters listed in section 4.3.8. A complete table of these error values is given in the appendix A.3. As the choice of the stabilisation parameter is of minor influence a graphical comparison of the velocity and pressure error obtained with the stabilisation parameter (4.44) and the element length i) is given in diagrams 5.13 and 5.14.

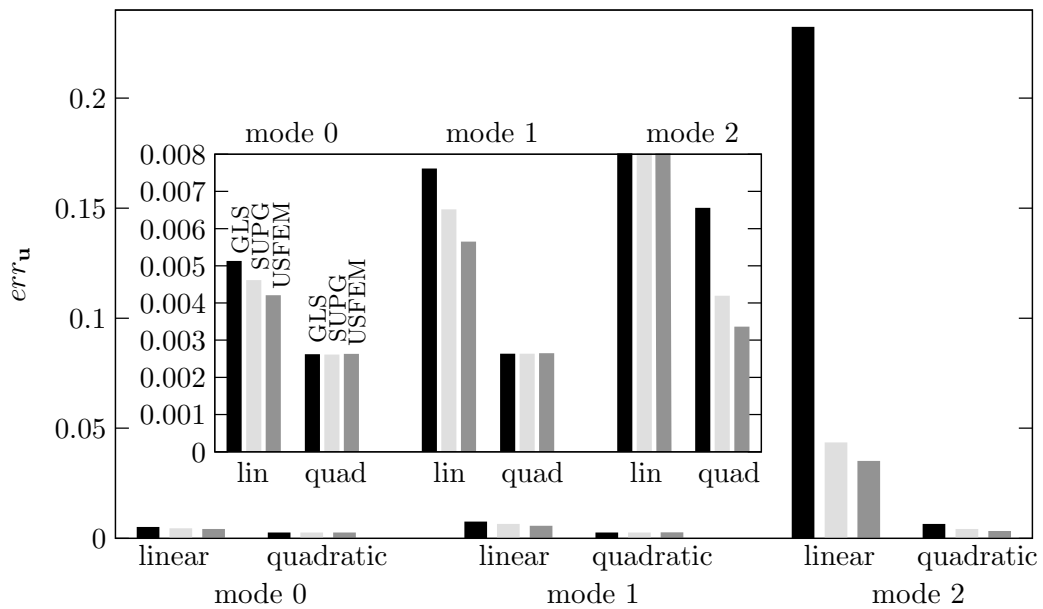


Figure 5.13: Velocity error obtained on differently distorted meshes with linear and quadratic elements and GLS, SUPG and USFEM configuration of the stabilisation

The superiority of quadratic elements observed in these diagrams is confirmed if also gradient errors are considered. In accordance with (5.44) a normalised \mathbf{H}^1 seminorm of

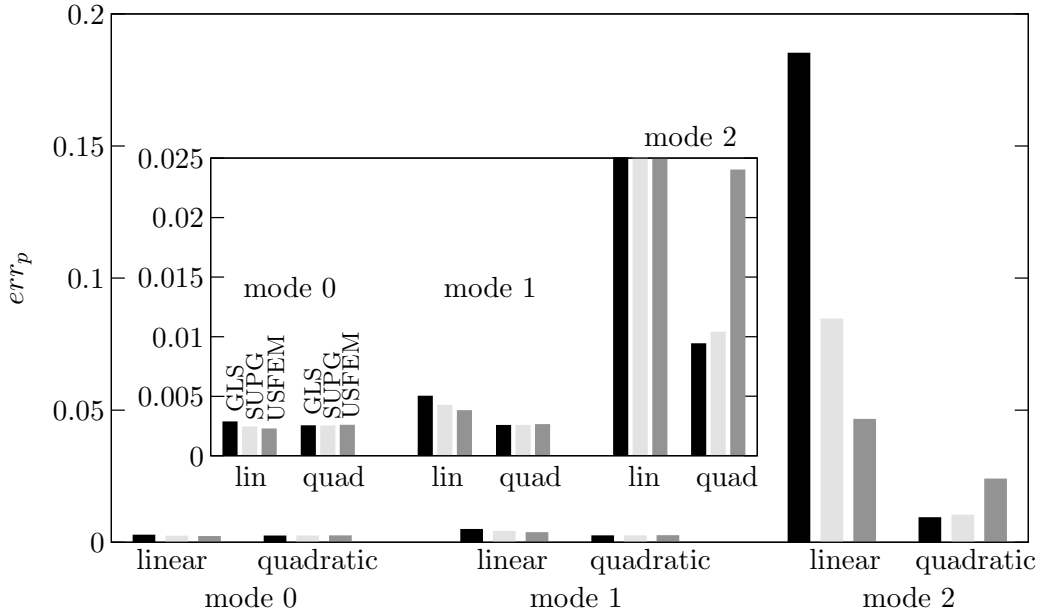


Figure 5.14: Pressure error obtained on differently distorted meshes with linear and quadratic elements and GLS, SUPG and USFEM configuration of the stabilisation

the error can be defined which is independent of the temporal decay

$$\begin{aligned} graderr_{\mathbf{u}} &:= \|\nabla \mathbf{u}^h - \nabla \mathbf{u}\|_0 e^{2a^2\pi^2 t\nu} \\ graderr_p &:= \|\nabla p^h - \nabla p\|_0 e^{4a^2\pi^2 t\nu}. \end{aligned} \quad (5.45)$$

The \mathbf{H}^1 seminorm of the error calculated with the element length definition i and for the three different modes of mesh distortion is given in the tables 5.1 and 5.2. These errors confirm the previous observations and show a particular sensitivity of the pressure gradient with respect to mesh distortion. Interestingly this sensitivity even increases when the SUPG version of the stabilisation is employed.

Table 5.1: Velocity and pressure error in normalised \mathbf{H}^1 seminorm on differently distorted meshes of linear elements

mode	$graderr_{\mathbf{u}}$	$graderr_p$	$graderr_{\mathbf{u}}$	$graderr_p$
	GLS	GLS	SUPG	SUPG
0	0.357003	0.356385	0.356671	0.356563
1	0.455323	0.448726	0.432784	0.431555
2	2.894864	7.005269	2.049585	15.375787

From these results a number of observations can be made.

- With the same number of unknowns quadratic elements perform substantially better than linear ones.
- On a perfectly squared mesh the performance of linear elements depends upon the value α within the stabilisation operator. The quadratic element is independent thereof. This highlights the impact of the inconsistency of linear elements.

Table 5.2: Velocity and pressure error in normalised \mathbf{H}^1 seminorm on differently distorted meshes of quadratic elements

mode	$graderr_{\mathbf{u}}$ GLS	$graderr_p$ GLS	$graderr_{\mathbf{u}}$ SUPG	$graderr_p$ SUPG
0	0.042845	0.082813	0.043054	0.083754
1	0.059931	0.109139	0.058817	0.110863
2	0.405593	0.912929	0.281089	2.893050

- Mesh distortion significantly increases the errors obtained with linear elements. The mesh distortion of mode 2 has a devastating effect on linear elements.
- Quadratic elements are insensitive to the distortion mode 1 and only slightly affected by the distortion mode 2.

On the heavily distorted mesh in mode 2 USFEM calculations, i.e. $\alpha = 1$ are possible only for some stabilisation parameter and in those cases require very small parameters m_e . A side effect thereof is insufficient pressure stabilisation and thus an increased pressure error for USFEM calculations on the distortion mode 2.

The above allows to draw the conclusion that substantial mesh distortion can be coped with when higher order elements are employed where the edge and centre nodes are perfectly placed. Further GLS or also SUPG versions of the stabilisation, i.e. $\alpha = -1$ or $\alpha = 0$, respectively, should be preferred.

Misplaced edge and centre nodes

In a second test case the KIM-MOIN problem discretised by 16×16 nine-noded elements is used to access the sensitivity of the element with respect to misplaced edge nodes. Misplacement of edge and centre nodes can have a huge impact on the accuracy reached with higher order elements. However usually there is no need to allow arbitrary placement of the non-corner nodes in elements inside the domain. Only at curved boundaries edge nodes of higher order elements have to be adjusted.

Nevertheless the effect of misplaced edge nodes in the interior of the domain shall be considered in order to investigate the error sensitivity due to such displacements. The interest is focused here on edge nodes displaced perpendicular to the undistorted element edge while still residing on the centre of the now curved edge. The element mid nodes are placed at the centres of the distorted elements.

The distorted meshes under consideration are depicted in figure 5.15 where the offset of the edge node perpendicular to the undistorted element edge d is varied between $0 \leq d \leq 1.5h$ where h denotes the distance of two adjacent nodes in the original mesh, i.e. half the original element length.

The square root of the elemental area is taken as element length and the errors are computed according to (5.44). The diagrams in figure 5.16 show the evolution of the time normalised velocity and pressure error depending on the distortion d and obtained with GLS or SUPG variants of the stabilisation.

From the diagrams in figure 5.16 it can be observed that small or moderate displace-

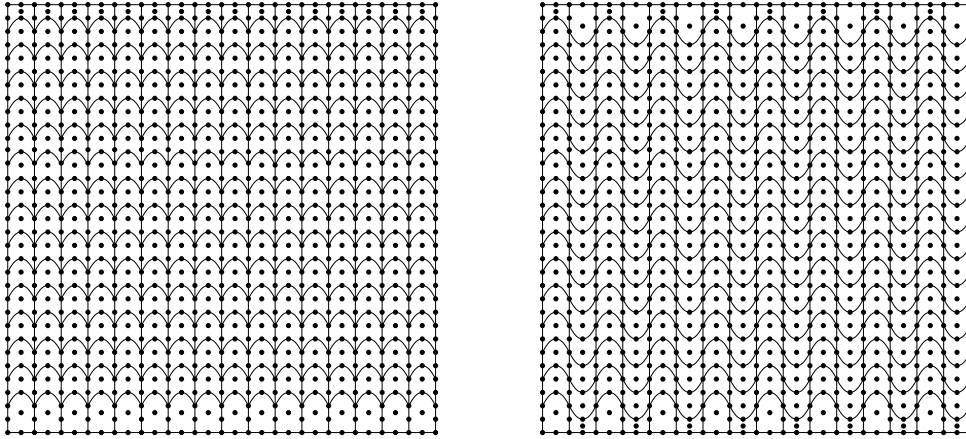


Figure 5.15: Distorted quadratic element meshes with offset edge nodes from left to right: distortion mode 3 and distortion mode 4

ments of the edge node perpendicular to the straight edge can be done safely without introducing velocity or pressure errors due to mesh distortion. Huge deflections of the edge node yield clear deterioration of the results. It is further observed that the SUPG type of the stabilisation method, i.e. $\alpha = 0$ yields significantly smaller errors in velocity and pressure than GLS when high edge node offset are considered. Badly approximated second derivatives are able to affect quadratic elements also if high distortion has to be considered. In most practical cases, however, good geometry approximation should be possible by placing the edge node with $-0.5h \leq d \leq 0.5h$, i.e. with an offset of up to a quarter of the element length and using SUPG or GLS.

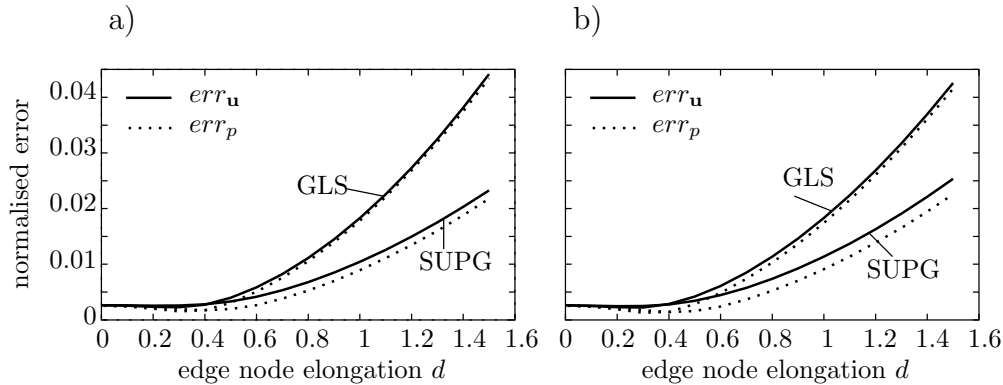


Figure 5.16: Evolution of the normalised error depending upon the offset d of the edge nodes in distortion a) mode 3 and b) mode 4

A different behaviour is observed if an USFEM version of the stabilisation is employed, i.e. if $\alpha = 1$ (where still $\eta = 0$ is used). In this case an elemental constant m_e determined according to (5.40) has to be employed. The errors obtained on the two meshes depicted in figure 5.15 are displayed in figure 5.17 along with the evolution of the parameter m_e .

The diagram in figure 5.17 shows that the errors obtained for USFEM and the distortion mode 3 are much larger than those of all other cases. Additionally the pressure error here significantly exceeds the corresponding velocity error. This effect is due to the necessary drop in the parameter m_e . Along with a reduced m_e the stabilisation parameter $\tau_{M,e}$ decreases and so does the influence of the stabilisation terms. Consequently a limit is

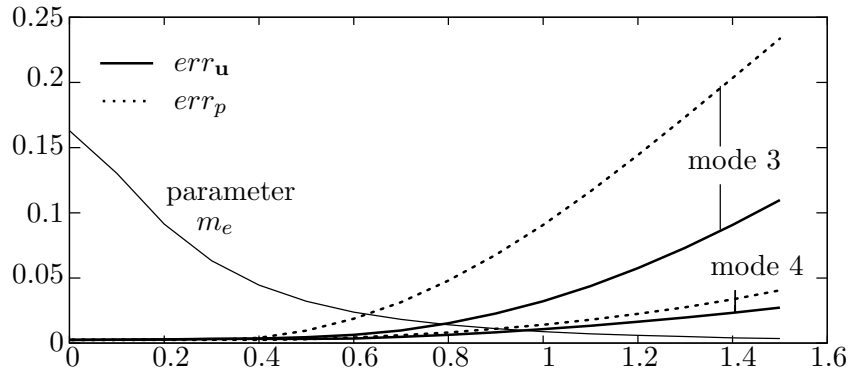


Figure 5.17: Evolution of the normalised error obtained with USFEM stabilisation for distortion modes 3 and 4 along with the parameter m_e

reached at which insufficient pressure stabilisation occurs and zero pressure modes begin to spoil the solution. However, such pressure modes are highly mesh dependent and thus only observed for the distortion mode 3 where all elements exhibit the same distortion. In practical situations this will rarely be the case. Nevertheless these results confirm that SUPG or GLS simulations are somewhat preferable compared to USFEM which may require a determination of m_e within every time step when the mesh is moving.

5.3.3 Flow past cylinder

Incompressible flow past a rigid cylinder at a REYNOLDS number of $Re = 100$ is a classical test case. The problem has been used e.g. by BROOKS and HUGHES [35] for the validation of the SUPG method and it has been investigated with respect to linear elements of high aspect ratio by MITTAL [181]. The present investigation particularly refers to that latter paper. Parts of the computations reported in [181] are repeated here and some further test cases are considered. Thus comparisons of the behaviour of linear and quadratic elements can be presented.

The geometry and the mesh data used is depicted in figure 5.18. Three different meshes of linear four-noded elements are employed differing only in the region close to the cylinder. The number of elements along the diagonal line a is 36, 48 and 90 yielding a total number of elements of 4424, 5192 and 7880 for the linear meshes A4, B4 and C4, respectively. The elements along a are concentrated towards the cylinder such that a maximal aspect ratio of the order of magnitude of 10^1 , 10^3 and 10^5 results for the three respective meshes A4, B4 and C4.

A second set of three meshes A9, B9 and C9 of quadratic nine-noded elements is defined in the same way by taking half the number of elements compared to the linear case along every edge yielding in total a quarter of the respective linear elements.

The fluid has a viscosity of $\nu = 0.005$ and a density of $\rho^F = 1.0$. A horizontal inflow velocity of $u_\infty = 0.5$ is prescribed. At the top and bottom boundary the flow is allowed to slip frictionless along the wall. Following MITTAL in all cases a time step of $\Delta t = 0.125$ has been used. GLS stabilisation, i.e. $\eta = 0.0$, $\alpha = -1.0$ and $\beta = -1.0$ is employed.

For very stretched elements the element definitions given in section 4.3.8 significantly differ. In order to access these differences the element length definitions according to i, vi

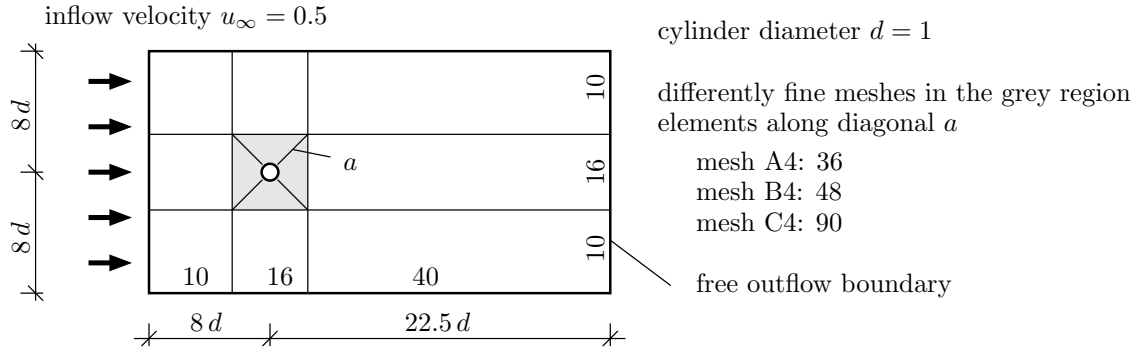


Figure 5.18: Flow past cylinder, geometry and mesh data

and vii, i.e. based on the square root of the elemental area and the minimal and maximal element lengths, respectively, are compared. In table 5.3 the STROUHAL numbers for the different cases are presented. The STROUHAL number is defined by

$$\text{St} = \frac{d}{t_c u_\infty} \quad (5.46)$$

and represents a dimensionless frequency. The duration of a period in the oscillations of the lift force is the characteristic time t_c employed to evaluate (5.46). The maximal and minimal obtained STROUHAL number differs less than 3% which is just half the variation obtained by MITTAL on the Q1Q1 mesh in [181].

Table 5.3: STROUHAL number for different element length measures and on different meshes

mesh	number of elements	number of nodes	aspect ratio	element length vi STROUHAL number	element length vii STROUHAL number	element length i STROUHAL number
A4	4424	4558	10	0.16949	0.16878	0.16913
B4	5192	5326	10^3	0.16807	0.16701	0.16736
C4	7880	8014	10^5	0.16878	0.16807	0.16842
A9	1106	4558	10	0.17131	0.17131	0.17167
B9	1298	5326	10^3	0.17094	0.17058	0.17058
C9	1970	8014	10^5	0.17131	0.17131	0.17131

It is further observed that quadratic elements in all cases yield a slightly higher STROUHAL number indicating that even for the very fine meshes employed around the cylinder quadratic elements are able to offer more accurate results. Also the mean value of the drag coefficient on the cylinder obtained with quadratic elements is higher than when linear elements are used.

The temporal evolution of the coefficients of lift and drag according to

$$C_l = \frac{2F_l}{\rho^F u_\infty d} \quad \text{and} \quad C_d = \frac{2F_d}{\rho^F u_\infty d}$$

where F_l and F_d denote the lift and drag force, respectively, obtained with different element length definitions are compared in the diagrams 5.19 to 5.22 for the meshes A4 and C9. The respective results obtained on the meshes B4, C4, A9 and B9 are given in the appendix A.4. In figure 5.22 the pressure profile obtained on the mesh C9 and with minimal element length v_i is given to highlight the slight oscillation obtained in this case. This was the only sign of an ‘instability’ that could be found in this investigation. Using the other two definitions for the element length h_k on the mesh C9 yields very similar results. The legend in figure 5.19 also applies to all the following diagrams.

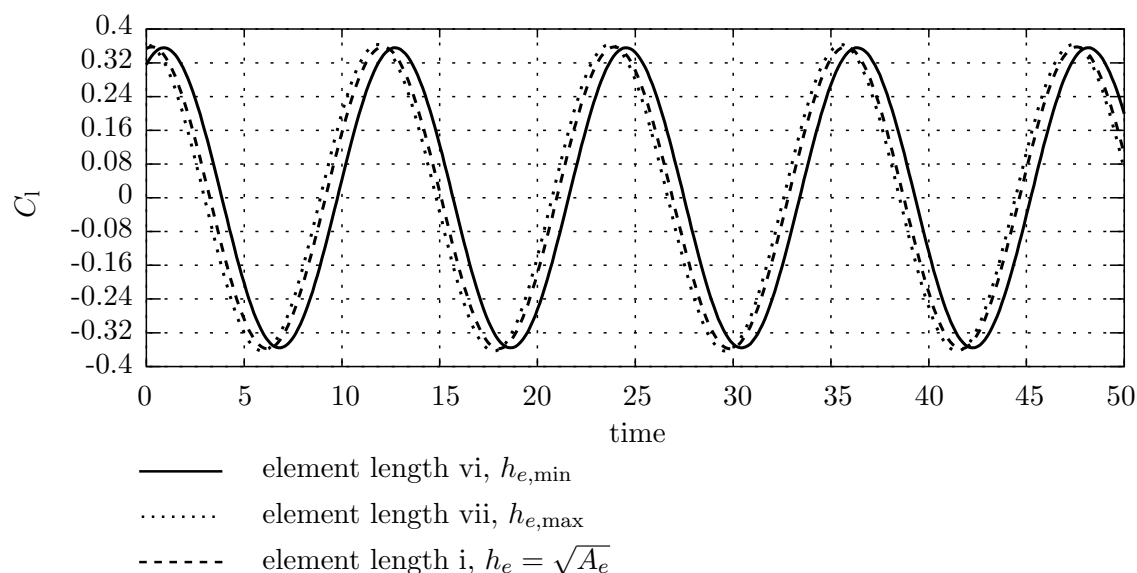


Figure 5.19: Lift coefficient obtained on mesh A4 with three different element length definitions within the stabilisation parameter

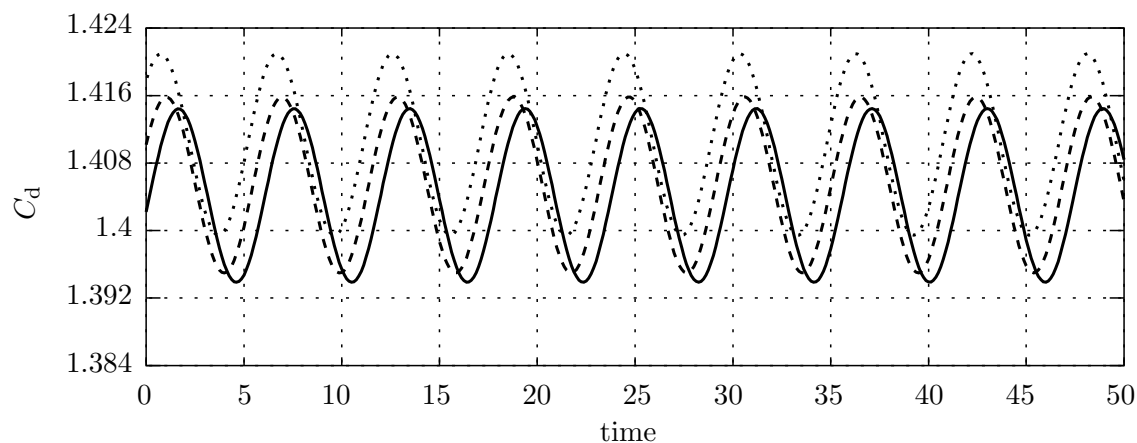


Figure 5.20: Drag coefficient obtained on mesh A4 with three different element length definitions within the stabilisation parameter

Additionally the normalised pressure distribution along the cylinder is given for every case. The normalised pressure is computed from

$$C_p = \frac{2(p - p_0)}{\rho u_\infty^2} + 1$$

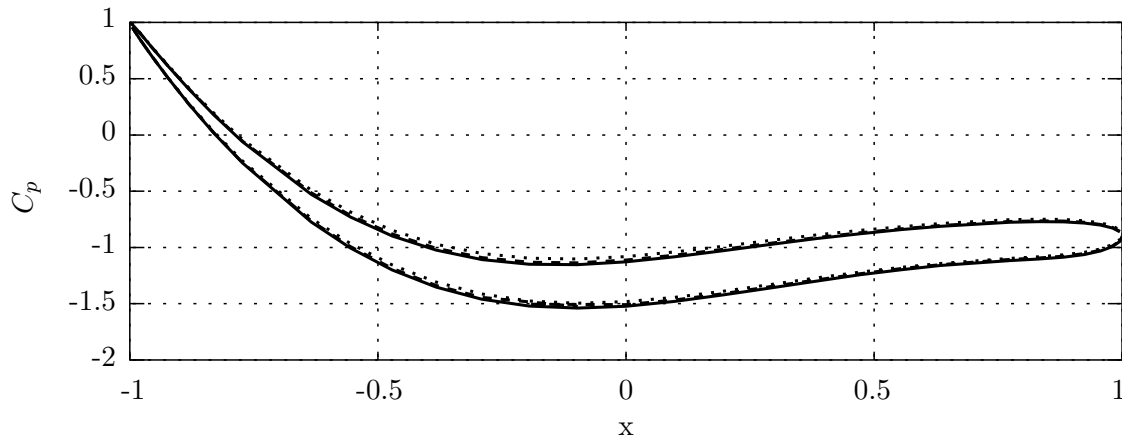


Figure 5.21: Pressure profile along the cylinder obtained on mesh A4 with three different element length definitions within the stabilisation parameter

where p_0 denotes the pressure at the leading point of the cylinder. Following Mittal in [181] the pressure distribution is projected to the horizontal, i.e. x -direction. The pressure distribution is evaluated at a time instant when the lift coefficient reaches its a maximum value.

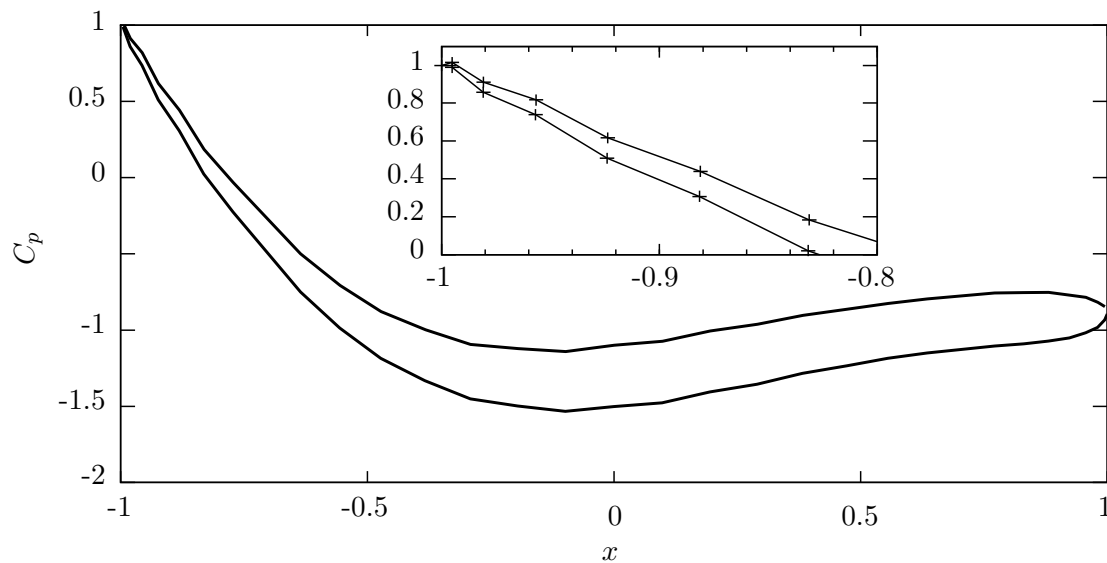


Figure 5.22: Slightly oscillating pressure profile with close-up view obtained on Mesh C9 with minimal element length v_i

The results give rise to a number of observations.

- The influence of the element length within the stabilisation parameter is only minor even in the case of highly stretched elements.
- When linear elements are employed a deviation in the lift coefficient for the element length $h_{e,\max}$ is observed. This indicates slight over-stabilisation.
- In contrast to the results reported in [181] no instabilities are observed. Even the pressure profile remains correct apart from a tiny disposition to oscillations between corner and edge node pressure values when the minimal element length is used on

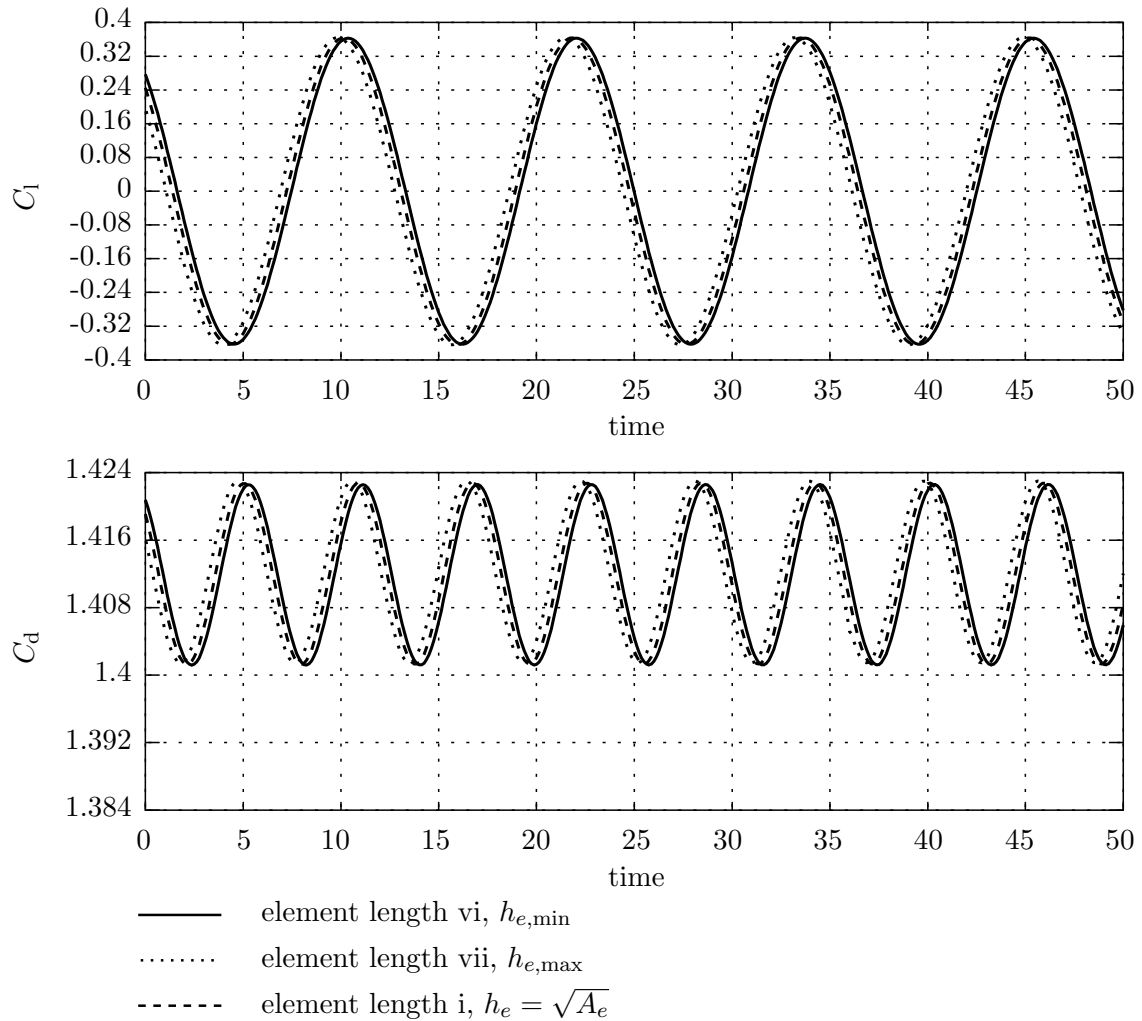


Figure 5.23: Lift and drag coefficients obtained on mesh C9 with three different element length definitions within the stabilisation parameter

a quadratic mesh.

- Quadratic elements yield even better results. They are surprisingly insensitive to the choice of the element length as long as sufficient pressure stabilisation is ensured.

While still offering very good results highly stretched elements yield badly conditioned matrices and thus the solution may require particular consideration. The iterative solver package AZTEC has been used for the meshes A4, B4, C4 and A9 while a direct solver had to be employed for the remaining cases B9 and C9. However as the condition problem is related to single nodes or degrees of freedom of highly stretched elements appropriate scaling of the respective lines of the overall system of equations could be introduced removing the problem if such elements have to be used.

In [181] MITTAL draws the conclusion that the use of a minimal element length works best. It is thus supposed here that the inaccuracy at high aspect ratio observed by MITTAL is mainly due to the inconsistency of linear elements. This effect increases the amount of numerical dissipation along with the increase of the stabilisation itself.

5.4 Summary

Stable FSI algorithms require a flow solver which is reliable also at critical parameters.

At very small time step sizes and steep velocity gradients perpendicular to the flow numerical oscillations are observed in simulations with stabilised finite fluid elements. These oscillations are due to a dominance of the inertia term compared with viscous effects and indicate a singular perturbed problem. Compared to the dominating mass term the convection stabilisation becomes insufficient allowing convection type of wiggles to enter the simulation.

Using a stabilisation variant which contains a zeroth order term within the stabilisation operator reduces the dominating term which has a revitalising effect on the convection stabilisation. However, this stabilisation variant must not be used in conjunction with linear elements where it may have a devastating effect on the accuracy.

As a second critical parameter distorted meshes are considered. Consistently stabilised finite elements are potentially very insensitive to mesh distortion provided that quadratic and higher order elements with perfectly placed edge nodes and mid nodes are used. The method further shows insensitive to the actual choice of the element length within the stabilisation parameter. Even when highly stretched elements are used very little influences are observed in particular when higher order elements are employed. For linear elements an error which scales with the amount of stabilisation has to be expected due to the inherent inconsistency of such elements.

Chapter 6

FSI coupling

This chapter is devoted to an investigation of the solver for the coupled problem including the structural field, the fluid field and the interaction of the two which appears as an additional challenge. Building upon the work of MOK [182] and WALL [227] (also [183, 228]) some improvements of the FSI coupling algorithm are presented here. The main part of this chapter is intended to clarify the *artificial added mass effect*. This effect is responsible for an inherent instability of sequentially coupled FSI algorithms applied to systems of light-weight structures and incompressible flows.

6.1 Introduction

A variety of schemes has been proposed and used to solve FSI and other surface coupled problems. An overview over recent developments can be found in the special issue on FSI [187] where various approaches are discussed. A summary of different FSI problems treated by reduced models can be found in the encyclopedia article by OHAYON [186] where the structural-acoustic problem but also sloshing in elastic structures is treated.

Monolithic schemes which require that the entire coupled problem is eventually cast into one system of equations have been reported for example by HÜBNER et al. [130, 226] and HEIL [123]. However such schemes suffer from the disadvantage that potentially rather badly conditioned overall matrices may be obtained. A possibly even more important drawback lies in the fact that such schemes do not allow to couple existing fluid and structural solvers but rather require a specified overall framework.

A higher popularity has been gained by partitioned schemes which allow to use specifically designed codes on the different fields. Smaller and better conditioned subsystems are solved instead of one overall problem. Among others the group of TEZDUYAR [208, 221, 224], DETTMER and PERIĆ [63, 64], MATTHIES et al. [179, 180], PIPERNO [193, 194] and RANK et al. [199, 200] employ partitioned approaches to compute surface coupled systems. A significant amount of work in the field of partitioned coupling schemes is due to FARHAT and his group [77, 195].

Sequentially staggered schemes are a particularly appealing subclass of partitioned algorithms. However these schemes exhibit an inherent instability when used on fluid-structure interaction problems where incompressible flows are considered. Surprisingly the instability depends upon the densities of fluid and structure and also on the geometry of the domain [38, 182, 183, 228]. Clearly sequential coupling introduces an explicit flavour into the computation even if both partitions themselves are solved implicitly. Thus restrictions on the time step have to be expected. Observations however show that decreasing the time step size causes an increase of the instability. The instability

is inherent in the scheme itself and has been named ‘artificial added mass effect’ since major parts of the fluid act as an extra mass on the structural degrees of freedom at the coupling interface. In sequentially staggered schemes the fluid forces depend upon predicted structural interface displacements rather than the correct ones and thus contain a portion of incorrect coupling forces. It is this ‘artificial’ contribution to the coupling which yields the instability.

Already in 1977 FELIPPA et al. reported an upper limit on the time step size for acoustic FSI [79]. The maximal time step size obtained there depends on the ratio of structural and fluid mass density but it is independent of the temporal discretisation scheme. Applying the results of FELIPPA et al. to the limit case of incompressible flow which goes along with an infinite speed of sound, predicts immediate instability irrespective of the time step size.

It shall be shown in the subsequent analysis that the problem posed by the artificial added mass effect is not quite as bad as that.

6.2 Partitioned FSI algorithm and its details

The present work is exclusively concerned with partitioned FSI approaches. Within such schemes it is the task of the coupling algorithm to ensure that the kinematic coupling condition (2.51) as well as the dynamic continuity (2.52) are satisfied.

Partitioned strong coupling schemes converge to the solution of the monolithic scheme and are thus able to satisfy discrete versions of the kinematic and dynamic coupling conditions exactly. However these schemes require sub-iterations and thus in terms of efficiency weak or loose coupling partitioned schemes could be preferred. The latter approach manages with just one solution of either field per time step but it consequently lacks accurate fulfilment of the coupling conditions.

Subsequently an unified approach for a general partitioned algorithm is described which can be specified to a loosely or strongly coupled version. The strongly coupled or iterative scheme of the algorithmic framework for FSI has been proposed by LE TALLEC et al. [166].

6.2.1 A general partitioned algorithm

The algorithm of consideration is restricted to synchronous time discretisations with equal time step size Δt on both fields. Additionally to the time step superscript n the subscript i denoting the iteration number in the strongly coupled version of the scheme is introduced.

The algorithm is based on the temporally and spatially discretised equations of structure and fluid given by (2.23) and (4.41), (4.42) respectively. The subscript Γ denotes the restriction of a vector of nodal values to those lines referring to interface degrees of freedom.

Starting from known solutions up to the time level t^n the following algorithmic steps have to be taken in order to compute the new coupled solution at t^{n+1} . Specifications of the single steps are given in subsequent sections.

1. **Start step.** Compute structural predictor $\mathbf{d}_{\Gamma, \text{P}}^{n+1} = \mathbf{d}_{\Gamma, 0}^{n+1}$ in Ω_S for the interface displacements at t^{n+1} , set $i = 0$.

- 2a. **Mesh step.** Solve fluid mesh on mesh domain Ω_G for new positions \mathbf{r}_{i+1}^{n+1} ($\mathbf{d}_{\Gamma,i}^{n+1}$).
- 2b. Compute new grid velocity $\mathbf{u}_{i+1}^{G,n+1}$ ($\mathbf{d}_{\Gamma,i}^{n+1}$) according to (3.33).
- 3a. **Fluid step.** Derive a new fluid velocity along wet surface $\mathbf{u}_{\Gamma,i+1}^{n+1}$ ($\mathbf{d}_{\Gamma,i}^{n+1}$) to be used as DIRICHLET boundary condition on the fluid domain according to section 6.2.3.
- 3b. Integrate fluid vectors and matrices on Ω_F^{n+1} and solve nonlinear discrete flow equations iteratively for new fluid velocity \mathbf{u}_{i+1}^{n+1} ($\mathbf{d}_{\Gamma,i}^{n+1}$) and pressure field \mathbf{p}_{i+1}^{n+1} ($\mathbf{d}_{\Gamma,i}^{n+1}$). Consider external fluid forces if present.
- 3c. Determine fluid forces on the interface $\mathbf{f}_{\Gamma,i+1}^{n+1}$ ($\mathbf{d}_{\Gamma,i}^{n+1}$).
4. **Structural step.** Solve structural equations (2.23) iteratively for new structural displacement $\tilde{\mathbf{d}}_{i+1}^{n+1}$ where the fluid forces $\mathbf{f}_{\Gamma,i+1}^{n+1}$ ($\mathbf{d}_{\Gamma,i}^{n+1}$) and external loads are exerted on the structure.
5. *For iterative schemes only:* Determine relaxation parameter $\omega_i \in \mathbb{R}^+$ according to the methods reported in [183, 228].
6. *For iterative schemes only:* Compute relaxed update of predicted interface position.

$$\mathbf{d}_{\Gamma,i+1}^{n+1} = \omega_i \tilde{\mathbf{d}}_{\Gamma,i+1}^{n+1} + (1 - \omega_i) \mathbf{d}_{\Gamma,i}^{n+1} \quad (6.1)$$

7. *For iterative schemes only:* Check convergence. If not converged, then set $i \rightarrow i + 1$ and continue with 2.
8. Proceed to next time step by setting $n \rightarrow n + 1$

In iteratively staggered schemes the predicted interface displacement $\mathbf{d}_{\Gamma,P}^{n+1}$ can be regarded the zeroth iteration and is thus also termed $\mathbf{d}_{\Gamma,0}^{n+1}$ in step 1 of the above algorithm. With regard to the analysis of the artificial added mass effect in loosely coupled schemes the former notation is preferred in the sequel.

6.2.2 Structural predictor

A variety of predictors can be employed to find a starting guess for the interface displacement in the new time step. The easiest version is given by the simple choice

$$\mathbf{d}_{\Gamma,P}^{n+1} = \mathbf{d}_{\Gamma}^n, \quad (6.2)$$

which is zeroth order accurate in time and has been proposed for partitioned FSI procedures by FELIPPA et al. in [78, 79]. In sequentially staggered schemes the accuracy is determined by the lowest order ingredient and thus a predictor of higher order than the above is highly desirable.

A first order accurate prediction which has been suggested by PIPERNO in [192] is obtained from

$$\mathbf{d}_{\Gamma,P}^{n+1} = \mathbf{d}_{\Gamma}^n + \Delta t \dot{\mathbf{d}}_{\Gamma}^n. \quad (6.3)$$

A second order accurate predictor reading

$$\mathbf{d}_{\Gamma,P}^{n+1} = \mathbf{d}_{\Gamma}^n + \Delta t \left(\frac{3}{2} \dot{\mathbf{d}}_{\Gamma}^n - \frac{1}{2} \dot{\mathbf{d}}_{\Gamma}^{n-1} \right) \quad (6.4)$$

can also be found in [192].

While the actual choice of the predictor does not influence the solution when sub-iterations are performed it has a significant impact on sequential staggered schemes. There it does not only determine the order of temporal accuracy but also highly influences the actual onset of the instability due to the artificial added mass effect. A detailed analysis of this effect is presented in section 6.3.

6.2.3 Fluid velocity boundary condition

The structural interface displacement obtained in step 1 of the above algorithm needs to be transformed into an interface velocity in order to provide the DIRICHLET boundary condition for the fluid field. With an interpolation which is first order accurate in time this velocity is obtained from

$$\mathbf{u}_\Gamma^{n+1} = \frac{\mathbf{d}_{\Gamma,P}^{n+1} - \mathbf{d}_{\Gamma,P}^n}{\Delta t}. \quad (6.5)$$

Equation (6.5) is a backward Euler discretisation of the fluid velocity at the coupling interface Γ . Accurate conservation of the size of the fluid domain Ω^F requires to employ a velocity which is consistent with the time discretisation scheme of the fluid field. The time discretisations schemes one-step- θ method (3.13) and BDF2 (3.14) can be cast into the general form

$$\bar{\mathbf{a}} = \frac{\mathbf{u}^{n+1} - \mathbf{u}^n}{\Delta t}, \quad (6.6)$$

where $\bar{\mathbf{a}}$ is an average acceleration within the time step from time level n to $n + 1$ which is assumed constant in both discretisation schemes while being approximated differently in either case. Thus the interface displacement of the fluid field can be obtained from integrating $\bar{\mathbf{a}}$ according to

$$\int_{t^n}^{t^{n+1}} \left(\int_{t^n}^t \bar{\mathbf{a}} \, d\tau + \mathbf{u}^n \right) dt = \mathbf{r}^{n+1} - \mathbf{r}^n \quad (6.7)$$

where kinematic continuity requires that the fluid and structural motion coincide within the time step, i.e. $\mathbf{r}^{n+1} - \mathbf{r}^n = \mathbf{d}_{\Gamma,P}^{n+1} - \mathbf{d}_{\Gamma,P}^n$. Evaluating (6.7) and using (6.6) yields a second order discretisation of the fluid boundary velocity reading

$$\mathbf{u}_\Gamma^{n+1} = 2 \frac{\mathbf{d}_{\Gamma,P}^{n+1} - \mathbf{d}_{\Gamma,P}^n}{\Delta t} - \mathbf{u}_\Gamma^n. \quad (6.8)$$

Equation (6.8) can be interpreted as a trapezoidal rule for the interface velocity and it correctly preserves the size of the fluid domain, i.e. it extends geometric conservation to the boundary of the domain. Consequently (6.8) poses the preferable fluid boundary condition which should be used whenever possible. Despite the desirable property of geometrical correctness (6.8) exhibits the tendency of the trapezoidal rule to oscillations and has thus to be replaced by the dissipating condition (6.5) in some sensitive cases.

6.2.4 Structural force boundary condition

Care has also to be taken to obtain the fluid forces which are transferred to the structure. For flows with very low viscosity the coupling is occasionally performed by just exerting the fluid pressures on the structure according to

$$\mathbf{F}_p = - \int_{\Gamma} \bar{p} \mathbf{n} d\gamma. \quad (6.9)$$

For low and moderate REYNOLDS number flows which are considered here the flow friction along the structure should not be neglected and thus

$$\mathbf{F}_{\sigma} = \int_{\Gamma} (2\mu\boldsymbol{\varepsilon}(\mathbf{u}) - \bar{p}\mathbf{I}) \cdot \mathbf{n} d\gamma \quad (6.10)$$

should be evaluated rather than (6.9). However (6.10) suffers from several drawbacks. As the velocities are approximated by C^0 continuous finite element shape functions the viscous tractions exhibit jumps at the element borders and consequently the evaluation of (6.10) does not fit very well into the nodal based data structure of a finite element code. Due to the need to calculate spatial derivatives of the velocity \mathbf{u} the forces \mathbf{F}_{σ} further exhibit an order of accuracy in space which is one order lower than the approximation of the velocity.

Much more accuracy can be squeezed out of the fluid solution by evaluating consistent nodal forces which are also strongly recommended by GRESHO and SANI in [107]. Nodal forces are defined in the discrete setting. In the fully stabilised case given in (4.41) these forces can be obtained from

$$\mathbf{f}_{\Gamma}^F = \frac{1}{\delta} \bar{\mathbf{M}}_{\Gamma}^F(\mathbf{u})\mathbf{u} + \bar{\mathbf{K}}_{\Gamma}^F(\mathbf{u})\mathbf{u} + \bar{\mathbf{N}}_{\Gamma}(\mathbf{u}) + \bar{\mathbf{G}}_{\Gamma}(\mathbf{u})\mathbf{p} - \frac{1}{\delta} \bar{\mathbf{f}}_{b,\Gamma}^F, \quad (6.11)$$

where the subscript Γ denotes the restriction of the respective matrix or vector to the lines corresponding to the interface degrees of freedom. It is worth noting that the nodal fluid force vector \mathbf{f}^F and also \mathbf{f}_{Γ}^F as defined in section 4.3.6 expresses the right hand side of the discrete flow equations normalised by the fluid density ρ^F . Consequently it has the unit force per density and needs to be multiplied by the fluid density in order to obtain the physical coupling forces which will be denoted by \mathbf{f}_{Γ} .

Forces according to (6.11) have a number of desirable properties.

- Consistent nodal forces share the order of accuracy of the pressure and velocity approximation.
- Forces according to (6.11) fit into an element based data structure and are easy to implement.
- Consistent nodal forces account for the influence of the stabilisation and thus the effect of the virtual bubble enriching the approximation space.

When no stabilisation is applied an equivalent expression to (6.11) can be found by considering (3.23).

6.3 Artificial added mass effect

6.3.1 Introduction

Sequential staggered schemes applied to incompressible flows interacting with light-weight structures exhibit an instability which has been named artificial added mass effect. This effect already mentioned by WALL et al. in [228] and LE TALLEC and MOURO in [166] has been investigated by means of a reduced model problem in [38] where it is shown that the onset of the instability can be predicted well within the simplified problem. In [38] CAUSIN et al. reformulate the continuous fluid problem and perform their analysis on a simplified version of the Pressure-POISSON equation which reduces to $-\Delta p = 0$ with appropriate boundary conditions. They eventually give a discrete added mass operator in terms of the discretised Pressure-POISSON equation.

The analysis presented subsequently follows [87] and shows how to obtain an expression of the discrete added mass operator in terms of matrices which are usually computed within fluid codes solving the incompressible Navier-Stokes equations for the primary unknowns \mathbf{u} and p . It further shows why more accurate time discretisation yields an earlier onset of the instability. Also the effect of residual based stabilisation for elements not satisfying the inf-sup condition is considered.

According to the properties of the instability the following observations have repeatedly been reported.

- With decreasing Δt the instability occurs earlier.
- The mass ratio between fluid and structure has a significant influence on the stability of the staggered system. The larger the mass ratio ρ^F/ρ^S the worse the instability gets.
- Numerical observations indicate that increased fluid viscosity increases the instability while increased structural stiffness causes a light decreasing effect.
- The actual onset of unconditional instability depends upon the particular combination of temporal discretisation items where the most inaccurate combination yields best stability properties.

6.3.2 Added mass operator for LBB stable fluid elements

Basic discrete equations

In order to perform a general stability analysis of the coupled problem the spatially discretised flow equations still continuous in time are required. The influence of the particular time discretisation shall be considered subsequently. For inf-sup stable elements where no stabilisation is applied the time continuous matrix equations read

$$\mathbf{M}^F \dot{\mathbf{u}} + \mathbf{N}(\mathbf{u}) + \mathbf{K}^F \mathbf{u} + \mathbf{G}p = \mathbf{f}_\Gamma^F \quad (6.12)$$

$$\mathbf{G}^T \mathbf{u} = \mathbf{0} \quad (6.13)$$

where the matrices and vectors are defined in section 3.3.2. In view of the intended analysis no body forces and tractions are considered in (6.12). Thus the right hand side exclusively consists of FSI-coupling forces along Γ . Equivalently the structural system of

equations reads

$$\mathbf{M}^S \ddot{\mathbf{d}} + \mathbf{F}_{\text{int}}^S(\mathbf{d}) = -\mathbf{f}_\Gamma \quad (6.14)$$

where the damping term has been neglected. The structural interface forces pose the only load on the structure. As the structural equations were discretised directly its right hand side consists of real, physical forces.

Simplifications required for the analysis

Some further simplifications are made in order to ease the analysis.

- The discretisation of fluid and structural field is assumed conforming along the interface Γ .
- Both field equations are regarded as linear.
- The influence of mesh motion and thus the change of all coefficient matrices is negligible.
- The structural density ρ^S remains constant.
- No physical structural damping is assumed.

The first one of the above assumptions simply eases the presentation while the others are reasonable as the instability of consideration is observed very early in the computation when no significant nonlinearity has been built up. In order to perform an eigenvalue analysis of the amplification operator of the coupling procedure the assumption of linearity is further crucial as nonlinear eigenvalues for nonlinear operators are not defined. However the insight obtained from the analysis also transfers to the nonlinear problem.

To simplify further the fluid stiffness and convective term in (6.12) are omitted. This is reasonable at very small time steps where the behaviour of the flow is governed by inertia and incompressibility. Thus this simplification allows to highlight clearly the reason of the instability.

The added mass operator

The assumption that the coefficient matrices do not change in time allows to use the ALE time derivative of the divergence equation (6.13) yielding

$$\left. \frac{\partial (\mathbf{G}^T \mathbf{u})}{\partial t} \right|_x = \overline{\mathbf{G}^T \dot{\mathbf{u}}} = \mathbf{G}^T \dot{\mathbf{u}} = \mathbf{0}. \quad (6.15)$$

The simplified fluid system of equations is now split up into degrees of freedom belonging to the interior of the fluid domain and others at the interface. The split matrices and vectors are labelled by the subscripts I and Γ indicating the interior and interface, respectively. Replacing (6.13) by (6.15) and using the simplifications the fluid system of equations reads

$$\begin{bmatrix} \mathbf{M}_{\text{II}}^F & \mathbf{M}_{\text{I}\Gamma}^F & \mathbf{G}_{\text{I}} \\ \mathbf{M}_{\Gamma\text{I}}^F & \mathbf{M}_{\Gamma\Gamma}^F & \mathbf{G}_{\Gamma} \\ \mathbf{G}_{\text{I}}^T & \mathbf{G}_{\Gamma}^T & \mathbf{0} \end{bmatrix} \begin{bmatrix} \dot{\mathbf{u}}_{\text{I}} \\ \dot{\mathbf{u}}_{\Gamma} \\ \mathbf{p} \end{bmatrix} = \begin{bmatrix} \mathbf{0} \\ \mathbf{f}_{\Gamma}^F \\ \mathbf{0} \end{bmatrix}. \quad (6.16)$$

In (6.16) the interface acceleration is prescribed according to the structural predictor. Thus the problem can be solved for the remaining accelerations and pressures which depend on $\dot{\mathbf{u}}_\Gamma$ and are given by

$$\mathbf{p} = \left(\mathbf{G}_I^T (\mathbf{M}_{II}^F)^{-1} \mathbf{G}_I \right)^{-1} \left(-\mathbf{G}_I^T (\mathbf{M}_{II}^F)^{-1} \mathbf{M}_{II}^F + \mathbf{G}_I^T \right) \dot{\mathbf{u}}_\Gamma, \quad (6.17)$$

$$\dot{\mathbf{u}}_I = - (\mathbf{M}_{II}^F)^{-1} \mathbf{M}_{II}^F \dot{\mathbf{u}}_\Gamma + (\mathbf{M}_{II}^F)^{-1} \mathbf{G}_I \left(\mathbf{G}_I^T (\mathbf{M}_{II}^F)^{-1} \mathbf{G}_I \right)^{-1} \left\{ \mathbf{G}_I^T (\mathbf{M}_{II}^F)^{-1} \mathbf{M}_{II}^F - \mathbf{G}_I^T \right\} \dot{\mathbf{u}}_\Gamma. \quad (6.18)$$

Employing the second line of the system (6.16) the normalised interfacial coupling force vector \mathbf{f}_Γ^F can be expressed in terms of the interface acceleration reading

$$\mathbf{f}_\Gamma^F = \left\{ \left(\mathbf{M}_{\Gamma I}^F (\mathbf{M}_{II}^F)^{-1} \mathbf{G}_I - \mathbf{G}_\Gamma \right) \left(\mathbf{G}_I^T (\mathbf{M}_{II}^F)^{-1} \mathbf{G}_I \right)^{-1} \left(\mathbf{G}_I^T (\mathbf{M}_{II}^F)^{-1} \mathbf{M}_{II}^F - \mathbf{G}_I^T \right) - \mathbf{M}_{\Gamma I}^F (\mathbf{M}_{II}^F)^{-1} \mathbf{M}_{II}^F + \mathbf{M}_{\Gamma \Gamma}^F \right\} \dot{\mathbf{u}}_\Gamma. \quad (6.19)$$

Due to the normalisation of the flow equations the discrete operator in curly brackets has the dimension of a volume. It can be normalised by a characteristic volume of the support of a fluid node v^F to recover a discrete representation of the added mass operator.

$$\mathcal{M}_{\mathcal{A}} := \frac{1}{v^F} \left(\mathbf{M}_{\Gamma I}^F (\mathbf{M}_{II}^F)^{-1} \mathbf{G}_I - \mathbf{G}_\Gamma \right) \left(\mathbf{G}_I^T (\mathbf{M}_{II}^F)^{-1} \mathbf{G}_I \right)^{-1} \left(\mathbf{G}_I^T (\mathbf{M}_{II}^F)^{-1} \mathbf{M}_{II}^F - \mathbf{G}_I^T \right) - \frac{1}{v^F} \mathbf{M}_{\Gamma I}^F (\mathbf{M}_{II}^F)^{-1} \mathbf{M}_{II}^F + \frac{1}{v^F} \mathbf{M}_{\Gamma \Gamma}^F \quad (6.20)$$

Employing the added mass operator (6.20) yields the physical fluid forces at the coupling boundary

$$\mathbf{f}_\Gamma = \rho^F v^F \mathcal{M}_{\mathcal{A}} \dot{\mathbf{u}}_\Gamma = m^F \mathcal{M}_{\mathcal{A}} \dot{\mathbf{u}}_\Gamma \quad (6.21)$$

where m^F denotes a characteristic mass of a fluid node, i.e. $m^F = \rho^F v^F$. The added mass operator $\mathcal{M}_{\mathcal{A}}$ contains the condensed fluid equations and maps a dimensionless interface acceleration onto an also dimensionless force vector at the interface Γ . Thus the operator is purely geometrical. It can be observed from (6.20) that the discrete added mass operator is symmetric and positive.

A further interesting simplification is to use a lumped fluid mass matrix. Then the off-diagonal blocks of the mass matrix vanish and assuming a regular mesh the main blocks are replaced by

$$\mathbf{M}_{II}^F = 2 v^F \mathbf{I}_{II} \quad \text{and} \quad \mathbf{M}_{\Gamma \Gamma}^F = v^F \mathbf{I}_{\Gamma \Gamma} \quad (6.22)$$

yielding the simple expression

$$\mathcal{M}_{\mathcal{A}} = \mathbf{I}_{\Gamma \Gamma}^F + 2 \mathbf{G}_\Gamma \left(\mathbf{G}_I^T \mathbf{G}_I \right)^{-1} \mathbf{G}_\Gamma^T \quad (6.23)$$

for the lumped added mass operator. Expression (6.23) indicates that the eigenvalues of the added mass operator exceed one. It can further be observed that the discrete gradient operator matrix \mathbf{G}_I needs to have full rank if the added mass operator exists, i.e. if the flow equations have a unique solution.

6.3.3 Added mass operator for stabilised finite elements

Stabilised discrete equations

A matrix representation of the stabilised flow problem still continuous in time replacing (6.12) and (6.13) reads

$$\overline{\mathbf{M}}^{\text{F}}(\mathbf{u})\dot{\mathbf{u}} + \overline{\mathbf{N}}^{\text{F}}(\mathbf{u}) + \overline{\mathbf{G}}(\mathbf{u})\mathbf{p} = \overline{\mathbf{f}}_{\Gamma}^{\text{F}} \quad (6.24)$$

$$\overline{\mathbf{G}}_{\text{M}}^{\text{T}}\dot{\mathbf{u}} + \overline{\mathbf{G}}_{\text{K}}^{\text{T}}(\mathbf{u})\mathbf{u} - \overline{\mathbf{C}}\mathbf{p} = \mathbf{0}, \quad (6.25)$$

where the single matrices are defined in section 4.3.6. As in the unstabilised case the fluid momentum balance equation (6.24) has been normalised by the fluid density ρ^{F} .

Some simplifications

In order to perform an analysis simplifications similar to the unstabilised case have to be made. Thus the system (6.24) and (6.25) is considered in the limit of very small time step size. Recalling the limit of the stabilisation parameter $\lim_{\Delta t \rightarrow 0} \tau_{\text{Me}} = 1$ from section 5.2.2 it can be observed from (6.25) or also (4.42) that in the regime of small time steps the leading terms of $\overline{\mathbf{G}}_{\text{M}}^{\text{T}}$ and $\overline{\mathbf{G}}_{\text{K}}^{\text{T}}$ are of the same order of magnitude in Δt . While for very small time steps the stiffness terms in (6.24) are of minor influence compared to the mass terms this is not the case in (6.25). In order to still reduce the system (6.24), (6.25) to one relating pressures and accelerations the continuity equation

$$\nabla \cdot \mathbf{u} = 0 \quad \text{is replaced by} \quad \delta \nabla \cdot \dot{\mathbf{u}} = 0, \quad (6.26)$$

which can be done provided that a divergence free initial velocity field is used. The substitution (6.26) does not change the system but rather somewhat anticipates the effect of temporal discretisation.

Along with the restriction to stabilisation variants with $\eta = 0$, i.e. no additional zeroth order term within the stabilisation operator, this allows to write the system (6.24) and (6.25) in the small time step limit in terms of nodal accelerations $\dot{\mathbf{u}}$ and nodal pressure values \mathbf{p} and to obtain the simplified system

$$\mathbf{M}^{\text{F}}\dot{\mathbf{u}} + \mathbf{G}\mathbf{p} = \mathbf{f}_{\Gamma}^{\text{F}} \quad (6.27)$$

$$\overline{\overline{\mathbf{G}}}^{\text{T}}\dot{\mathbf{u}} - \overline{\mathbf{C}}\mathbf{p} = \mathbf{0} \quad (6.28)$$

where the bar has been dropped on the matrices of the first line indicating that the stabilisation terms here are of higher order in Δt and thus of minor influence. In (6.28) the matrix $\overline{\overline{\mathbf{G}}}^{\text{T}}$ represents the sum

$$\mathbf{q}^{\text{T}}\overline{\overline{\mathbf{G}}}^{\text{T}}\dot{\mathbf{u}} = \mathbf{q}^{\text{T}}\left(\overline{\mathbf{G}}_{\text{M}}^{\text{T}} + \mathbf{G}^{\text{T}}\right)\dot{\mathbf{u}} = -\beta \sum_e \tau_{\text{Me}} (\dot{\mathbf{u}}, \delta \nabla q)_{\Omega_e} - \beta \delta (\nabla \cdot \dot{\mathbf{u}}, q)_{\Omega_{\text{F}}^{2+1}}. \quad (6.29)$$

The matrices $\overline{\mathbf{G}}_{\text{M}}^{\text{T}}$ and \mathbf{G}^{T} have been defined in section 4.3.6 and section 3.3.2, respectively. As the parameter β scales the pressure test function and thus the entire matrix equation (6.28) $\beta = 1$ might be assumed here without loss of generality.

Added mass operator in the stabilised case

Analogous to (6.16) the system

$$\begin{bmatrix} \mathbf{M}_{\text{II}}^{\text{F}} & \mathbf{M}_{\text{I}\Gamma}^{\text{F}} & \mathbf{G}_{\text{I}} \\ \mathbf{M}_{\text{I}\Gamma}^{\text{F}} & \mathbf{M}_{\text{II}}^{\text{F}} & \mathbf{G}_{\text{I}} \\ \overline{\mathbf{G}}_{\text{I}}^{\text{T}} & \overline{\mathbf{G}}_{\text{I}}^{\text{T}} & -\overline{\mathbf{C}} \end{bmatrix} \begin{bmatrix} \dot{\mathbf{u}}_{\text{I}} \\ \dot{\mathbf{u}}_{\text{I}\Gamma} \\ \mathbf{p} \end{bmatrix} = \begin{bmatrix} \mathbf{0} \\ \mathbf{f}_{\text{I}\Gamma}^{\text{F}} \\ \mathbf{0} \end{bmatrix} \quad (6.30)$$

is obtained which yields the fluid acceleration and pressure depending on a prescribed interface acceleration $\dot{\mathbf{u}}_{\text{I}\Gamma}$ according to

$$\mathbf{p} = \left(\overline{\mathbf{G}}_{\text{I}}^{\text{T}} (\mathbf{M}_{\text{II}}^{\text{F}})^{-1} \mathbf{G}_{\text{I}} + \overline{\mathbf{C}} \right)^{-1} \left(\overline{\mathbf{G}}_{\text{I}}^{\text{T}} - \overline{\mathbf{G}}_{\text{I}}^{\text{T}} (\mathbf{M}_{\text{II}}^{\text{F}})^{-1} \mathbf{M}_{\text{I}\Gamma}^{\text{F}} \right) \dot{\mathbf{u}}_{\text{I}\Gamma} \quad (6.31)$$

$$\begin{aligned} \dot{\mathbf{u}}_{\text{I}} = - \left((\mathbf{M}_{\text{II}}^{\text{F}})^{-1} \mathbf{M}_{\text{I}\Gamma}^{\text{F}} + (\mathbf{M}_{\text{II}}^{\text{F}})^{-1} \mathbf{G}_{\text{I}} \left(\overline{\mathbf{G}}_{\text{I}}^{\text{T}} (\mathbf{M}_{\text{II}}^{\text{F}})^{-1} \mathbf{G}_{\text{I}} + \overline{\mathbf{C}} \right)^{-1} \right. \\ \left. \left(\overline{\mathbf{G}}_{\text{I}}^{\text{T}} - \overline{\mathbf{G}}_{\text{I}}^{\text{T}} (\mathbf{M}_{\text{II}}^{\text{F}})^{-1} \mathbf{M}_{\text{I}\Gamma}^{\text{F}} \right) \right) \dot{\mathbf{u}}_{\text{I}\Gamma}. \end{aligned} \quad (6.32)$$

Inserting (6.31) and (6.32) into the second line of the split system (6.30) and multiplying by the fluid density ρ^{F} yields the physical fluid force at the coupling interface Γ

$$\mathbf{f}_{\Gamma} = \rho^{\text{F}} v^{\text{F}} \mathcal{M}_{\mathcal{A}\text{stab}} \dot{\mathbf{u}}_{\text{I}\Gamma} = m^{\text{F}} \mathcal{M}_{\mathcal{A}\text{stab}} \dot{\mathbf{u}}_{\text{I}\Gamma} \quad (6.33)$$

with the added mass operator in the stabilised case given by

$$\begin{aligned} \mathcal{M}_{\mathcal{A}\text{stab}} := & \frac{1}{v^{\text{F}}} \left(\mathbf{M}_{\text{I}\Gamma}^{\text{F}} (\mathbf{M}_{\text{II}}^{\text{F}})^{-1} \mathbf{G}_{\text{I}} - \mathbf{G}_{\text{I}} \right) \left(\overline{\mathbf{G}}_{\text{I}}^{\text{T}} (\mathbf{M}_{\text{II}}^{\text{F}})^{-1} \mathbf{G}_{\text{I}} + \overline{\mathbf{C}} \right)^{-1} \\ & \left(\overline{\mathbf{G}}_{\text{I}}^{\text{T}} (\mathbf{M}_{\text{II}}^{\text{F}})^{-1} \mathbf{M}_{\text{I}\Gamma}^{\text{F}} - \overline{\mathbf{G}}_{\text{I}}^{\text{T}} \right) \\ & - \frac{1}{v^{\text{F}}} \mathbf{M}_{\text{I}\Gamma}^{\text{F}} (\mathbf{M}_{\text{II}}^{\text{F}})^{-1} \mathbf{M}_{\text{I}\Gamma}^{\text{F}} + \frac{1}{v^{\text{F}}} \mathbf{M}_{\text{I}\Gamma}^{\text{F}}. \end{aligned} \quad (6.34)$$

With a lumped mass matrix the operator reduces to

$$\mathcal{M}_{\mathcal{A},\text{stab}} = \mathbf{I}_{\text{I}\Gamma}^{\text{F}} + 2\mathbf{G}_{\Gamma} \left(\overline{\mathbf{G}}_{\text{I}}^{\text{T}} \mathbf{G}_{\text{I}} + v^{\text{F}} \overline{\mathbf{C}} \right)^{-1} \overline{\mathbf{G}}_{\Gamma}^{\text{T}}. \quad (6.35)$$

The expression (6.35) suggests that some of the eigenvalues of the added mass operator might exceed one. While a strict mathematical prove of the positivity of the second term in (6.35) appears difficult or even impossible the operator (6.35) physically describes the same as (6.23) and maps an interface acceleration $\dot{\mathbf{u}}_{\text{I}\Gamma}$ onto an interface force vector. Corresponding to the composition of the added mass operator this interface force vector consists of two parts. The first ones are forces due to nodal inertia which are obtained from the first term in (6.35). The second part of these forces are forces due to incompressibility resulting from the second term of (6.35). If $2\mathbf{G}_{\Gamma} \left(\overline{\mathbf{G}}_{\text{I}}^{\text{T}} \mathbf{G}_{\text{I}} + v^{\text{F}} \overline{\mathbf{C}} \right)^{-1} \overline{\mathbf{G}}_{\Gamma}^{\text{T}}$ was strictly non-positive, i.e if one would obtain

$$\dot{\mathbf{u}}^{\text{T}} \left(2\mathbf{G}_{\Gamma} \left(\overline{\mathbf{G}}_{\text{I}}^{\text{T}} \mathbf{G}_{\text{I}} + v^{\text{F}} \overline{\mathbf{C}} \right)^{-1} \overline{\mathbf{G}}_{\Gamma}^{\text{T}} \right) \dot{\mathbf{u}} \leq 0 \quad \text{for all possible } \dot{\mathbf{u}} \quad (6.36)$$

this would be equivalent to exclusively negative energies generated by the incompressibility at the interface. In other words (6.36) would imply that all possible interface accelerations result in either no interfacial forces or such of the opposite direction to the interface acceleration. This is physically strongly unreasonable. It is thus not far-fetched to assume that the second term in (6.35) exhibits at least some positive eigenvalues and the overall eigenvalue of the added mass operator in the stabilised case exceeds one.

As the largest eigenvalue of the added mass operator governs the stability limit the added mass operator in the stabilised case deserves a closer look.

Discussion of the influence of stabilisation

While seemingly very similar to the added mass operator obtained in the unstabilised case (6.23) the operator (6.35) exhibits some significant differences. A first difference is the presence of the stabilisation matrix $\overline{\mathbf{C}}$ which is required as the matrix \mathbf{G} is not of full rank. Thus the positive matrix $\overline{\mathbf{C}}$ ensures that the term in brackets can be inverted. If $\overline{\mathbf{C}}$ is chosen too small this expression exhibits very small eigenvalues which might increase the maximal eigenvalue of the added mass operator. Thus the properly chosen amount of stabilisation is crucial. An alternative interpretation is that due to stabilisation the incompressibility condition is relaxed an effect which is caused by the presence of the matrix $\overline{\mathbf{C}}$. In this sense fluid stabilisation to some extent also stabilises the artificial added mass effect. However there is no direct influence of the time step size in (6.34) or (6.35) as all the over-lined matrices depend linearly on δ while the remaining matrices are independent of the time step size. Consequently the onset of a dramatic instability at reduced time step size may well have further reasons.

A second important difference to the unstabilised case is the now obtained unsymmetry of the added mass operator caused by $\overline{\mathbf{G}} \neq \mathbf{G}$. A closer look at (6.29) reveals

$$\begin{aligned} \overline{\mathbf{qG}}^T \dot{\mathbf{u}} &= - \sum_e \{ \tau_{Me} (\dot{\mathbf{u}} \cdot \mathbf{n}, \delta q)_{\partial\Omega_e} + \delta(1 - \tau_{Me}) (\nabla \cdot \dot{\mathbf{u}}, q)_{\Omega_e} \} \\ &= \mathbf{q\tilde{G}}^T \dot{\mathbf{u}} + \sum_e \delta(1 - \tau_{Me}) \mathbf{qG}_e^T \dot{\mathbf{u}}, \end{aligned} \quad (6.37)$$

where \mathbf{G}_e^T denotes the contribution of element e to \mathbf{G}^T . Thus for $\delta t \rightarrow 0$ and $\tau_{Me} \rightarrow 1$ the stabilised version of the continuity equation yields a matrix $\overline{\mathbf{G}}^T$ which contains a contribution of the original operator matrix \mathbf{G}^T that vanishes for very small time steps where $\tau_{Me} \rightarrow 1$. It further contains a boundary integral term $\tilde{\mathbf{G}}^T$ emerging from integration by parts. From (6.37) it can be observed that the continuity equation within the domain is cancelled at the small time step limit while the remaining boundary term demands global mass conservation by balancing the amount of inflow and outflow with the changes of the domain due to a displacement of the interface Γ .

Stability of the stabilised flow problem (4.32) has been shown in section 5.2.3 by means of a model problem. This stability now implies that the expression $\overline{\mathbf{G}}_I^T \mathbf{G}_I + v^F \overline{\mathbf{C}}$ in (6.35) can be inverted. However due to the unsymmetry of this matrix which increases with decreasing time step size the minimal eigenvalue might be rather small compared to the unstabilised case. This yields a possibly large maximal eigenvalue of the overall added

mass operator. An increased eigenvalue of the added mass operator however results in an earlier onset of the instability as it will be shown in section 6.3.4.

Numerical investigations confirm the above interpretation. As the matrix $\bar{\mathbf{G}}_M^T$ is required for the consistency of the stabilisation method in the transient case and does not contribute to the stabilising effects of the stabilisation terms it can be omitted without sacrificing stability of the fluid equations. In particular it has been observed that removing the matrix $\bar{\mathbf{G}}_M^T$ and thus introducing a consistency error restores the stability for small time step sizes at least for some time discretisation schemes. However this omission is not meant to be used for practical computations but rather understood as a means to clarify the effect of stabilisation on the artificial added mass effect.

A derivation of a discrete representation of the added mass operator reveals that while in an unstabilised case this operator is purely geometrical in the stabilised case it depends upon the time step size.

6.3.4 Influence of the discretisation in time

Introducing the physical coupling force (6.21) or (6.33) into the discrete linearised structural equation (6.14) which has been split into interface degrees of freedom at Γ and remaining ones yields

$$\begin{bmatrix} \mathbf{M}_{\Pi}^S & \mathbf{M}_{\Pi\Gamma}^S \\ \mathbf{M}_{\Gamma\Pi}^S & \mathbf{M}_{\Gamma\Gamma}^S \end{bmatrix} \begin{bmatrix} \ddot{\mathbf{d}}_{\Pi} \\ \ddot{\mathbf{d}}_{\Gamma} \end{bmatrix} + \begin{bmatrix} \mathbf{K}_{\Pi}^S & \mathbf{K}_{\Pi\Gamma}^S \\ \mathbf{K}_{\Gamma\Pi}^S & \mathbf{K}_{\Gamma\Gamma}^S \end{bmatrix} \begin{bmatrix} \mathbf{d}_{\Pi} \\ \mathbf{d}_{\Gamma} \end{bmatrix} = \begin{bmatrix} \mathbf{0} \\ -m^F \mathcal{M}_{\mathcal{A}} \dot{\mathbf{u}}_{\Gamma} \end{bmatrix}, \quad (6.38)$$

where within the staggered scheme the fluid interface acceleration $\dot{\mathbf{u}}_{\Gamma}$ is obtained from a structural prediction of the new interface displacement. The matrix \mathbf{K}^S denotes the structural tangent stiffness obtained from a linearisation of the internal structural forces $\mathbf{N}^S(\mathbf{d})$.

Equation (6.38) reveals why $\mathcal{M}_{\mathcal{A}}$ is named ‘added mass operator’. Identifying the fluid interface acceleration $\dot{\mathbf{u}}_{\Gamma}$ with the structural interface acceleration $\ddot{\mathbf{d}}_{\Gamma}$ shows that the product $m^F \mathcal{M}_{\mathcal{A}}$ works as an additional mass on the interface degrees of freedom.

In the context of the coupled FSI problem the overall time discretisation scheme is composed of the single schemes applied on the fluid and structural field, the structural predictor and the way of determining the fluid DIRICHLET boundary condition. For the subsequent analysis the time discretisation schemes employed to solve a temporally discretised version of (6.38) are distinguished into two main classes. One class of such overall time discretisation methods yields fluid and structural interface accelerations depending upon a limited number of previous interface positions. These schemes shall be termed *schemes with limited recursion*. On the other hand there are schemes which yield expressions for the accelerations of the two fields which depend upon all previously computed interface positions. Those formulations will be called *recursive* or also *fully recursive*.

Within the subsequent analysis discretisation items of different order of accuracy are combined. Clearly the lowest order contribution governs the overall order of accuracy making some of the considered schemes rather unattractive. However the combinations serve to enhance understanding rather than being applicable schemes. It can further be observed that a combination of higher order discretisation items worsens the stability problems.

Schemes with limited recursion

The stability or instability of the scheme (6.38) solved in a sequentially staggered manner depends upon the particular time discretisation employed. The most stable version of the structural generalised- α time discretisation scheme is obtained when maximal numerical dissipation is involved, i.e. when the spectral radius of the scheme is set to $\rho_\infty = 0.0$. This yields the parameter

$$\alpha_m = -1, \quad \alpha_f = 0, \quad \beta = 1, \quad \gamma = \frac{3}{2}.$$

Using these parameters in (2.21), (2.22) and (2.26) to (2.24) allows to obtain an expression for the structural acceleration in terms of displacements reading

$$\ddot{\mathbf{d}}^\alpha = \frac{1}{\Delta t^2} (2\mathbf{d}^{n+1} - 5\mathbf{d}^n + 4\mathbf{d}^{n-1} - \mathbf{d}^{n-2}). \quad (6.39)$$

The fluid acceleration $\dot{\mathbf{u}}_\Gamma$ is also expressed in terms of structural displacements. Using backward EULER time integration, the zeroth order interface predictor (6.2) and the first order interpolation of the boundary condition at the interface yields

$$\dot{\mathbf{u}}_\Gamma^{n+1} = \frac{1}{\Delta t^2} (\mathbf{d}_\Gamma^n - 2\mathbf{d}_\Gamma^{n-1} + \mathbf{d}_\Gamma^{n-2}). \quad (6.40)$$

Inserting (6.39) into the discrete linearised structural system of equations gives

$$\mathbf{M}^S \frac{1}{\Delta t^2} (2\mathbf{d}^{n+1} - 5\mathbf{d}^n + 4\mathbf{d}^{n-1} - \mathbf{d}^{n-2}) + \mathbf{K}^S \mathbf{d}^{n+1} = \mathbf{f}^{n+1}, \quad (6.41)$$

where \mathbf{f}^{n+1} represents forces on the structure at the new time level $n + 1$. For very small time steps (6.41) is dominated by the structural mass term while the stiffness loses influence. Omitting the stiffness and lumping the mass term in a temporally discretised version of (6.38) allows to reduce the system to the interfacial degrees of freedom according to

$$m^S (2\mathbf{d}_\Gamma^{n+1} - 5\mathbf{d}_\Gamma^n + 4\mathbf{d}_\Gamma^{n-1} - \mathbf{d}_\Gamma^{n-2}) + m^F \mathcal{M}_\mathcal{A} (\mathbf{d}_\Gamma^n - 2\mathbf{d}_\Gamma^{n-1} + \mathbf{d}_\Gamma^{n-2}) = \mathbf{0}. \quad (6.42)$$

As the added mass operator $\mathcal{M}_\mathcal{A}$ is a real positive matrix all vectors in (6.42) can be expanded in terms of the eigenvectors \mathbf{v}_i of $\mathcal{M}_\mathcal{A}$, i.e. $\mathbf{d}_\Gamma^n = \sum_i d_i^n \mathbf{v}_i$. The scalar coefficients d_i have to satisfy

$$2d_i^{n+1} - 5d_i^n + 4d_i^{n-1} - d_i^{n-2} + \mu_i \frac{m^F}{m^S} (d_i^n - 2d_i^{n-1} + d_i^{n-2}) = 0, \quad (6.43)$$

where μ_i represents the i th eigenvalue of $\mathcal{M}_\mathcal{A}$. Inserting the amplification factor λ_i with $d_i^{n+1} = \lambda_i d_i^n$ into (6.43) yields the characteristic polynomial of (6.43) associated with μ_i .

$$2\lambda_i^3 - 5\lambda_i^2 + 4\lambda_i - 1 + \mu_i \frac{m^F}{m^S} (\lambda_i^2 - 2\lambda_i + 1) = p(\lambda_i) = 0 \quad (6.44)$$

All solutions λ_i of (6.44) have to satisfy $|\lambda_i| \leq 1$ if the scheme (6.42) is stable. The diagram in figure 6.1 shows an array of curves $p(\lambda_i)$ for an increasing maximal eigenvalue of the added mass operator and fixed mass ratio of $m^F/m^S = 1$. The curve exhibits a double

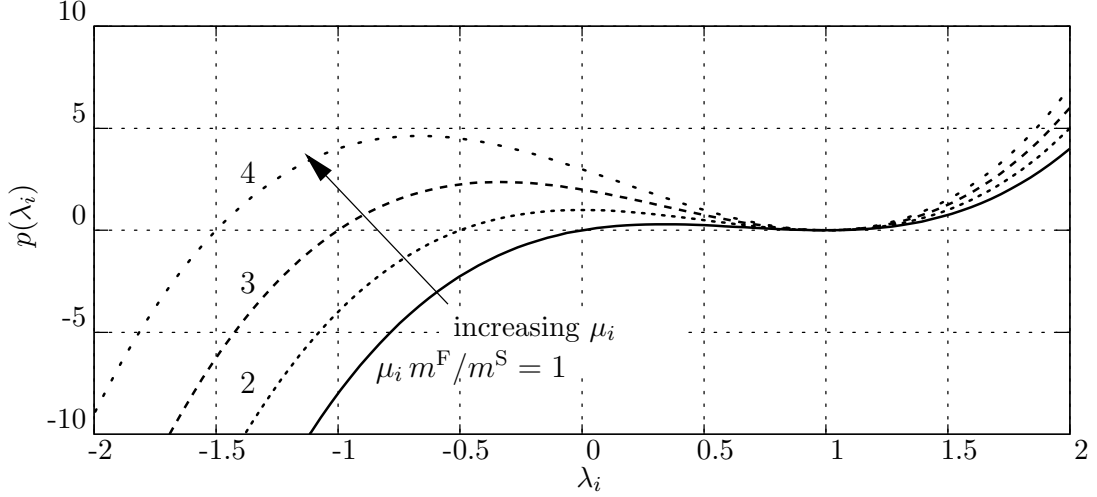


Figure 6.1: Polynomial $p(\lambda_i)$ according to (6.44) for different values of μ_i

root at $\lambda_i = 1$ which is a typical behaviour of polynomials obtained from extrapolations. It can be observed that increasing μ_i (or equivalently increasing the mass ratio) shifts the lowest root further left increasing its absolute value.

Using the double root $\lambda_{i;1,2} = 1$ a third root is found by solving the remaining linear equation

$$2\lambda_{i;3} - 1 + \mu_i \frac{m^F}{m^S} = 0,$$

yielding $\lambda_{i;3} \leq 1/2$. The system is unstable if $\lambda_{i;3} < -1$ which gives the instability condition

$$\frac{m^F}{m^S} \max_i \mu_i > 3. \quad (6.45)$$

While the third order polynomial (6.44) allows to be solved exactly this is no longer possible when more complicated time discretisation schemes are employed. Observing that the potential instability is found for $\lambda_i < -1$ rather than $\lambda_i > 1$ the approach in [38] is pursued noting that $p(-\infty) = -\infty$ and $p(-1) = -12 + 4 m^F / m^S \mu_i$. A change in sign between $p(-\infty)$ and $p(-1)$ indicates a solution $p(\lambda^*) = 0$ with $\lambda^* < -1$ which again yields the instability condition (6.45).

As all the ingredients of the above scheme are very good-natured in the sense that high numerical damping on both the structural and fluid part is involved, (6.45) is a very permissive result. Repeating the analysis by using BDF2 (3.14) rather than BE to discretise the fluid part in time yields

$$\dot{\mathbf{u}}_{\Gamma}^{n+1} = \frac{1}{2 \Delta t^2} (3\mathbf{d}_{\Gamma}^n - 7\mathbf{d}_{\Gamma}^{n-1} + 5\mathbf{d}_{\Gamma}^{n-2} - \mathbf{d}_{\Gamma}^{n-3}). \quad (6.46)$$

In this case the characteristic polynomial is given by

$$4\lambda_i^4 - 10\lambda_i^3 + 8\lambda_i^2 - 2\lambda_i + \mu_i \frac{m^F}{m^S} (3\lambda_i^3 - 7\lambda_i^2 + 5\lambda_i - 1) = p(\lambda_i) = 0$$

and yields the instability condition

$$\frac{m^F}{m^S} \max_i \mu_i > \frac{3}{2}. \quad (6.47)$$

Changing from first order accurate BE to BDF2 on the fluid part of the problem results in an instability condition which is twice as restrictive. In table 6.1 the instability constants C_{inst} of the instability condition

$$\frac{m^F}{m^S} \max_i \mu_i > C_{\text{inst}} \quad (6.48)$$

obtained with generalised- α time integration (with $\rho_\infty = 0$) of the structural domain, first order interpolation at the interface Γ (6.5) and the different structural predictors (6.2)-(6.4) are summarised.

Table 6.1: Instability constant C_{inst} in condition (6.48) obtained for sequentially staggered fluid-structure interaction schemes depending upon the structural predictors (6.2)-(6.4) and the fluid time discretisation scheme

predictor	BE	BDF2
0th order	3	$\frac{3}{2}$
1st order	$\frac{3}{5}$	$\frac{3}{10}$
2nd order	$\frac{1}{3}$	$\frac{1}{6}$

It shows that increased accuracy results in a significantly earlier onset of the instability. Another remarkable result is that switching from BE to BDF2 on the fluid domain results in an instability condition twice as restrictive.

Remark 6.3.1 More accurate extrapolation in time yields a closer restriction of the stability constant. Similar observations have been made by HUND in [145] where higher order predictors eventually caused divergence of an iterative approach used for multiscale structural analysis. This effect appears to be inherent in polynomial extrapolation and reminds of the well known shrinking stability domain for higher order backward differentiation formulae [112].

Remark 6.3.2 In the present context one might be interested in the general behaviour of characteristic polynomials resulting from time discretisation schemes with limited recursion. Apparently such polynomials do always exhibit a double root at $\lambda = 1$ which is related to the fact that a constant displacement corresponds to zero velocity and also zero acceleration.

Schemes with fully recursive characteristics

Coupling schemes which employ the TR for fluid time integration or use the geometrically correct version for the DIRICHLET boundary condition on the fluid structure interface (6.8) are a little more difficult to treat than the previous ones. Such algorithms do not exhibit an expression for the predicted fluid interface acceleration in terms of a limited number

of previous interface displacements comparable to (6.40) but rather require all previous interface positions to be considered, i.e. cycle down to the initial conditions.

To sample the following scheme is considered:

- structure: generalised- α with $\rho_\infty = 0$
- fluid:
 - time discretisation: TR
 - predictor: zeroth order (6.2)
 - Dirichlet boundary condition: first order (6.5)

Here the particular influence of the trapezoidal rule employed on the fluid domain shall be investigated. The results obtained for a fully second order scheme with TR and a second order accurate predictor and boundary condition are even more restrictive.

While the structural acceleration is given by the expression (6.39), the fluid acceleration is obtained from

$$\dot{\mathbf{u}}_\Gamma^{n+1} = \frac{1}{\Delta t^2} (2\mathbf{d}_\Gamma^n - 4\mathbf{d}_\Gamma^n + 2\mathbf{d}_\Gamma^{n-1}) - \dot{\mathbf{u}}_\Gamma^n,$$

which cannot be expressed exclusively in interface displacements. The amplification of the scheme thus depends upon the actual time step. Assuming that the initial condition includes zero acceleration of the interface, i.e. $\dot{\mathbf{u}}_\Gamma^0 = \mathbf{0}$ the first step ($n = 0$) yields

$$2\mathbf{d}_\Gamma^1 - 5\mathbf{d}_\Gamma^0 + \mathcal{M}\mathcal{A} \frac{m^F}{m^S} 2\mathbf{d}_\Gamma^0 = \mathbf{0}$$

and the characteristic polynomial

$$2\lambda - 5 + 2\mu_i \frac{m^F}{m^S} = p(\lambda) = 0.$$

With $p(\lambda = -\infty) = -\infty$ and $p(\lambda = -1) = -7 + 2\mu_i m^F/m^S$ one obtains the instability condition for the first step which is unstable if

$$\max_i \mu_i \frac{m^F}{m^S} > \frac{7}{2} \quad (6.49)$$

is satisfied. With $n = 1$

$$2\mathbf{d}_\Gamma^2 - 5\mathbf{d}_\Gamma^1 + 4\mathbf{d}_\Gamma^0 + \mathcal{M}\mathcal{A} \frac{m^F}{m^S} (2\mathbf{d}_\Gamma^1 - 6\mathbf{d}_\Gamma^0) = \mathbf{0}$$

is obtained and so is

$$2\lambda^2 - 5\lambda + 4 + \mu_i \frac{m^F}{m^S} (2\lambda - 6) = p(\lambda) = 0.$$

As $p(\lambda = -\infty) = \infty$ and $p(\lambda = -1) = 11 - 8\mu_i m^F/m^S$ the corresponding instability condition reads

$$\max_i \mu_i \frac{m^F}{m^S} > \frac{11}{8}. \quad (6.50)$$

Analogously the next ($n = 2$) step gives

$$2\mathbf{d}_\Gamma^3 - 5\mathbf{d}_\Gamma^2 + 4\mathbf{d}_\Gamma^1 - \mathbf{d}_\Gamma^0 + \mathcal{M}_\mathcal{A} \frac{m^F}{m^S} (2\mathbf{d}_\Gamma^2 - 6\mathbf{d}_\Gamma^1 + 8\mathbf{d}_\Gamma^0) = \mathbf{0},$$

which by means of the characteristic polynomial

$$2\lambda^3 - 5\lambda^2 + 4\lambda - 1 + \mu_i \frac{m^F}{m^S} (2\lambda^2 - 6\lambda + 8) = p(\lambda) = 0$$

yields the instability limit of the third step reading

$$\max_i \mu_i \frac{m^F}{m^S} > \frac{3}{4}. \quad (6.51)$$

The instability conditions of all further steps n is obtained accordingly. It is given by

$$\max_i \mu_i \frac{m^F}{m^S} > \frac{12}{8n} \quad \text{for } n > 1, \quad (6.52)$$

which shows that the scheme with fixed geometry and mass ratio becomes unstable after a limited number of steps irrespective of the mass ratio or the added mass operator themselves. Similar results can be obtained when the coupling condition (6.8) is employed. Additionally, the combination of higher order ingredients (time discretisation scheme, predictor, coupling condition) and a recursive scheme destabilises even faster.

Thus a fluid time discretisation scheme which employs the trapezoidal rule (or also the one-step- θ scheme with $\theta \neq 1$) or the geometrically correct coupling condition (6.8) cannot be employed in a sequentially staggered scheme if stable long-time simulations are to be guaranteed.

6.3.5 Consequences of the artificial added mass effect

Summarising the previous results it can be stated that sequentially staggered schemes yield an instability condition of the form (6.48) where the maximal eigenvalue of the added mass operator $\max_i \mu_i$ is larger than one. The constant C_{inst} on the other hand is smaller than one for all schemes with an accuracy which is of interest. With respect to the mass ratio different cases can be considered.

- Fluid mass density larger is than structural mass density. This is the case for interactions of water with light structures able to swim such as foils from synthetics. A wide variety of technical fluid-structure interaction processes falls into this category. Such problems simulated by a simple sequentially staggered scheme will definitely be unstable.
- Fluid and mass density are of comparable magnitude. Typical applications include biological or physiological flows like blood flow-vessel interaction. Sequentially staggered simulations of such problems are typically unstable. In fact instabilities observed in sequential blood flow simulations were one driving force for the investigation of the artificial added mass effect [38, 80].
- The structural mass density is significantly larger than the fluid one. This is the case for most interactions of structures with airflow. Here conditionally stable sequential computations might be possible. Additionally these applications frequently require compressible flow where the artificial added mass effect has not been observed.

Altogether it has to be concluded that the artificial added mass effect excludes sequential partitioned schemes for a wide range of interesting applications.

6.3.6 General instability

It remains the question if by intelligently tuning the discretisation items a scheme can be defined which is stable irrespective of the mass ratio. In [193, 194] modifications at the load- and motion transfer in the context of coupled aeroelastic problems are suggested to improve the accuracy and stability of the overall scheme which show beneficial in particular for compressible flow.

However it turns out that when incompressible flow is considered these modifications might postpone the onset of the instability while being unable to actually prevent it. Irrespective of the particular time discretisation schemes the sequential staggered coupling scheme itself carries an inherent instability as stated by the following theorem.

Theorem 4 *For every sequentially staggered scheme constructed as described in section 6.2.1, a mass ratio m^F/m^S exists at which the overall algorithm becomes unstable.*

Proof. For every sequentially staggered scheme the structural predictor for the displacement of the interface Γ at time level $n + 1$ contains previous structural information up to time level n only. Thus the general appearance of the scheme is

$$\sum_{j=0}^{n+1} a_j \mathbf{d}_\Gamma^j + \mathcal{M}_A \frac{m^F}{m^S} \sum_{k=0}^n b_k \mathbf{d}_\Gamma^k = \mathbf{0}, \quad (6.53)$$

where $a_j, b_k \in \mathbb{R}$ are the coefficients defining the particular time discretisation scheme. Equation (6.53) yields the characteristic polynomial

$$p^S(\lambda) + \mu_i \frac{m^F}{m^S} p^F(\lambda) = p(\lambda) = 0, \quad (6.54)$$

where the polynomial defined by the time discretisation of the structure is denoted by $p^S(\lambda) = \sum_{j=0}^{n+1} a_j \lambda^j$ while the polynomial $p^F(\lambda) = \sum_{k=0}^n b_k \lambda^k$ contains the temporal discretisation of the fluid partition, the type of the structural predictor and Dirichlet coupling velocity. The polynomial $p^S(\lambda)$ is one degree higher in λ due to the sequential structure of the problem. Thus one obtains

$$\frac{p^S(\lambda = -\infty)}{p^F(\lambda = -\infty)} < 0,$$

i.e. both polynomials are of different sign in the infinite negative. As the polynomials are continuous this implies that a point $\lambda^* < -1$ can be found which satisfies

$$\frac{p^S(\lambda^*)}{p^F(\lambda^*)} < 0.$$

Consequently there exists a positive coefficient a such that

$$p^S(\lambda^*) + a p^F(\lambda^*) = 0.$$

Hence for $a = \max_i \mu_i m^F/m^S$ the characteristic polynomial (6.54) exhibits a solution with $|\lambda^*| > 1$ and the underlying scheme is unstable. \square

6.3.7 Further influences on the artificial added mass effect

For a simplified coupled model problem an added mass operator can be defined the eigenvalues of which precisely predict the onset of instabilities as shown by CAUSIN et al. in [38]. Real fluid structure interaction problems however introduce a significant number of additional influences. There are physical effects which bring more complexity.

- First of all fluid viscosity and structural stiffness the latter possibly including contributions from geometric nonlinearities cannot be ignored within such applications. Using implicit time discretisation on both fields results in an stabilising effect of structural stiffness on the added mass instability. Viscous fluid forces however increase the influence of the instability. Clearly both effects depend upon the time step Δt as a reduced time step size decreases the influence of the stiffness terms compared to the mass matrices.
- Further there are nonlinearities due to the convective fluid term and also material or geometrical nonlinearities of the structural behaviour. Typically simulations start from a reference configuration and zero velocities. Nonlinearities not dominating within the first few steps build up and preclude the existence of a linear added mass operator the eigenvalues of which could precisely predict the stability or instability of a calculation for the entire simulation time.
- Additional nonlinearities also emerge from the geometrical changes due to the displacement of the interface Γ . Changing geometry means changing integration domain and thus a change of all coefficient matrices encountered.
- Frequently compressible structures are employed where a change of the effective structural density ρ^S has to be expected which may also influence potential instabilities.

Thus the physical fluid-structure interaction problem is highly nonlinear. However the insight gained by considering a linearised version and the stability thereof significantly helps to understand the instability of the problem at hand. While the analysis performed does not necessarily allow to predict the onset of the instability precisely it explains why stable schemes for the interaction of incompressible flow and light-weight structures have not been found.

6.3.8 Numerical investigation

The classical driven cavity problem equipped with a thin flexible bottom is used to numerically investigate the added mass instability within a full fluid structure interaction environment. The example which is taken from [182, 183, 228] is depicted in figure 6.2. The fluid domain is discretised by 32×32 stabilised bilinear elements. The structure is modelled by 32×1 geometrically nonlinear wall elements.

The influence of different parameters and discretisation schemes on the onset of the instability within the time interval $t \in [0 \text{ s}; 100 \text{ s}]$ shall be examined. To diagnose stability or instability the history of the vertical component of the FSI coupling force at node A is monitored. Oscillations in the coupling force indicate instability.

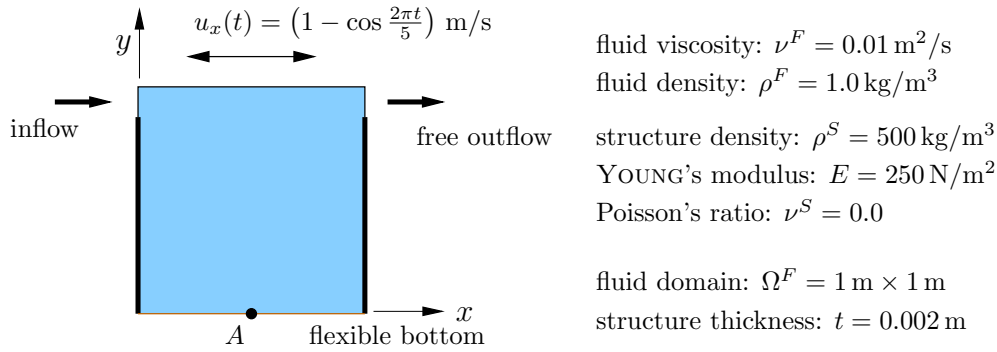


Figure 6.2: Geometry and material data of driven cavity example with flexible bottom

The default algorithm is the most stable scheme to be found. Generalised- α time integration of the structure with zero spectral radius and BE on the fluid domain is used. Further the simple predictor (6.2) and DIRICHLET boundary condition (6.5) are employed. At a time step of $\Delta t = 0.1$ s the problem can stably be integrated in time up to at least 1000 time steps.

The influence of the structural density ρ^S is compared for BE and BDF2 time discretisation on the fluid domain. From the prediction summarised in table 6.1 it is expected that roughly half the structural density required to stably integrate with BDF2 suffices if BE is used on the fluid domain. Starting from the default parameter setting and decreasing the structural density ρ^S the simulation becomes unstable towards the end of the investigated time interval at $\rho^S = 321$ kg/m³. The onset of this instability is depicted in the diagram in figure 6.3.

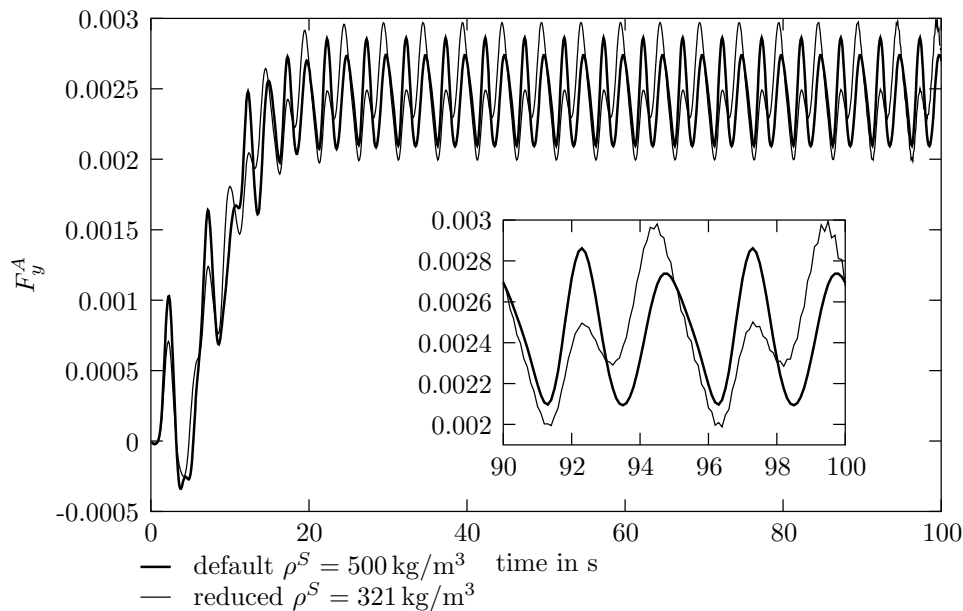


Figure 6.3: Evolution of the vertical coupling force at point A for the default configuration of parameters and a problem with lower structural mass density both evaluated with BE time discretisation of the fluid

A similar procedure is repeated with BDF2 time discretisation on the fluid domain. In

this case the problem is unstable at $\rho^S = 500 \text{ kg/m}^3$ and the structural density is increased until the simulation remains stable within the time interval of interest. Results are shown in the diagram in figure 6.4. Increasing the structural mass density from $\rho^S = 500 \text{ kg/m}^3$ to $\rho^S = 550 \text{ kg/m}^3$ delays the onset of the instability and also slightly damps the instability itself. At $\rho^S = 590 \text{ kg/m}^3$ no instability is observed within the time interval of interest.

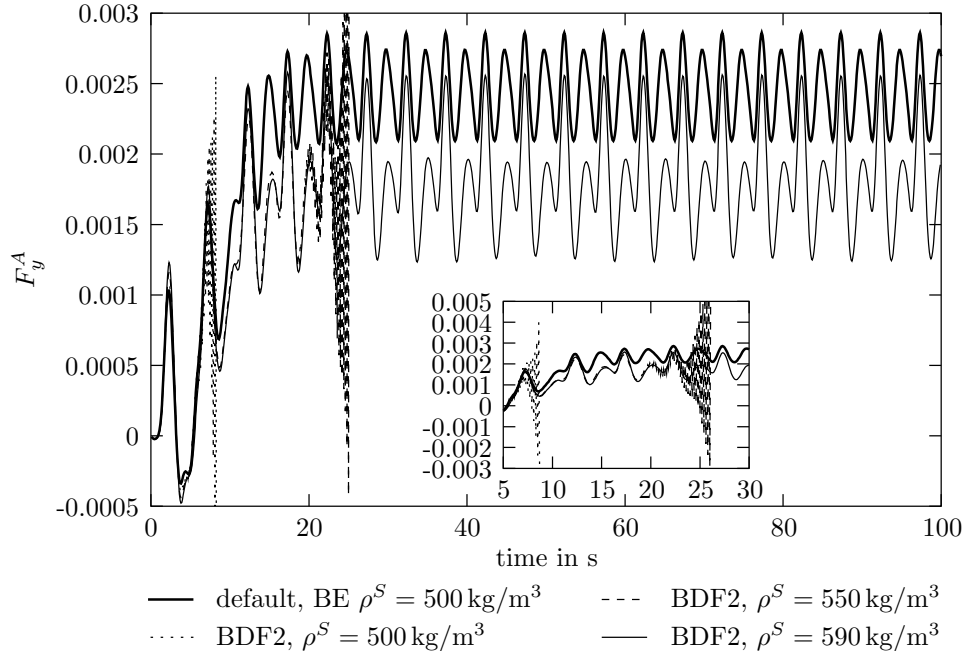


Figure 6.4: Evolution of the vertical coupling force at point A obtained with the default parameter setting and problems with different structural mass densities obtained with BDF2 time discretisation on the fluid field

The influence of the structural stiffness shall be considered next. Departing again from the default configuration with BE, $\Delta t = 0.1 \text{ s}$ and $\rho^S = 500 \text{ kg/m}^3$ the structural stiffness is reduced aiming at a scheme which becomes unstable within the time interval of interest. However, this is not to be reached, indicating that the default parameter configuration is actually stable even without the help of the structural stiffness.

The influence of the structural predictor is also worth to be investigated. Employing the first order accurate predictor (6.3) rather than (6.2) yields an immediately unstable scheme at $\rho^S = 500 \text{ kg/m}^3$ even if BE is used to integrate the fluid equations in time. Using the second order accurate predictor (6.4) the behaviour gets even worse as shown in the diagram 6.5. From table 6.1 an estimate of the structural density necessary to stabilise the simulation can be obtained by using the ratio of the stability constants calculated with different predictors. The zeroth order predictor is stable down to $\rho^S = 322 \text{ kg/m}^3$, thus the first order predictor should be stable for structural densities exceeding $\rho^S = 1610 \text{ kg/m}^3$. This prediction fits very well as the first stable simulation with the first order predictor is obtained at $\rho^S = 1635 \text{ kg/m}^3$. Similar observations can be made when the second order accurate predictor is used which yields an instability condition nine times as rigorous as the zeroth order one. Thus the smallest structural density which should allow a stable

computation is $\rho^S = 2898 \text{ kg/m}^3$. Actually at $\rho^S = 2300 \text{ kg/m}^3$ no oscillations are observed within the time interval of interest while oscillations occur within the next few time steps.

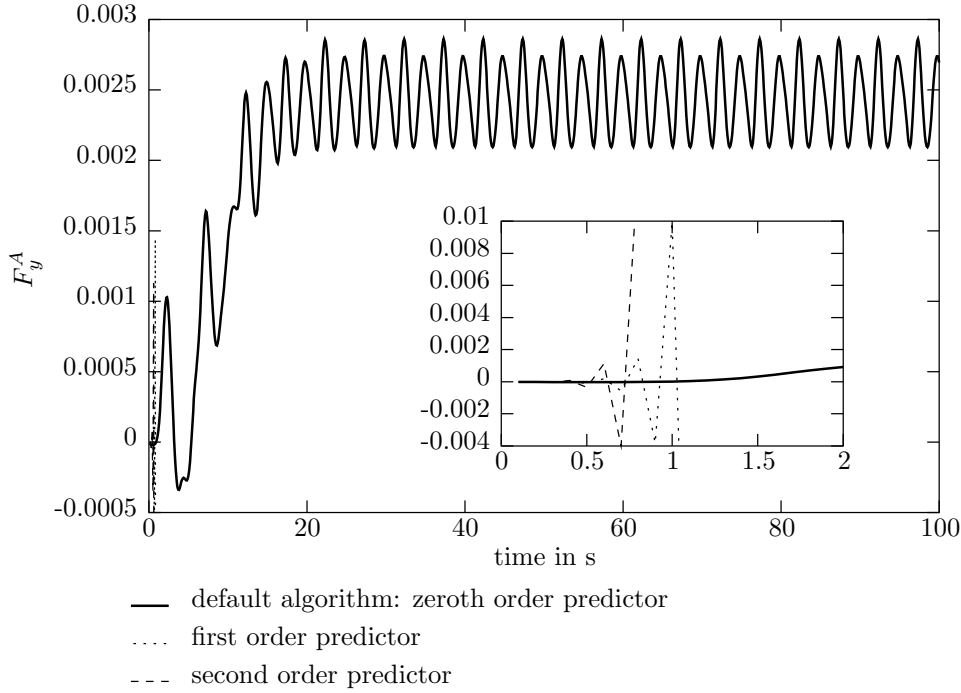


Figure 6.5: Evolution of the vertical coupling force at point A evaluated with default parameter setting and different predictors: within the first few time steps violent instabilities are observed if higher order predictors are employed

The influence of the time step size is investigated by starting again from BE time integration on the fluid domain and $\Delta t = 0.1 \text{ s}$ with $\rho^S = 500 \text{ kg/m}^3$. Stable computations up to $t = 100$ can be obtained for all $\Delta t \geq 0.005 \text{ s}$ where rapidly growing instabilities are observed for smaller time steps. The temporal evolution of the vertical component of the coupling force at point A is depicted in diagram 6.6. Due to the previous test regarding the structural stiffness it is suspected that the sudden onset of the instability is not caused by the decreasing influence of the structural stiffness but rather by an increase of the maximal eigenvalue of $\mathcal{M}_{\mathcal{A}_{\text{stab}}}$ caused by a dominating influence of the stabilisation operator $\bar{\mathbf{G}}_{\text{M}}^T$.

The effect of stabilisation at small time steps is considered by removing the stabilisation operator $\bar{\mathbf{G}}_{\text{M}}^T$. This causes a consistency error within the stabilisation which scales with the influence of the transient term. Removing this term apparently restores temporal stability for schemes which have been stable for larger time steps thus stressing that the instability at very small time steps is caused by the influence of the stabilisation terms. A simulation with a time step size of $\Delta t = 0.0001 \text{ s}$ which gets unstable immediately for the correctly stabilised formulation can be performed when BE, the zeroth order predictor (6.2) and the first order boundary condition (6.5) are employed.

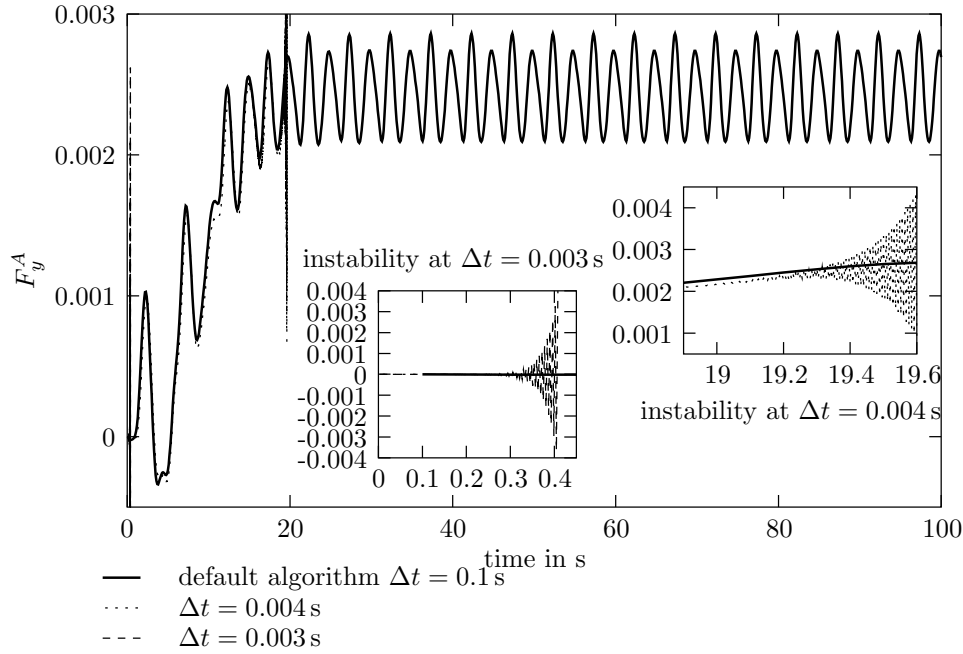


Figure 6.6: Evolution of the vertical coupling force at point A evaluated with different time step sizes and zoom on the regions where instabilities occur; temporally stable integrations are obtained for all $\Delta t \geq 0.005$ s

Some results are depicted in the diagram in figure 6.7 where the solid line represents a computation with default parameter setting but a time step of $\Delta t = 0.003$ s and without the influence of the stabilisation matrix $\bar{\mathbf{G}}_M^T$. The simulation has been stopped after 10000 stable steps without any sign of an instability. Interestingly the same computation including $\bar{\mathbf{G}}_M^T$ gets unstable before the absolute time $t = 0.4$ s is reached as it can be observed in diagram 6.6. A significantly different behaviour is observed if the fluid is integrated by the trapezoidal rule. In this case a scheme with instationary characteristics is obtained which gets unstable irrespective of the maximal eigenvalue of the added mass operator. Removing the stabilisation matrix $\bar{\mathbf{G}}_M^T$ slightly delays the onset of the instability but cannot prevent its onset.

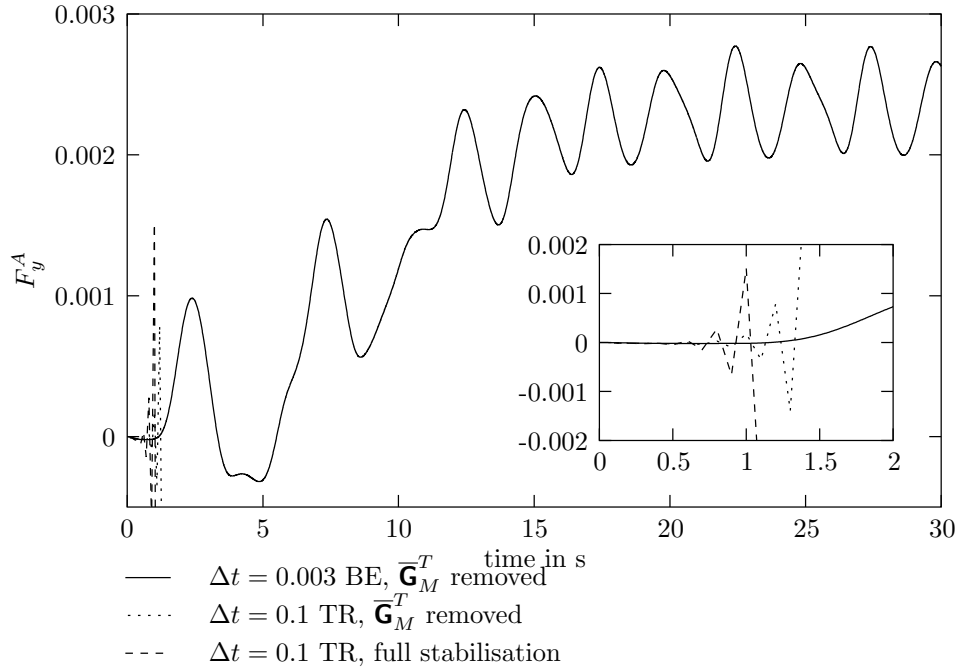


Figure 6.7: Evolution of the vertical coupling force at point A for consistently stabilised fluid and removed stabilisation matrix $\overline{\mathbf{G}}_M^T$

6.4 Stable partitioned schemes

For the applications considered here the artificial added mass effect excludes the use of simple sequentially staggered schemes. In order to derive a convergent method which is highly parameter independent further effort has to be made. Within this work an accelerated iteratively coupled scheme is employed which has shown to be robust and reliable.

6.4.1 Iteratively staggered schemes and the need for relaxation

The use of sub-iterations allows to converge the overall solution within every time step to the solution of the respective monolithic scheme. Thus, dynamic and kinematic continuity are satisfied up to a discretisation error. However, it has been observed that convergence of the iterative scheme is not always guaranteed [182, 183]. In particular CAUSIN et al. [38] have shown that the artificial added mass effect present in sequentially staggered schemes also influences the convergence properties of the corresponding iteratively staggered approach. The analysis in [38] reveals that relaxation with a relaxation parameter $\omega < 1$ is required in the limit of $\Delta t \rightarrow 0$ to obtain convergence of the iteration over the fields. And indeed even for transonic aeroelastic analysis convergence problems at small Δt are reported as for example in a recent paper by MASSJUNG [174].

Consequently relaxation serves to do two important jobs. Firstly it enables convergence making the scheme feasible. By choosing an optimal or nearly optimal relaxation parameter it secondly accelerates convergence increasing the efficiency of the numerical method. This is an important feature as iterations over the fields of fluid and structure

tend to be rather time consuming.

A heuristic and user-input dependent way to get convergence has been reported by TEZDUYAR et al. in [222]. Within the ‘block-iterative coupling’ approach described in [222] the iteration between the fluid and structural field is performed in the core loop, i.e. the coupling conditions are satisfied for iterates of the fluid and structural solution. Thus convergence over the fields can be achieved by an artificial increase of the structural left hand side mass matrix. The structural residual vector is left unchanged ensuring that a converged solution is correct. Thus convergence difficulties of the coupled problem are shifted onto the structural equations while the amount of shift required remains a-priori unknown.

Methods to obtain an appropriate relaxation parameter automatically have been developed by MOK et al. in [182, 183, 228]. Within the present work the AITKEN method is used preferably. This cheap and easy approach to determine ω is based upon AITKEN’s acceleration scheme for vector sequences according to IRONS and TUCK [146]. While no rigorous analysis of the convergence properties of the AITKEN method is available it has shown to work very well in various numerical applications.

The AITKEN method provides a possible specification of step 5. in section 6.2.1 where the following sub-steps have to be performed.

5a. Determine the difference of the present and previous interface position according to

$$\Delta \mathbf{d}_{\Gamma,i+1}^{n+1} = \mathbf{d}_{\Gamma,i}^{n+1} - \tilde{\mathbf{d}}_{\Gamma,i+1}^{n+1}.$$

5b. Compute AITKEN factor

$$\mu_i^{n+1} = \mu_{i-1}^{n+1} + (\mu_{i-1}^{n+1} - 1) \frac{(\Delta \mathbf{d}_{\Gamma,i}^{n+1} - \Delta \mathbf{d}_{\Gamma,i+1}^{n+1})^T \Delta \mathbf{d}_{\Gamma,i+1}^{n+1}}{(\Delta \mathbf{d}_{\Gamma,i}^{n+1} - \Delta \mathbf{d}_{\Gamma,i+1}^{n+1})^2} \quad \text{for } i > 0,$$

where the initial AITKEN factor of a new time step is given by $\mu_0^{n+1} = \mu_{\max}^n$ and the very first factor of a simulation is $\mu_0^1 = 0$.

5c. Obtain relaxation parameter from

$$\omega_i = 1 - \mu_i^{n+1}.$$

The above steps involve global vector operations only and are thus cheap in terms of CPU and memory. It can further be observed that the AITKEN method is easy to implement.

An alternative to the AITKEN relaxation parameter is the method of steepest descent or gradient method which can be found in [183]. This approach involves the solution of an auxiliary coupled problem to determine the relaxation parameter ω and is thus considerably more expensive. A strong advantage of the gradient method is the availability of a convergence analysis.

6.4.2 Projection based semi-implicit scheme

While sub-iterations with proper relaxation allow to integrate the FSI problem stably in time an iteratively staggered scheme requires a significant number of fluid and structure field solutions per time step. More efficient formulations are thus desirable.

The artificial added mass instability is intrinsically related to the incompressibility condition. The fluid pressure is highly sensitive with respect to the correctly determined fluid-structure interface position and yields heavily wrong coupling forces for slightly incorrect predictions of the structural interface motion. Thus implicit coupling of the pressure is unavoidable.

Motivated by this fact FERNÁNDEZ et al. propose a semi-implicit FSI coupling scheme in [80]. Solving the flow equations using a CHORIN type projection scheme decouples the pressure solution from the inversion of the remaining operator. Thus the viscous and convective terms are solved once per time step while the projection step which yields the pressure has to be repeated iteratively until convergence of the fluid and structural solution is obtained. Conditional stability of the scheme is proven by FERNANDEZ et al. in [80].

6.5 Summary

A partitioned FSI algorithm is used which can be formulated in an efficient sequentially partitioned version and a stable iteratively staggered variant. Accurate exchange of coupling data requires that a fluid interface condition is used which is consistent with the fluid time discretisation. Nodal fluid forces are exerted on the structure rather than integrated stresses. These forces exhibit the order of accuracy of the primary variables and fit very well into a nodal based data structure.

The artificial added mass effect which is an instability of the sequential version of the partitioned algorithm is closely related to the incompressibility of the flow. From an analysis of the coupled system instability conditions are deduced. These conditions show that the instability depends upon the maximal eigenvalue of the added mass operator and the time discretisation schemes used on the fluid and structure. Even more important the instability is highly influenced by the ratio of the fluid and structural mass density. Whenever fluid and structural densities are comparable the instability is almost unavoidable. Only in cases where the fluid is much lighter than the structure conditionally stable schemes might be possible.

The analysis further reveals that higher temporal accuracy necessarily yields earlier instability. It is also shown that there are discretisation schemes for the fluid field as for example the trapezoidal rule which yield an instability condition that gets increasingly restrictive with every further time step. Such schemes necessarily fail to work.

Extending the idea which yields the instability condition it can also be shown that no unconditionally stable staggered algorithm can be designed. Consequently stable partitioned schemes have to be iteratively staggered where at least the coupling forces due to fluid pressure have to be treated implicitly.

Chapter 7

Numerical Examples

In addition to the academic examples used in the previous chapters to highlight particular numerical effects a number of applications of the entire FSI interaction scheme are presented within this chapter. These examples are not only designed to demonstrate the capability of the algorithm but also to present some characteristics of FSI problems including modelling and simulation issues.

7.1 Introduction

7.1.1 General algorithmic information and modelling

Throughout residual based stabilised finite elements with equal order interpolation of velocity and pressure have been used on the fluid domain. The structural field is discretised by geometric nonlinear wall elements or nonlinear, three-dimensional shell elements for two-dimensional and three-dimensional problems, respectively. In all cases the interaction of the fluid and structural field is achieved by subiterations where the AITKEN relaxation strategy has been employed. Typically four up to maximal ten iterations over the fields are required to converge the coupled problem.

The examples described here are given with the full data required to rerun the problems. This not only includes geometry and full material data along with discretisation information but also details of the modelling process. These ‘tricks’ usually not published are however closely related to the coupled nature of FSI problems and offer further insight into the complexity thereof. It also appears likely that the modelling information given here might help and inspire the solution of similar difficulties.

7.1.2 A few comments on computational tools

All applications have been simulated using the research code of the Institute of Structural Mechanics called `ccarat`. Contributions to this code and improvements thereof have been made in the progress of this work. The research finite element program of the institute had been relaunched in the programming language C in 2002 as a much wider framework than the parent FORTRAN code. The major work has been done by GEE who provided an excellent computational environment which is gratefully acknowledged. Almost every FSI example which was simulated during the course of this work also highly relied on the restart facility which is based on a binary input and output module. This restart offers an immense flexibility by allowing not only a modification of material parameters or time step sizes but also a change in NEUMANN and also DIRICHLET boundary conditions or the

number of processors used to run the problem in parallel. This core module was added to `ccarat` by KÜTTLER who also provided a highly valuable support.

The design of the new `ccarat` allows to compile a sequential or a parallel MPI based version. In particular the three-dimensional examples have been run in parallel on two to four processors.

Iterative solvers and preferably the solver package AZTEC (see [225] for product details) have been employed to solve the resulting fluid system of equations. In particular a stabilised biconjugate gradient (BiCGSTAB) method along with a symmetric GAUSS-SEIDEL preconditioner or an incomplete LU preconditioner have been used within most examples. Alternatively a GMRES method also available within the AZTEC package has been employed.

The mesh and structural system of equations tends to be smaller and much less demanding. Here a direct solver or for larger problems a conjugate gradient method available within the AZTEC package have done a good job.

The program GID of CIMNE in Barcelona [46] has been used for preprocessing and mesh generation and to some extent also in the postprocessing stage, in particular for the three-dimensional problems. For two-dimensional problems the visualisation tool `visual2` has been employed [110].

7.2 Bridge cross section in laminar flow

This example is designed to simulate the fundamental behaviour of the flow around a plate girder bridge cross section. The problem geometry is inspired by the Tacoma Narrows bridge which is famous for its collapse in 1940.

It was a finding of the studies initiated by this collapse that vortex-shedding excitation and flutter instability of a suspension bridge can be represented by a spring-supported model of the cross section. Compared to a coupled analysis of the entire bridge and the surrounding three-dimensional flow this offers substantial savings while still exhibiting the advantages of a numerical simulation. In contrast to wind tunnel tests numerical analysis may be performed much faster and at lower expenses. In particular preliminary studies of general shapes might efficiently be performed numerically.

7.2.1 Geometry and material data

The geometry and boundary conditions of the two-dimensional problem which are adopted from the work of HÜBNER [129] are depicted in figure 7.1. A section of 1 m of the bridge profile is fixed at its centre in x -direction and supported by a spring with a linear stiffness of $k_y = 2.467$ kN/m in y -direction. Additionally a torsional spring of $k_\alpha = 126.33$ kNm is attached. As fluid-rigid body interaction is not directly supported within the present code the cross section is modelled by a very stiff structure with YOUNG's modulus of $E_{\text{art}} = 5 \times 10^9$ kN/m² and supported by two vertical linear springs of a stiffness of $k_y/2$ and a horizontal distance of $d = 14.31$ m. Two additional truss members of E_{art} and unit area introduced on either side of the bridge profile allow to reach this distance. This corresponds to a linearisation of the torsional stiffness as described in the diploma thesis of HILCHENBACH [126]. With a structural mass density of $\rho^S = 823$ kg/m² the total mass

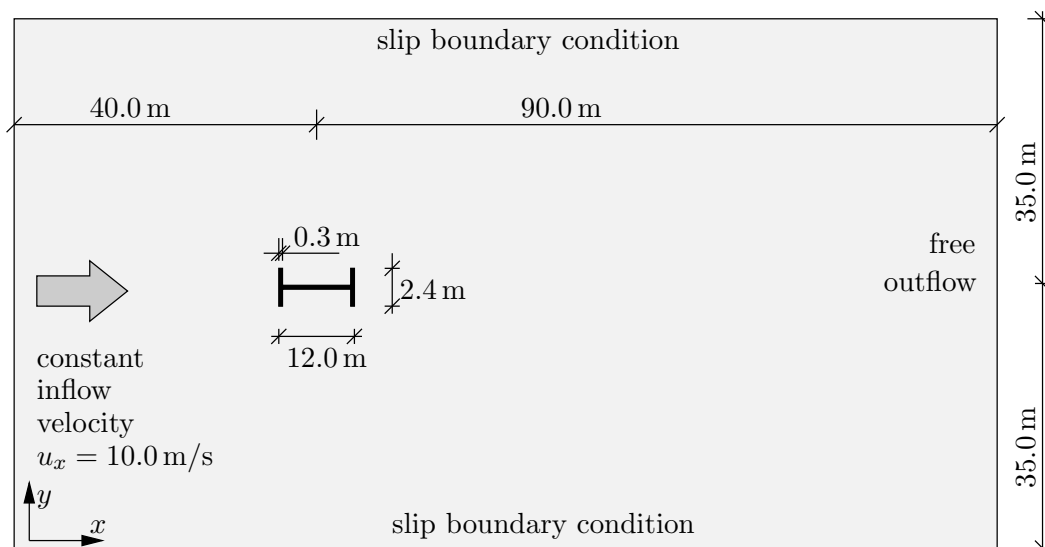


Figure 7.1: Geometry of bridge cross section in flow field

of the cross section per meter length of the bridge is 4000 kg/m and a total moment of inertia of about $80000 \text{ kg m}^2/\text{m}$ can be obtained.

The corresponding eigenfrequency of the vertical cross sectional mode is $f_y = 0.125 \text{ Hz}$ while a free rotation would take place at an eigenfrequency of $f_\alpha = 0.20 \text{ Hz}$. These frequencies are close to those of the Tacoma Narrows bridge reported in [165]. The fluid is rather viscous with a kinematic viscosity of $\nu = 0.08 \text{ m}^2/\text{s}$ and the mass density of air $\rho^F = 1.25 \text{ kg/m}^3$.

Altogether this example is very good-natured and an immediate convergence of the iteration over the fields is obtained.

7.2.2 Modelling and discretisation

Using the width of the bridge $L = 12 \text{ m}$ as a characteristic length of the flow a REYNOLDS number of $\text{Re} = 1500$ results for the problem. Clearly wind passing a bridge corresponds to much higher REYNOLDS numbers and has to be treated as highly turbulent flow. However, due to the sharp edges of the present cross section the flow pattern is governed by the bridge deck geometry and the influence of the actual REYNOLDS number is minor. It is thus reasonable to expect that the fundamental coupled behaviour and the self-excitation of the system can be modelled while an accurate prediction of a wind flow pattern will not be achieved. This expectation is also supported by studies reported in [126, 129] where vortex-shedding at different cross sections is compared. The dimensionless characteristics such as the STROUHAL number as well as lift and drag coefficients of the flow across the present profile fit very well to values obtained for much higher REYNOLDS numbers as reported by LARSEN in [165]. In [165] also comparisons to wind tunnel section model tests are presented.

A total of 16028 bilinear four-noded elements is used to discretise the flow field and 208 structural elements are employed. The discretisation of the moving mesh manages with 15127 bilinear elements as a part of the fluid domain is modelled in EULERIAN formulation. Particular care has been taken to assure a regular mesh in the direct vicinity of the bridge

profile.

A time step size of $\Delta t = 0.02\text{ s}$ is used which allows a high resolution of the coupled dynamics. Starting the simulation the inflow velocity is accelerated according to

$$u_x = u_\infty \frac{1}{2} \left(\sin \left(\frac{\pi t}{2\text{ s}} - \frac{\pi}{2} \right) + 1 \right),$$

is employed where the surrounding flow speed is given by $u_\infty = 10\text{ m/s}$. This start-up generates a smooth flow acceleration within the first two seconds.

7.2.3 Results

The inflow velocity of 10 m/s suffices to cause an increasing excitation of the bridge deck which eventually yields failure if no additional damping occurs. The temporal evolution of the total vertical fluid force upon the profile is shown in diagram 7.2. Accordingly the overall fluid moment is given in diagram 7.3. Both diagrams show an apparently stable phase from about 50 s to 100 s where the lift force as well as the fluid moment of momentum exerted on the bridge deck is very similar to that of the respective fixed

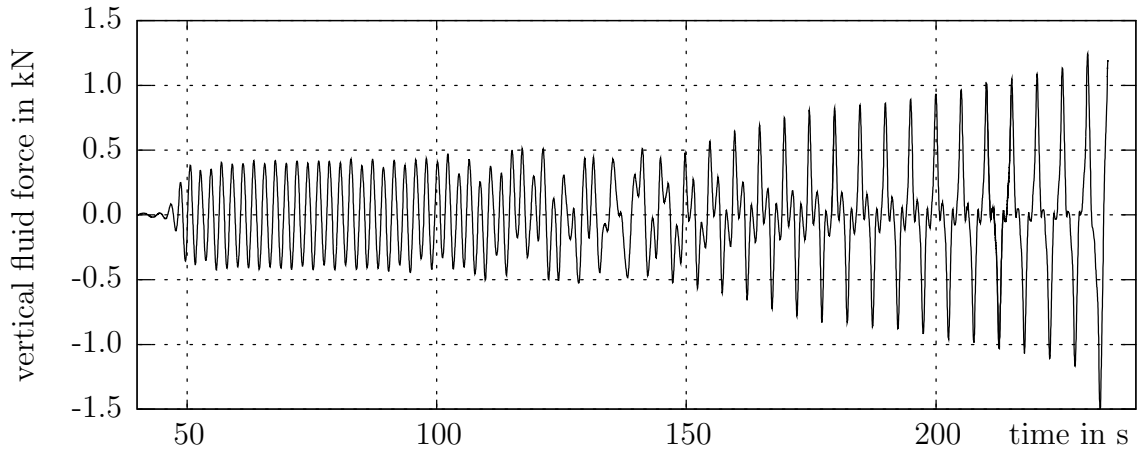


Figure 7.2: Temporal evolution of the total vertical fluid force exerted on the bridge cross section

cross section. But as soon as the vortex shedding has fully developed a second frequency corresponding to the torsional oscillation of the bridge cross section sets in. While the initial structural motion is a slight vertical translation, the rotational mode dominates soon after. After about 150 s this effect eventually takes over and an increasing torsional oscillation is observed. The rapid growth of the peak fluid force and angular momentum prior to the end of the simulation is caused by the linearisation of the torsional spring.

The transition in the dynamics caused by the fluid-structure interaction can also be expressed in the STROUHAL numbers. Using the height of the cross section as characteristic length scale, i.e. $L = 2.4\text{ m}$ the initial STROUHAL number $St_1 = 0.112$ equals that of the fixed cross section (see [126, 129]). After the coupled system has developed the STROUHAL number is $St_2 = 0.048$.

Images of the flow field along with the displaced structure are given in figure 7.4 as well as in the colour chart in figure 7.5. In figure 7.4 stream lines are plotted on the pressure field and the pressure scale of figure 7.5 applies also here. The time instants depicted

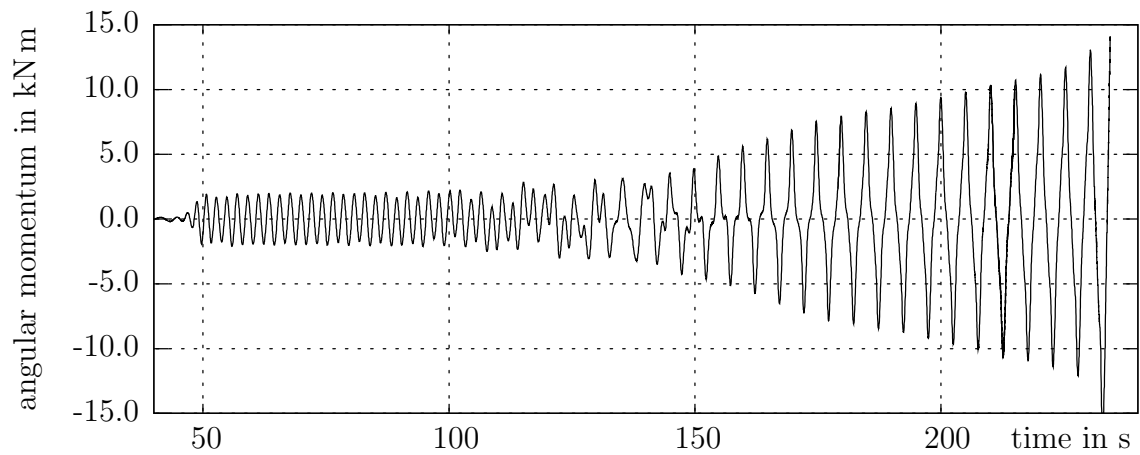


Figure 7.3: Temporal evolution of the total angular fluid momentum exerted on the bridge cross section

correspond to peak values in the lift force and the torsional moment as it can be observed from the diagrams 7.2 and 7.3.

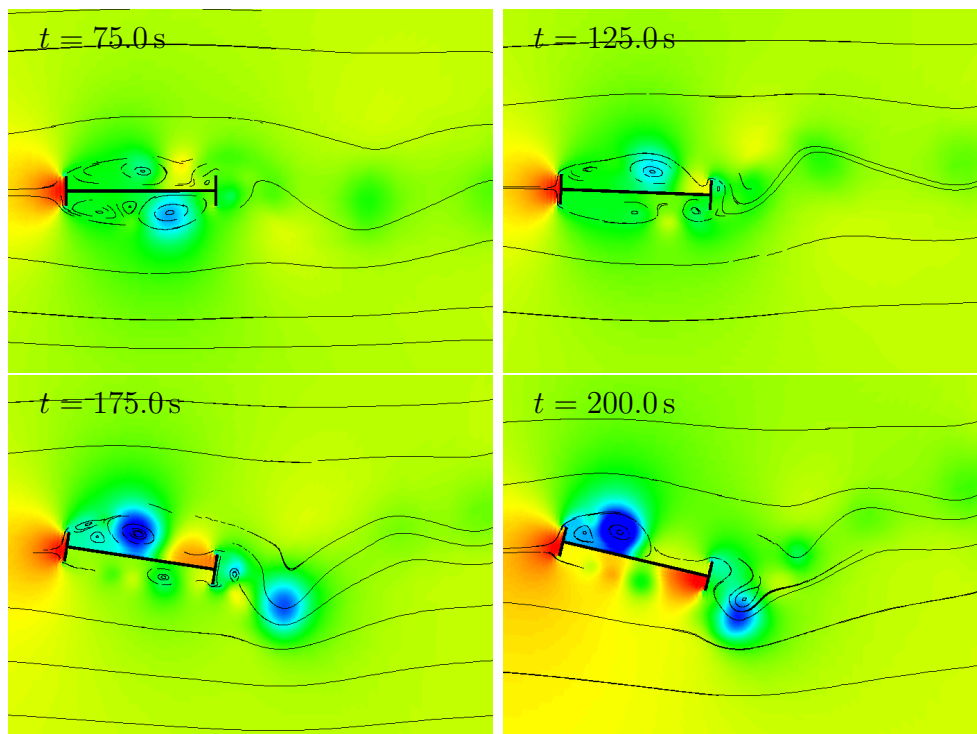


Figure 7.4: Stream lines on pressure field

The horizontal velocity at different time instants is presented on the left hand side of figure 7.5. It nicely highlights the significant influence of the structural motion on the flow field. The horizontal velocity increases in the course of the simulation. This effect can also be observed for the pressure where in particular zones of negative pressure grow in strength as a result of the rotation of the cross section. The mutual excitation of cross section and intensity of the vortices is shown in figure 7.5. The close up views on the right hand side of figure 7.5 further give an impression of the mesh and its motion. These results agree well with those obtained by HÜBNER reported in [129].

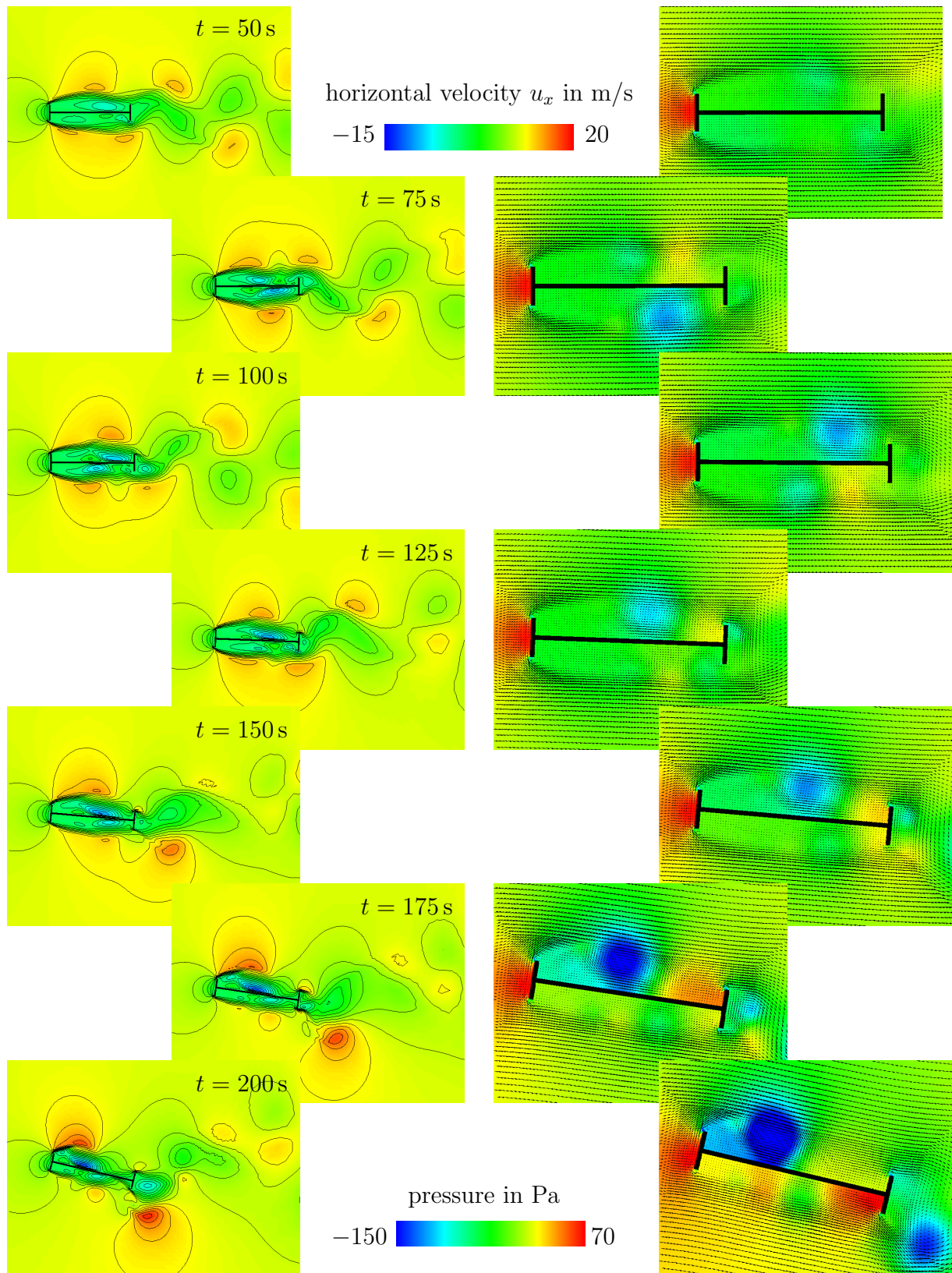


Figure 7.5: Snapshots of bridge deck at different instants in time: Horizontal velocity with isolines (left) close-up view of cross section area with velocity arrows on pressure field (right)

7.3 Channel with backward facing step and membrane

The present numerical example has been designed for several purposes. It demonstrates the capability of the fluid-structure interaction scheme to simulate the highly transient dynamics of a membrane structure interacting with air flow. It is also used to compare a simulation computed with linear elements to one performed with quadratic elements of the SERENDIPITY type.

7.3.1 Geometry and material data

The geometry of the initial problem is depicted in Figure 7.6. In order to relax the membrane and thus allowing pure bending deformation without inducing membrane stresses the structure is relaxed in a preliminary step by moving the point *A* 0.1 cm to the left.

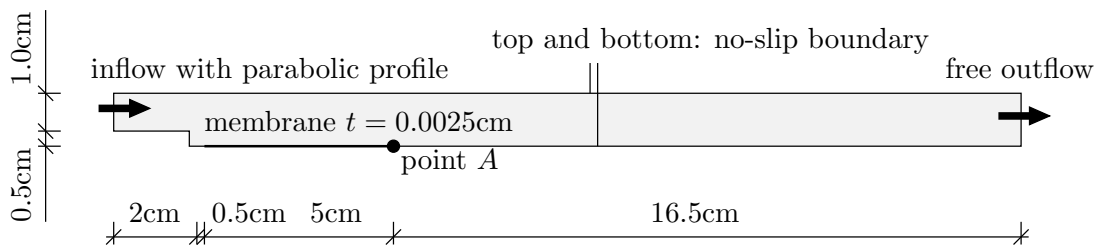


Figure 7.6: Initial geometry of backward facing step problem

The fluid has the material data of dry air at about 25° C, i.e. a kinematic viscosity of $\nu = 0.146 \text{ cm}^2/\text{s}$ and a density of $\rho^F = 0.0012 \text{ g/cm}^3$. The deformation of the slack membrane passed by the flow is governed by bending and thus small strains which justifies the assumption of a linear ST.VENANT-KIRCHHOFF material law. The structural YOUNG'S modulus is $E = 1.0 \times 10^8 \text{ g/s}^2\text{cm}$ representing a soft rubber like material while POISSON'S ratio has been set to $\nu^S = 0.2$. The structural mass density is $\rho^S = 0.5 \text{ g/cm}^3$.

The inflow velocity is increased linearly in time within the first 0.048 s of the computation. Eventually the air enters the domain with a maximal velocity of 120 cm/s at the centre of the inflow boundary line. No-slip boundary conditions are applied at the top and bottom of the channel.

7.3.2 Discretisation and initial membrane relaxation

Discretisation in space and time

In order to avoid an initially curved structure the bottom membrane is created as a plane. Five or two elements are used in thickness direction of the membrane with linear or quadratic elements, respectively. This largely reduces shear locking. The quadratic structural elements of the SERENDIPITY type are under-integrated by 2×2 GAUSS points. Overall 21200 linear or 5280 quadratic SERENDIPITY elements are employed on three fields yielding a total of 21908 or 16547 nodes, respectively. Prior to the actual computation the membrane is relaxed by moving the point *A* to the left.

Initial set-up

The moving action of point A consists of two preliminary steps with differing boundary conditions and material parameters. These steps are not used to model any real physical action but rather supply the initial state for the simulation. The inflow boundary condition is fixed to zero during these steps. Within a first preliminary step point A moves to the left at constant velocity. At the same time a constant external pressure at the outside of the membrane ensures that the structure buckles towards the inner part forcing some fluid to leave the domain. After a few large time steps a static situation is reached. The problem is restarted from this state for a second preliminary step where the external pressure is removed. This causes the fluid domain to enlarge again and thus inflow at the free outflow boundary condition. Despite being ill posed the step can be run with fingers kept crossed to a steady state and provides the initial shape of the membrane.

The initial steps are made good-natured by evoking artificial damping. To this end BE is used on the fluid and a very low spectral radius on the structural domain which causes significant numerical damping in both fields. Further an increased fluid viscosity of 5.146 cm/s is initially employed.

After adjusting the viscosity to the value of air and selecting less dissipative time discretisation schemes the simulation of the physical problem is started. The slack membrane interacts with the flow exhibiting almost exclusively bending deformation. Thus the structure is extremely soft and sensitive to the fluid forces. The highly transient nature of the problem requires a time step of $\Delta t = 1.0 \times 10^{-4}$ s.

The dynamic behaviour of the present membrane problem exhibits an initial snap-through which is damped by the action of the flow but nevertheless highly transient. Consequently it is necessary to increase the inflow velocity fast enough to avoid negative pressures due to the sudden enlargement of the fluid domain. This would cause an inflow at the free outflow boundary and thus an ill-posed problem.

7.3.3 Results on two meshes

Dynamics of a physically very sensitive system

An impression of the highly transient dynamics of the coupled problem is given in the figures 7.7 and 7.8 where the absolute value of the velocity field is depicted. These results are obtained on the linear and quadratic SERENDIPITY meshes, respectively. It can be observed that the dynamic behaviour computed on the two different discretisations is initially very similar while the two evolutions separate soon after the initial phase of 0.048 s. This separation is also obvious from the vertical displacement of the membrane centre point as depicted in diagram 7.9. At the latest after 0.125 s the two simulations predict a different behaviour. In particular a comparison of the close-up view of the membrane area as presented in figure 7.10 reveals a smoother flow behaviour obtained with linear elements. As far as the flow field is concerned this additional smoothness is caused by numerical damping induced by the inconsistency of linear elements. The discretisation by quadratic SERENDIPITY elements admits the development of more vortices which govern the overall dynamics. However different structural stiffnesses seem to play a significant role, too. The results suggest that five linear elements used in membrane thickness direction might not suffice to remove shear locking effects in particular as those elements are

very stretched due to restrictions imposed by the resolution of the fluid field along the interface.

In a sense these distinctly disjoint results are unfavourable and indicate that at least one of the solutions is not converged. The results suggest that a better approximation is obtained by quadratic elements while even here a finer mesh would be beneficial. A convergence study verifying the coupled dynamics has not yet been performed due to limitations in the available computational resources. However the suggestion shall be made here that even with finer resolutions in space and time a unique solution will be hard to obtain. It is the characteristic of the physics governing the dynamics of the present problem that it is highly nonlinear. It is thus also due to the physical sensitivity of the coupled system that small perturbations immensely effect the temporal evolution of the system.

Computational effort

The computational effort required on both discretisations is comparable. The reduced number of unknowns resulting from quadratic SERENDIPITY elements does not pay off. It is rather balanced by an increased number of non zero values within the overall coefficient matrix. Thus the time consumed by the solver on either mesh is comparable. On a personal computer with Intel core 2 duo processor T7200 with 2.0 GHz the simulation of one time step took about 530 s. Consequently the overall computing time for one of the discretisations simulated for more than 4500 time steps on the same machine amounts about a month.

Performance of the partitioned solver

Due to the very thin and flexible structure the present membrane problem poses a special difficulty for the partitioned solver. Even if the fluid mass density is much smaller than the structural one this example can by no means be treated by a sequentially staggered scheme. A considerable artificial added mass effect is observed which also harms the iteratively staggered procedure, i.e. a large number of iterations is needed in every time step. Up to 15 or even 20 iterations over the fields are required to obtain a converged coupled solution while a non monotone convergence behaviour is observed in this iteration.

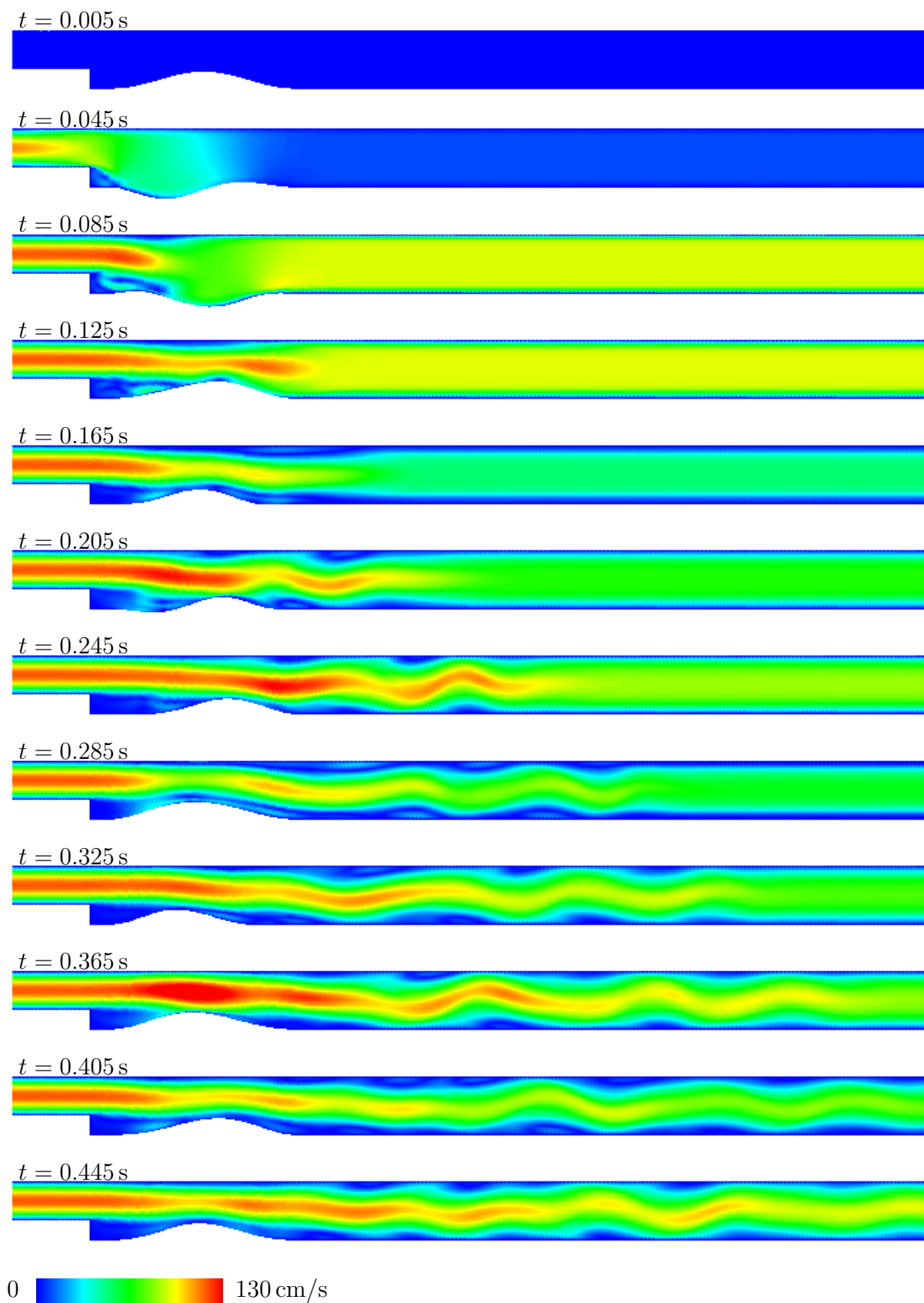


Figure 7.7: Evolution of absolute value of the fluid velocity $|\mathbf{u}|$ obtained on linear elements

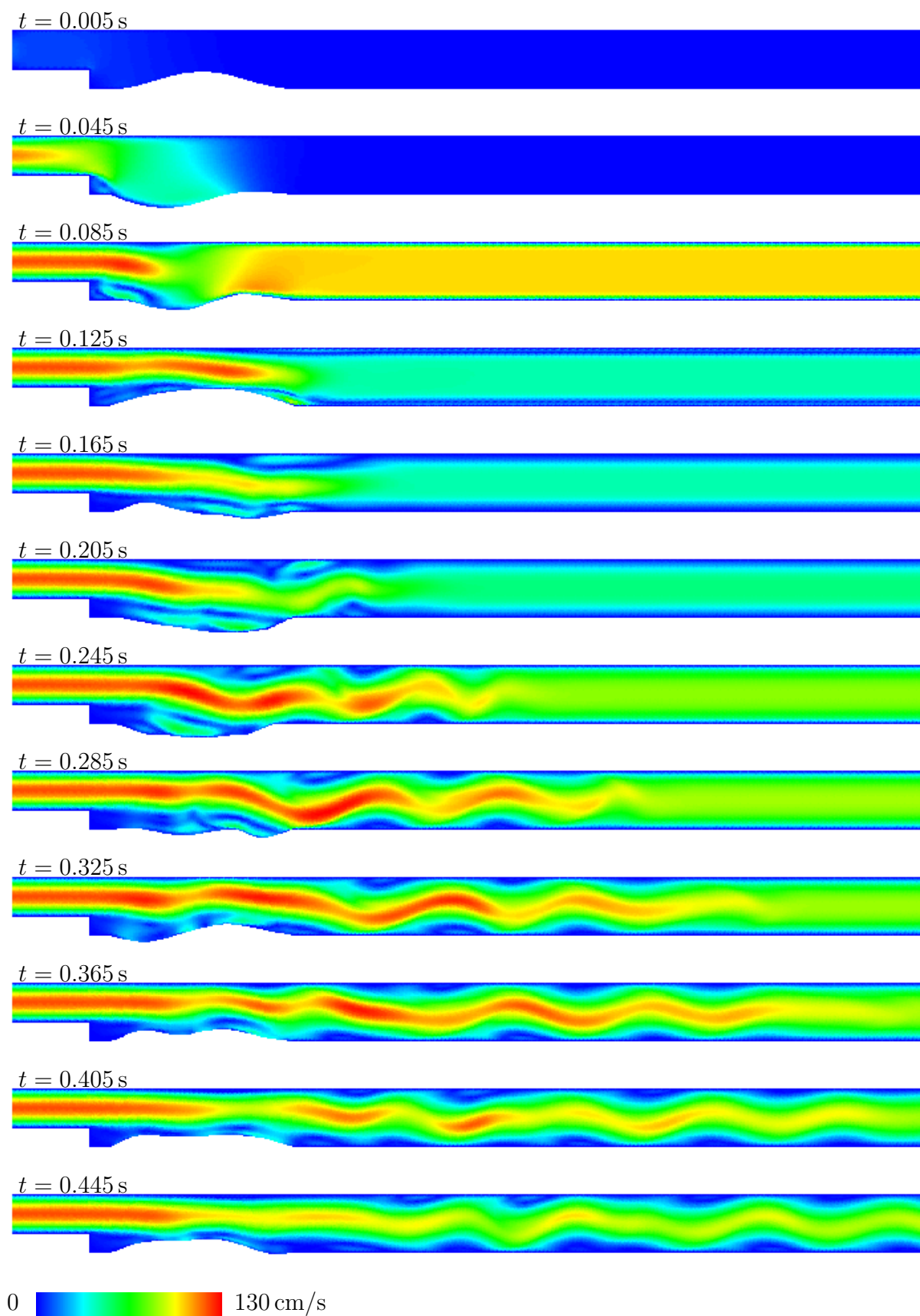


Figure 7.8: Evolution of absolute value of the fluid velocity $|\mathbf{u}|$ obtained on quadratic SERENDIPITY elements

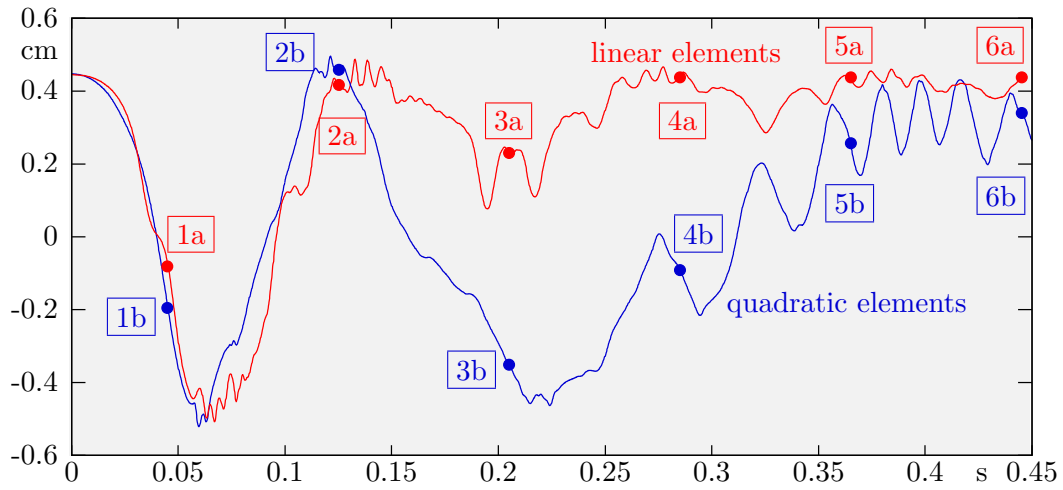


Figure 7.9: Temporal evolution of vertical displacement of membrane mid point

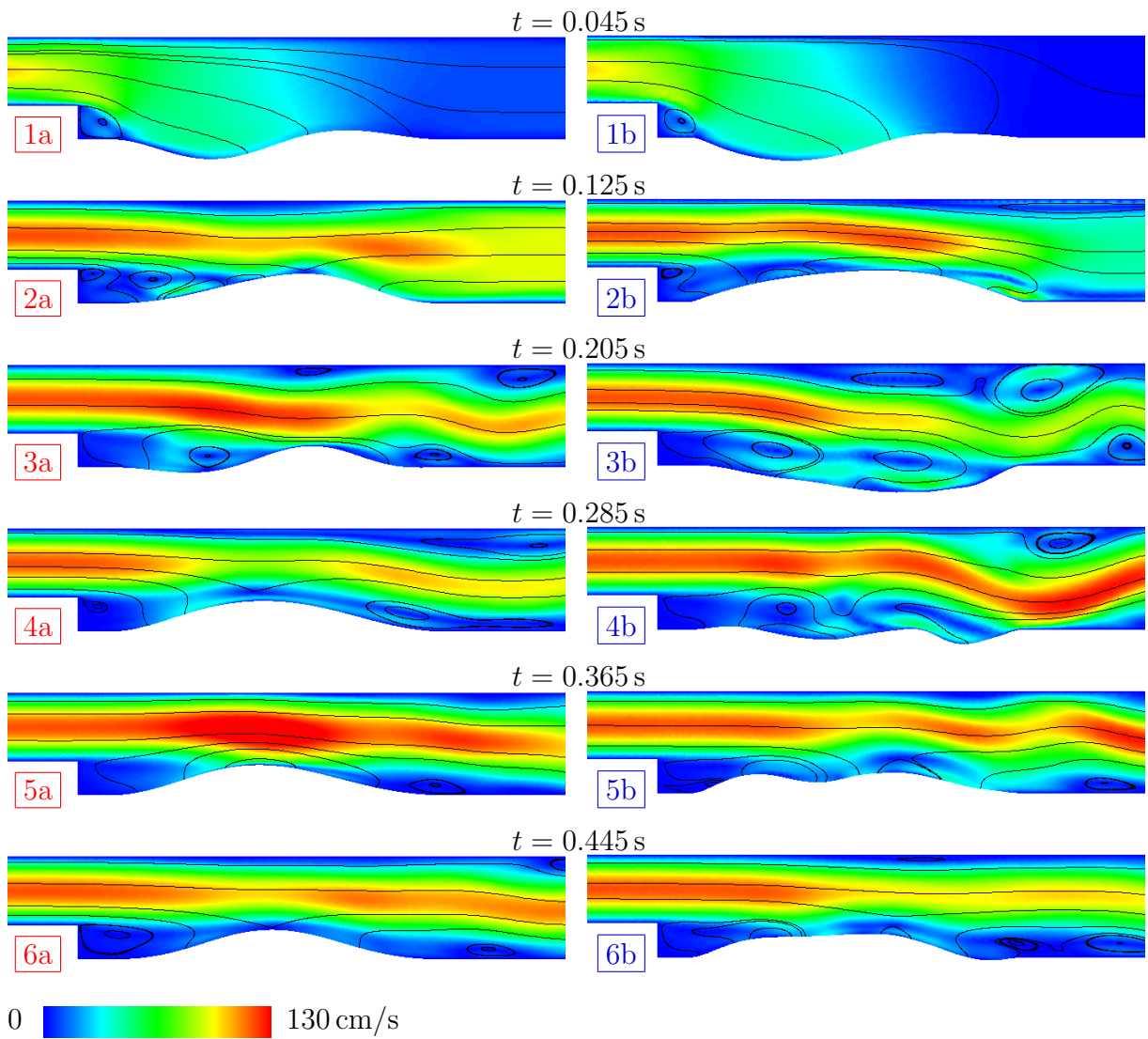


Figure 7.10: Close-up view of membrane area; streamlines on absolute value of velocity obtained on the linear (left) and quadratic (right) mesh

7.4 Vibrating U-pipe

Coriolis flowmeters are an elegant way to measure the mass flow rate in a pipe. The measuring unit inside such a flowmeter is a flexible tube which in its classical form is U-shaped, clamped at both ends and passed by the flow. The pipe is subject to a forced vibration in the cantilever mode at angular frequency ω_f . This oscillation induces opposite and time dependent CORIOLIS forces within the fluid in the inflow and outflow part of the tube. Thus the resulting vibration is not just the enforced bending but accompanied by an amount of torsion depending upon the frequency ratio f_t/f_f where f_t denotes the eigenfrequency of the torsional mode.

7.4.1 Geometry and material data

Geometry and material parameters of the sample tube are given in figure 7.11 where the tube is fully clamped at the in- and outflow boundaries.

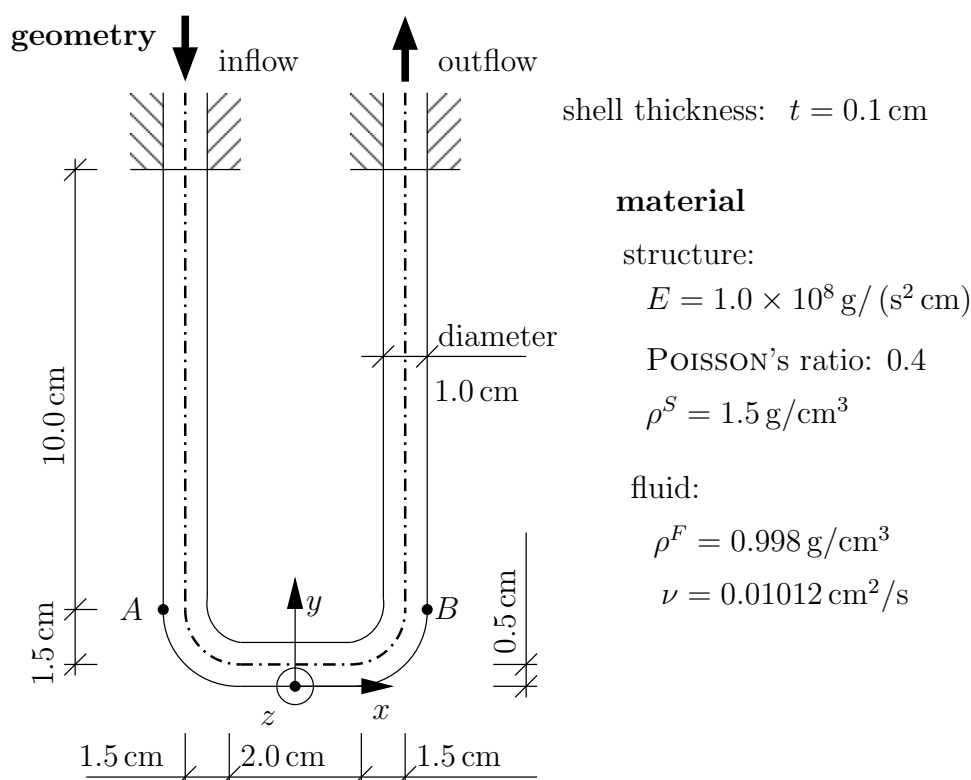


Figure 7.11: Geometry and material of flowmeter tube

In contrast to technical flowmeters which are made of metals here the tube material is a rubber like compressible neo-HOOKEAN type of material which yields large deflections of the overall system and thus allows to highlight the physical effect. Graviatational forces of the water inside the tube are considered while effect of gravitation on the shell itself is neglected. The inflow velocity of the water inside the tube is prescribed to $u_y = 15$ cm/s.

7.4.2 Modelling and discretisation

The mesh of the tube itself consists of 5120 linear four-noded shell elements enriched by means of the enhanced assumed strain method (EAS) to remove locking inherent in linear elements [15]. Further the Assumed Natural Strains (ANS) method is used to avoid parasitic transverse shear strains, i.e. removing shear locking. Scaled director conditioning as described in [99, 100] with a scaling factor of $\mathcal{C} = 10.0$ is employed to improve the conditioning of the resulting structural system of equations.

The fluid domain is meshed by 11520 stabilised trilinear hexahedral elements. A major part of the fluid domain is accompanied by a deformable mesh field consisting of 10240 pseudo structural elements. Thus the overall mesh while still being quite coarse for the problem consists of 26880 elements yielding a total of 94924 degrees of freedom on three fields. To resolve the higher frequencies of interest adequately a small time step of $\Delta t = 0.005$ s is used.

A harmonic force of a frequency of $f_f = 7.685$ Hz close to the eigenfrequency of the torsional mode f_t is applied on the tip of the clamped tube pointing in z -direction. The force is distributed over the area of the part of the pipe which is parallel to the x -axis.

In this example the choice of suitable boundary conditions for the fluid field poses an interesting challenge. Clearly at the inflow boundary the fluid velocity is prescribed in a classical DIRICHLET type of boundary condition. At the outflow, however, the velocity cannot be prescribed as this would implicitly determine the volume of the fluid and pose a problem that an unmodified partitioned procedure cannot handle. An escape for this so-called incompressibility dilemma has been given in [164]. Specifying an adequate NEUMANN boundary condition at the outflow would be an easy workaround. However, due to gravity pointing in z -direction the pressure distribution at the end cross section of the structure is unknown. A priori determination of the stress distribution at the outflow boundary surface also fails due to the transient nature of the problem. Circumventing all these difficulties the fluid domain is extended as depicted in figure 7.12. An additional bent part of the pipe which is rigid allows to end the computational domain at a level of constant gravity potential which is chosen to $z = 2$ cm. Thus a NEUMANN boundary condition can be prescribed here and determines the pressure level inside the tube.

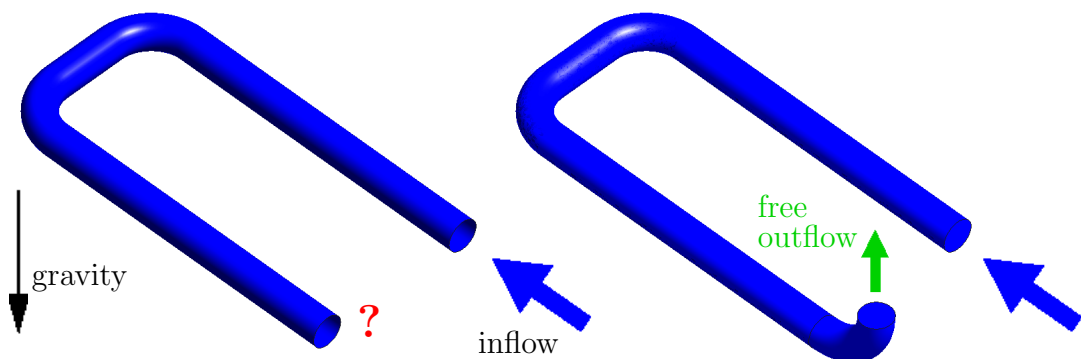


Figure 7.12: Isometric view on fluid (left) and structural domain (right); extension of the fluid domain allows to state correct boundary conditions

7.4.3 Results

The resulting tube oscillation is not just the expected bending but also an increasing torsional replay which is due to the CORIOLIS forces induced in the two arms of the pipe during the up and down cycles. In figure 7.13 the evolution of the vertical displacements at the reference corner points A and B is depicted along with the displacement difference.

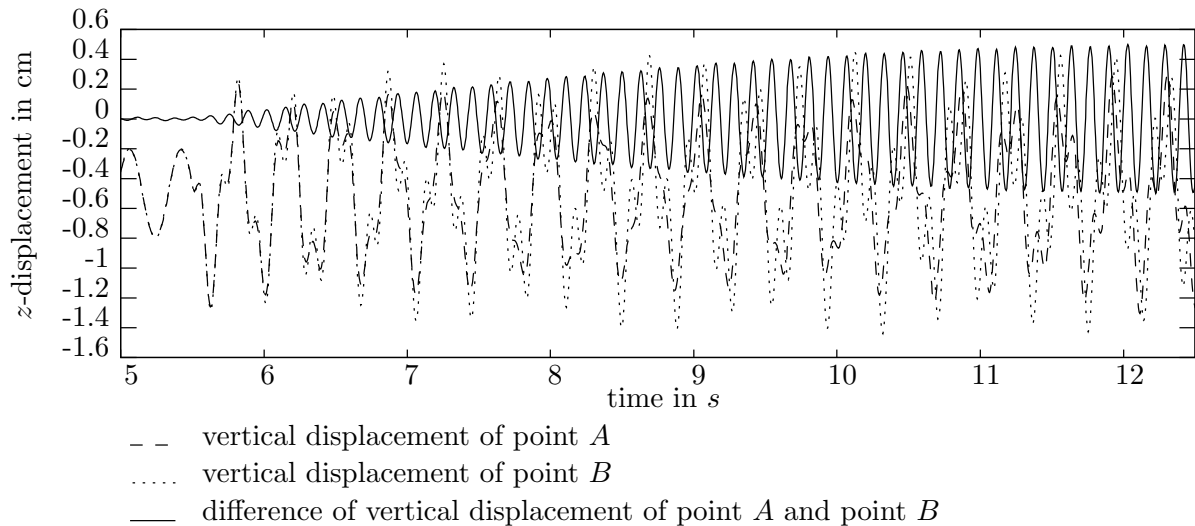


Figure 7.13: Vertical displacement at the two points A and B along with displacement difference between those points

In order to ensure the well-posedness of the problem the flow passing the tube as well as the gravitational forces have to be built up over a period in time. This startup was finished at 4.0 s when the system oscillated in the first bending mode and its corresponding eigenfrequency as it can be seen in the first part of the diagram in figure 7.13. At 5.5 s the periodic vertical tip force is switched on. This initiates a forced vibration on the first, the bending eigenmode of the structure. The evolution of the increasing contribution of the torsional mode can be observed from the increasing displacement difference of the two reference points A and B of the shell. In every cycle a portion of the bending energy is transferred to the torsional mode resulting in an increasing torsional oscillation.

As a consequence of physical as well as numerical damping the torsional oscillation eventually reaches a constant amplitude and the overall system remains stable.

A zoom into the diagram 7.13 is given in the first part of colour chart 7.14 where five time instants are marked indicating the configurations depicted subsequently. The view on the deformed shell clearly shows the torsional displacement caused by the CORIOLIS forces. A U-pipe filled with water at rest does not excite the unsymmetric part of the structural response. Correspondingly the vertical fluid velocity is depicted on cutting surfaces in the second column of figure 7.14. High velocity in z -direction at the point B can be observed for those configurations which show almost no torsional displacement. In the third column of figure 7.14 the absolute value of the velocity is depicted on cuts of the deformed configuration. It can be observed that the velocity due to the torsional oscillation well dominates the longitudinal flow velocity inside the tube.

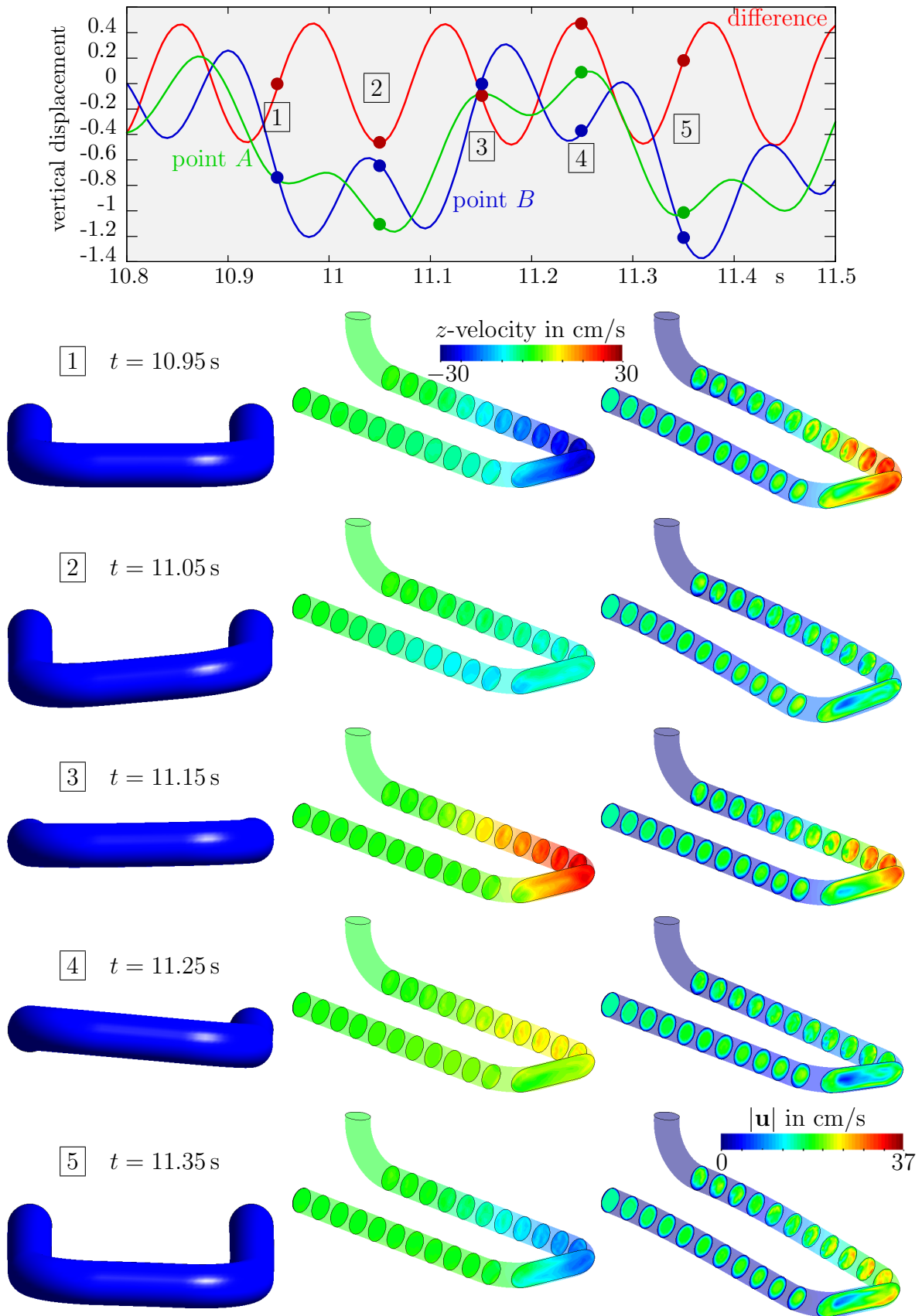


Figure 7.14: Detail of diagram 7.13 and deformed structure viewed in z -direction, vertical fluid velocity on undeformed configuration and absolute value of fluid velocity on deformed configuration (from left to right)

Chapter 8

Summary and Conclusions

8.1 Summary

This work is devoted to improvements of a partitioned fluid-structure interaction algorithm which is based on an ALE flow formulation with stabilised finite elements and a nonlinear structural solver. In a sense the objective has been twofold. In the first instance a detailed theoretical revisit of the fundamentals of the flow solver and to some extent also the coupling algorithm has been made in order to establish and confirm its accuracy and stability properties. As a result of these methodological considerations a number of changes within the code itself arose enhancing convergence and stability of the formulation.

The most important ambition of this work is to increase the understanding of the numerical algorithm and details thereof. In particular the matter of geometric conservation and its connection to stability of flow simulations on deforming domains appeared as a key question for stable and reliable algorithms. Within this work a stability criterion in terms of a maximal allowable time step size depending upon the mesh velocity could be confirmed and interpreted. In particular the interpretation reveals why the potential instability of convective ALE schemes has been suspected but not been found in practical applications. It has further been shown how a flow solver on a deforming domain has to be constructed such that it is stable independently of the mesh velocity.

Another key problem regarding the understanding of the theoretical fundamentals of the algorithm is the so-called artificial added mass effect. This is an inherent instability of sequentially coupled partitioned FSI algorithms used with incompressible flows. Especially the combination of light-weight structures and incompressible flows yields an almost immediate blow-up of weak coupling schemes. Within this work an analysis could be established explaining the instability and identifying the parameters it is influenced by. This analysis confirms the numerical observations described in the dissertation of MOK [182]. It shows why more accurate time discretisation accelerate the instability and it highlights the role of the fluid and structural mass density ratio. Consequences of the use of a stabilised FEM for the fluid field in the context of the artificial added mass effect at very small time steps have been considered. Instability conditions for various combinations of discretisation schemes could be established. It has been proved that there is no possibility to construct a sequentially staggered scheme which would be stable irrespective of the mass density ratio of fluid and structure.

Additionally the stabilised finite element formulation for fluid elements on deforming domains was revisited within this work. Here some modifications could be introduced which guarantee that the stability with respect to the motion of the reference system is not influenced by the stabilisation terms. Consequently the stability properties of

the model problem can be transferred to the stabilised NAVIER-STOKES equations on deforming domains.

Further considerations regard the behaviour of the stabilised finite element method for incompressible flows in critical situations such as highly distorted meshes and steep gradients. Numerical test cases were employed to gain the desired experience required to answer questions which are hard to be accessed analytically.

The methodological considerations brought a number of changes within the code. Along with the modifications parts of the code have been rewritten in order to derive and implement a fully linearised version of the stabilised fluid element. The computation of the elemental right hand side vector has been reformulated. Both these changes resulted in a significantly faster convergence of the nonlinear iterations within the fluid field. Extra accuracy for the coupled problem has been gained by introducing consistent nodal forces and a correctly obtained flow velocity boundary condition as coupling data. Additionally the introduction of second order accurate time discretisation schemes for the flow equations opened the door for a fully second order FSI algorithm.

Altogether the iteratively staggered FSI algorithm based on an ALE flow formulation of the incompressible NAVIER-STOKES equations with stabilised finite elements and a nonlinear structural finite element solver is regarded as settled and theoretically sound. In particular the stability issue of the flow solver on deforming domains could be clarified and an analysis of the artificial added mass effect has been presented.

8.2 Prospectus

The focus of the present work is to improve an existing approach and to deepen the understanding of the methodological fundamentals. Now a very general partitioned FSI solver for incompressible flow and highly flexible structures is available which is second order accurate, stable and offers reliable results for a broad variety of problems.

However a work like the present project will never be finished in the sense that all questions would have been answered and all problems solved. It is rather interrupted by the fact that time has passed. So a variety of interesting issues remains. Continuing the present investigations one might wish to clarify the exact interaction of the artificial added mass effect with the stabilisation of the fluid elements. Or one might well wonder if there is an intelligent way to higher order fluid elements. And what would such an element look like? Is there anything like ‘optimal stabilisation’?

And an even higher need for further progress is found away from the fundamentals. It is still most urgent to speed up the entire algorithm which would allow larger examples closer to realistic applications to be simulated at an acceptable accuracy. In particular the simulation of large scale three-dimensional problems are currently quite at the limit. Modifications of the coupling approach are presently investigated and shall make the simulation more efficient. In this context it appears interesting to work out in which range of parameters, i.e. for which applications semi-explicit coupling schemes might work well. Additional speed-up could also be gained by optimising the solver of the resulting nonlinear system of equations. A matter which has not been touched at all within this work.

As the overall FSI algorithm runs stably a very interesting challenge would be the

implementation of adaptivity with respect to the temporal but also the spatial resolution. As a prerequisite a stable overall algorithm would have to be established which allows different time step sizes within the single fields. Analogously non-matching grids at the interface would have to be treated.

Another very important direction of future work is the extension of the class of problems that can be dealt with. It appears very promising to customise the algorithm to special applications such as building wind interaction, particular pipe flow problems or biological flows. Such a specialisation to a class of sub-problems appears to be twofold. On the one hand the derivation and implementation of additional models or nonlinear material laws is required which would increase the complexity of the model. On the other hand the restriction to a particular type of application would very likely allow to built in some a-priori knowledge about the problem. This could possibly reduce the computational effort and at the same time increase the accuracy of the simulation.

In any case the present approach appears to be promising and worth to built on.

Appendix A

Some further information

A.1 The kinematic formulae in a deforming frame of reference

Two kinematic formulae the first of which is the geometric conservation law (3.5) and the second is the REYNOLDS transport theorem are used within this work without derivation. However the basic coordinate transformations and required ALE equations heavily rely upon these formulae and thus a derivation shall be given here.

A.1.1 Geometric conservation law

The derivation for the geometric conservation law or EULER formula follows [230] and starts from an expression of the mesh determinant reading

$$J_t \delta_{ij} = \frac{\partial x_i}{\partial \chi_\alpha} a_{j\alpha}, \quad (\text{A.1})$$

where $a_{j\alpha}$ is the cofactor of $\partial x_i / \partial \chi_\alpha$ and a summation over $\alpha \in 1, 2, 3$ is applied. In a three-dimensional case one obtains this factor to

$$a_{j\alpha} = \frac{\partial x_k}{\partial \chi_\beta} \frac{\partial x_l}{\partial \chi_\gamma} - \frac{\partial x_k}{\partial \chi_\gamma} \frac{\partial x_l}{\partial \chi_\beta},$$

where $\{j, k, l\} = \{1, 2, 3\}$ and $\{\alpha, \beta, \gamma\} = \{1, 2, 3\}$ and cyclic permutations thereof. From (A.1) one obtains the possible expressions for the JACOBIAN determinant with $i = j$

$$J_t = \frac{\partial x_1}{\partial \chi_\alpha} a_{1\alpha} = \frac{\partial x_2}{\partial \chi_\alpha} a_{2\alpha} = \frac{\partial x_3}{\partial \chi_\alpha} a_{3\alpha}$$

Thus a time derivation of J_t at a fixed point of reference can be expressed by

$$\left. \frac{\partial J_t}{\partial t} \right|_{\mathbf{x}} = \frac{\partial u_k^G}{\partial \chi_\alpha} a_{k\alpha},$$

where $\partial \mathbf{x} / \partial t|_{\mathbf{x}} = \mathbf{u}^G$ has been used. Applying further the chain rule yields

$$\left. \frac{\partial J_t}{\partial t} \right|_{\mathbf{x}} = \frac{\partial u_k^G}{\partial x_j} \frac{\partial x_j}{\partial \chi_\alpha} a_{k\alpha} \quad (\text{A.2})$$

$$= \frac{\partial u_k^G}{\partial x_j} J_t \delta_{jk} \quad (\text{A.3})$$

$$= J_t \nabla \cdot \mathbf{u}^G, \quad (\text{A.4})$$

i.e. the desired geometric conservation law.

A.1.2 Reynolds transport theorem

The REYNOLDS transport theorem allows to express the time derivative of the spatial integral of a time dependent function with respect to a spatially moving system of reference

$$\frac{\partial}{\partial t} \Big|_{\boldsymbol{\chi}} \int_{V_t} f(\mathbf{x}, t) \, dV_t,$$

where V_t is a volume fixed in the reference system $\boldsymbol{\chi}$.

In order to derive the theorem the differential volume element is transferred back to the reference system and the relation $\mathbf{x} = \mathbf{x}(\boldsymbol{\chi})$ is employed yielding

$$\begin{aligned} \frac{\partial}{\partial t} \Big|_{\boldsymbol{\chi}} \int_{V_t} f(\mathbf{x}, t) \, dV_t &= \int_{V_0} \frac{\partial}{\partial t} \Big|_{\boldsymbol{\chi}} (f(\mathbf{x}(\boldsymbol{\chi}), t) J_t) \, dV_0 \\ &= \int_{V_0} \frac{\partial}{\partial t} \Big|_{\boldsymbol{\chi}} f(\mathbf{x}(\boldsymbol{\chi}), t) J_t \, dV_0 + \int_{V_0} f(\mathbf{x}, t) \frac{\partial J_t}{\partial t} \Big|_{\boldsymbol{\chi}} \, dV_0 \end{aligned} \quad (\text{A.5})$$

The time derivative in the first term of (A.5) can be evaluated by the chain rule

$$\frac{\partial f(\mathbf{x}(\boldsymbol{\chi}), t)}{\partial t} \Big|_{\boldsymbol{\chi}} = \frac{\partial f(\mathbf{x}, t)}{\partial \mathbf{x}} \frac{\partial \mathbf{x}}{\partial t} \Big|_{\boldsymbol{\chi}} + \frac{\partial f(\mathbf{x}, t)}{\partial t} \Big|_{\mathbf{x}} \quad (\text{A.6})$$

Inserting (A.6) into (A.5) yields

$$\frac{\partial}{\partial t} \Big|_{\boldsymbol{\chi}} \int_{V_t} f(\mathbf{x}, t) \, dV_t = \int_{V_0} \left(\frac{\partial f(\mathbf{x}, t)}{\partial t} \Big|_{\mathbf{x}} + \mathbf{u}^G \cdot \nabla f(\mathbf{x}, t) + f(\mathbf{x}, t) \nabla \cdot \mathbf{u}^G \right) J_t \, dV_0,$$

where (A.4) and the definition of the mesh velocity has been used. This equation can be reformulated as an integral over the time dependent domain V_t

$$\frac{\partial}{\partial t} \Big|_{\boldsymbol{\chi}} \int_{V_t} f(\mathbf{x}, t) \, dV_t = \int_{V_t} \left(\frac{\partial f(\mathbf{x}, t)}{\partial t} \Big|_{\mathbf{x}} + \nabla \cdot (\mathbf{u}^G f(\mathbf{x}, t)) \right) \, dV_t \quad (\text{A.7})$$

and yields the REYNOLDS transport theorem in an ALE frame of reference reading

$$\frac{\partial}{\partial t} \Big|_{\boldsymbol{\chi}} \int_{V_t} f(\mathbf{x}, t) \, dV_t = \int_{V_t} \frac{\partial f(\mathbf{x}, t)}{\partial t} \Big|_{\mathbf{x}} \, dV_t + \int_{\Gamma_t} f(\mathbf{x}, t) \mathbf{u}^G \cdot \mathbf{n} \, d\Gamma_t. \quad (\text{A.8})$$

In the special case of an EULERian frame of reference the theorem allows to express the material time derivative of the integral over a function $f(\mathbf{x}, t)$ and thus the arbitrary system $\boldsymbol{\chi}$ is identified with the material coordinates \mathbf{X} yielding the well known expression

$$\frac{\partial}{\partial t} \Big|_{\mathbf{X}} \int_{V_t} f(\mathbf{x}, t) \, dV_t = \int_{V_t} \frac{\partial f(\mathbf{x}, t)}{\partial t} \Big|_{\mathbf{x}} \, dV_t + \int_{\Gamma_t} f(\mathbf{x}, t) \mathbf{u} \cdot \mathbf{n} \, d\Gamma_t \quad (\text{A.9})$$

which is the REYNOLDS transport theorem in an EULERian frame of reference.

A.2 Some mathematical background

A.2.1 The scalar product

The notation $(a, b)_\Omega$ is used short for

$$(a, b)_\Omega = \int_\Omega ab \, d\Omega, \quad (\text{A.10})$$

where a and b may represent tensors of first or second order.

A.2.2 Lax-Milgram lemma

The lemma named after the Hungarian mathematician Peter David LAX and Artur Norton MILGRAM guarantees the solvability of a variational problem of the form

$$a(u, v) = (f, v) \quad \text{for all } v \in V. \quad (\text{A.11})$$

In (A.11) $a(u, v)$ denotes a bilinear form and v can be regarded a test or weighting function in a weak formulation. The problem (A.11) has a unique solution if the bilinear form a is bounded, i.e.

$$|a(u, v)| \leq C \|u\| \|v\| \quad (\text{A.12})$$

and coercive which means that

$$a(u, u) \geq c \|u\|^2 \quad (\text{A.13})$$

with $0 < c < C < \infty$ is guaranteed. For symmetric positive definite operators a the constant c is an lower bound on the lowest eigenvalue of a thus ensuring that the left hand side of (A.11) is bounded away from being singular. Further the inequality

$$c \|u\| \leq \sup_{0 \neq v \in V} \frac{(f, v)}{\|v\|} \quad (\text{A.14})$$

holds.

In more general cases coercivity requires that for every admissible solution $u \in V$ at least one test function v can be found, such that $a(u, v) > 0$. For further reference one might consult for example [4].

A.2.3 Some inequalities

Some inequalities are required in coercivity analyses and shall thus be summarised here.

Cauchy-Schwarz inequality

For two terms a and b

$$(a, b)_\Omega \leq \|a\|_\Omega \|b\|_\Omega \quad (\text{A.15})$$

is satisfied. This CAUCHY-SCHWARZ inequality follows from geometrical considerations. It is sharp in the case that a can be expressed as $a = \lambda b$ where λ is a positive constant.

The ε -inequality

The ε -inequality states that for any a and b and for any strictly positive ε

$$\varepsilon a^2 + \frac{1}{4\varepsilon} b^2 \geq ab \quad (\text{A.16})$$

is satisfied. It can easily be derived from a binomial formula. The inequality becomes an equality in the case of $a > 0$ and $b > 0$ when the parameter ε satisfies $\varepsilon = b/(2a)$.

Inverse inequalities

The inverse inequalities required within the present work are related to a particular spatial discretisation or rather, valid on a single element. In a discrete space it is possible to bound higher derivatives by lower ones, i.e.

$$C_{0e} h_e^2 \|\nabla \mathbf{v}\|_{\Omega_e}^2 \leq \|\mathbf{v}\|_{\Omega_e}^2 \quad \text{for all } \mathbf{v} \in \mathbf{V}_e^h \quad (\text{A.17})$$

with a positive elemental constant C_{0e} which depends upon the order and geometry of the element. Likewise an inequality one order higher can be stated which is used to adjust the stabilisation parameter to the element order and geometry. The inequality stated in section 4.3.7 reads

$$C_e h_e^2 \|\Delta \mathbf{v}\|_{\Omega_e}^2 \leq \|\nabla \mathbf{v}\|_{\Omega_e}^2 \quad \text{for all } \mathbf{v} \in \mathbf{V}_e^h. \quad (\text{A.18})$$

The constants in (A.17) and (A.18) satisfy $C_{0e} > C_e$ as shown in [116]. The sharp constant within a particular element can be obtained from the solution of an elemental eigenvalue problem. For more information on inverse inequalities consult for instance the textbook by BRENNER and SCOTT [30].

A.3 Errors in Kim-Moin flow

The L^2 errors obtained on three differently distorted meshes with a variety of stabilisation parameters and variants of the stabilisation operator are given here. These values complete the KIM-MOIN problem as presented in section 5.3.2.

On the heavily distorted mesh in mode 2 no convergent USFEM solution could be obtained for most of the stabilisation parameters.

Table A.1: L^2 error in velocity and pressure on undistorted meshes of linear elements for different choices of the stabilisation parameter

τ	$err_{\mathbf{u}}$ GLS	err_p GLS	$err_{\mathbf{u}}$ SUPG	err_p SUPG	$err_{\mathbf{u}}$ USFEM	err_p USFEM
i	0.005130	0.002877	0.004614	0.002460	0.004212	0.002287
ii	0.005267	0.002919	0.004729	0.002505	0.004319	0.002360
iii	0.005130	0.002877	0.004614	0.002460	0.004212	0.002287
iv	0.005130	0.002877	0.004614	0.002460	0.004212	0.002287
v	0.004815	0.002885	0.004524	0.002676	0.004274	0.002552
vi	0.005130	0.002877	0.004614	0.002460	0.004212	0.002287
vii	0.005130	0.002877	0.004614	0.002460	0.004212	0.002287

Table A.2: L^2 error in velocity and pressure on undistorted meshes of quadratic elements for different choices of the stabilisation parameter

τ	$err_{\mathbf{u}}$ GLS	err_p GLS	$err_{\mathbf{u}}$ SUPG	err_p SUPG	$err_{\mathbf{u}}$ USFEM	err_p USFEM
i	0.002624	0.002560	0.002617	0.002544	0.002631	0.002597
ii	0.002623	0.002562	0.002616	0.002546	0.002627	0.002543
iii	0.002624	0.002560	0.002617	0.002544	0.002631	0.002597
iv	0.002624	0.002560	0.002617	0.002544	0.002631	0.002597
v	0.002631	0.002561	0.002624	0.002546	0.002612	0.002526
vi	0.002624	0.002560	0.002617	0.002544	0.002631	0.002597
vii	0.002624	0.002560	0.002617	0.002544	0.002631	0.002597

Table A.3: L^2 error in velocity and pressure on mode 1 distorted meshes of linear elements for different choices of the stabilisation parameter

τ	$err_{\mathbf{u}}$ GLS	err_p GLS	$err_{\mathbf{u}}$ SUPG	err_p SUPG	$err_{\mathbf{u}}$ USFEM	err_p USFEM
i	0.007613	0.005044	0.006514	0.004266	0.005650	0.003835
ii	0.007695	0.004969	0.006593	0.004199	0.005752	0.003802
iii	0.007513	0.004839	0.006460	0.004083	0.005620	0.003638
iv	0.007376	0.004821	0.006444	0.004207	0.005667	0.003829
v	0.006994	0.004825	0.006353	0.004376	0.005777	0.004045
vi	0.007422	0.004913	0.006456	0.004251	0.005654	0.003840
vii	0.007785	0.005177	0.006575	0.004321	0.005679	0.003908

Table A.4: L^2 error in velocity and pressure on mode 1 distorted meshes of quadratic elements for different choices of the stabilisation parameter

τ	$err_{\mathbf{u}}$ GLS	err_p GLS	$err_{\mathbf{u}}$ SUPG	err_p SUPG	$err_{\mathbf{u}}$ USFEM	err_p USFEM
i	0.002638	0.002581	0.002637	0.002587	0.002655	0.002662
ii	0.002636	0.002581	0.002635	0.002590	0.002691	0.002886
iii	0.002638	0.002580	0.002637	0.002587	0.002656	0.002662
iv	0.002642	0.002583	0.002641	0.002589	0.002663	0.002670
v	0.002648	0.002584	0.002644	0.002588	–	–
vi	0.002642	0.002583	0.002641	0.002589	0.002662	0.002670
vii	0.002635	0.002579	0.002634	0.002586	0.002647	0.002656

Table A.5: L^2 error in velocity and pressure on mode 2 distorted meshes of linear elements for different choices of the stabilisation parameter

τ	$err_{\mathbf{u}}$ GLS	err_p GLS	$err_{\mathbf{u}}$ SUPG	err_p SUPG
i	0.232357	0.185340	0.043555	0.084645
ii	0.134009	0.120765	0.055546	0.058709
iii	0.108969	0.102256	0.057660	0.061274
iv	0.087337	0.085032	0.058018	0.057737
v	0.087531	0.087089	0.058085	0.059084
vi	0.087356	0.085038	0.058027	0.057756
vii	0.419851	0.272936	0.043516	0.155843

Table A.6: L^2 error in velocity and pressure on mode 2 distorted meshes of quadratic elements for different choices of the stabilisation parameter

τ	$err_{\mathbf{u}}$ GLS	err_p GLS	$err_{\mathbf{u}}$ SUPG	err_p SUPG
i	0.006558	0.009451	0.004198	0.010419
ii	0.006135	0.008265	0.004601	0.010309
iii	0.005910	0.008046	0.004624	0.010148
iv	0.004953	0.007794	0.004212	0.006309
v	0.005621	0.008779	0.004048	0.004463
vi	0.004952	0.007793	0.004212	0.006316
vii	0.006916	0.010307	0.004510	0.018528

A.4 Flow around rigid cylinder

The subsequent diagrams complete the results obtained from $Re = 100$ flow around a rigid cylinder reported in section 5.3.3. The lift coefficients and drag coefficients for the meshes B4, C4, A9 and B9 are given here.

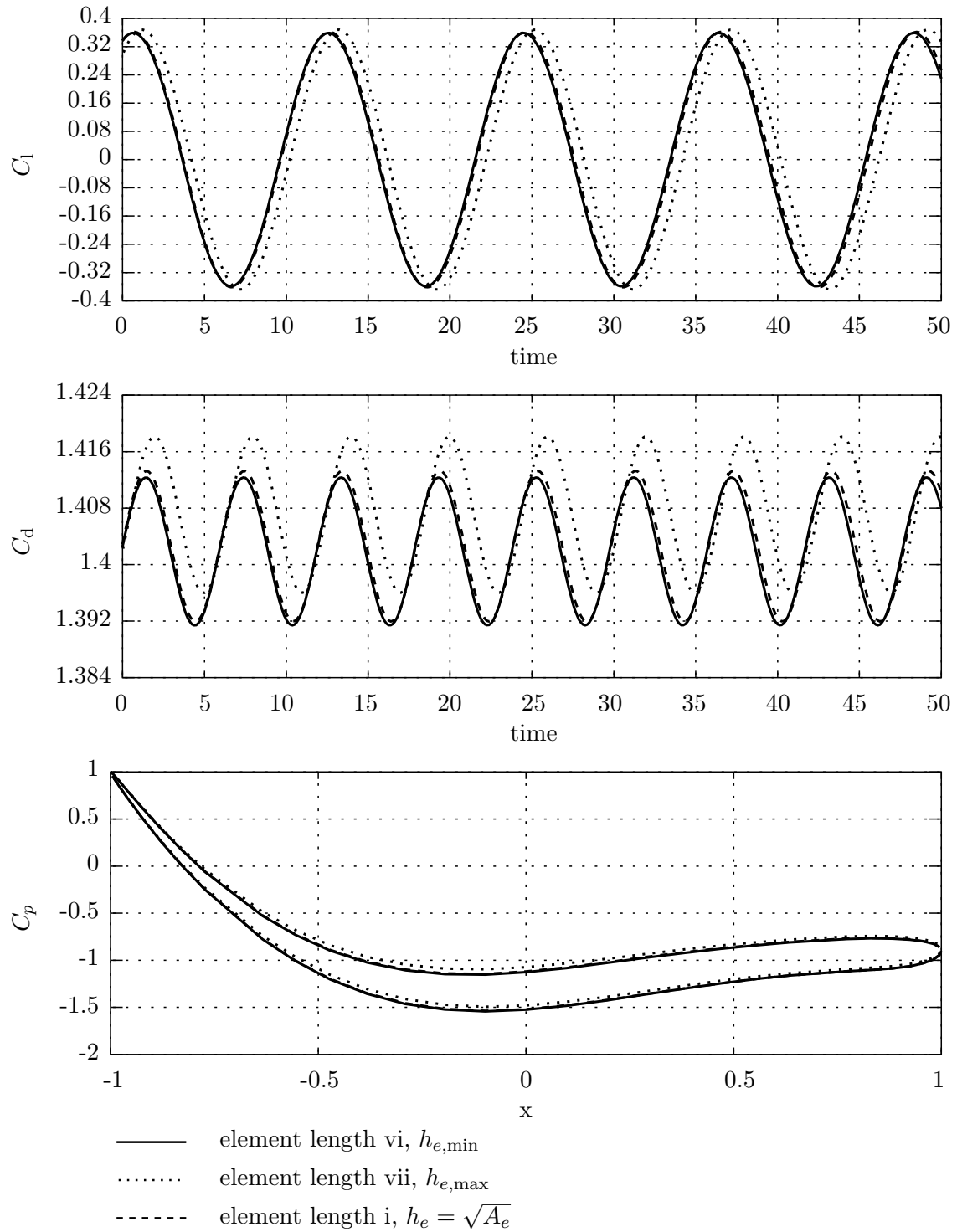


Figure A.1: Lift and drag coefficients and pressure profile obtained on mesh B4 with three different element length definitions within the stabilisation parameter

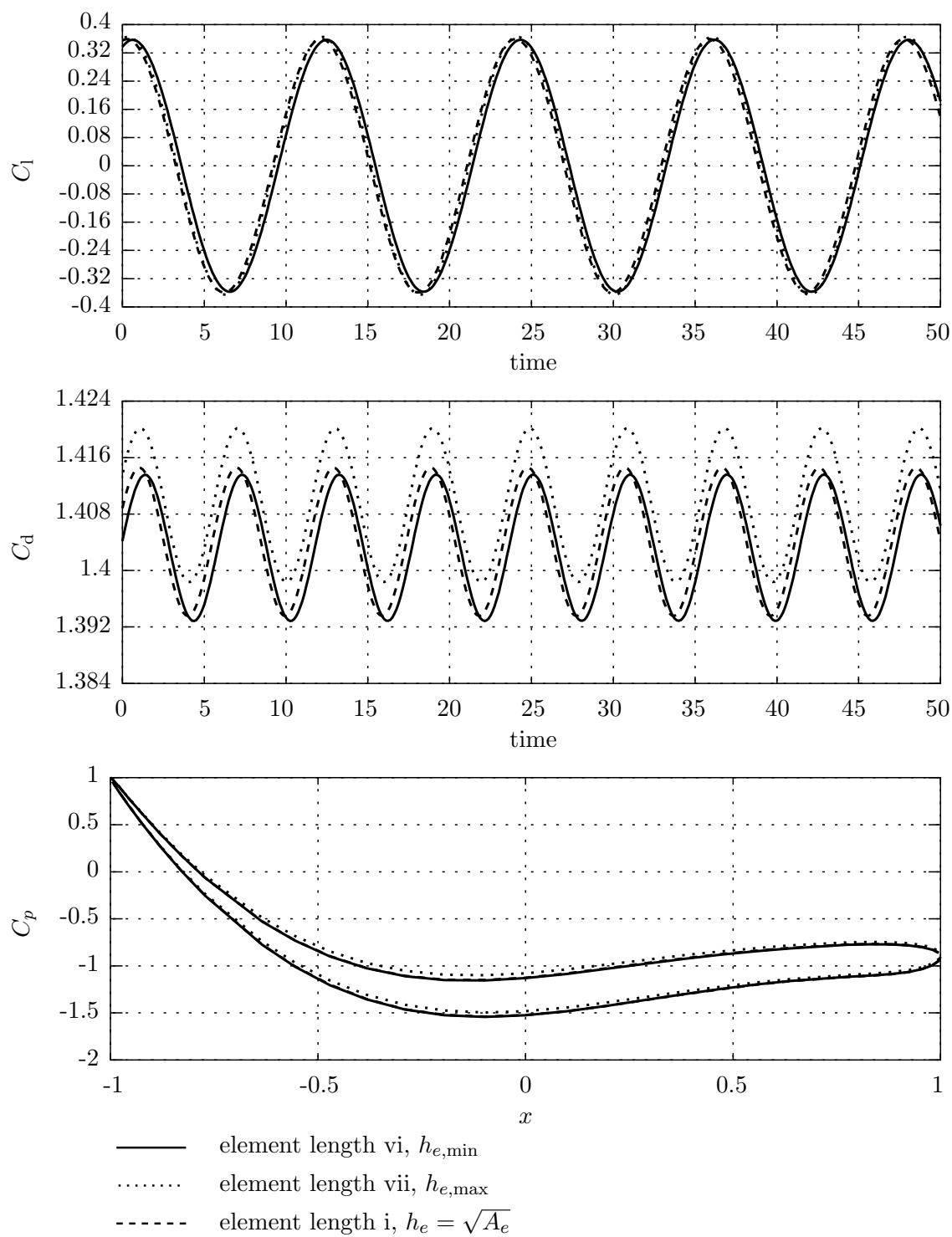


Figure A.2: Lift and drag coefficients and pressure profile obtained on mesh C4 with three different element length definitions within the stabilisation parameter

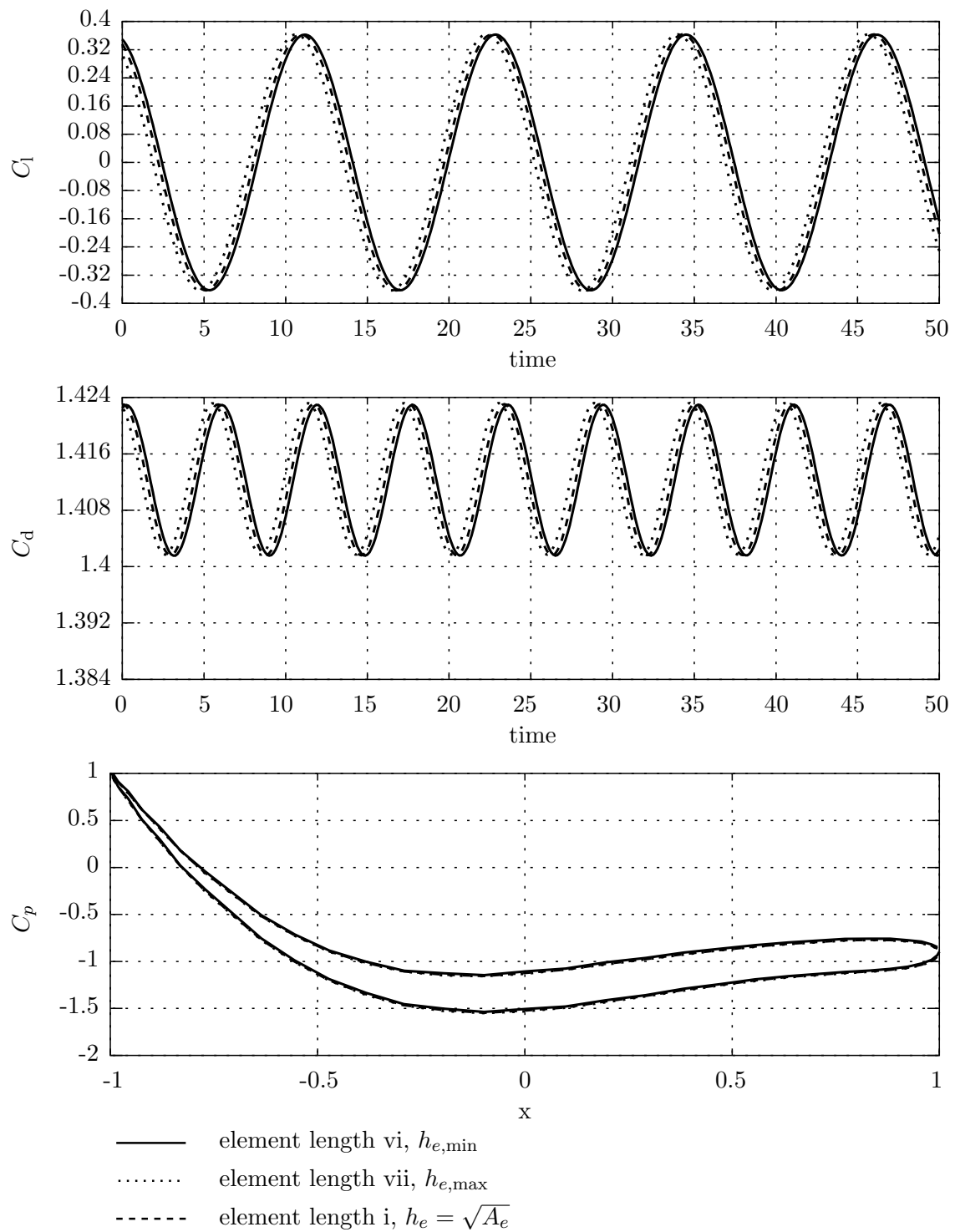


Figure A.3: Lift and drag coefficients and pressure profile obtained on mesh A9 with three different element length definitions within the stabilisation parameter

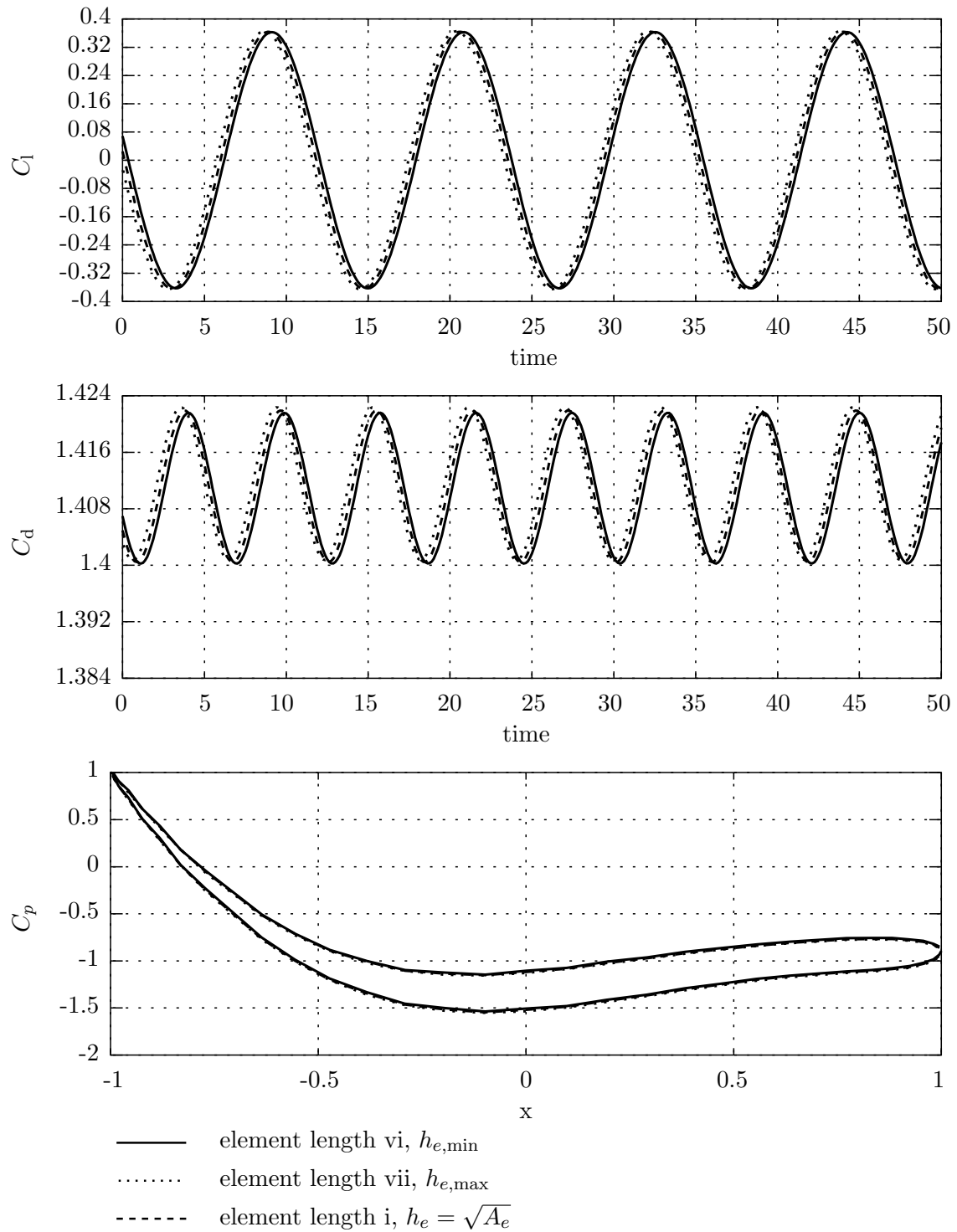


Figure A.4: Lift and drag coefficients and pressure profile obtained on mesh B9 with three different element length definitions within the stabilisation parameter

References

- [1] **Akin, J., Tezduyar, T. (2004)**: ‘Calculation of the advective limit of the SUPG stabilization parameter for linear and higher-order elements.’, *Computer Methods in Applied Mechanics and Engineering*, Vol. 193, pp. 1909–1922.
- [2] **Altenbach, J., Altenbach, H. (1994)**: *Einführung in die Kontinuumsmechanik*, Teubner, Stuttgart.
- [3] **Aris, R. (1962)**: *Vectors, Tensors, and the Basic Equations of Fluid Mechanics*, Prentice-Hall, Englewood Cliffs, New Jersey.
- [4] **Babuška, I., Aziz, A. K. (1972)**: ‘Survey lectures on the mathematical foundations of the finite element method’, in: **Aziz, A. K.** (ed.), *The Mathematical Foundations of the Finite Element Method with Applications to Partial Differential Equations*, Academic Press, Inc., New York, pp. 5–359.
- [5] **Badia, S., Codina, R. (2006)**: ‘Analysis of a stabilized finite element approximation of the transient convection-diffusion equation using an ALE framework’, *SIAM Journal on Numerical Analysis*, Vol. 44, pp. 2159–2197.
- [6] **Baiocchi, C., Brezzi, F. (1993)**: ‘Virtual bubbles and Galerkin-least-squares type of methods (Ga.L.S.)’, *Computer Methods in Applied Mechanics and Engineering*, Vol. 105, pp. 125–141.
- [7] **Barrenechea, G., Valentin, F. (2002)**: ‘An unusual stabilized finite element method for a generalized Stokes problem.’, *Numerische Mathematik*, Vol. 92, pp. 652–677.
- [8] **Barth, T., Bochev, P. B., Gunzburger, M. D., Shadid, J. N. (2004)**: ‘A taxonomy of consistently stabilized finite element methods for the Stokes problem.’, *SIAM Journal on Scientific Computing*, Vol. 25, pp. 1585–1607.
- [9] **Bathe, K.-J. (1982)**: *Finite Element Procedures in Engineering Analysis*, Prentice Hall, New Jersey.
- [10] **Bathe, K.-J., Pontaza, J.-P. (2002)**: ‘A flow-condition-based interpolation mixed finite element procedure for higher Reynolds number fluid flows.’, *Mathematical Models & Methods in Applied Sciences*, Vol. 12, pp. 525–539.
- [11] **Bathe, K.-J., Zhang, H. (2002)**: ‘A flow-condition-based interpolation finite element procedure for incompressible fluid flows.’, *Computers and Structures*, Vol. 80, pp. 1267–1277.
- [12] **Behr, M. A., Franca, L. P., Tezduyar, T. E. (1993)**: ‘Stabilized finite element methods in applied mechanics and engineering.’, *Computer Methods in Applied Mechanics and Engineering*, Vol. 104, pp. 31–48.
- [13] **Belytschko, T., Kennedy, J. M. (1978)**: ‘Computer methods for subassembly simulation.’, *Nuclear Engineering and Design*, Vol. 49, pp. 17–38.
- [14] **Bischoff, M. (1999)**: *Theorie und Numerik einer dreidimensionalen Schalenformulierung*, Phd thesis, Institut für Baustatik, Universität Stuttgart.
- [15] **Bischoff, M., Ramm, E. (2000)**: ‘On the physical significance of higher order kinematic and static variables in a three-dimensional shell formulation.’, *International Journal of Solids and Structures*, Vol. 37, pp. 6933–6960.

- [16] **Bischoff, M., Wall, W. A., Bletzinger, K.-U., Ramm, E. (2004)**: ‘Models and finite elements for thin-walled structures’, in: **Stein, E., de Borst, R., Hughes, T. J. R.** (eds.), *Encyclopedia of Computational Mechanics, Volume 2 Solids and Structures*, Wiley, pp. 59–137.
- [17] **Blasco, J., Codina, R. (2001)**: ‘Space and time error estimates for a first-order, pressure stabilized finite element method for the incompressible Navier-Stokes equations.’, *Applied Numerical Mathematics*, Vol. 38, pp. 475–497.
- [18] **Blom, F. J. (2000)**: ‘Considerations on the spring analogy.’, *International Journal for Numerical Methods in Fluids*, Vol. 32, pp. 647–668.
- [19] **Bochev, P. B., Dohrmann, C. R., Gunzburger, M. D. (2006)**: ‘Stabilization of low-order mixed finite elements for the Stokes equations.’, *SINUM*, Vol. 44, pp. 82–101.
- [20] **Bochev, P. B., Gunzburger, M. D. (2005)**: ‘An absolutely stable pressure-Poisson stabilized finite element method for the Stokes equations.’, *SIAM J. Numer. Anal.*, Vol. 42/3, pp. 1189–1207.
- [21] **Bochev, P. B., Gunzburger, M. D., Lehoucq, R. B. (2007)**: ‘On stabilized finite element methods for the Stokes problem in the small time step limit.’, *International Journal for Numerical Methods in Fluids*, Vol. 53, pp. 573–597.
- [22] **Bochev, P. B., Gunzburger, M. D., Shadid, J. N. (2004)**: ‘On inf-sup stabilized finite element methods for transient problems.’, *Computer Methods in Applied Mechanics and Engineering*, Vol. 193, pp. 1471–1489.
- [23] **Bochev, P. B., Gunzburger, M. D., Shadid, J. N. (2004)**: ‘Stability of the SUPG finite element method for transient advection-diffusion problems.’, *Computer Methods in Applied Mechanics and Engineering*, Vol. 193, pp. 2301–2323.
- [24] **Bochev, P. B., Shadid, J. N., Gunzburger, M. D. (2002)**: ‘On stabilized finite element methods for transient problems with varying time scales.’, in: *Proceedings of the Fifth World Congress on Computational Mechanics 2002, Vienna, Austria*.
- [25] **Boffi, D., Gastaldi, L. (2004)**: ‘Stability and geometric conservation laws for ALE formulations.’, *Computer Methods in Applied Mechanics and Engineering*, Vol. 193, pp. 4717–4739.
- [26] **Bonet, J., Wood, R. D. (1997)**: *Nonlinear Continuum Mechanics for Finite Element Analysis*, Cambridge University Press.
- [27] **Braack, M., Burman, E., John, V., Lube, G. (2006)**: ‘Stabilized finite element methods for the generalized Oseen problem.’, *Computer Methods in Applied Mechanics and Engineering*, Vol. 196, pp. 853–866.
- [28] **Braess, D. (1997)**: *Finite Elemente - Theorie, schnelle Löser und Anwendungen in der Elastizitätstheorie*, Springer, Berlin.
- [29] **Brenner, S. C., Carstensen, C. (2004)**: ‘Finite element methods’, in: **Stein, E., de Borst, R., Hughes, T. J. R.** (eds.), *Encyclopedia of Computational Mechanics, Volume 1 Fundamentals*, Wiley, pp. 74–118.
- [30] **Brenner, S. C., Scott, L. R. (1994)**: *The mathematical theory of finite element methods*, Springer-Verlag, New York.
- [31] **Brezzi, F., Bristeau, M.-O., Franca, L. P., Mallet, M., Rogé, G. (1992)**: ‘A relationship between stabilized finite element methods and the Galerkin method with bubble functions.’, *Computer Methods in Applied Mechanics and Engineering*, Vol. 96, pp. 117–129.
- [32] **Brezzi, F., Fortin, M. (1991)**: *Mixed and Hybrid Finite Element Methods*, Vol. 15 of *Springer Series in Computational Mathematics*, Springer, New York.
- [33] **Brezzi, F., Franca, L. P., Hughes, T. J. R., Russo, A. (1996)**: ‘Stabilization techniques and subgrid scales capturing’, in: *Proceedings of the Conference State of the Art in Numerical Analysis*, York, England.
- [34] **Brezzi, F., Russo, A. (1994)**: ‘Choosing bubbles for advection-diffusion problems.’, *Mathematical Models and Methods in Applied Sciences*, Vol. 4, pp. 571–587.

- [35] **Brooks, A., Hughes, T. J. R. (1982)**: ‘Streamline upwind/Petrov-Galerkin formulations for convection dominated flows with particular emphasis on the incompressible Navier-Stokes equations.’, *Computer Methods in Applied Mechanics and Engineering*, Vol. 32, pp. 199–259.
- [36] **Büchter, N., Ramm, E. (1992)**: ‘Shell theory versus degeneration - a comparison in large rotation finite element analysis.’, *International Journal of Numerical Methods in Engineering*, Vol. 34, pp. 39–59.
- [37] **Büchter, N., Ramm, E., Roehl, D. (1994)**: ‘Three-dimensional extension of nonlinear shell formulation based on the enhanced assumed strain concept.’, *International Journal of Numerical Methods in Engineering*, Vol. 37, pp. 2551–2568.
- [38] **Causin, P., Gerbeau, J.-F., Nobile, F. (2005)**: ‘Added-mass effect in the design of partitioned algorithms for fluid-structure problems.’, *Computer Methods in Applied Mechanics and Engineering*, Vol. 194, pp. 4506–4527.
- [39] **Chiandussi, G., Bugeda, G., Oñate, E. (2000)**: ‘A simple method for automatic update of finite element meshes.’, *Communications in Numerical Methods in Engineering*, Vol. 16, pp. 1–19.
- [40] **Chorin, A. J. (1968)**: ‘Numerical solution of the Navier-Stokes equations.’, *Mathematics of Computation*, Vol. 22, pp. 745–762.
- [41] **Chorin, A. J. (1969)**: ‘On the convergence of discrete approximation to the Navier-Stokes equations.’, *Mathematics of Computation*, Vol. 23, pp. 341–353.
- [42] **Chung, J., Hulbert, G. M. (1993)**: ‘A time integration algorithm for structural dynamics with improved numerical dissipation: The generalized- α method.’, *Journal of Applied Mathematics*, Vol. 60, pp. 371–375.
- [43] **Ciarlet, P. G. (2002)**: *The Finite Element Method for Elliptic Problems*, Classics in Applied Mathematics, SIAM, 2. edn.
- [44] **Ciarlet, P. G., Lions, J. L. (eds.) (1991)**: *Finite Element Methods (Part 1)*, Vol. II of *Handbook of Numerical Analysis*, North-Holland, Amsterdam.
- [45] **Ciarlet, P. G., Lions, J. L. (eds.) (1996)**: *Finite Element Methods (Part 2) - Numerical Methods for Solids (Part 2)*, Vol. IV of *Handbook of Numerical Analysis*, North-Holland, Amsterdam.
- [46] CIMNE, <http://gid.cimne.upc.es/>: *GID*.
- [47] **Codina, R. (1998)**: ‘Comparison of some finite element methods for solving the diffusion-convection-reaction equation.’, *Computer Methods in Applied Mechanics and Engineering*, Vol. 156, pp. 185–210.
- [48] **Codina, R. (2000)**: ‘A nodal-based implementation of a stabilized finite element method for incompressible flow problems.’, *International Journal for Numerical Methods in Fluids*, Vol. 33, pp. 737–766.
- [49] **Codina, R. (2000)**: ‘On stabilized finite element methods for linear systems of convection-diffusion-reaction equations.’, *Computer Methods in Applied Mechanics and Engineering*, Vol. 188, pp. 61–82.
- [50] **Codina, R. (2000)**: ‘Stabilization of incompressibility and convection through orthogonal subscales in finite element methods.’, *Computer Methods in Applied Mechanics and Engineering*, Vol. 190, pp. 1579–1599.
- [51] **Codina, R. (2001)**: ‘A stabilized finite element method for generalized stationary incompressible flows.’, *Computer Methods in Applied Mechanics and Engineering*, Vol. 190, pp. 2681–2706.
- [52] **Codina, R. (2002)**: ‘Stabilized finite element approximation of transient incompressible flows using orthogonal subscales.’, *Computer Methods in Applied Mechanics and Engineering*, Vol. 191, pp. 4295–4321.
- [53] **Codina, R. (2007)**: ‘Analysis of a stabilized finite element approximation of the Oseen equations using orthogonal subscales.’, *Applied Numerical Mathematics*, in press.

- [54] **Codina, R., Blasco, C. (1997)**: ‘A finite element formulation for the Stokes problem allowing equal velocity–pressure interpolation.’, *Computer Methods in Applied Mechanics and Engineering*, Vol. 143, pp. 373–391.
- [55] **Codina, R., Blasco, J. (2000)**: ‘Analysis of a pressure-stabilized finite element approximation of the stationary Navier-Stokes equations.’, *Numerische Mathematik*, Vol. 87, pp. 59–81.
- [56] **Codina, R., Blasco, J. (2000)**: ‘Stabilized finite element method for the transient Navier-Stokes equations based on a pressure gradient projection.’, *Computer Methods in Applied Mechanics and Engineering*, Vol. 182, pp. 277–300.
- [57] **Codina, R., Principe, J., Guasch, O., Badia, S. (2007)**: ‘Time dependent subscales in the stabilized finite element approximation of incompressible flow problems.’, *Computer Methods in Applied Mechanics and Engineering*, Vol. 196, pp. 2413–2430.
- [58] **Codina, R., Soto, O. (2004)**: ‘Approximation of the incompressible Navier-Stokes equations using orthogonal subscale stabilization and pressure segregation on anisotropic finite element meshes.’, *Computer Methods in Applied Mechanics and Engineering*, Vol. 193, pp. 1403–1419.
- [59] **Codina, R., Zienkiewicz, O. C. (2002)**: ‘CBS versus GLS stabilization of the incompressible Navier-stokes equations and the role of the time step as stabilization parameter.’, *Communications in Numerical Methods in Engineering*, Vol. 18, pp. 99–112.
- [60] **Crisfield, M. (1997)**: *Non-linear Finite Element Analysis of Solid and Structures, Volume 2: Advanced Topics*, John Wiley & Sons.
- [61] **Degand, C., Farhat, C. (2002)**: ‘A three-dimensional torsional spring analogy method for unstructured dynamic meshes.’, *Computers and Structures*, Vol. 80, pp. 305–316.
- [62] **Dettmer, W., Perić, D. (2003)**: ‘An analysis of the time integration algorithms for the finite element solutions of incompressible Navier-Stokes equations based on a stabilised formulation.’, *Computer Methods in Applied Mechanics and Engineering*, Vol. 192, pp. 1177–1226.
- [63] **Dettmer, W., Perić, D. (2006)**: ‘A computational framework for fluid-rigid body interaction: Finite element formulation and applications.’, *Computer Methods in Applied Mechanics and Engineering*, Vol. 195, pp. 1633–1666.
- [64] **Dettmer, W., Perić, D. (2006)**: ‘A computational framework for fluid-structure interaction: Finite element formulation and applications.’, *Computer Methods in Applied Mechanics and Engineering*, Vol. 195, pp. 5754–5779.
- [65] **Dohrmann, C. R., Bochev, P. B. (2004)**: ‘A stabilized finite element method for the Stokes problem based on polynomial pressure projections.’, *International Journal for Numerical Methods in Fluids*, Vol. 46, pp. 183–201.
- [66] **Donea, J. (1983)**: ‘Arbitrary Lagrangian-Eulerian finite element methods’, in: **Hughes, T. J. R., Belytschko, T.** (eds.), *Computational Methods for Transient Analysis*, Elsevier Science Publishers B. V., pp. 473–516.
- [67] **Donea, J., Fasoli-Stella, P., Giuliani, S. (1977)**: ‘Lagrangian and Eulerian finite element techniques for transient fluid-structure interaction problems’, in: *Transactions of the 4th SMIRT Conference*, Vol. B, San Francisco.
- [68] **Donea, J., Giuliani, S., Halleux, J. P. (1982)**: ‘An arbitrary Lagrangian-Eulerian finite element method for transient dynamic fluid-structure interactions.’, *Computer Methods in Applied Mechanics and Engineering*, Vol. 33, pp. 689–723.
- [69] **Donea, J., Huerta, A. (1989)**: *Finite element methods for flow problems*, Wiley.
- [70] **Donea, J., Huerta, A., Ponthot, J.-P., Rodríguez-Ferran, A. (2004)**: ‘Arbitrary Lagrangian-Eulerian finite element methods’, in: **Stein, E., de Borst, R., Hughes, T. J. R.** (eds.), *Encyclopedia of Computational Mechanics, Volume 1 Fundamentals*, Wiley, pp. 413–437.
- [71] **Douglas, J., Wang, J. (1989)**: ‘An absolutely stabilized finite element method for the Stokes problem.’, *Mathematics of Computation*, Vol. 52, pp. 495–508.

- [72] **Engel, M., Griebel, M. (2006)**: ‘Flow simulation on moving boundary-fitted grids and application to fluid-structure interaction problems.’, *International Journal for Numerical Methods in Fluids*, Vol. 50, pp. 437–468.
- [73] **Farhat, C. (2004)**: ‘CFD-based nonlinear computational aeroelasticity’, in: **Stein, E., de Borst, R., Hughes, T. J. R.** (eds.), *Encyclopedia of Computational Mechanics, Volume 3 Fluids*, Wiley, J., pp. 459–480.
- [74] **Farhat, C., Degand, C., Koobus, B., Lesoinne, M. (1998)**: ‘Torsional springs for two-dimensional dynamic unstructured fluid meshes.’, *Computer Methods in Applied Mechanics and Engineering*, Vol. 163, pp. 231–245.
- [75] **Farhat, C., Geuzaine, P. (2004)**: ‘Design and analysis of robust ALE time-integrators for the solution of unsteady flow problems on moving grids.’, *Computer Methods in Applied Mechanics and Engineering*, Vol. 193, pp. 4073–4095.
- [76] **Farhat, C., Geuzaine, P., Grandmont, C. (2001)**: ‘The discrete geometric conservation law and the nonlinear stability of ALE schemes for the solution of flow problems on moving grids.’, *Journal of Computational Physics*, Vol. 174, pp. 669–694.
- [77] **Farhat, C., van der Zee, K. G., Geuzaine, P. (2006)**: ‘Provably second-order time-accurate loosely-coupled solution algorithms for transient nonlinear computational aeroelasticity.’, *Computer Methods in Applied Mechanics and Engineering*, Vol. 195, pp. 1973–2001.
- [78] **Felippa, C., Park, K. (1980)**: ‘Staggered transient analysis procedures for coupled mechanical systems: Formulation.’, *Computer Methods in Applied Mechanics and Engineering*, Vol. 24, pp. 61–111.
- [79] **Felippa, C., Park, K., de Runtz, J. (1977)**: ‘Stabilization of staggered solution procedures for fluid-structure interaction analysis.’, in: **Belytschko, T., Geers, T.** (eds.), *Computational Methods for Fluid-Structure Interaction Problems*, Vol. 26, AMS, AMD, New York, pp. 95–124.
- [80] **Fernandez, M. A., Gerbeau, J.-F., Grandmont, C. (2007)**: ‘A projection semi-implicit scheme for the coupling of an elastic structure with an incompressible fluid.’, *International Journal for Numerical Methods in Engineering*, Vol. 69, pp. 794–821.
- [81] **Ferziger, J. H., Perić, M. (1997)**: *Computational Methods for Fluid Dynamics*, Springer.
- [82] **Fletcher, C. A. J. (1991)**: *Computational Techniques for Fluid Dynamics, Volume 1*, Springer-Verlag, Berlin.
- [83] **Formaggia, L., Nobile, F. (1999)**: ‘A stability analysis for the arbitrary Lagrangian Eulerian formulation with finite elements.’, *East-West Journal of Numerical Mathematics*, Vol. 7, pp. 105–131.
- [84] **Formaggia, L., Nobile, F. (2004)**: ‘Stability analysis of second-order time accurate schemes for ALE-FEM.’, *Computer Methods in Applied Mechanics and Engineering*, Vol. 193, pp. 4097–4116.
- [85] **Förster, Ch., Genkinger, S., Neumann, M., Wall, W. A., Ramm, E. (2006)**: *Multifield Problems in Solid and Fluid Mechanics*, Vol. 28 of *Lecture Notes in Applied and Computational Mechanics*, chap. Fluid-Structure Interaction of Incompressible Flows and Thin-Walled Structures., Springer, Berlin/Heidelberg, pp. 187–218.
- [86] **Förster, Ch., Wall, W. A., Ramm, E. (2006)**: ‘On the geometric conservation law in transient flow calculations on deforming domains.’, *International Journal for Numerical Methods in Fluids*, Vol. 50, pp. 1369–1379.
- [87] **Förster, Ch., Wall, W. A., Ramm, E. (2007)**: ‘Artificial added mass instabilities in sequential staggered coupling of nonlinear structures and incompressible viscous flows.’, *Computer Methods in Applied Mechanics and Engineering*, Vol. 196, pp. 1278–1293.
- [88] **Förster, Ch., Wall, W. A., Ramm, E. (2007)**: ‘On residual based stabilisation methods for transient problems at small time increments’, *submitted*.
- [89] **Förster, Ch., Wall, W. A., Ramm, E. (2007)**: ‘Stabilised finite element formulation for incompressible flow on distorted meshes.’, *submitted*.

- [90] **Franca, L. P.** (ed.) (1998): *Special Issue on Advances in Stabilized Methods in Computational Mechanics*, Vol. 166 of *Computer Methods in Applied Mechanics and Engineering*, Elsevier.
- [91] **Franca, L. P., Farhat, C.** (1995): ‘Bubble functions prompt unusual stabilized finite element methods.’, *Computer Methods in Applied Mechanics and Engineering*, Vol. 123, pp. 299–308.
- [92] **Franca, L. P., Farhat, C., Lesoinne, M., Russo, A.** (1998): ‘Unusual stabilized finite element methods and residual free bubbles.’, *International Journal for Numerical Methods in Fluids*, Vol. 27, pp. 159–168.
- [93] **Franca, L. P., Frey, S. L., Hughes, T. J. R.** (1992): ‘Stabilized finite element methods: I. Application to the advective-diffusive model.’, *Computer Methods in Applied Mechanics and Engineering*, Vol. 95, pp. 253–276.
- [94] **Franca, L. P., Hauke, G., Masud, A.** (2006): ‘Revisiting stabilized finite element methods for the advective-diffusive equation.’, *Computer Methods in Applied Mechanics and Engineering*, Vol. 195, pp. 1560–1572.
- [95] **Franca, L. P., Hughes, T. J. R.** (1988): ‘Two classes of mixed finite element methods.’, *Computer Methods in Applied Mechanics and Engineering*, Vol. 69, pp. 89–129.
- [96] **Franca, L. P., Valentin, F.** (2000): ‘On an improved unusual stabilized finite element method for the advective-reactive-diffusive equation.’, *Computer Methods in Applied Mechanics and Engineering*, Vol. 190, pp. 1785–1800.
- [97] **Galdi, G. P., Layton, W. J.** (2000): ‘Approximation of the larger eddies in fluid motion II: a model of space filtered flow.’, *Mathematical Models and Methods in Applied Sciences*, Vol. 10, pp. 343–350.
- [98] **Gear, C. W.** (1971): *Numerical initial value problems in ordinary differential equations*, Prentice-Hall, Englewood Cliffs, New Jersey.
- [99] **Gee, M.** (2004): *Effiziente Lösungsstrategien in der nichtlinearen Schalenmechanik*, Phd thesis, Institut für Baustatik, Universität Stuttgart.
- [100] **Gee, M., Ramm, E., Wall, W. A.** (2005): ‘Parallel multilevel solution of nonlinear shell structures.’, *Computer Methods in Applied Mechanics and Engineering*, Vol. 194, pp. 2513–2533.
- [101] **Geuzaine, P., Grandmont, C., Farhat, C.** (2003): ‘Design and analysis of ALE schemes with provable second-order time-accuracy for inviscid and viscous flow simulations.’, *Journal of Computational Physics*, Vol. 191, pp. 206–227.
- [102] **Girault, V., Raviart, P.-A.** (1980): *Finite Element Methods for Navier-Stokes Equations*, Vol. 5 of *Springer Series in Computational Mathematics*, Springer, Berlin.
- [103] **Gravemeier, V.** (2003): *The Variational Multiscale Method for Laminar and Turbulent Incompressible Flow*, Ph.D. Thesis, Institut für Baustatik, Universität Stuttgart.
- [104] **Gravemeier, V.** (2006): ‘The variational multiscale method for laminar and turbulent flow.’, *Archives of Computational Methods in Engineering - State of the Art Reviews*, Vol. 13, pp. 249–324.
- [105] **Gravemeier, V., Wall, W. A., Ramm, E.** (2004): ‘A three-level finite element method for the instationary incompressible Navier-Stokes equations.’, *Computer Methods in Applied Mechanics and Engineering*, Vol. 193, pp. 1323–1366.
- [106] **Gravemeier, V., Wall, W. A., Ramm, E.** (2005): ‘Large eddy simulation of turbulent incompressible flows by a three-level finite element method.’, *International Journal for Numerical Methods in Fluids*, Vol. 48, pp. 1067–1099.
- [107] **Gresho, P. M., Sani, R. L.** (1998): *Incompressible flow and the finite element method*, Wiley.
- [108] **Guillard, H., Farhat, C.** (2000): ‘On the significance of the geometric conservation law for flow computations on moving meshes.’, *Computer Methods in Applied Mechanics and Engineering*, Vol. 190, pp. 1467–1482.

- [109] **Gunzburger, M. D. (1989)**: *Finite element methods for viscous incompressible flows: a guide to theory, practice and algorithms*, Academic Press.
- [110] **Haines, B., Giles, M. (1992)**: *Visual2 User's and Programmer's Manual*, Massachusetts Institute of Technology, Cambridge, <http://raphael.mit.edu/visual2/visual2.html>.
- [111] **Hairer, E., Nørsett, S. P., Wanner, G. (1991)**: *Solving Ordinary Differential Equations I - Nonstiff Problems*, Vol. 8 of *Springer Series in Computational Mathematics*, Springer, Berlin.
- [112] **Hairer, E., Wanner, G. (1996)**: *Solving Ordinary Differential Equations II - Stiff and Differential-Algebraic Problems*, Vol. 14 of *Springer Series in Computational Mathematics*, Springer, Berlin.
- [113] **Harari, I. (2002)**: 'Spatial stability of semidiscrete formulations for parabolic problems', in: *Proceedings of the Fifth World Congress on Computational Mechanics 2002, Vienna, Austria*.
- [114] **Harari, I. (2004)**: 'Stability of semidiscrete formulations for parabolic problems at small time steps.', *Computer Methods in Applied Mechanics and Engineering*, Vol. 193, pp. 1491–1516.
- [115] **Harari, I., Hauke, G. (2007)**: 'Semidiscrete formulations for transient transport at small time steps.', *submitted to International Journal for Numerical Methods in Fluids*.
- [116] **Harari, I., Hughes, T. J. R. (1992)**: 'What are c and h?: Inequalities for the analysis and design of finite element methods.', *Computer Methods in Applied Mechanics and Engineering*, Vol. 97, pp. 157–192.
- [117] **Harari, I., Hughes, T. J. R. (1994)**: 'Stabilized finite element methods for steady advection-diffusion with production.', *Computer Methods in Applied Mechanics and Engineering*, Vol. 115, pp. 165–191.
- [118] **Hauke, G. (2002)**: 'A simple subgrid scale stabilized method for the advection-diffusion-reaction equation.', *Computer Methods in Applied Mechanics and Engineering*, Vol. 191, pp. 2925–2947.
- [119] **Hauke, G., Doweidar, M. H. (2005)**: 'Fourier analysis of semi-discrete and space-time stabilized methods for the advective-diffusive-reactive equation: I. SUPG.', *Computer Methods in Applied Mechanics and Engineering*, Vol. 194, pp. 45–81.
- [120] **Hauke, G., Doweidar, M. H. (2005)**: 'Fourier analysis of semi-discrete and space-time stabilized methods for the advective-diffusive-reactive equation: II. SGS.', *Computer Methods in Applied Mechanics and Engineering*, Vol. 194, pp. 691–725.
- [121] **Hauke, G., Doweidar, M. H. (2006)**: 'Fourier analysis of semi-discrete and space-time stabilized methods for the advective-diffusive-reactive equation: III SGS/GSGS', *Computer Methods in Applied Mechanics and Engineering*, Vol. 195, pp. 6158–6176.
- [122] **Hauke, G., Doweidar, M. H., Miana, M. (2006)**: 'Proper intrinsic scales for a-posteriori multiscale error estimation', *Computer Methods in Applied Mechanics and Engineering*, Vol. 195, pp. 3983–4001.
- [123] **Heil, M. (2004)**: 'An efficient solver for the fully coupled solution of large-displacement fluid-structure interaction problems.', *Computer Methods in Applied Mechanics and Engineering*, Vol. 193, pp. 1–23.
- [124] **Heinemann, A.**: *Human Thorax, Lung, 3D reconstruction from CT-scans*, Zeppelinzentrum Karlsruhe, Germany, <http://www.rad-zep.de>, visited on 21. December 2006.
- [125] **Heywood, J. G., Rannacher, R., Turek, S. (1996)**: 'Artificial boundaries and flux and pressure conditions for the incompressible Navier-Stokes equations.', *International Journal for Numerical Methods in Fluids*, Vol. 22, pp. 325–352.
- [126] **Hilchenbach, C. F. (2004)**: *Simulation der Wechselwirkung von Wind und umströmten Brückenquerschnitten*, Diplomarbeit, Institut für Baustatik, Universität Stuttgart.
- [127] **Hirt, C. W., Amsden, A. A., Cook, J. L. (1974)**: 'An arbitrary Lagrangian-Eulerian computing method for all flow speeds.', *Journal of Computational Physics*, Vol. 14, pp. 227–253.

- [128] **Hirt, C. W., Amsden, A. A., Cook, J. L. (1997)**: ‘An arbitrary Lagrangian-Eulerian computing method for all flow speeds.’, *Journal of Computational Physics*, Vol. 135, pp. 203–216, reprint from 1974.
- [129] **Hübner, B. (2003)**: *Simultane Analyse von Bauwerk-Wind-Wechselwirkungen*, Ph.D. Thesis, Institut für Statik, Universität Braunschweig.
- [130] **Hübner, B., Walhorn, E., Dinkler, D. (2004)**: ‘A monolithic approach to fluid-structure interaction using space-time finite elements.’, *Computer Methods in Applied Mechanics and Engineering*, Vol. 193, pp. 2087–2104.
- [131] **Huerta, A., Rodriguez-Ferran, A. (eds.) (2000)**: *Special Issue on The Arbitrary Lagrangian-Eulerian Formulation*, Vol. 193 issues 39–41 of *Computer Methods in Applied Mechanics and Engineering*, Elsevier.
- [132] **Hughes, T. J. R. (1987)**: ‘Recent progress in the development and understanding of SUPG methods with special reference to the compressible Euler and Navier-Stokes equations.’, *International Journal for Numerical Methods in Fluids*, Vol. 7, pp. 1261–1275.
- [133] **Hughes, T. J. R. (1995)**: ‘Multiscale phenomena: Green’s functions, the Dirichlet-to-Neumann formulations, subgrid scale models, bubbles and the origins of stabilized methods.’, *Computer Methods in Applied Mechanics and Engineering*, Vol. 127, pp. 387–401.
- [134] **Hughes, T. J. R. (2000)**: *The Finite Element Method – Linear Static and Dynamic Finite Element Analysis*, Dover Publications, Mineola, New York.
- [135] **Hughes, T. J. R., Brooks, A. (1979)**: ‘A multi-dimensional upwind scheme with no cross wind diffusion’, in: **Hughes, T. J. R. (ed.)**, *Finite Element for convection Dominated Flows*, Vol. 34, ASME, AMD, pp. 19–35.
- [136] **Hughes, T. J. R., Brooks, A. (1982)**: ‘A theoretical framework for Petrov-Galerkin methods with discontinuous weighting function’, in: **Gallagher, R. H. (ed.)**, *Finite Elements in Fluids*, Vol. 4, Wiley, Chichester, pp. 47–65.
- [137] **Hughes, T. J. R., Engel, G., Mazzei, L., Larson, M. G. (2000)**: ‘The continuous Galerkin method is locally conservative.’, *Journal of Computational Physics*, Vol. 163, pp. 467–488.
- [138] **Hughes, T. J. R., Feijoo, G. R., Mazzei, L., Quincy, J.-B. (1998)**: ‘The variational multiscale method - a paradigm for computational mechanics.’, *Computer Methods in Applied Mechanics and Engineering*, Vol. 166, pp. 3–24.
- [139] **Hughes, T. J. R., Franca, L. P., Balestra, M. (1986)**: ‘A new finite element formulation for computational fluid dynamics: V. circumventing the Babuska-Brezzi condition: A stable Petrov-Galerkin formulation of the Stokes problem accommodating equal-order interpolation.’, *Computer Methods in Applied Mechanics and Engineering*, Vol. 59, pp. 85–99.
- [140] **Hughes, T. J. R., Franca, P., Hulbert, G. M. (1989)**: ‘A new finite element formulation for computational fluid dynamics: VIII. The Galerkin/least-squares method for advective-diffusive equations.’, *Computer Methods in Applied Mechanics and Engineering*, Vol. 73, pp. 173–189.
- [141] **Hughes, T. J. R., Mazzei, L., Jansen, K. E. (2000)**: ‘Large Eddy Simulation and the variational multiscale method.’, *Computing and Visualization in Science*, Vol. 3, pp. 47–59.
- [142] **Hughes, T. J. R., Oberai, A. A., Mazzei, L. (2001)**: ‘Large eddy simulation of turbulent channel flows by the variational multiscale method.’, *Physics of Fluids*, Vol. 13, pp. 1784–1799.
- [143] **Hughes, T. J. R., Scovazzi, G., Franca, L. P. (2004)**: ‘Multiscale and stabilized method’, in: **Stein, E., de Borst, R., Hughes, T. J. R. (eds.)**, *Encyclopedia of Computational Mechanics, Volume 3 Fluids*, Wiley, pp. 5–59.
- [144] **Hughes, T. J. R., Wells, G. N. (2005)**: ‘Conservation properties for the Galerkin and stabilised forms of the advection-diffusion and incompressible Navier-Stokes equations.’, *Computer Methods in Applied Mechanics and Engineering*, Vol. 194, pp. 1141–1159.
- [145] **Hund, A. (2007)**: *Hierarchische Mehrskalenmodellierung des Versagens von Werkstoffen mit Mikrostruktur*, Ph.D. Thesis, Institut für Baustatik und Baudynamik, Universität Stuttgart.

- [146] **Irons, B., Tuck, R. (1969)**: ‘A version of the Aitken accelerator for computer implementation.’, *International Journal for Numerical Methods in Engineering*, Vol. 1, pp. 275–277.
- [147] **Jansen, E. K., Collis, S. S., Whiting, C., Shakib, F. (1999)**: ‘A better consistency for low-order stabilized finite element methods.’, *Computer Methods in Applied Mechanics and Engineering*, Vol. 174, pp. 153–170.
- [148] **John, V. (2000)**: *Large Eddy Simulation of Turbulent Incompressible Flows*, Vol. 34 of *Lecture Notes in Computational Science and Engineering*, Springer, Berlin.
- [149] **John, V. (2002)**: ‘Higher order finite element methods and multigrid solvers in a benchmark problem for the 3d Navier-Stokes equations.’, *International Journal for Numerical Methods in Fluids*, Vol. 40, pp. 775–798.
- [150] **John, V. (2006)**: ‘On the efficiency of linearization schemes and coupled multigrid methods in the simulation of a 3d flow around a cylinder.’, *International Journal for Numerical Methods in Fluids*, Vol. 50, pp. 845–862.
- [151] **John, V., Liakos, A. (2006)**: ‘Time-dependent flow across a step: the slip with friction boundary condition’, *International Journal for Numerical Methods in Fluids*, Vol. 50, pp. 713–731.
- [152] **Kawahara, M., Ohmiya, K. (1985)**: ‘Finite element analysis of density flow using the velocity correction method.’, *International Journal for Numerical Methods in Fluids*, Vol. 5, pp. 981–993.
- [153] **Kelly, W. W., Nakazawa, S., Zienkiewicz, O. C. (1980)**: ‘A note on anisotropic balancing dissipation in the finite element methods approximation to convective diffusion problems.’, *International Journal for Numerical Methods in Engineering*, Vol. 15, pp. 1705–1711.
- [154] **Khurram, R. A., Masud, A. (2006)**: ‘A multiscale/stabilized formulation of the incompressible Navier-Stokes equations for moving boundary flows and fluid-structure interaction’, *Computational Mechanics*, Vol. 38, pp. 403–416.
- [155] **Kim, J., Moin, P. (1985)**: ‘Application of a fractional-step method to incompressible Navier-Stokes equations.’, *Journal of Computational Physics*, Vol. 59, pp. 308–323.
- [156] **Kjellgren, P., Hyvärinen, J. (1998)**: ‘An arbitrary Lagrangian-Eulerian finite element method.’, *Computational Mechanics*, Vol. 21, pp. 81–90.
- [157] **Knabner, P., Angermann, L. (2000)**: *Numerik partieller Differentialgleichungen*, Springer, Berlin.
- [158] **Kohno, H., Bathe, K.-J. (2005)**: ‘Insight into the flow-condition-based interpolation finite element approach: Solution of steady-state advection-diffusion problems.’, *International Journal for Numerical Methods in Engineering*, Vol. 63, pp. 197–217.
- [159] **Kohno, H., Bathe, K.-J. (2005)**: ‘On the flow-condition-based interpolation approach for incompressible fluids.’, in: **Bathe, K.-J.** (ed.), *Computational Fluid and Solid Mechanics*, Elsevier.
- [160] **Kohno, H., Bathe, K.-J. (2006(?))**: ‘A 9-node quadrilateral FCBI element for incompressible Navier-Stokes flows.’, *Communications in Numerical Methods in Engineering*.
- [161] **Koobus, B., Farhat, C. (1999)**: ‘Second-order time-accurate and geometrically conservative implicit schemes for flow computations on unstructured dynamic meshes.’, *Computer Methods in Applied Mechanics and Engineering*, Vol. 170, pp. 103–129.
- [162] **Kuhl, D. (1996)**: *Stabile Zeitintegrationsalgorithmen in der nichtlinearen Elastodynamik dünnwandiger Tragwerke*, Ph.D. Thesis, Institut für Baustatik, Universität Stuttgart.
- [163] **Kuhl, D., Ramm, E. (1999)**: ‘Generalized energy-momentum method for non-linear adaptive shell dynamics.’, *Computer Methods in Applied Mechanics and Engineering*, Vol. 178, pp. 343–366.
- [164] **Küttler, U., Förster, Ch., Wall, W. A. (2006)**: ‘A solution for the incompressibility dilemma in partitioned fluid-structure interaction with pure Dirichlet fluid domains.’, *Computational Mechanics*, Vol. 38, pp. 417–429.
- [165] **Larsen, A. (1998)**: ‘Advances in aeroelastic analyses of suspension and cable-stayed bridges.’, *Journal of Wind Engineering and Industrial Aerodynamics*, Vol. 74–76, pp. 73–90.

- [166] **Le Tallec, P., Mouro, J. (2001)**: ‘Fluid structure interaction with large structural displacements.’, *Computer Methods in Applied Mechanics and Engineering*, Vol. 190, pp. 3039–3067.
- [167] **Lesoinne, M., Farhat, C. (1996)**: ‘Geometric conservation laws for flow problems with moving boundaries and deformable meshes, and their impact on aeroelastic computations.’, *Computer Methods in Applied Mechanics and Engineering*, Vol. 134, pp. 71–91.
- [168] **Löhner, R., Yang, C. (1996)**: ‘Improved ALE mesh velocities for moving bodies.’, *Communications in Numerical Methods in Engineering*, Vol. 12, pp. 599–608.
- [169] **Löhner, R., Yang, C., Cebal, J., Baum, J. D., Luo, H., Pelessone, D., Charman, C. (1995)**: ‘Fluid-structure interaction using a loose coupling algorithm and adaptive unstructured grids’, in: **Hafez, M., Oshima, K.** (eds.), *Computational Fluid Dynamics Review 1995*, Wiley.
- [170] **MAGEBA**, <http://www.mageba.ch/upload/pics/>: *Schrägseilbrücke ausgerüstet mit mageba Pendellager (Rocker bearing)*, visited on 21. December 2006.
- [171] **Malvern, L. (1969)**: *Introduction to the mechanics of a continuous medium*, Prentice-Hall, London.
- [172] **Markour, G. A., Mouroutis, Z. S., Charmpis, D. C., Papadrakakis, M. (2007)**: ‘The ortho-semi-torsional (OST) spring analogy methods for 3d mesh moving boundary problems.’, *Computer Methods in Applied Mechanics and Engineering*, Vol. 196, pp. 747–765.
- [173] **Marsden, J., Hughes, T. J. R. (1983)**: *Mathematical foundations of elasticity*, Prentice-Hall.
- [174] **Massjung, R. (2006)**: ‘Discrete conservation and coupling strategies in nonlinear aeroelasticity.’, *Computer Methods in Applied Mechanics and Engineering*, Vol. 196, pp. 91–102.
- [175] **Masud, A. (2006)**: ‘Effects of mesh motion on the stability and convergence of ALE based formulations for moving boundary flows’, *Computational Mechanics*, Vol. 38, pp. 430–439.
- [176] **Masud, A., Hughes, T. J. R. (1997)**: ‘A space-time Galerkin/least-squares finite element formulation of the Navier-Stokes equations for moving domain problems.’, *Computer Methods in Applied Mechanics and Engineering*, Vol. 146, pp. 91–126.
- [177] **Masud, A., Xia, K. (2005)**: ‘A stabilized mixed finite element method for nearly incompressible elasticity.’, *Journal of Applied Mechanics*, Vol. 72, pp. 711–720.
- [178] **Masud, A., Xia, K. (2006)**: ‘A variational multiscale method for inelasticity: Application to superelasticity in shape memory alloys.’, *Computer Methods in Applied Mechanics and Engineering*, Vol. 195, pp. 4512–4531.
- [179] **Matthies, H. G., Niekamp, R., Steindorf, J. (2006)**: ‘Algorithms for strong coupling procedures.’, *Computer Methods in Applied Mechanics and Engineering*, Vol. 195, pp. 2028–2049.
- [180] **Matthies, H. G., Steindorf, J. (2003)**: ‘Partitioned strong coupling algorithms for fluid-structure interaction.’, *Computers and Structures*, Vol. 81, pp. 805–812.
- [181] **Mittal, S. (2000)**: ‘On the performance of high aspect ratio elements for incompressible flows.’, *Computer Methods in Applied Mechanics and Engineering*, Vol. 188, pp. 269–287.
- [182] **Mok, D. P. (2001)**: *Partitionierte Lösungsansätze in der Strukturmechanik und der Fluid-Struktur-Interaktion*, Ph.D. Thesis, Institut für Baustatik, Universität Stuttgart.
- [183] **Mok, D. P., Wall, W. A. (2001)**: ‘Partitioned analysis schemes for the transient interaction of incompressible flows and nonlinear flexible structures’, in: *Proceedings of Trends in Computational Structural Mechanics*, W.A. Wall, K.-U. Bletzinger and K. Schweizerhof (Eds.), pp. 689–698.
- [184] **Norburn, S., Silvester, D. (1998)**: ‘Stabilised vs. stable mixed methods for incompressible flow.’, *Computer Methods in Applied Mechanics and Engineering*, Vol. 166, pp. 131–141.
- [185] **Oden, J. T. (1972)**: *Finite Elements of Nonlinear Continua*, McGraw-Hill.
- [186] **Ohayon, R. (2004)**: ‘Fluid-structure interaction problems’, in: **Stein, E., de Borst, R., Hughes, T. J. R.** (eds.), *Encyclopedia of Computational Mechanics, Volume 2 Solids and Structures*, Wiley, pp. 683–693.

- [187] **Ohayon, R., Kvamsdal, T. (eds.) (2006)**: *Special issue on Fluid-Structure Interaction*, Vol. 195, issues 17-18 of *Computer Methods in Applied Mechanics and Engineering*, Elsevier.
- [188] **Oñate, E. (1998)**: ‘Derivation of stabilized equations for numerical solution of advective-diffusive transport and fluid flow problems.’, *Computer Methods in Applied Mechanics and Engineering*, Vol. 151, pp. 233–265.
- [189] **Oñate, E., Gracia, J., Idelsohn, S. R. (2004)**: ‘Ship hydrodynamics’, in: **Stein, E., de Borst, R., Hughes, T. J. R. (eds.)**, *Encyclopedia of Computational Mechanics, Volume 3 Fluids*, Wiley, pp. 580–610.
- [190] **Oñate, E., Gracia, J., Idelsohn, S. R., Pin, F. D. (2006)**: ‘Finite calculus formulations for finite element analysis of incompressible flows. Eulerian, ALE and Lagrangian approaches.’, *Computer Methods in Applied Mechanics and Engineering*, Vol. 195, pp. 3001–3037.
- [191] **Oñate, E., Miquel, J., Hauke, G. (2006)**: ‘Stabilized formulation for the advection-diffusion-absorption equation using finite calculus and linear finite elements.’, *Computer Methods in Applied Mechanics and Engineering*, Vol. 195, pp. 3926–3946.
- [192] **Piperno, S. (1997)**: ‘Explicit/implicit fluid/structure staggered procedures with a structural predictor and fluid subcycling for 2d inviscid aeroelastic simulations’, *International Journal for Numerical Methods in Fluids*, Vol. 25, pp. 1207–1226.
- [193] **Piperno, S., Farhat, C. (2000)**: ‘Design of efficient partitioned procedures for the transient solution of aeroelastic problems.’, *Revue Européenne des Elements Finis*, Vol. 9, pp. 655–680.
- [194] **Piperno, S., Farhat, C. (2001)**: ‘Partitioned procedures for the transient solution of coupled aeroelastic problems - Part II: energy transfer analysis and three-dimensional applications’, *Computer Methods in Applied Mechanics and Engineering*, Vol. 190, pp. 3147–3170.
- [195] **Piperno, S., Farhat, C., Larrouturou, B. (1995)**: ‘Partitioned procedures for the transient solution of coupled aeroelastic problems. Part I: Model problem, theory and two-dimensional application’, *Computer Methods in Applied Mechanics and Engineering*, Vol. 124, pp. 79–112.
- [196] **Pironneau, O. (1989)**: *Finite Element Methods for Fluids*, Wiley, Chichester.
- [197] **Quateroni, A., Valli, A. (1997)**: *Numerical Approximations of Partial Differential Equations*, Vol. 23 of *Springer Series in Computational Mathematics*, Springer, Berlin.
- [198] **Rammerstorfer, F. G., Scharf, K., Fischer, F. D. (1990)**: ‘Storage tanks under earthquake loading.’, *Applied Mechanic Reviews*, Vol. 43, pp. 261–282.
- [199] **Rank, E., Halfmann, A., Scholz, D., Glück, M., Breuer, M., Durst, F., Kaiser, U., Bergmann, D., Wagner, S. (2005)**: ‘Wind loads on lightweight structures: Numerical simulation and wind tunnel tests’, *GAMM Mitteilungen*, Vol. 28, pp. 73–89.
- [200] **Rank, E., Scholz, D., Halfmann, A., Glück, M., Breuer, M., Durst, F. (2003)**: ‘Fluid-structure interaction in civil engineering’, in: *Computational Fluid and Solid Mechanics, K.J. Bathe (ed.)*, Vol. 2, pp. 1488–1491.
- [201] **Rannacher, R. (1998)**: ‘A posteriori error estimation in least-squares stabilized finite element schemes.’, *Computer Methods in Applied Mechanics and Engineering*, Vol. 166, pp. 99–114.
- [202] **Rannacher, R. (2004)**: ‘Incompressible viscous flows’, in: **Stein, E., de Borst, R., Hughes, T. J. R. (eds.)**, *Encyclopedia of Computational Mechanics, Volume 3 Fluids*, Wiley, J., pp. 155–181.
- [203] Rheonik Messgeräte GmbH, <http://www.rheonik.com>: *General Construction of a RHEONIK Mass Flowmeter*.
- [204] **Rothe, E. (1930)**: ‘Zweidimensionale parabolische Randwertaufgaben als Grenzfall eindimensionaler Randwertaufgaben.’, *Mathematische Annalen*, Vol. 102, pp. 650–670.
- [205] **Russo, A. (2006)**: ‘Streamline-upwind Petrov/Galerkin method (SUPG) vs residual-free bubbles (RFB).’, *Computer Methods in Applied Mechanics and Engineering*, Vol. 195, pp. 1608–1620.

- [206] **Sani, R. L., Shen, J., Pironneau, O., Gresho, P. M. (2005)**: ‘Pressure boundary condition for the time-dependent incompressible Navier-Stokes equations’, *International Journal for Numerical Methods in Fluids*.
- [207] **Stein, E., Barthold, F.-J. (1996)**: ‘Elastizitätstheorie’, in: **Mehlhorn, G.** (ed.), *Der Ingenieurbau, Werkstoffe, Elastizitätstheorie*, Ernst & Sohn, Berlin, pp. 165–428.
- [208] **Stein, K., Tezduyar, T., Benney, R. (2002)**: ‘Applications in airdrop systems: Fluid-structure interaction modeling’, in: *Proceedings of the Fifth World Congress on Computational Mechanics 2002, Vienna, Austria*.
- [209] **Stenberg, R. (1990)**: ‘Error analysis of some finite element methods for the Stokes problem.’, *Mathematics of Computation*, Vol. 54, pp. 495–508.
- [210] **Stewart, J. R., Hughes, T. J. R. (1998)**: ‘A tutorial in elementary finite element error analysis: A systematic presentation of a priori and a posteriori error estimates.’, *Computer Methods in Applied Mechanics and Engineering*, Vol. 158, pp. 1–22.
- [211] **Taylor, C. A., Hughes, T. J. R., Zarins, C. K. (1998)**: ‘Finite element modeling of blood flow in arteries.’, *Computer Methods in Applied Mechanics and Engineering*, Vol. 158, pp. 155–196.
- [212] **Temam, R. (1985)**: *Navier-Stokes equations: theory and numerical analysis*, North Holland, Amsterdam, 3. edn.
- [213] **Tezduyar, T., Behr, M., Mittal, S., Johnson, A. (1992)**: ‘Computation of unsteady incompressible flows with the stabilized finite element methods: Space-time formulations, iterative strategies and massively parallel implementations.’, in: **Smolinski, P., Liu, W. K., Hulbert, G., Tamma, K.** (eds.), *New Methods in Transient Analysis*, Vol. 143, ASME, AMD, pp. 7–24.
- [214] **Tezduyar, T., Sathe, S. (2003)**: ‘Stabilization parameters in SUPG and PSPG formulations.’, *Journal of Computational and Applied Mechanics*, Vol. 4, pp. 71–88.
- [215] **Tezduyar, T. E. (2001)**: ‘Adaptive determination of the finite element stabilization parameters.’, in: *Proceedings of the ECCOMAS Computational Fluid Dynamics Conference*, Swansea.
- [216] **Tezduyar, T. E. (2003)**: ‘Computation of moving boundaries and interfaces and stabilization parameters.’, *International Journal for Numerical Methods in Fluids*, Vol. 43, pp. 555–575.
- [217] **Tezduyar, T. E. (2004)**: ‘Finite element methods for fluid dynamics with moving boundaries and interfaces’, in: **Stein, E., de Borst, R., Hughes, T. J. R.** (eds.), *Encyclopedia of Computational Mechanics, Volume 3 Fluids*, Wiley, pp. 545–577.
- [218] **Tezduyar, T. E., Behr, M. (1992)**: ‘A new strategy for finite element computations involving moving boundaries and interfaces - the deforming-spatial-domain/space-time procedure: I. The concept and the preliminary numerical tests.’, *Computer Methods in Applied Mechanics and Engineering*, Vol. 94, pp. 339–351.
- [219] **Tezduyar, T. E., Mittal, S., Ray, S. E., Shih, R. (1992)**: ‘Incompressible flow computations with stabilized bilinear and linear equal-order-interpolation velocity-pressure elements.’, *Computer Methods in Applied Mechanics and Engineering*, Vol. 95, pp. 221–242.
- [220] **Tezduyar, T. E., Osawa, Y. (2000)**: ‘Finite element stabilization parameters computed from element matrices and vectors.’, *Computer Methods in Applied Mechanics and Engineering*, Vol. 190, pp. 411–430.
- [221] **Tezduyar, T. E., Sathe, S., Keedy, R., Stein, K. (2006)**: ‘Space-time finite element techniques for computation of fluid-structure interactions.’, *Computer Methods in Applied Mechanics and Engineering*, Vol. 195, pp. 2002–2027.
- [222] **Tezduyar, T. E., Sathe, S., Stein, K. (2006)**: ‘Solution techniques for the fully discretized equations in computation of fluid-structure interactions with the space-time formulations’, *Computer Methods in Applied Mechanics and Engineering*, Vol. 195, pp. 5743–5753.
- [223] **Thomas, P. D., Lombard, C. K. (1979)**: ‘Geometric conservation law and its application to flow computations on moving grids.’, *AIAA Journal*, Vol. 17, pp. 1030–1037.

- [224] **Torii, R., Oshima, M., Kobayashi, T., Takagi, K., Tezduyar, T. E. (2006):** ‘Computer modeling of cardiovascular fluid-structure interactions with the deforming-spatial-domain/stabilized space-time formulation.’, *Computer Methods in Applied Mechanics and Engineering*, Vol. 195, pp. 1885–1895.
- [225] **Tuminaro, R. S., Heroux, M., Hutchinson, S. A., Shadid, J. N. (1999):** ‘Official Aztec user’s guide version 2.1’, *Report SAND99- 8801J, Massively Parallel Computing Research Laboratory*, Sandia National Laboratories, Albuquerque.
- [226] **Walhoern, E., Hübner, B., Kölke, A., Dinkler, D. (2003):** ‘Fluid-structure coupling within a monolithic model involving free surface flows’, in: *Computational Fluid and Solid Mechanics, K.J. Bathe (ed.)*, Vol. 2, pp. 1560–1563.
- [227] **Wall, W. A. (1999):** *Fluid-Struktur-Interaktion mit stabilisierten Finiten Elementen*, Ph.D. Thesis, Institut für Baustatik, Universität Stuttgart.
- [228] **Wall, W. A., Mok, D. P., Ramm, E. (1999):** ‘Partitioned analysis approach of the transient coupled response of viscous fluids and flexible structures’, in: *W. Wunderlich (Ed.), Solids, Structures and Coupled Problems in Engineering, Proceedings of the European Conference on Computational Mechanics ECCM ’99, Munich*.
- [229] **Wall, W. A., Ramm, E. (1998):** ‘Fluid-structure interaction based upon a stabilized (ALE) finite element method’, in: *E. Oñate and S. Idelsohn (Eds.), Computational Mechanics, Proceedings of the Fourth World Congress on Computational Mechanics WCCM IV, Buenos Aires, Argentina*.
- [230] **Warsi, Z. U. A. (1993):** *Fluid Dynamics - Theoretical and computational approaches*, CRC Press, Boca Raton.
- [231] **Whiting, C. (1999):** *Stabilized finite element methods for fluid dynamics using a hierarchical basis*, Ph.D. Thesis, Rensselaer Polytechnic Institute.
- [232] **Whiting, C. H., Jansen, K. E. (2001):** ‘A stabilized finite element method for the incompressible Navier-Stokes equations using a hierarchical basis.’, *International Journal for Numerical Methods in Fluids*, Vol. 35, pp. 93–116.
- [233] **Whiting, C. H., Jansen, K. E., Dey, S. (2003):** ‘Hierarchical basis for stabilized finite element methods for compressible flows.’, *Computer Methods in Applied Mechanics and Engineering*, Vol. 192, pp. 5167–5185.
- [234] **Wriggers, P. (2001):** *Nichtlineare Finite-Element-Methoden*, Springer, Berlin.
- [235] **Zienkiewicz, O. C. (2006):** ‘The background of error estimation and adaptivity in finite element computations.’, *Computer Methods in Applied Mechanics and Engineering*, Vol. 195, pp. 207–213.
- [236] **Zienkiewicz, O. C., Taylor, R. L. (2005):** *The Finite Element Method for Solid and Structural Mechanics*, Elsevier.
- [237] **Zienkiewicz, O. C., Taylor, R. L., Nithiarasu, P. (2005):** *The Finite Element Method for Fluid Dynamics*, Elsevier.
- [238] **Zienkiewicz, O. C., Taylor, R. L., Zhu, J. Z. (2005):** *The Finite Element Method: Its Basis and Fundamentals*, Elsevier.

Index

- ε -inequality, 162
- A-stability, 28
- accuracy, 36
- added mass operator, 119, 122
- advection-diffusion equation, 21, 50, 53, 60
- advection-diffusion-reaction equation, 22
- ALE
 - formulation, 7, 23–27
 - reference system, 24
- artificial added mass effect, 113, 118
- BUBNOV-GALERKIN scheme, 52
- backward EULER method, 28
- balance
 - of angular momentum, 9
 - of linear momentum, 10
- BB condition, *see* inf-sup condition
- BDF2, 29, 32, 35, 36, 42, 82, 101, 116, 126
- boundary conditions, 10, 18
- bubble
 - condensation, 59
 - functions, 59
- CAUCHY stresses, 9
- CAUCHY-SCHWARZ inequality, 161
- changing domain, 23
- characteristic GALERKIN procedure, 53
- coercivity, 42, 45, 50, 75–80, 88–161
- conservation
 - laws, 33
 - of energy, 17, 38
 - of linear momentum, 16, 34
 - of mass, 15
- consistent
 - nodal forces, 117
 - stabilisation, *see* residual based stabilisation
- consistent nodal forces, 86
- continuum mechanics
 - of fluids, 14
 - of structures, 8
- convection
 - dominated problem, 50
 - induced oscillations, 50
 - instability, *see* induced oscillations
 - stabilisation, 52
- convective
 - formulation, 16, 26
 - term, 14, 54
- coupling
 - conditions, 20
 - forces, 117
- crosswind diffusion, 52
- deforming domain, 24, 60
- differential-algebraic problem, 27
- discrete geometric conservation laws, 38
- discretisation, 12, 27
 - in space, 12, 30
 - in time, 13, 27
- divergence formulation, 16, 26
- EULERian formulation, 7, 14
- element length, 72
- equal order interpolation, 55, 57, 66
- finite
 - elements, 12, 27, 30, 52
 - increment calculus, 53
 - volumes, 52
- flow
 - conditioned based interpolation, 54
 - equations, 14
- flowmeter, 151
- fundamental ALE equation, 26
- GALERKIN weak form, *see* weak formulation
- GALERKIN/Least-Squares method, *see* GLS
- generalised- α method, 13, 125
- geometric conservation, 25, 34, 116
- GLS, 53, 65, 75

- HELMHOLTZ decomposition, 55
- higher order elements, 66, 74, 102, 146
- horizontal method of lines, 27
- incompressibility, 49, 55, 56
- incompressible NAVIER-STOKES equations,
 - see* NAVIER-STOKES equations
- inf-sup condition, 49–54, 57
- initial conditions, 10, 18
- instability, 52
- inverse inequality, 162
- LAGRANGEan formulation, 7
- LBB condition, *see* inf-sup condition
- linear elements, 73, 84, 88
- material time derivative, 9, 25
- mesh
 - distortion, 72, 99–107
 - velocity, 35
- method of lines, 27
- model problems, 20
- NAVIER-STOKES equations, 16
- NEWTONian fluid, 15
- nonlinearity, 64
- numerical
 - accuracy check, 36
 - diffusion, 50
 - example, 36, 94, 100, 107, 131, 153
- one-step- θ method, 28, 30, 32, 35, 36, 42, 53, 116
- operator splitting, 55
- orthogonal subscales, 59
- PECLET number, 21, 50, 52
- PETROV-GALERKIN scheme, 52
- partitioned algorithm, 114
- predictor, 115
- pressure
 - oscillations, 51
 - projection, 57
 - projection method, 55
 - stabilisation, 54
- principle of virtual work, 11
- projection, 66, 102
- PSPG, 64
- REYNOLDS number, 14, 18, 70
- reference configuration, 8
- relaxation, 136
- residual
 - based stabilisation, 52, 53, 55, 58, 73
 - free bubbles, 62
- STOKES problem, 21, 51, 56, 58
- STROUHAL number, 18
- second
 - DAHLQUIST barrier, 28
 - order backward differencing, *see* BDF2
- shear forces, 14
- singular diffusion equation, 22
- small time steps, 82
- stabilisation, 49, 52
 - parameter, 70, 87, 89, 107
- stability
 - of ALE formulations, 40, 74
 - unconditional, 46
- stiff partial differential equation, 27
- structural material, 9
- SUPG, 53
- system of reference, 7
- time
 - dependent sub scales, 65
 - step size limit, 42, 45
- trapezoidal rule, 28
- unresolved gradients, 50
- upwinding, 51, 52
- USFEM, 59, 64, 76, 106
- variational multiscale method, 62
- weak formulation, 11
- weighted residual method, 52
- wiggles, 49

Lebenslauf

- Name: Christiane Förster, geb. Küttler
Geburtsdatum: 5. August 1977
Geburtsort: Zwickau
Eltern: Matthias Küttler, Maria Kütter, geb. Dietrich
Nationalität: deutsch
Familienstand: verheiratet seit 15. Juli 2003 mit Dr. rer. nat. Clemens Förster
- 1984-1986: Besuch der Polytechnischen Oberschule „Max Reichpietsch“
in Thurm
- 1986-1990: Besuch der Polytechnischen Oberschule II Thurm
- 1990-1992: Besuch einer Leistungsklasse mit mathematisch-natur-
wissenschaftlichem Profil an der Oberschule Mülsen St. Micheln
- 1992-1996: Besuch des Gymnasiums „Am Sandberg“ Wilkau-Haßlau Außen-
stelle Mülsen St. Micheln (vormals Oberschule Mülsen St.
Micheln)
- Juni 1996: Abitur
- 1996 - 2001: Studium des Bauingenieurwesens
an der Technischen Universität Dresden
- November 1998: Aufnahme in die Studienstiftung des Deutschen Volkes
- August 2001: Abschluß als Diplomingenieur
- Januar 2002: Auszeichnung der Diplomarbeit
mit dem Kurt-Beyer-Preis der TU Dresden
- 2001-2002: Studium des „Civil and Computational Engineering“
an der University of Wales, Swansea
- September 2002: Abschluß als Master of Research
in „Computer Modelling in Engineering“
- Januar 2003 Auszeichnung der Masterarbeit mit dem „Earnest Hinton Prize“
des „Civil and Computational Engineering Centre“
der University of Wales, Swansea
- 2002-2006: Wissenschaftlicher Mitarbeiter am Institut für Baustatik und
Baudynamik Universität Stuttgart,
im selben Zeitraum auch Mitglied des Sonderforschungsbe-
reiches 404 „Mehrfeldprobleme in der Kontinuumsmechanik“
der Deutschen Forschungsgemeinschaft



Universität Stuttgart

ISBN 978-3-00-022267-2